

32

25

SACRAMENTO PLANT

N64-27286

code. 1

cat. 02

NASA W 56978

343 P.

STUDY OF HIGH EFFECTIVE

AREA RATIO NOZZLES FOR

SPACE CRAFT ENGINES

FINAL REPORT

Contract NAS 7-136

Report NAS 7-136-F, Volume 2

June, 1964

OTS PRICE

XEROX

\$ 19.75 ph

MICROFILM

\$ _____



Report NAS 7-136-F

STUDY OF HIGH EFFECTIVE AREA RATIO
NOZZLES FOR SPACECRAFT ENGINES

Final Report

Prepared under
Contract NAS 7-136

for

Western Operations Office
National Aeronautics and Space Administration
Santa Monica, California

FOREWORD

This final report is submitted in fulfillment of Contract No. NAS 7-136, conducted from 18 April 1962 to 18 February 1964. The report consists of two volumes. The first volume contains the technical discussion and results of the study, and the second volume contains the appendices with methods of calculation and detailed results.

The work was conducted at the Aerojet-General Liquid Rocket Operations in Sacramento, by the Research and Advanced Technology Division. The primary contributors to the report were V. H. Ransom, Project Manager of the first phase of the contract, F. X. McKeivitt, Project Engineer during the same period and Manager of the second phase; N. C. DeLeuze, Project Engineer during the second period, and J. D. Hwang, J. D. Tuls, A. A. Trujillo, and T. J. Walsh.

The contract was conducted for the National Aeronautics and Space Administration under the management of Mr. Henry Burlage, Jr., and the technical direction of Mr. Richard Cannova.

APPENDIX A
THERMOCHEMICAL AND CHEMICAL KINETIC
LOSS CALCULATION

FIGURE LISTFIGURE

Specific Impulse of N_2O_4 /Aerozine 50, $MR = 1.6$, $P_c = 25$ psia	1
Specific Impulse of N_2O_4 /Aerozine 50, $MR = 2.0$, $P_c = 25$ psia	2
Specific Impulse of NO /Aerozine 50, $MR = 2.4$, $P_c = 25$ psia	3
Specific Impulse of LO_2/LH_2 , $MR = 5.0$, $P_c = 25$ psia	4
Specific Impulse of LO_2/LH_2 , $MR = 6.0$, $P_c = 25$ psia	5
Specific Impulse of LO_2/LH_2 , $MR = 7.0$, $P_c = 25$ psia	6
Specific Impulse of F_2/H_2 , $MR = 7.0$, $P_c = 50$ psia	7
Specific Impulse of F_2/H_2 , $MR = 10.0$, $P_c = 50$ psia	8
Specific Impulse of F_2/H_2 , $MR = 13.0$, $P_c = 50$ psia	9
Specific Impulse of F_2/H_2 , $MR = 16.0$, $P_c = 50$ psia	10
Specific Impulse of N_2O_4 /Aerozine 50, $MR = 1.600$, $P_c = 100$ psia	11
Specific Impulse of N_2O_4 /Aerozine 50, $MR = 2.0$, $P_c = 100$ psia	12
Specific Impulse of N_2O_4 /Aerozine 50, $MR = 2.4$, $P_c = 100$ psia	13
Specific Impulse of LO_2/LH_2 , $MR = 5.0$, $P_c = 100$ psia	14
Specific Impulse of LO_2/LH_2 , $MR = 6.0$, $P_c = 100$ psia	15
Specific Impulse of LO_2/LH_2 , $MR = 7.0$, $P_c = 100$ psia	16
Specific Impulse of F_2/H_2 , $MR = 7.0$, $P_c = 100$ psia	17
Specific Impulse of F_2/H_2 , $MR = 10.0$, $P_c = 100$ psia	18
Specific Impulse of F_2/H_2 , $MR = 13.0$, $P_c = 100$ psia	19
Specific Impulse of F_2/H_2 , $MR = 16.0$, $P_c = 100$ psia	20
Specific Impulse of N_2O_4 /Aerozine 50, $MR = 1.6$, $P_c = 500$ psia	21
Specific Impulse of N_2O_4 /Aerozine 50, $MR = 2.0$, $P_c = 500$ psia	22
Specific Impulse of N_2O_4 /Aerozine 50, $MR = 2.4$, $P_c = 500$ psia	23
Specific Impulse of LO_2/LH_2 , $MR = 5.0$, $P_c = 500$ psia	24
Specific Impulse of LO_2/LH_2 , $MR = 6.0$, $P_c = 500$ psia	25
Specific Impulse of LO_2/LH_2 , $MR = 7.0$, $P_c = 500$ psia	26
Specific Impulse of F_2/H_2 , $MR = 10.0$, $P_c = 500$ psia	27
Specific Impulse of F_2/H_2 , $MR = 13.0$, $P_c = 500$ psia	28
Specific Impulse of F_2/H_2 , $MR = 16.0$, $P_c = 500$ psia	29
Specific Impulse of N_2O_4 /Alumizine, $P_c = 1000$ psia	30

FIGURE LIST (cont.)

FIGURE

Kinetic Effects for Bell Nozzle, N_2O_4 /Aerozine 50, MR = 1.6	31
Kinetic Effects for Bell Nozzle, N_2O_4 /Aerozine 50, MR = 2.0	32
Kinetic Effects for Bell Nozzle, N_2O_4 /Aerozine 50, MR = 2.4	33
Kinetic Effects for Bell Nozzle, O_2/H_2 , MR = 5.0	34
Kinetic Effects for Bell Nozzle, O_2/H_2 , MR = 6.0	35
Kinetic Effects for Bell Nozzle, O_2/H_2 , MR = 7.0	36
Kinetic Effects for Plug Nozzle, N_2O_4 /Aerozine 50, MR = 1.6	37
Kinetic Effects for Plug Nozzle, N_2O_4 /Aerozine 50, MR = 2.0	38
Kinetic Effects for Plug Nozzle, N_2O_4 /Aerozine 50, MR = 2.4	39
Kinetic Effects for Plug Nozzle, O_2/H_2 , MR = 5.0	40
Kinetic Effects for Plug Nozzle, O_2/H_2 , MR = 6.0	41
Kinetic Effects for Plug Nozzle, O_2/H_2 , MR = 7.0	42
Kinetic Effects for Forced-Deflection Nozzle, N_2O_4 /Aerozine 50, MR = 1.6	43
Kinetic Effects for Forced-Deflection Nozzle, N_2O_4 /Aerozine 50, MR = 2.0	44
Kinetic Effects for Forced-Deflection Nozzle, N_2O_4 /Aerozine 50, MR = 2.4	45
Kinetic Effects for Forced-Deflection Nozzle, LO_2/LH_2 , MR = 5.0	46
Kinetic Effects for Forced-Deflection Nozzle, LO_2/LH_2 , MR = 6.0	47
Kinetic Effects for Forced-Deflection Nozzle, LO_2/LH_2 , MR = 7.0	48
Effects of Assumed Recombination Rate Constant on Predicted Performance Loss	49
Effect of Departure From Chemical Equilibrium on Ideal Performance of a Bell Nozzle, $R_D/R_T = 1.0, 6.0$	50

I. ADIABATIC ONE-DIMENSIONAL FLOW THROUGH A NOZZLE

A discussion of the case of adiabatic quasi-one-dimensional, steady flow of a homogeneous mixture of ideal gases* is included in this appendix. It is assumed that the effects of diffusion, heat conduction, and viscosity are negligible.

The conservation equations are:

$$\rho v A = \dot{m} = \text{constant} \quad (\text{Eq 1})$$

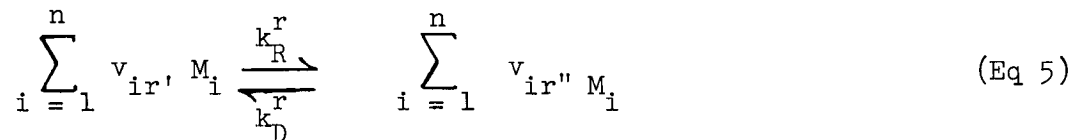
$$H + \frac{v^2}{2} = \text{constant} \quad (\text{Eq 2})$$

$$\frac{v dv}{dx} + \frac{1}{\rho} \frac{dp}{dx} = 0 \quad (\text{Eq 3})$$

and $A = A(x) \quad (\text{Eq 4})$

specifies the nozzle geometry.

Let the total number of chemical species such as M_i in the gas mixture be n , of which the first n_A are atomic species and the remaining $n - n_A$ are molecular species. The r^{th} chemical reaction taking place in the mixture is formally written as,



where $r = 1, 2, N$, and N is the total number of reactions, and k_R and k_D are the reaction rate parameters of the forward and backward chemical changes in the r^{th} reaction.

* Bray, K.N.C., Appleton, J.P., Atomic Recombination in Nozzles: Methods of Analysis for Flows with Complicated Chemistry, Department of Aeronautics and Astronautics, University of Southampton, April 1961

I, Adiabatic One-Dimensional Flow Through a Nozzle (cont.)

The total possible number of elementary, independent reactions is equal to the number of molecular species, $n - n_A$. At least this number of reactions must be postulated in order that the problem may be completely formulated. In fact, N will be greater than $n - n_A$ if a given chemical process, brought about by more than one different catalyst is treated as several different reactions; the number of reactions being equal to the number of catalysts. This may be necessary when the reaction rate is greatly affected by the nature of the catalyst. The above general statements are not intended to imply that all of the N reactions will be of equal importance in a given flow system.

The equations of state are:

$$P = \sum_{i=1}^n P_i = \frac{\rho TR}{W_t} \sum_{i=1}^n i \quad (\text{Eq. 6})$$

$$H = \sum_{i=1}^n \gamma_i \left\{ \int_{T^0}^T C_{pi} dT + \Delta H_{fi} \right\} W_i \quad (\text{Eq. 7})$$

There are $n - n_A$ differential continuity equations corresponding to the reactions (5), which will be written for the molecular species. The i_{th} of these equations is

$$\rho \frac{D\gamma_i}{Dt} = \sum W_T (v_{ir''} - v_{ir'}) \left\{ k_D^r \prod_{j=1}^n \left(\frac{\gamma_j}{W_T} \right)^{v_{jr''}} \right\} \quad (\text{Eq. 8})$$

where in the steady case $\frac{D}{Dt} \equiv v \frac{d}{dx}$. There are also n_A algebraic continuity equations for the atomic species,

$$\gamma_i \frac{W_i}{W_t} + \sum_{q=n_A+1}^n \left\{ S_{iq} \frac{W_i}{W_t} \right\} \gamma'_q = \Gamma_i \quad (\text{Eq. 9})$$

I, Adiabatic One-Dimensional Flow Through a Nozzle (cont.)

where Γ_i is the total mass fraction of the i_{th} atomic species in the gas mixture in both atomic and molecular forms, the S_{iq} is the number of atoms of the i_{th} species in the q_{th} molecular species.

If the chemical kinetic data suggests that the r^{th} reaction proceeds sufficiently fast to remain in chemical equilibrium, then the mass fractions of the species taking part in the reaction are related by the law of mass action; i.e.,

$$\frac{k_R^r}{k_D^r} = K_c^r = \prod_{i=1}^n \left(\frac{\rho Y_i}{W_T} \right)^{v_{ir}'' - v_{ir}'} \quad (\text{Eq 10})$$

Equation 10 then replaces one of the set of differential equations (Equation 8). If all the N reactions remain in equilibrium, then clearly, N laws of mass action may be written. However, it will be found that only $n - n_A$ of these are independent and they will replace the $n - n_A$ differential equations Equation 8.

If the chemical composition in the flow is fixed (frozen flow) then the laws of mass action are replaced by a set of equations

$$Y_i = C_i \quad (\text{Eq 11})$$

where C_i is a constant.

The general non-equilibrium nozzle flow problem is specified by the $n + 6$ equations (1) through (4) and (6) through (9) above, of which $n - n_A + 1$ are differential equations. The independent variable is x and the $w + 6$ dependent variables are: P, ρ, T, H, V, A and Y_i ($i = 1, 2, \dots, n$). It is assumed that the area distribution $A(x)$ is specified.

II. SUDDEN FREEZING

Bray performed exact calculations* for air flowing through a nozzle with a single reaction and found that, for a nozzle of large area ratio, three flow regions may be distinguished. These are:

1. A region of near equilibrium flow in which deviation from the infinite rate solution is small.
2. A transition region.
3. A region of nearly frozen flow in which the reaction has almost ceased.

If the area ratio is very large, a good approximation to the conditions at the exit of the nozzle may be obtained by reducing the transition region to a point, which is called the sudden freezing point. Upstream of this point, the flow is assumed to remain in complete equilibrium, so that the infinite rate solution applies. Downstream of the sudden freezing point, the reaction ceases and the composition of the gas remains frozen. This approximation cannot give the exact values of all the flow properties a long way downstream however well the sudden freezing point is chosen, because it does not take account of the entropy rise which actually occurs due to the nonequilibrium phase of the reaction. However, the errors may be very small.

The $n-n_A$ equations (Equation 8) are first written in the form

$$\frac{d Y_i}{d x} = \sum_{r=1} a_{ir} X^r \quad (\text{Eq 12})$$

where X^r , which represents the curly bracket in Equation 8, is given by

$$X^r = R_R^r - R_D^r \quad (\text{Eq 13})$$

*Bray, K.N.C., "Atomic Recombination in a Hypersonic Wind-Tunnel Nozzle," Journal Fluid Mechanics, Vol 6 (1959)

II, Sudden Freezing (cont.)

and

$$R_R^r = K_R^r \prod_{j=1}^h \left(\frac{\rho \gamma_j}{w_T} \right)^{v_{jr'}} \quad (\text{Eq 14})$$

$$R_D^r = K_D^r \prod_{j=1}^h \left(\frac{\rho \gamma_j}{w_T} \right)^{v_{jr''}} \quad (\text{Eq 15})$$

If the r_{th} reaction proceeds at an infinite rate and so remains in complete equilibrium, both R_R^r and R_D^r are infinite. The difference between these two infinite terms, which is proportional to the net rate of change of γ_i due to the r_{th} reaction, must then be determined from Equation 10 rather than from Equation 8. This argument suggests that, if the v_{th} reaction proceeds at a finite rate which is sufficiently fast to remain close to equilibrium, then

$$R_R^r \simeq R_D^r \quad (\text{Eq 16})$$

so that

$$\left| R_R^r \right| \gg \left| X^r \right| \quad (\text{Eq 17})$$

If equation 16 is nearly satisfied, then so is the law of mass action, Equation 10; thus, the quantities R_R^r and X^r in the criterion (16) may be evaluated on the basis that the r_{th} reaction remains in complete equilibrium. Evaluation of X^r under these conditions requires care. Calculated as the difference between R_R^r and R_D^r , where k_R^r and k_D^r are infinite according to the above equilibrium approximation, it is indeterminate. However, X^r is in fact finite, even for the infinite rate solution.

II, Sudden Freezing (cont.)

If the total number of reactions considered, N , is equal to the number of molecular species present $n - n_A$, then x^r can always be found from the system of equations (12) if the dY_i/dx values are suitably calculated (see below). On the other hand, if $N > (n - n_A)$, x^r cannot be determined in this way because there are more x^r values than there are equations (12). The physical explanation of the apparent anomaly is that, when the reactions are all close to equilibrium, the chemical problem is over-specified if $N > (n - n_A)$ because only $n - n_A$ laws of mass action are required to determine the composition. It is not then possible to determine the contributions of the individual reactions to dY_i/dx . Because of this difficulty, we shall assume in this section that $N = (n - n_A)$. The criterion (17) for the r^{th} reaction to be near equilibrium may be rewritten in the form

$$B^r \equiv \left| \frac{R_R^r}{X^r} \right|_e \gg 1 \quad (\text{Eq 18})$$

where the suffix e indicates that the functions are evaluated with the r_{th} reaction in equilibrium.

A criterion similar to (18) may be used to define a region in which the r^{th} reaction is nearly frozen, namely,

$$B^r \ll 1 \quad (\text{Eq 19})$$

However, this condition is not accurate to the same degree as (18), because the evaluation of B^r assuming that the r^{th} reaction is in equilibrium must lead to errors when this reaction is, in fact, nearly frozen.

The two conditions expressed by Equation 18 and 19, suggest a criterion, which may be used to define the sudden-freezing point. Since the sudden-freezing

II, Sudden Freezing (cont.)

point of a particular reaction lies between the near-equilibrium and near-frozen limits defined by Equation 18 and 19 respectively, we write

$$B^r = Q^r \quad (\text{Eq 20})$$

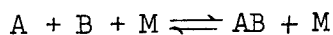
at the sudden-freezing point. The constants Q^r are expected to be of order unity. Clearly, equation (20) is purely empirical.

III. CALCULATION OF THERMOCHEMICAL AND CHEMICAL KINETIC DATA

Using a program in existence at Aerojet-General, the equilibrium one-dimensional performance and properties of the propellants O_2/H_2 , F_2/H_2 , N_2O_4 /Aerzine 50 and N_2O_4 /Alumizine were calculated for a range of mixture ratios and chamber pressures.* So that the effect of freezing on performance could be ascertained, performance calculations were also made for flows frozen at the nozzle entrance and at area ratios of 1, 2, and 5 for N_2O_4 /Aerzine 50 and LO_2/LH_2 . The results of all of the above calculation are given in Figures A-1 through A-30. The characteristic velocities are given in these figures, so that the thrust coefficient and thrust may be readily calculated.

In the application of the freezing point criterion, from the set of reactions which actually determine the chemical composition in the nozzle, one was chosen as dominant on the basis of its high concentration, and high heat of reaction. In addition to this reaction, as many of the other reactions as are required to adequately describe the gas composition in the nozzle are considered. The assumption is made that once the dominant reaction freezes, the entire flow is frozen from that point in the nozzle to the exit.

The diatomic recombination reaction takes place as follows:



where A and B are atomic species and M is an inert third body. In this program, the rate of recombination is determined from

$$R_R^F = k_F \frac{P}{W_T} \prod_{i=1}^J \left(\frac{P Y_i}{W_T} \right)^{v_i F} \quad (\text{Eq 21})$$

*For a description of the program see Grisman, P., Goldwasser, S., Petrozzi, P., Proceeding of the Propellant Thermodynamics and Handling Conference, Engineering Experiment Station Special Report No. 12, Ohio State University, June 1960.

III, Calculation of Thermochemical and Chemical Kinetic Data (cont.)

where the quantity $\frac{\rho}{w_T}$ outside the product represents the concentration of the inert third body, viz., $Y_M = 1$, and every atom and molecule present is considered equally effective as a third body. Therefore, only the concentrations of the recombining species, A and B, are required as input to calculate R_f .

The program can handle a reaction rate constant of the form

$$k_R^f = a T^b \exp(c/T)$$

where a, b, and c are constants for the reaction being considered. The required equilibrium rate of composition change along the nozzle is obtained by combining the composition data from the equilibrium solution and nozzle geometry data as follows:

$$\frac{dY_i}{dX} = \left(\frac{dY_i}{d\epsilon} \right) \left(\frac{d\epsilon}{dx} \right) \quad (\text{Eq 22})$$

Composition freezing is assumed to occur when B, below, is unity.

$$B = \left| \frac{R^f}{X^f} \right| \quad (\text{Eq 23})$$

The value of X is determined by solving a set of J simultaneous equations of the form:

$$\frac{dY_i}{dX} = \sum_{R=1}^J a_{iR} X^r, \quad i = 1, \dots, J \quad (\text{Eq 24})$$

III, Calculation of Thermochemical and Chemical Kinetic Data (cont.)

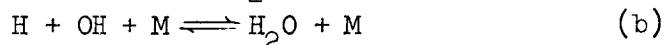
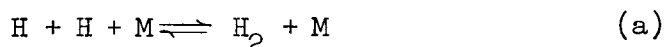
where the coefficients are determined as follows:

$$a_{ir} = \frac{T}{\rho v} (v_{ir''} - v_{ir'}) \quad (\text{Eq 25})$$

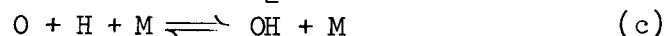
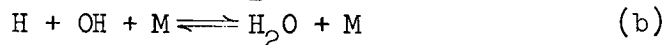
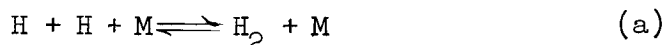
Note that in order to solve this set of equations, the number of reactions must equal the number of chemical species considered.

The calculation of dC/dx is based on simple one-dimensional expansion for the conventional contoured and conical nozzles. In the unconventional plug and forced-deflection nozzles, the gas flow at any axial location is not uniformly expanded. The approach for these cases was to calculate an average stream tube that would divide the flow field in half, i.e., 50% of the mass flow would lie on either side of this 50% stream tube. The gas flowing along this stream tube would then have an average value of fully expanded flow, and the new "equivalent" axial distance would be the distance along the 50% stream tube. The value of dA/dx for the 50% stream tube was then calculated and used in computing the kinetic losses for the plug and forced-deflection nozzles.

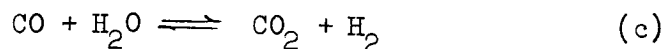
The two propellants considered were LO_2/LH_2 and $\text{N}_2\text{O}_4/\text{Aerzine 50}$. The set of reactions chosen to describe the recombination of LO_2/LH_2 is



with species, H, OH and H_2O being used to solve for X_F . For the recombination of $\text{N}_2\text{O}_4/\text{Aerzine 50}$, the set chosen was

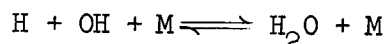


III, Calculation of Thermochemical and Chemical Kinetic Data (cont.)



Species used here to solve for X_f are H, OH, O, CO, NO, and H_2 .

The heat evolved by reaction (b) is, in each set, the greatest. Also, the concentrations of H and OH in the chamber as shown by the equilibrium calculations are, compared with other unrecombined species, high. Therefore, for both propellants



was taken as the reaction determining the freezing point*

$$k^f = 1.6 (10)^{17} \text{ cm}^6/\text{mole}^2 - \text{sec.}$$

Once the freezing area ratio in a nozzle is found, a specific impulse, taking into account departure from chemical equilibrium, is determined from curves such as those given in Figures 1 through 24.

The results of the freezing point calculations which were made only for $\text{N}_2\text{O}_4/\text{Aerazine 50}$ and LO_2/LH_2 are shown in Figures 31 through 48, where C_{EK} defined as

$$C_{EK} = 1 - \frac{\text{Is chemical non-equilibrium,}}{\text{Is equilibrium}} \quad (\text{Eq 26})$$

*The flow rate constant, k^f , of this reaction is from Baier, R. W., Byron, J. R., Armour, W. H., "Application of the Bray Criterion for Predicting Atomic Recombination Effects in Propulsion Systems," Aeronautics, 14 February 1962.

III, Calculation of Thermochemical and Chemical Kinetic Data (cont.)

is plotted against nozzle exit area ratio for constant ideal thrust. These data are for bell (vacuum Rao) nozzles with $0.2R_t$ downstream throat blend radius, plug nozzles, and forced-deflection nozzles having a base area ratio of 25. For the other nozzles considered in this report, estimates of C_{EK} were made based upon the results for the above nozzles. C_{EK} for the swirling flow nozzle was assumed to be the same as that for the bell nozzle having the same area ratio as the effective area ratio of the swirling flow nozzle. The annular nozzle losses were assumed to be the same as those for the forced-deflection nozzle. The losses for the aerodynamic and conical nozzles were taken to be the same as those for the bell nozzle.

Since the value of rate constants, k^f , at high temperatures are not known very accurately, the effect of changes in the value of k^f on the values of C_{EK} was studied for the propellant N_2O_4 /Aerozine-50; P_c , 100 psia; MR 2.0:1; and a bell nozzle exit area ratio of 60:1. The results are given in Figure 49. Increasing the presently used value by a factor of ten would approximately halve C_{EK} , and decreasing it by a factor of ten would approximately double C_{EK} .

The nozzle contours used in the computation of C_{EK} were the optimum ones based upon the expansion of a gas having a constant C_p/C_v of 1.2, for the nozzle exit area ratio being considered. Figures 31 through 48 show that, as might be expected, C_{EK} is considerably affected by thrust, i.e., throat radius, C_{EK} decreasing with increased thrust. Inasmuch as the curves of Figures 1 through 29 diverge with increasing area ratio, C_{EK} must increase with increasing area ratio since the changes in the optimum nozzle contour that are the result of increasing the nozzle exit area ratio change the freezing area ratio only slightly, for the same throat radius. The fact that the ideal specific impulse increases with increasing exit area ratio, thus making the throat radius smaller for a given ideal thrust, also tends to increase C_{EK} with exit area ratio.

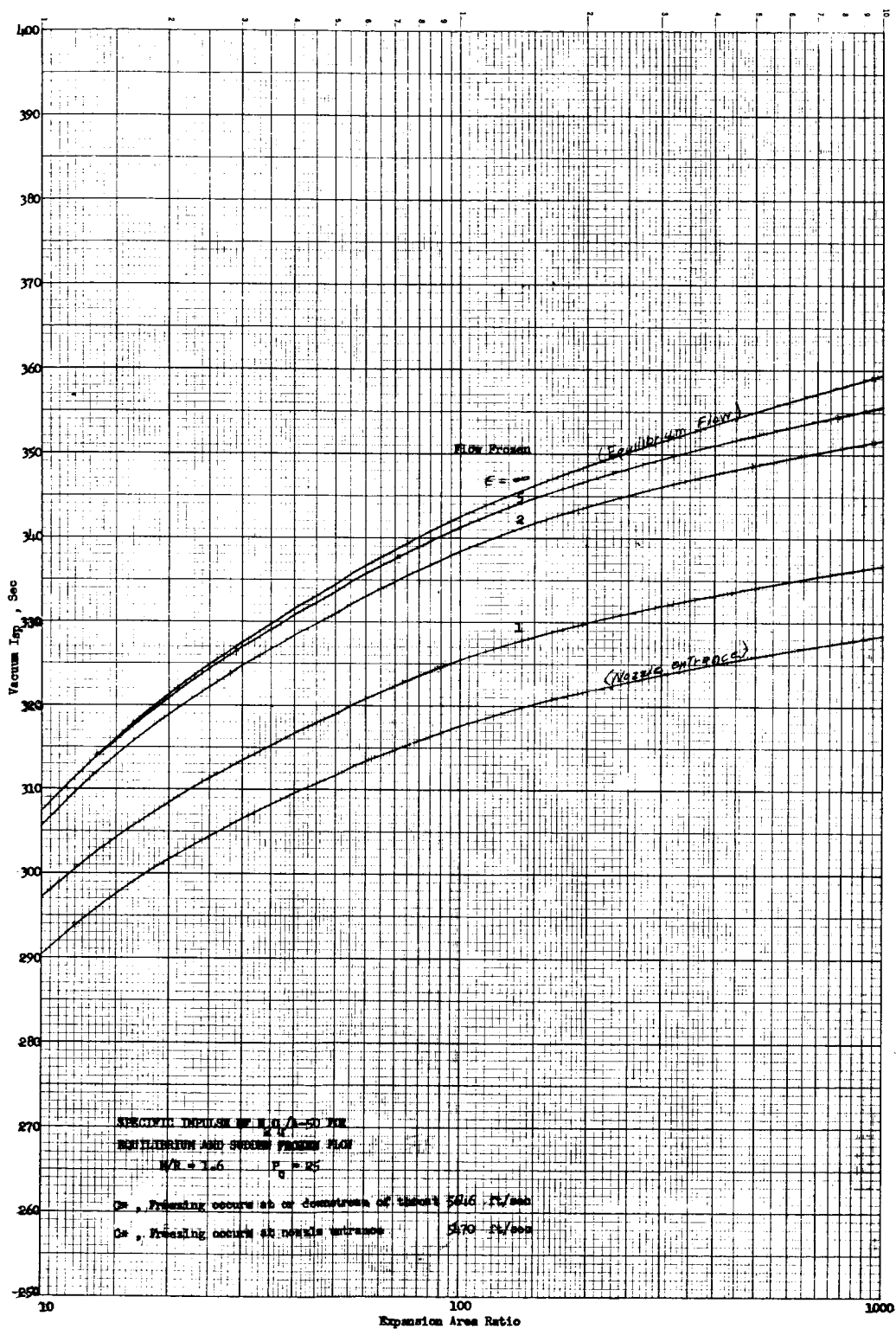
III, Calculation of Thermochemical and Chemical Kinetic Data

The losses are somewhat greater for the forced-deflection and plug nozzles than for the bell nozzles. The losses are also seen to increase with increasing mixture ratio and decreasing chamber pressure for both propellants.

To see what effect changing the contour might have on C_{ϵ_K} , it was computed for nozzles having 1.0 R_T and 6.0 R_T downstream blend radii. The results are plotted in Figure 50. Increasing the downstream radius does decrease C_{ϵ_K} . However, to achieve the same exit area ratio, in these cases, requires a longer nozzle. This effect is discussed in Section III-C.

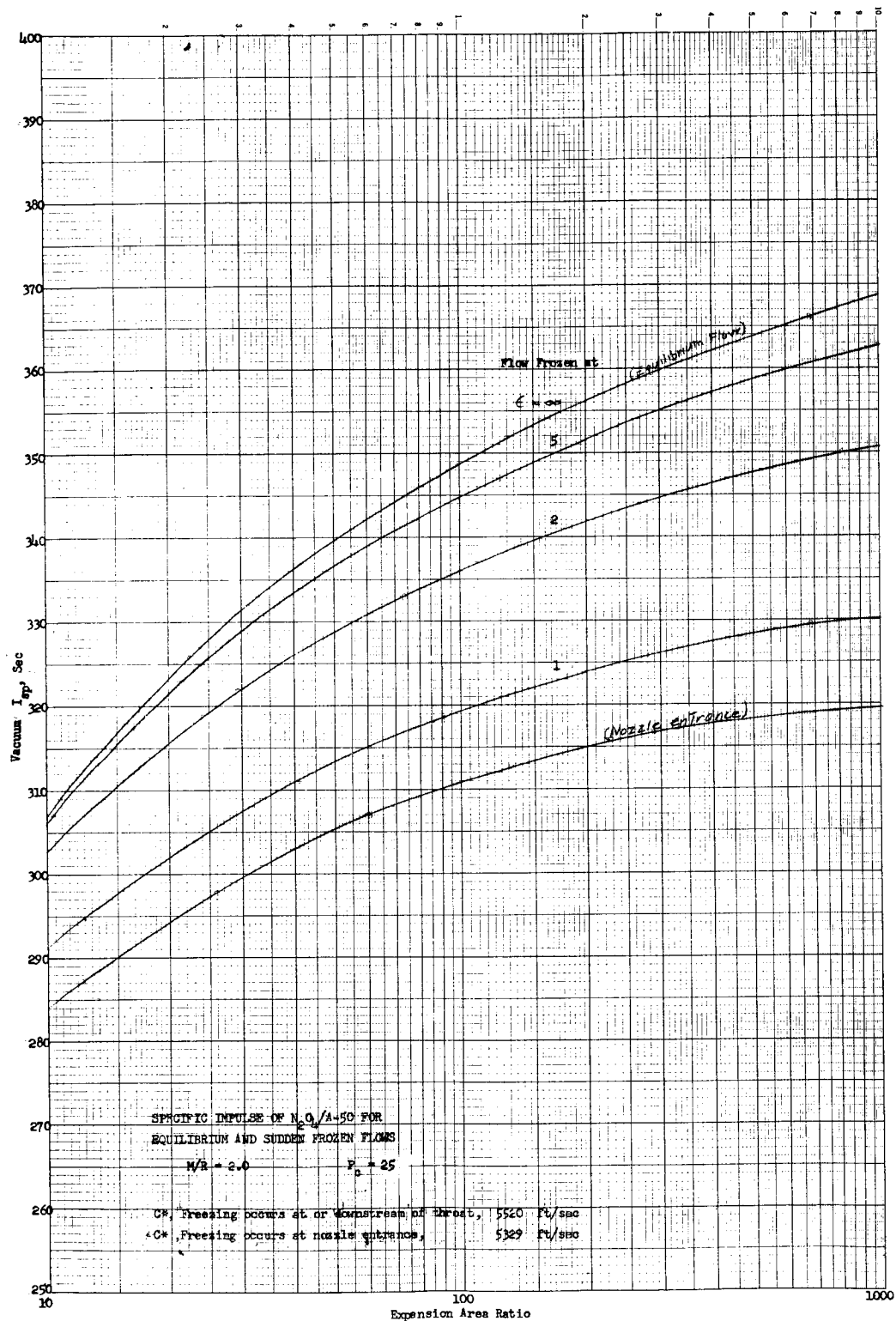
LIST OF SYMBOLS

A	Nozzle cross-sectional area
B^r	Defined by Equation 18
C_{pi}	Specific heat at constant pressure of the i th species
H	Specific enthalpy
ΔH_f	Heat of formation
K_C^r	Equilibrium constant, r th reaction
M_i	Chemical formula, i th species
N	Number of chemical reaction
Q^r	Defined by Equation 20
R	Universal gas constant
R_R^r, R_D^r	Defined by Equation 14 and 15 respectively
T	Temperature
$v_{ir'}$	Stoichiometric coefficient, i th reactant in the r th chemical reaction
$v_{ir''}$	Stoichiometric coefficient, i th product in the r th chemical reaction
v	Velocity
w_i	Molecular weight, i th species
W_T	Total molecular weight of gas mixture
k_R^r, k_D^r	Recombination rate constants
P_c	Chamber pressure
F	Ideal thrust
S_{iq}	Number of atoms of the i th species in the q th molecular species
x	Distance along nozzle axis



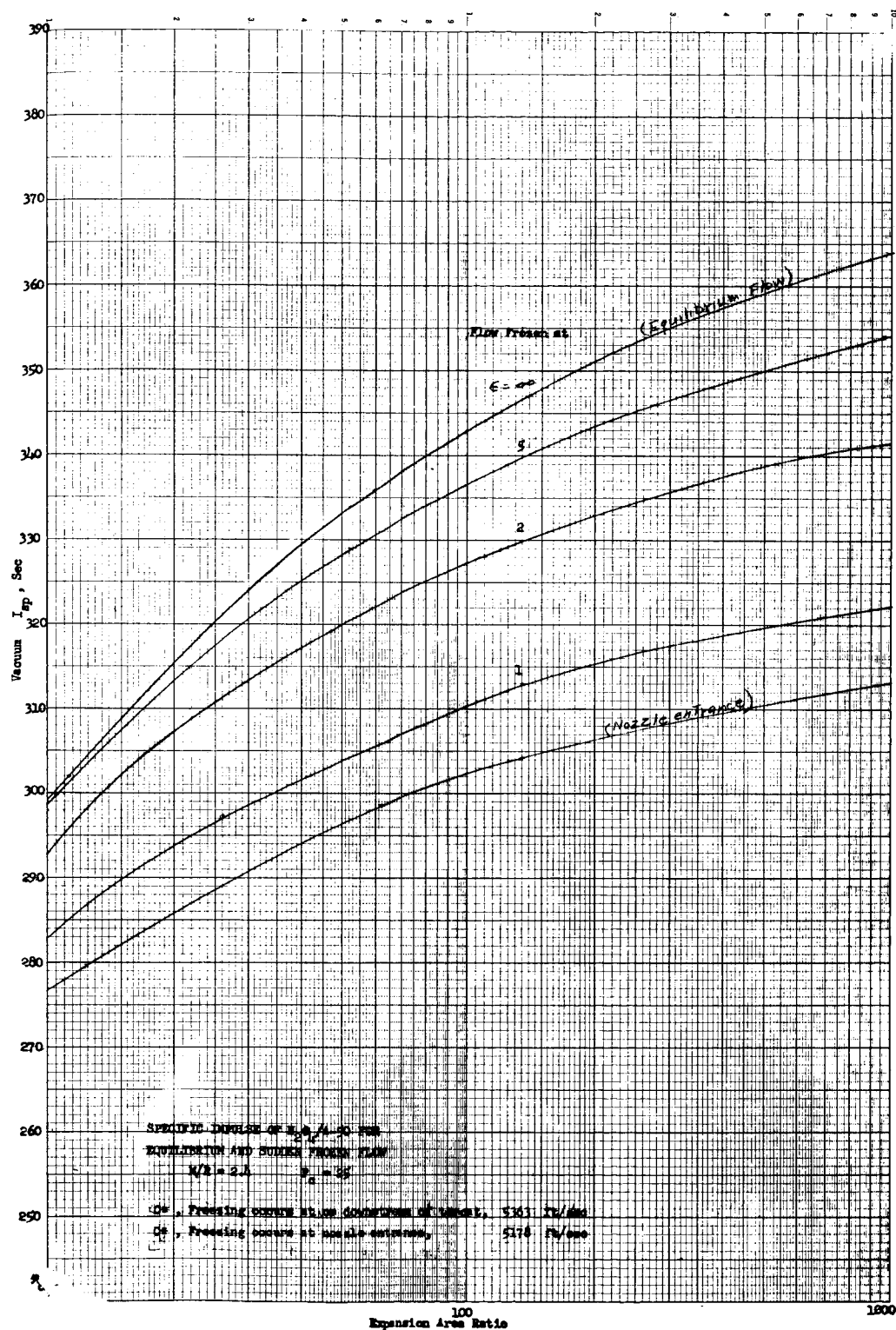
Specific Impulse of N_2O_4 /Aerozone 50, MR = 1.6, $P_c = 25$ psi

Figure 1



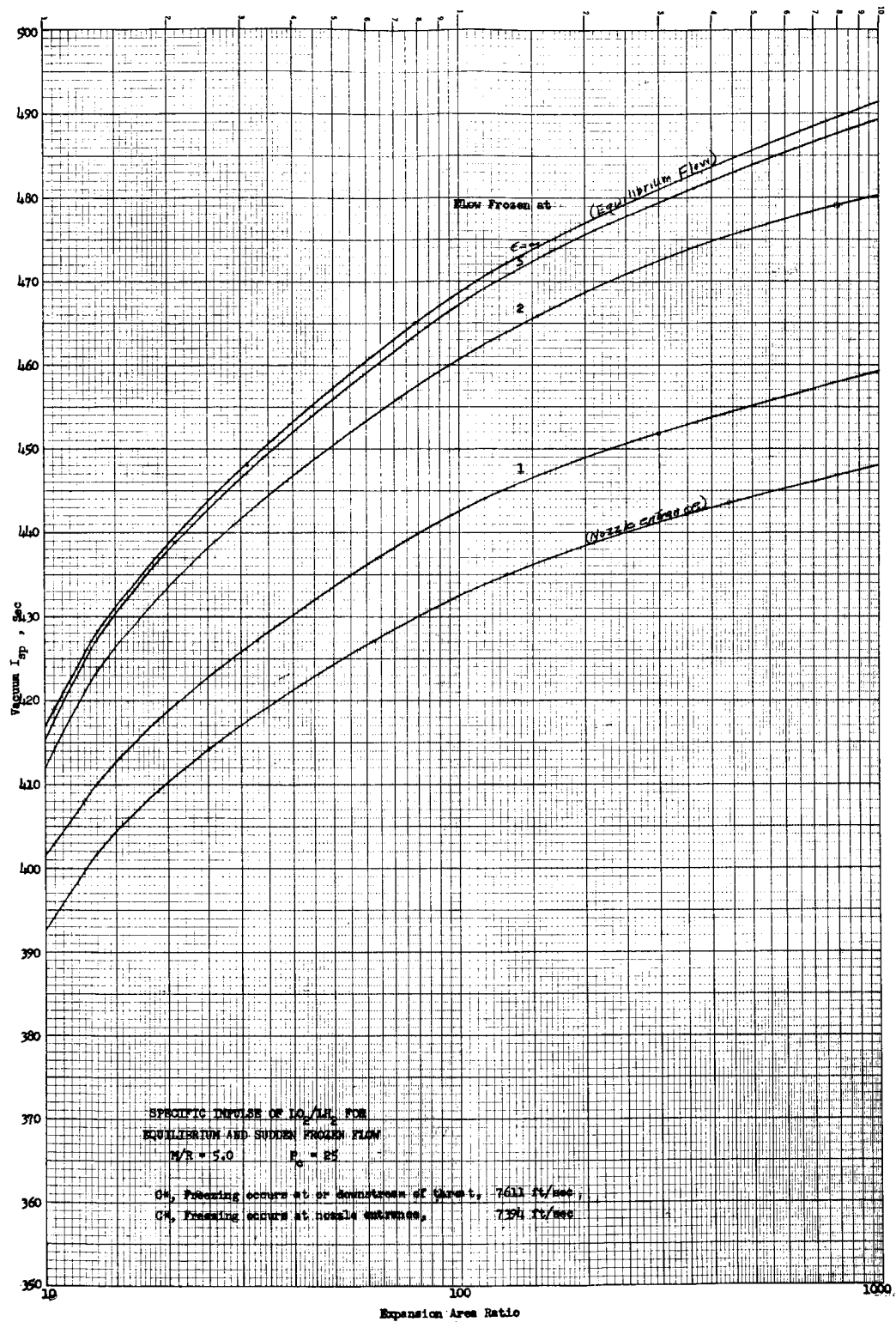
Specific Impulse of N_2O_4 /Aerozine 50, MR = 2.0, $P_c = 25$ psi

Figure 2



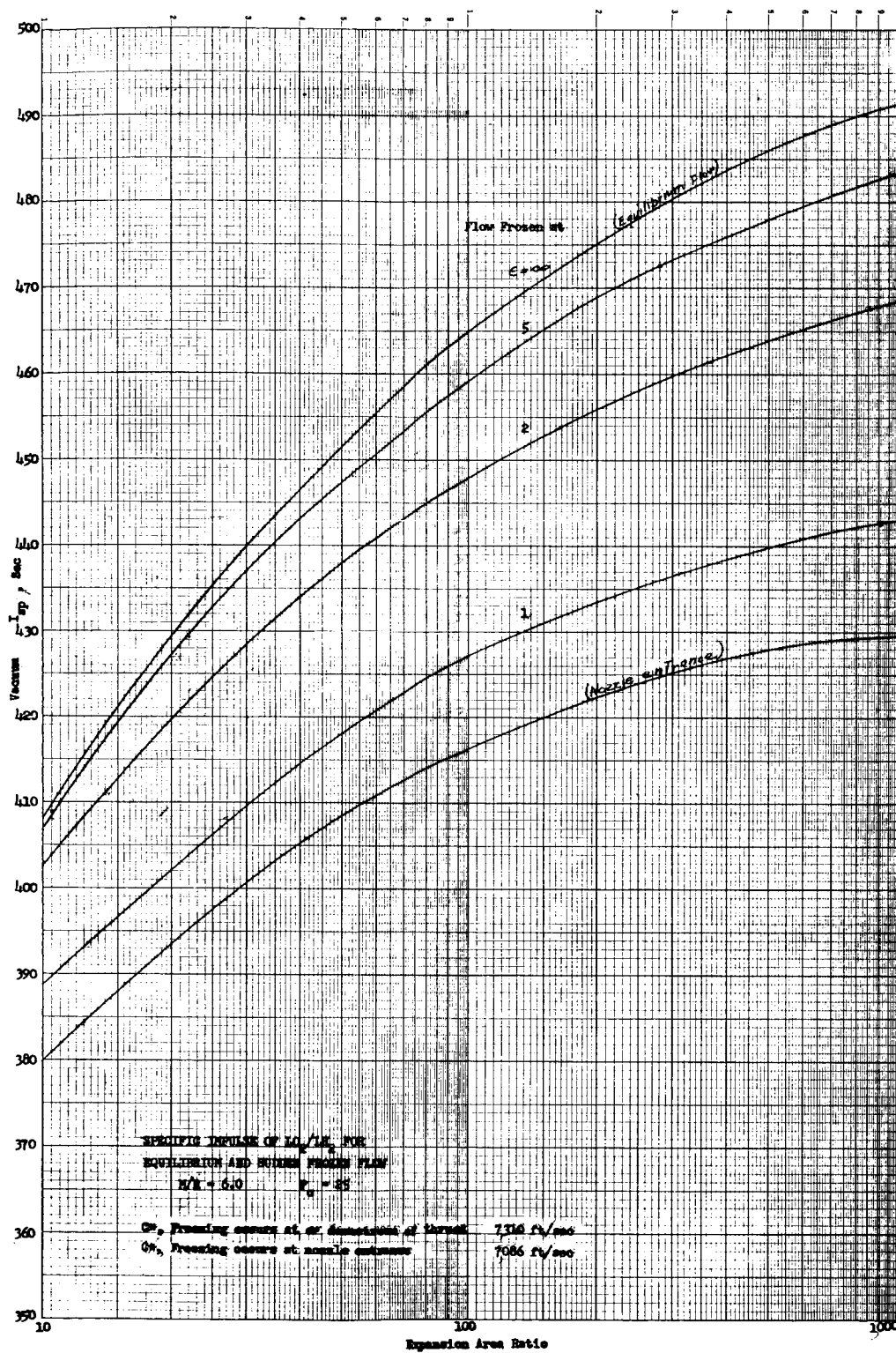
Specific Impulse of N_2O_4 /Aerozine 50, $MR = 2.4$, $P_c = 25$ psi

Figure 3



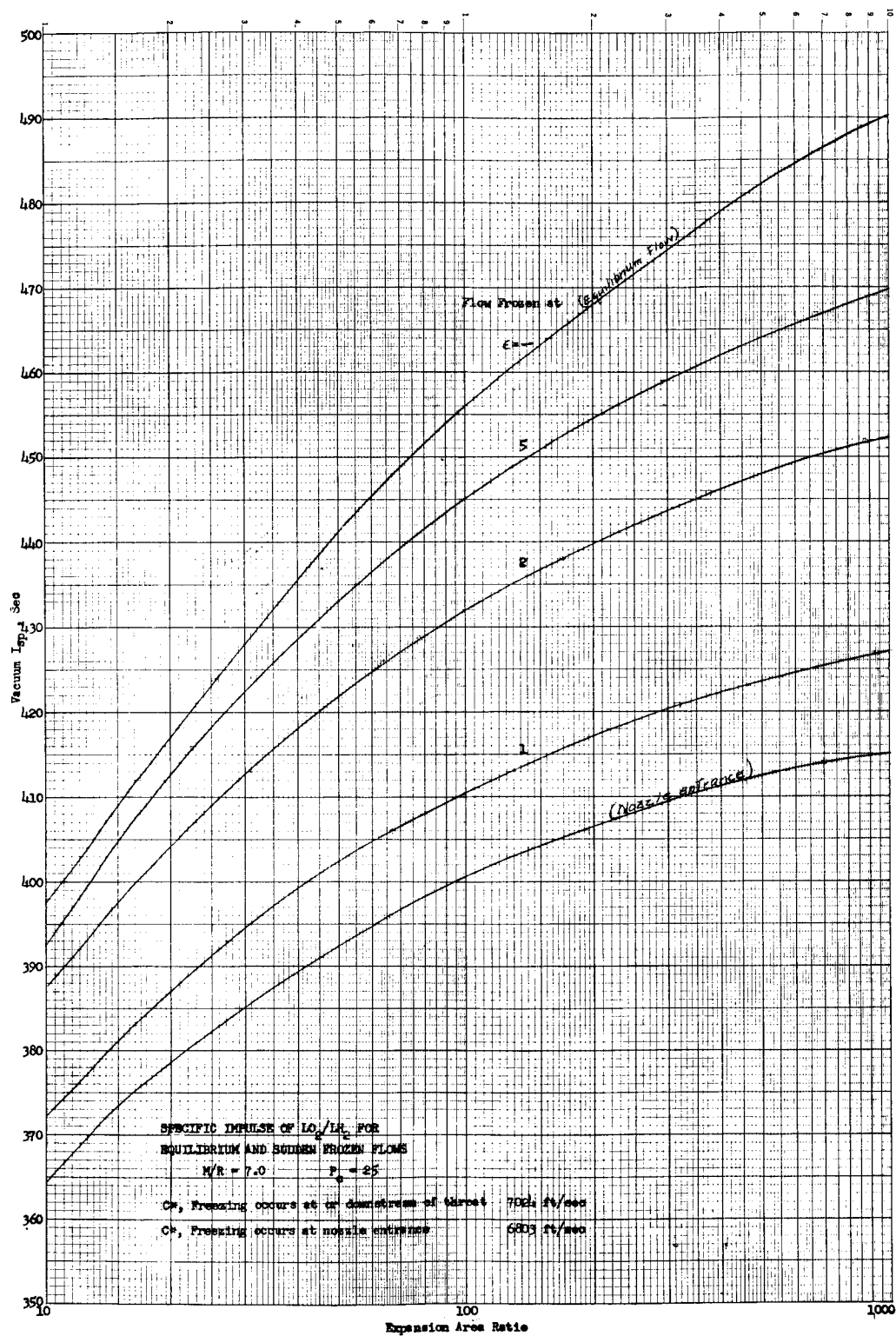
Specific Impulse of LO_2/LH_2 , $MR = 5.0$, $P_c = 25$ psi

Figure 4



Specific Impulse of LO_2/LH_2 , $MR = 6.0$, $P_c = 25$ psi

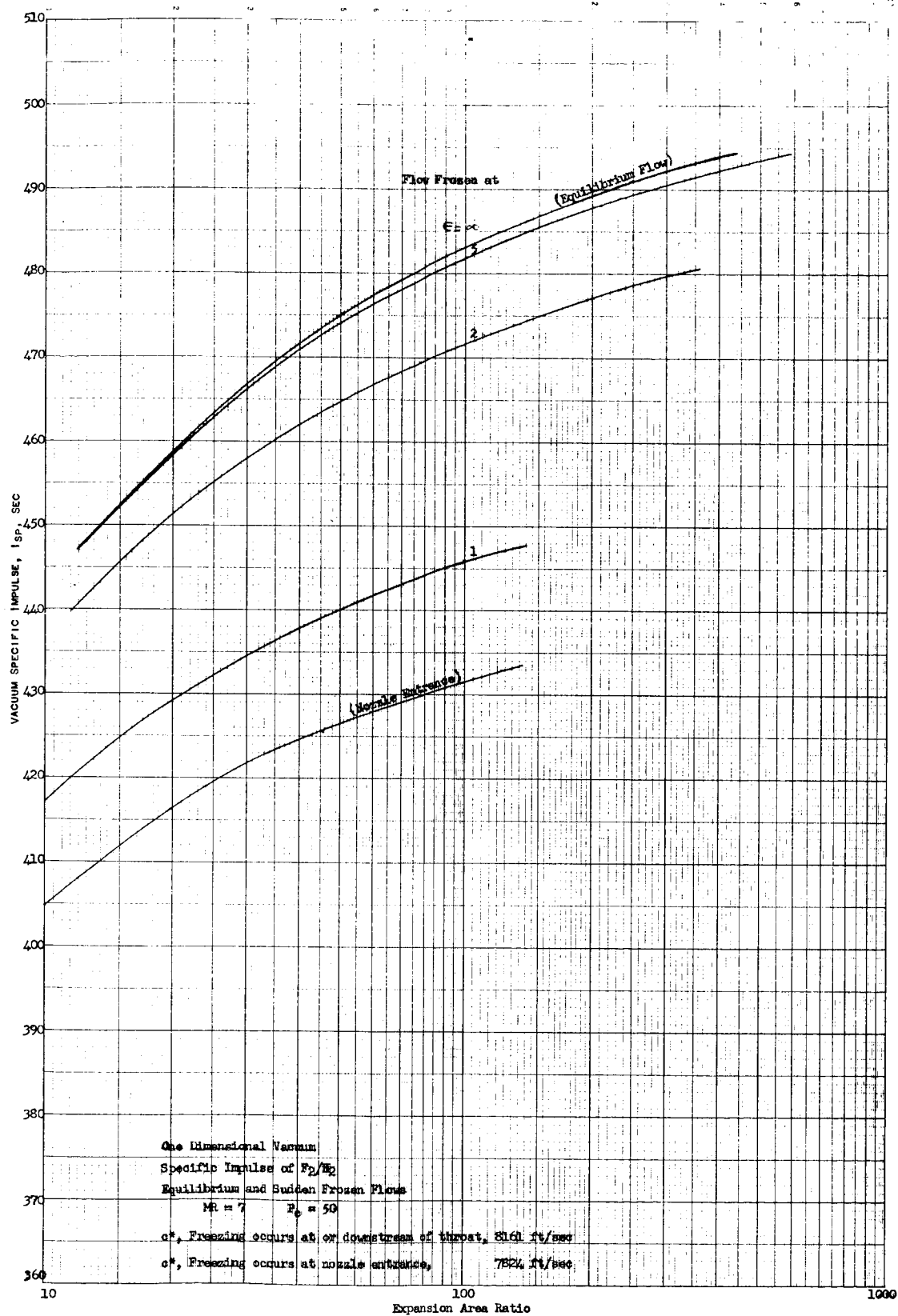
Figure 5



Specific Impulse of LO_2/LH_2 , $MR = 7.0$, $P_c = 25$ psi

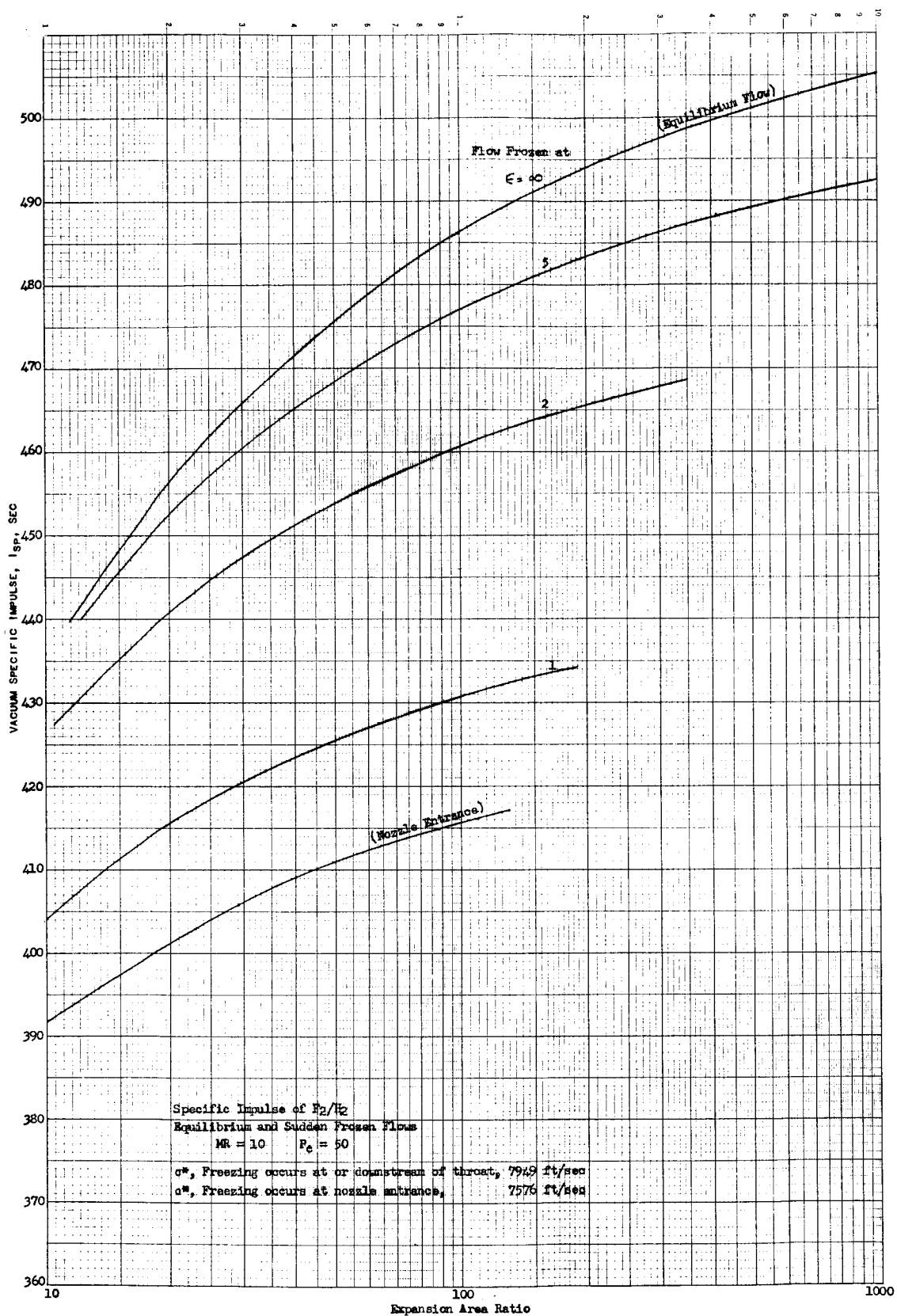
Figure 6

Report NAS 7-136-F, Appendix A



Specific Impulse of F_2/H_2 , $MR = 7.0$, $P_c = 50$ psia

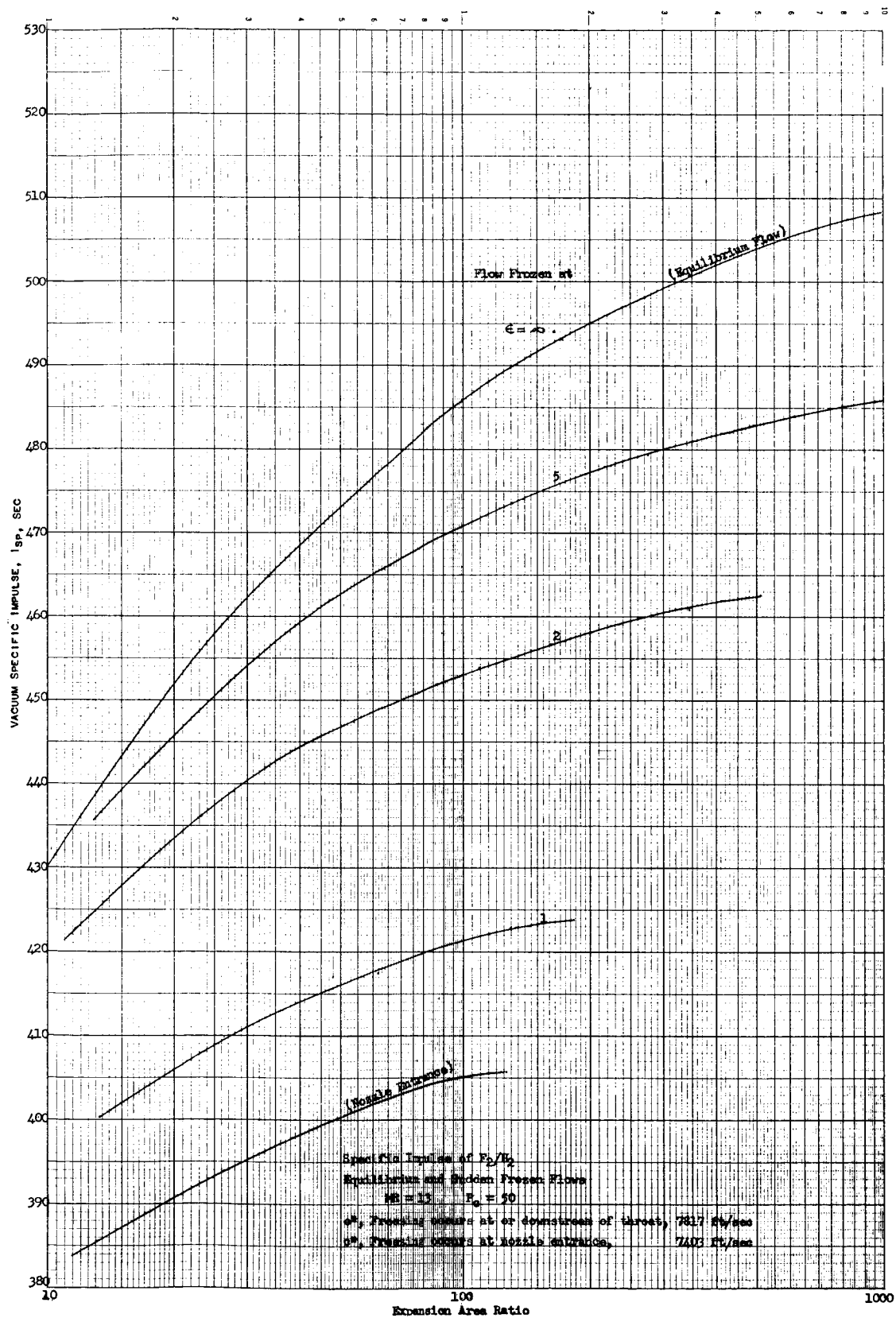
Figure 7



Specific Impulse of F_2/H_2 , $MR = 10.0$, $P_c = 50$ psia

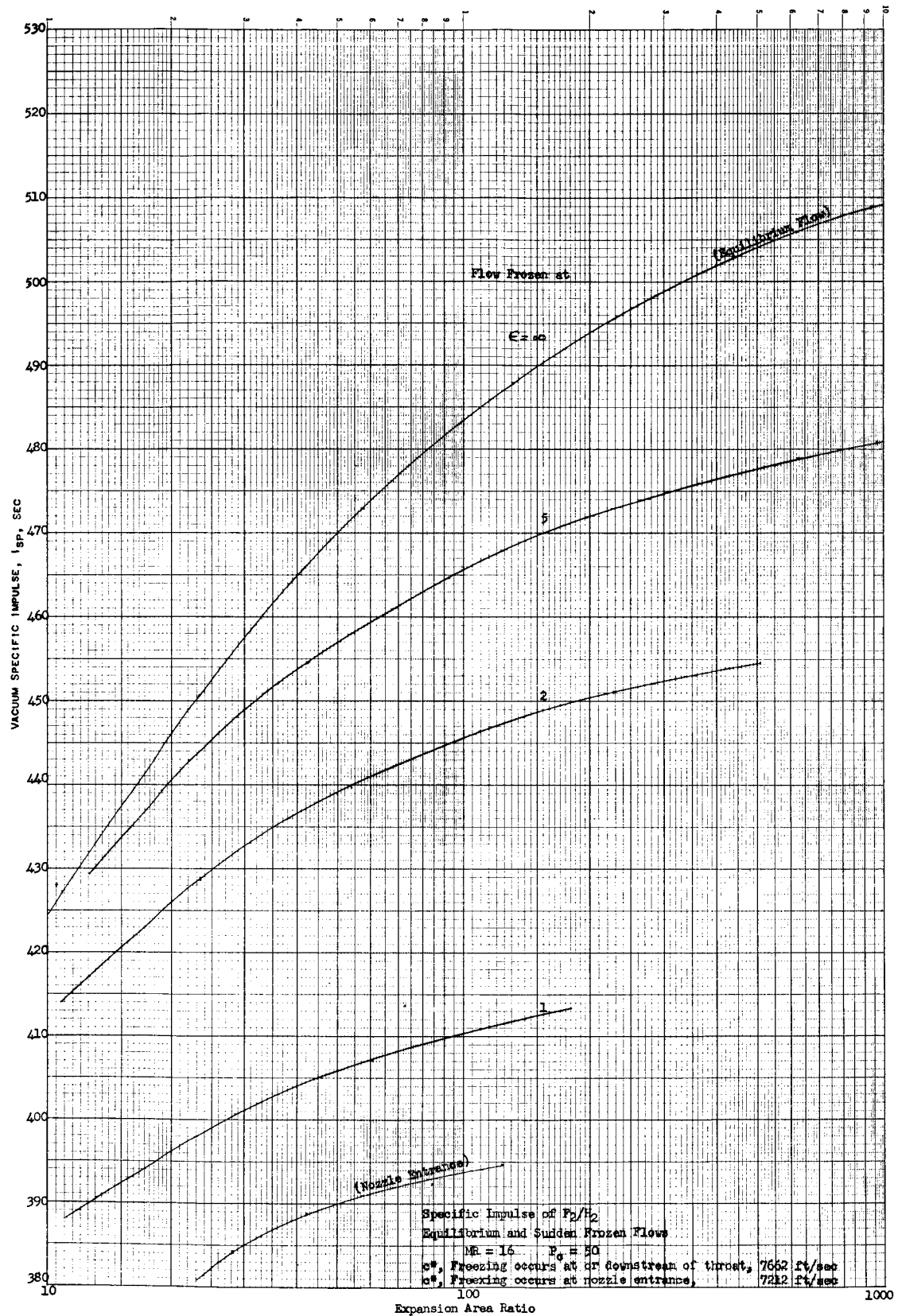
Figure 8

Report NAS 7-136-E, Appendix A



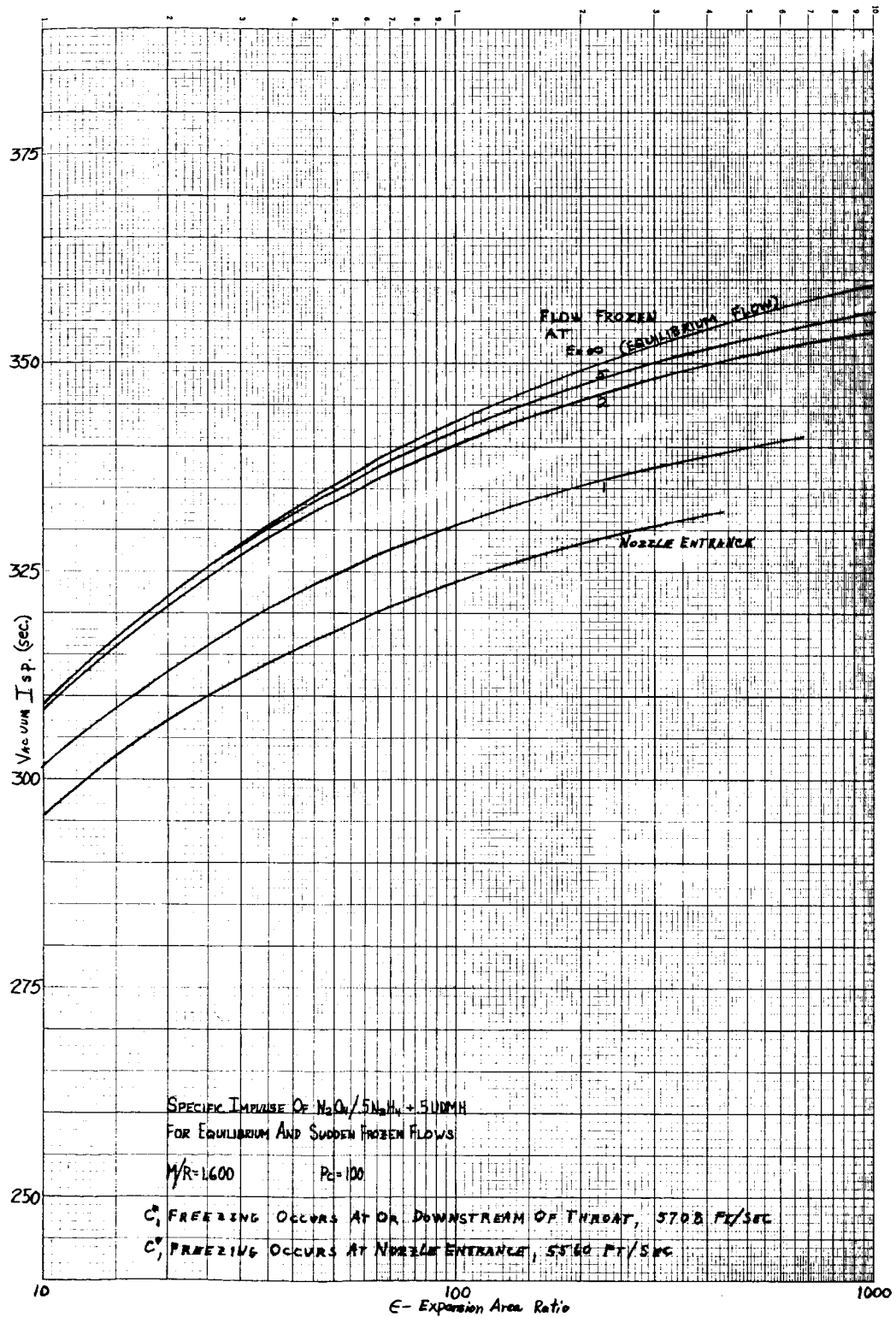
Specific Impulse of F_2/H_2 , $MR = 13.0$, $P_c = 50$ psia

Figure 9



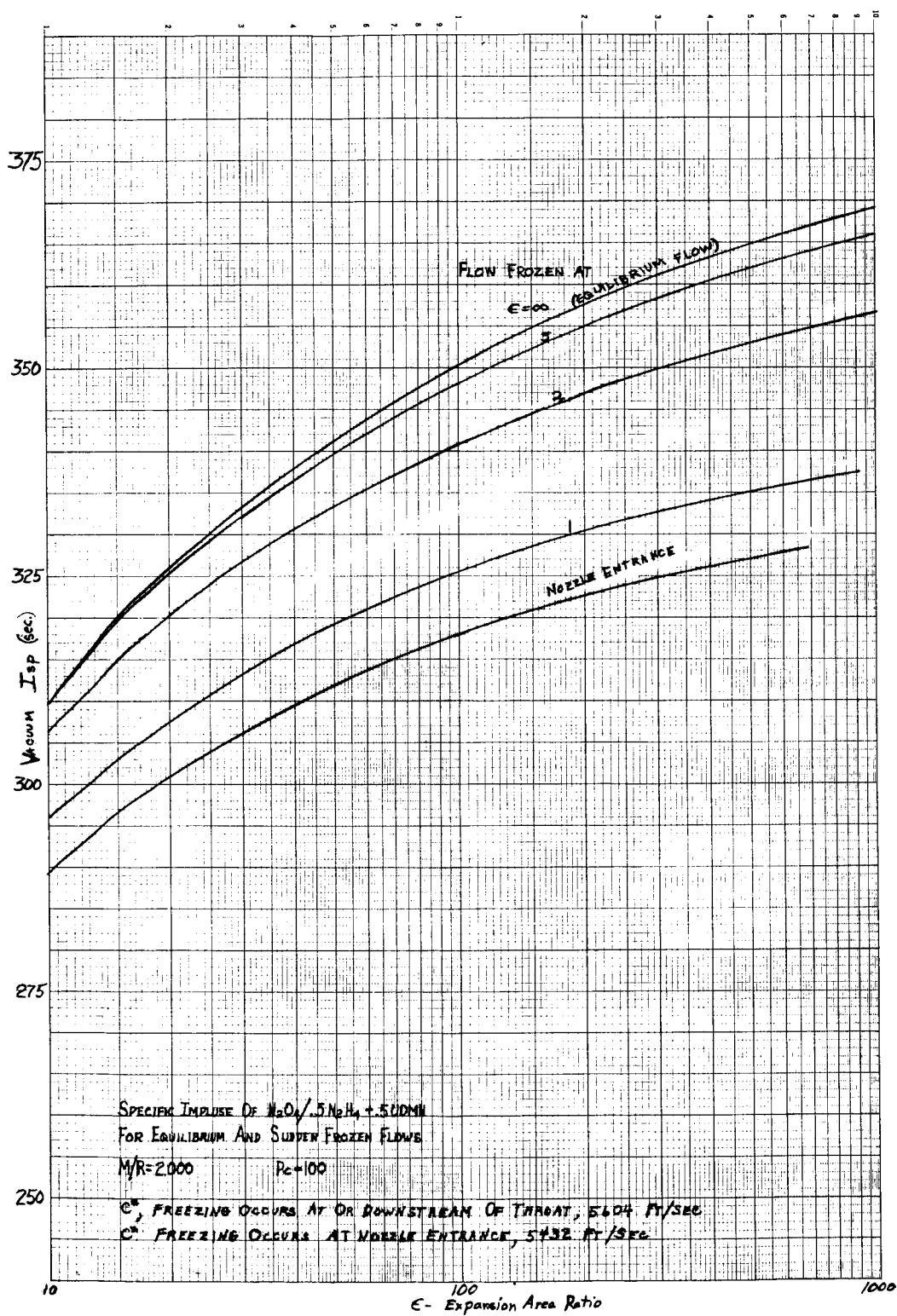
Specific Impulse of F_2/H_2 , MR = 16.0, $P_c = 50$ psia

Figure 10



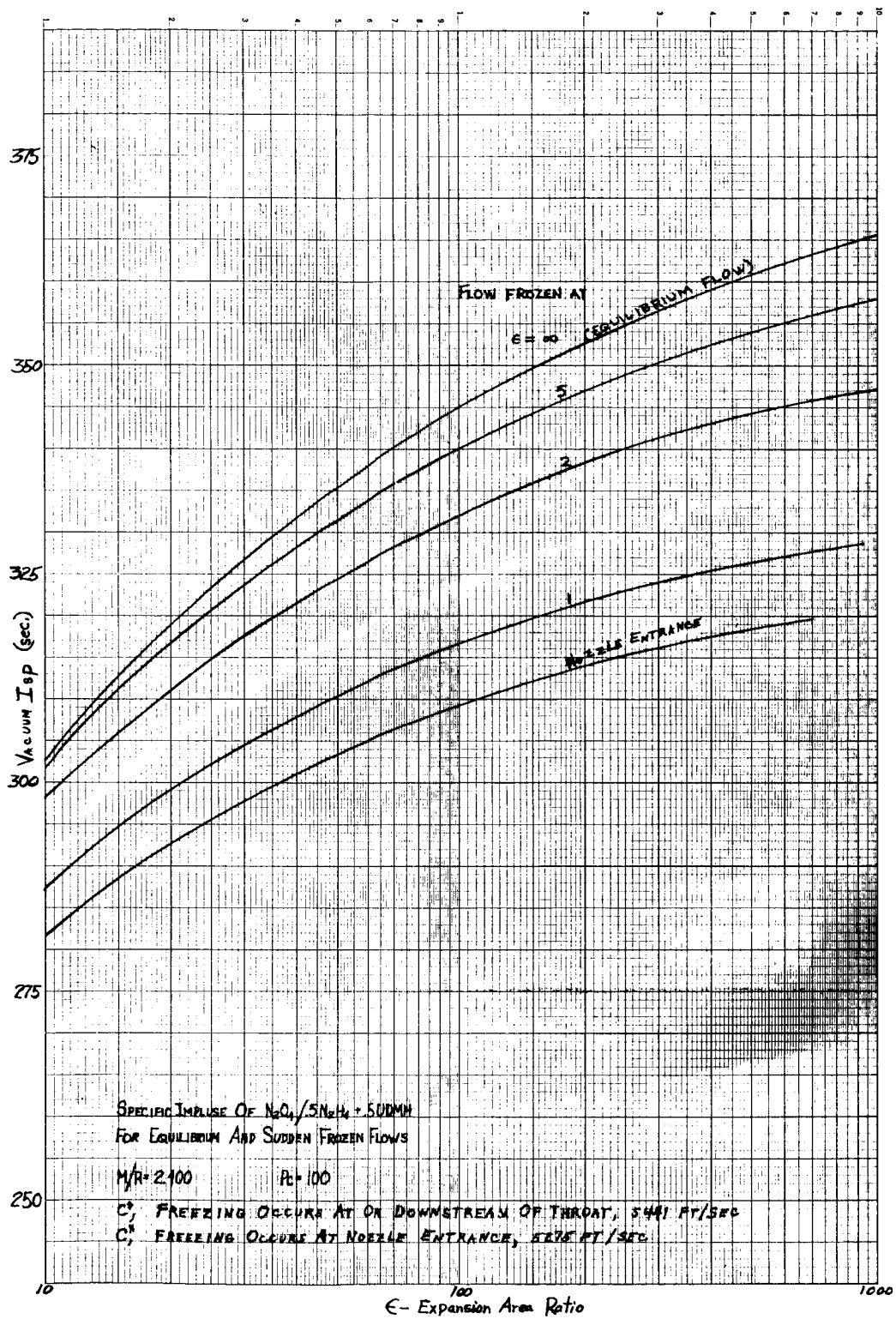
Specific Impulse of N_2O_4 /Aerozone 50, MR = 1.600 $P_c = 100$ psi

Figure 11



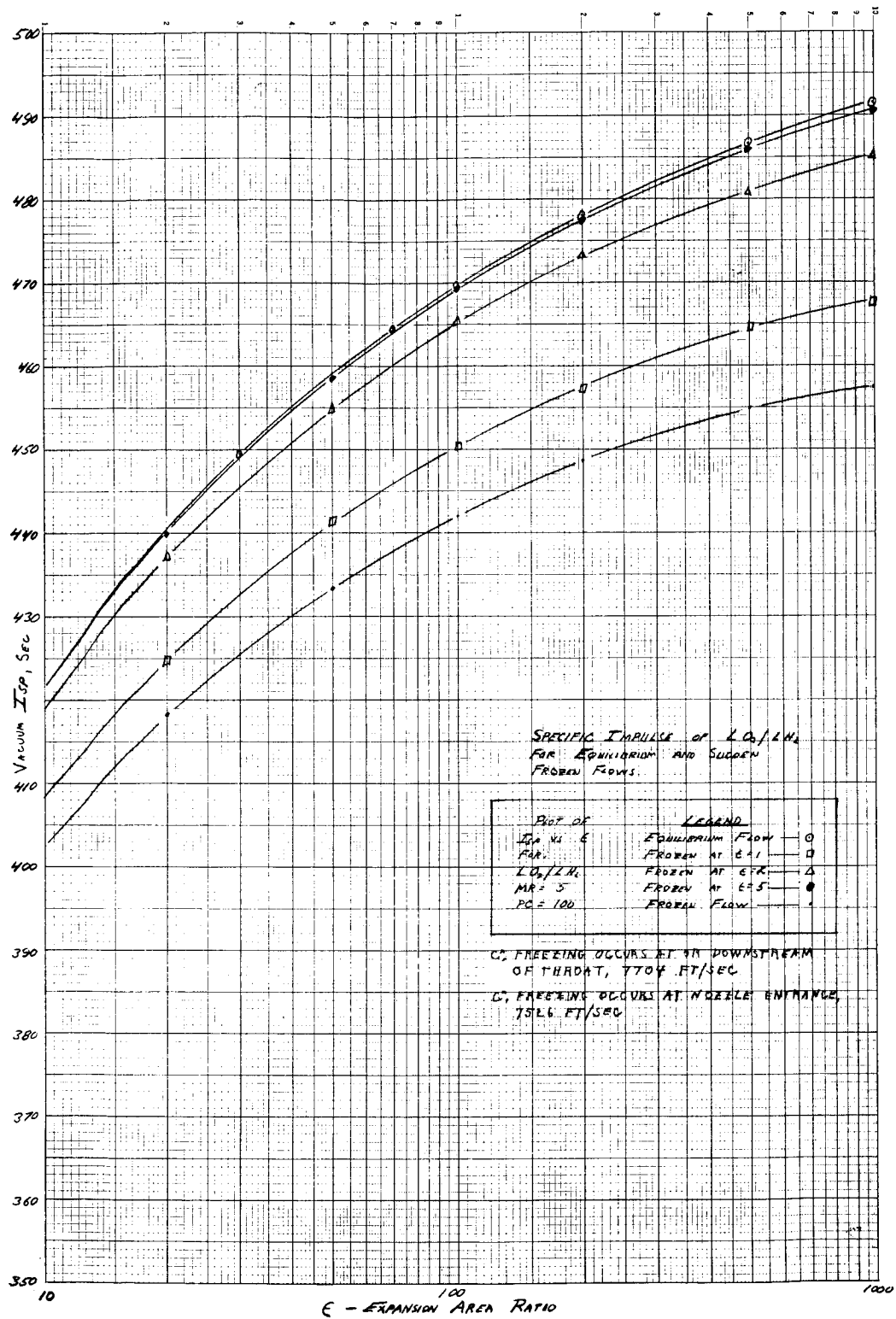
Specific Impulse of N_2O_4 /Aerozine 50, $MR = 2.0$, $P_c = 100$ psi

Figure 12



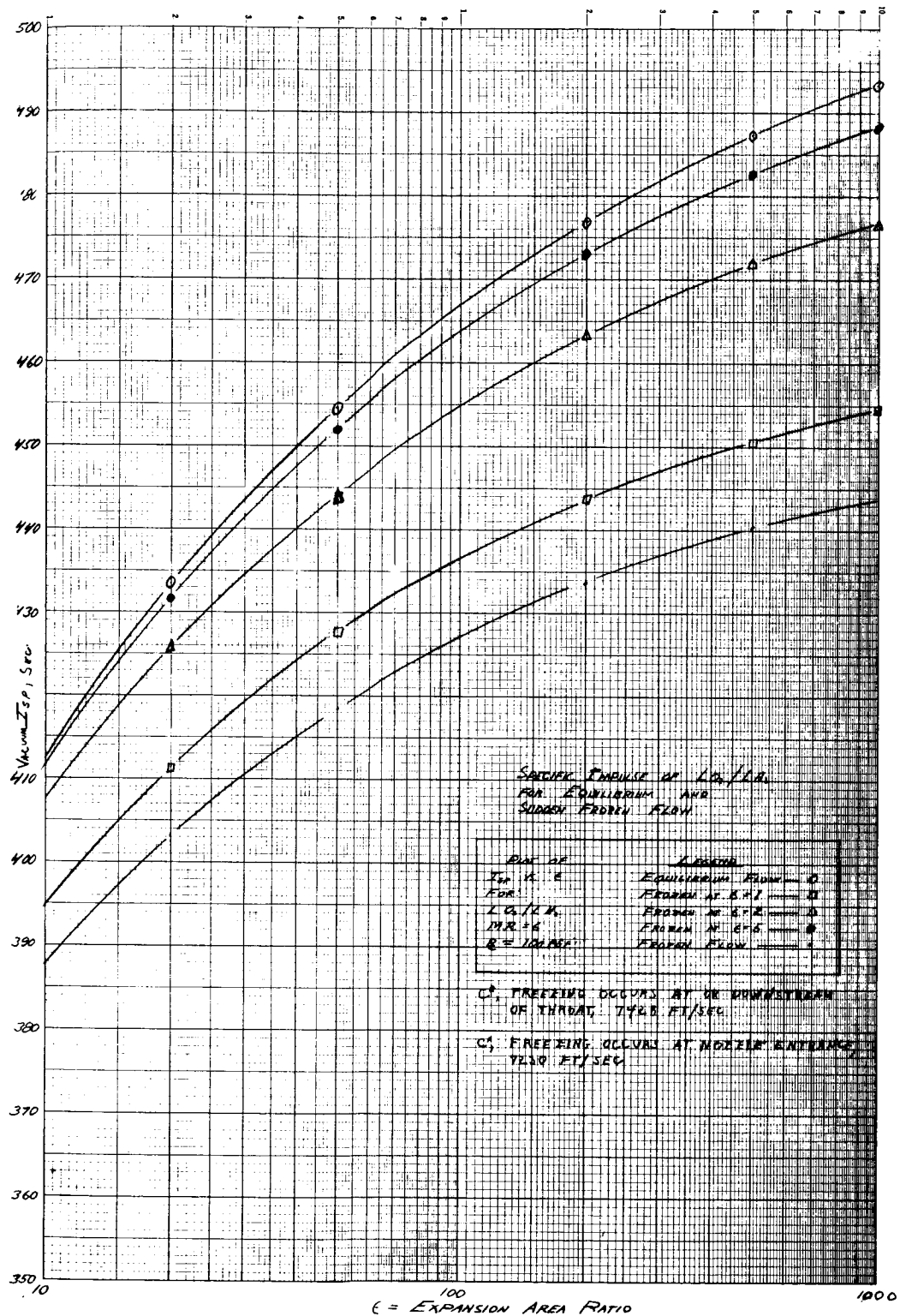
Specific Impulse of N_2O_4 /Aerazine 50, $MR = 2.4$, $P_c = 100$ psi

Figure 13



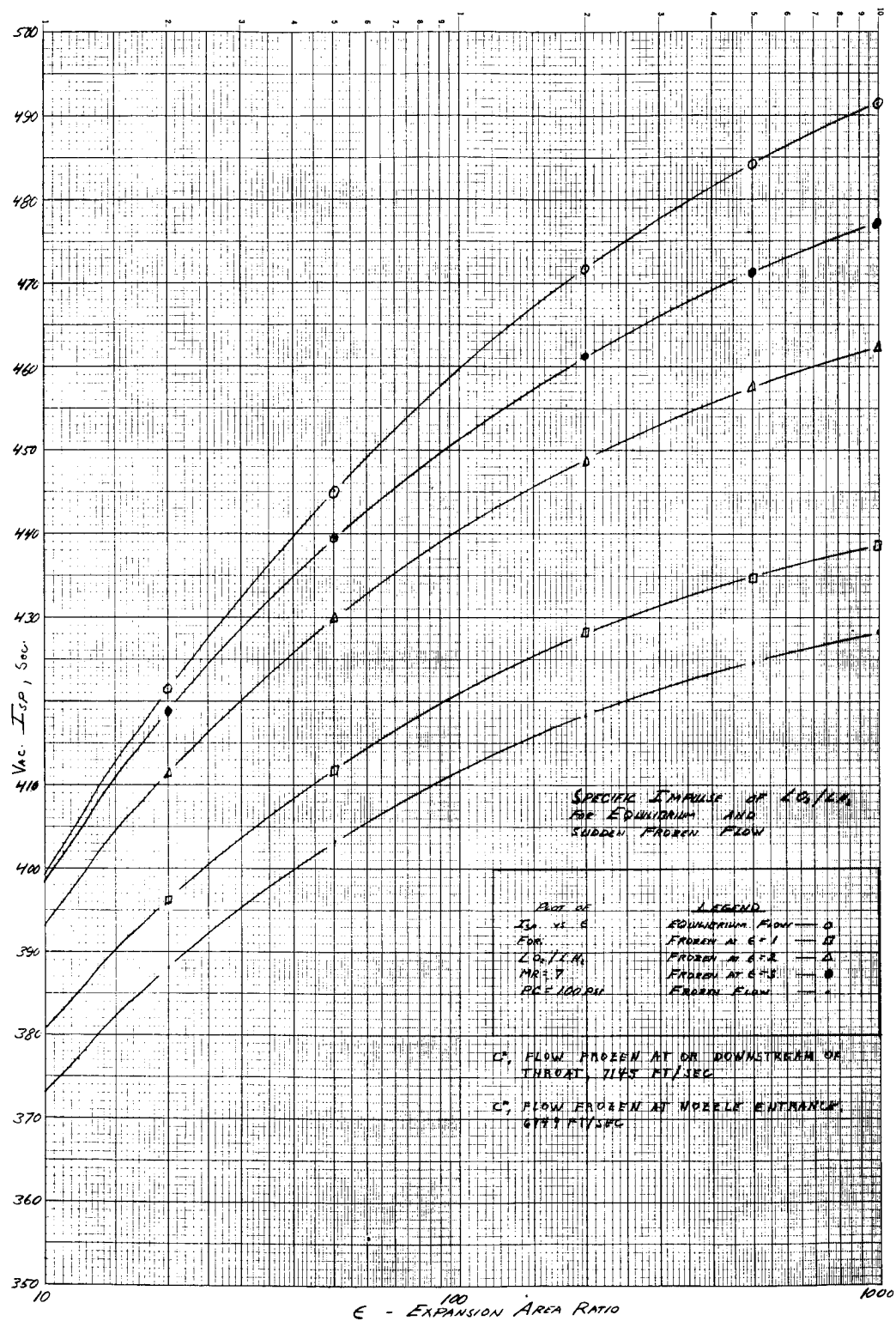
Specific Impulse of LO_2/LH_2 , $MR = 5.0$, $P_c = 100$ psi

Figure 14



Specific Impulse of LO_2/LH_2 , $MR = 6.0$, $P_c = 100$ psi

Figure 15



Specific Impulse of LO_2/LH_2 , $MR = 7.0$, $P_c = 100$ psi

Figure 16

Report NAS 7-136-F, Appendix A

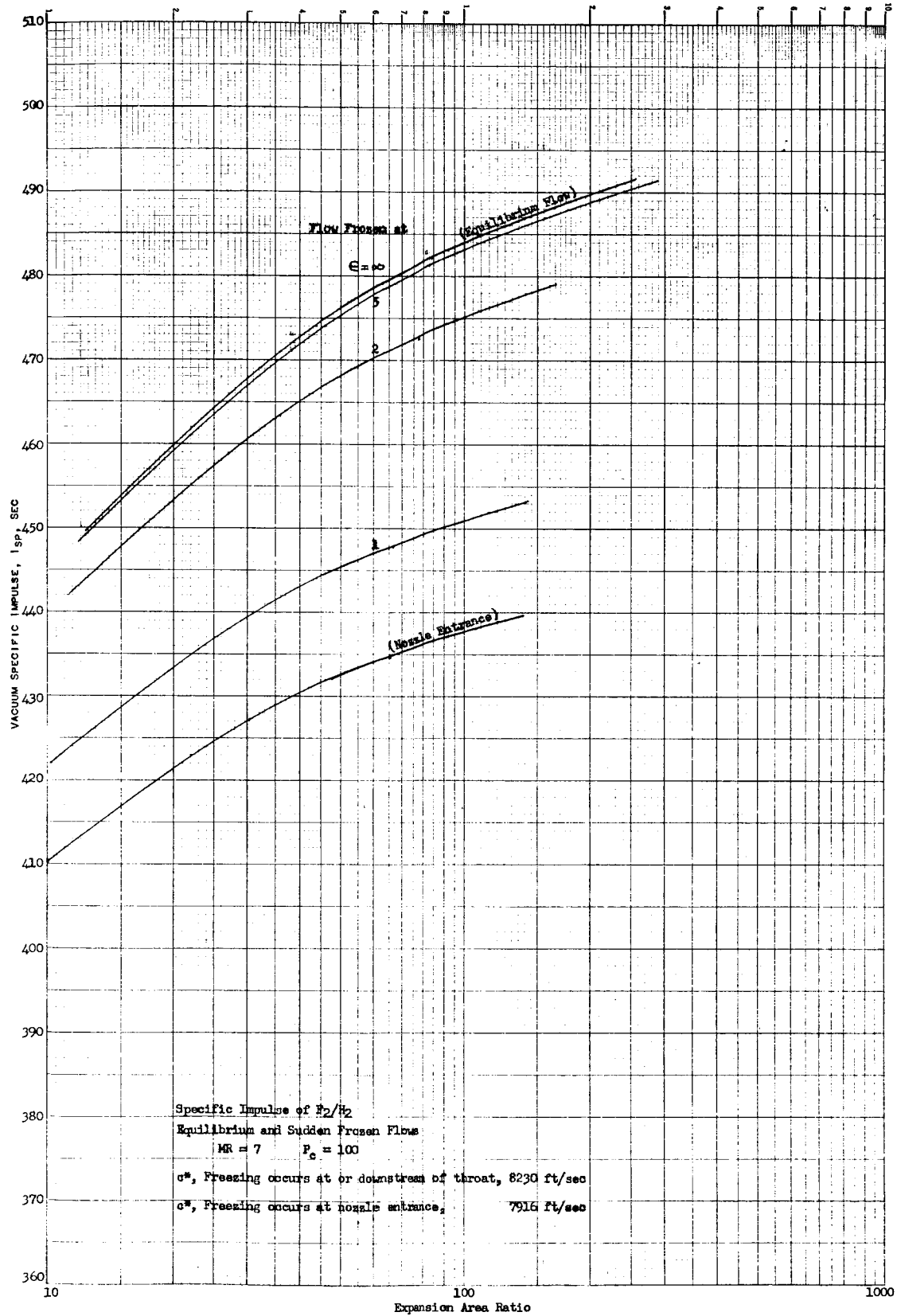
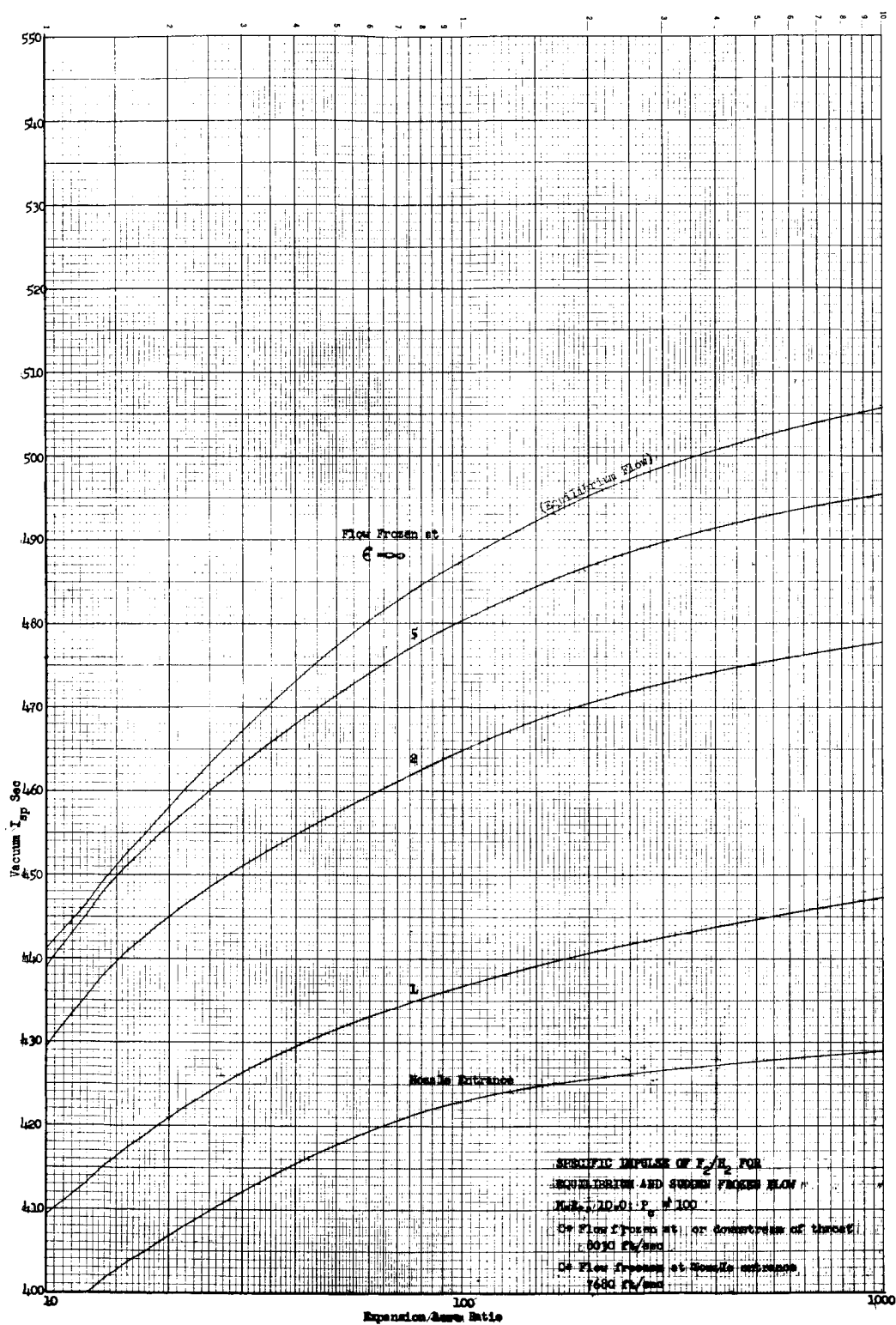
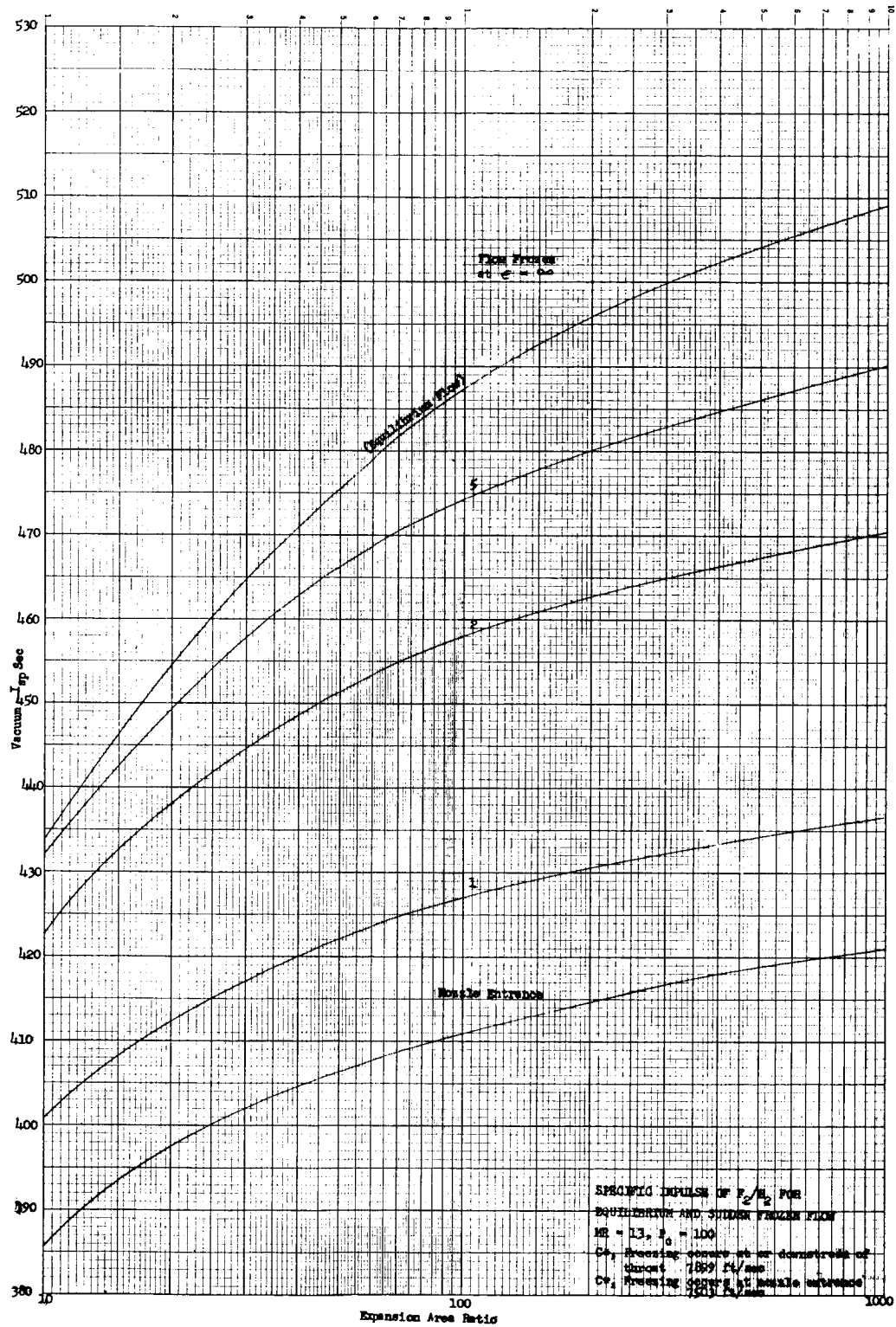


Figure 17



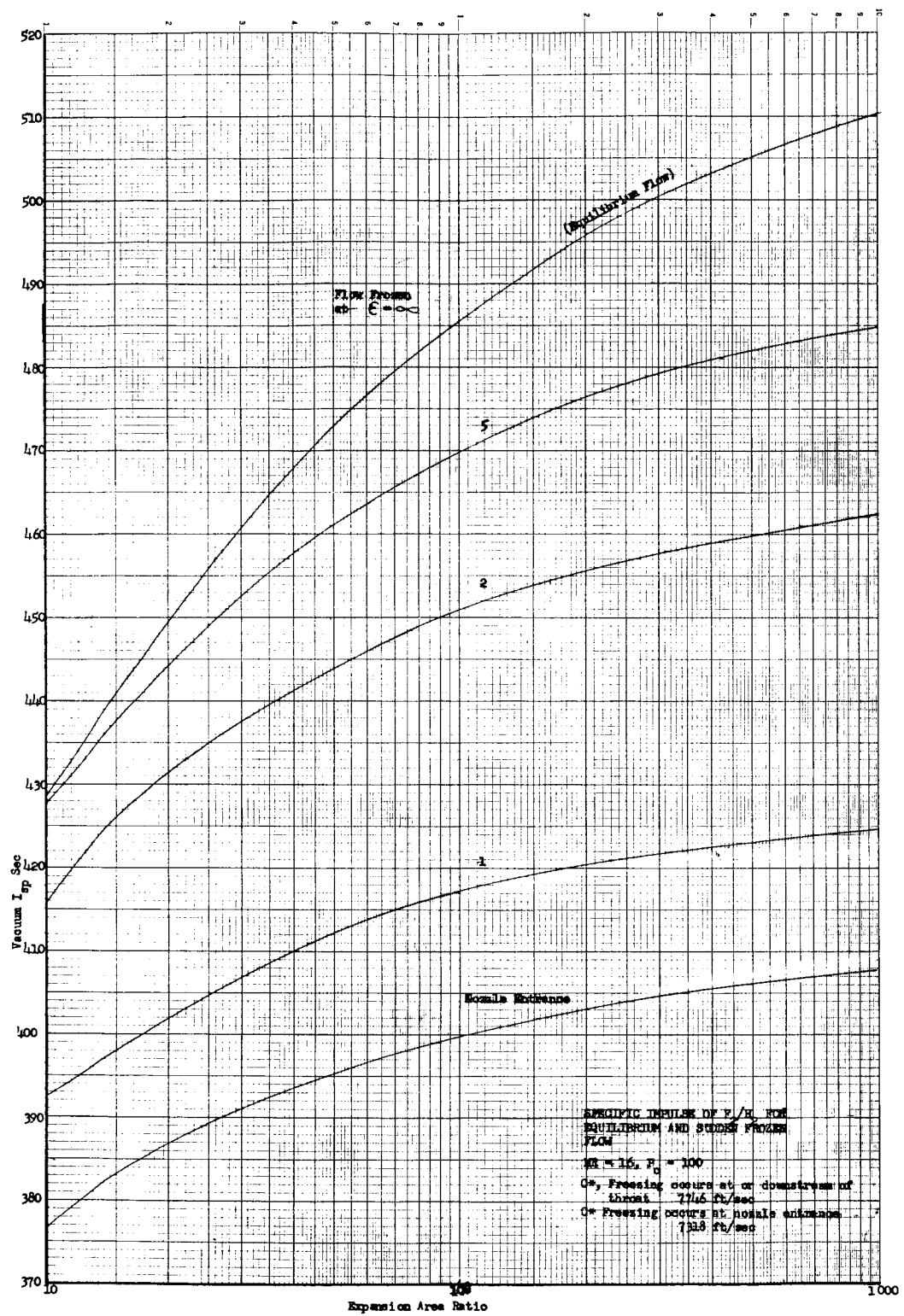
Specific Impulse of F_2/H_2 , $MR = 10.0$, $P_c = 100$ psi

Figure 18



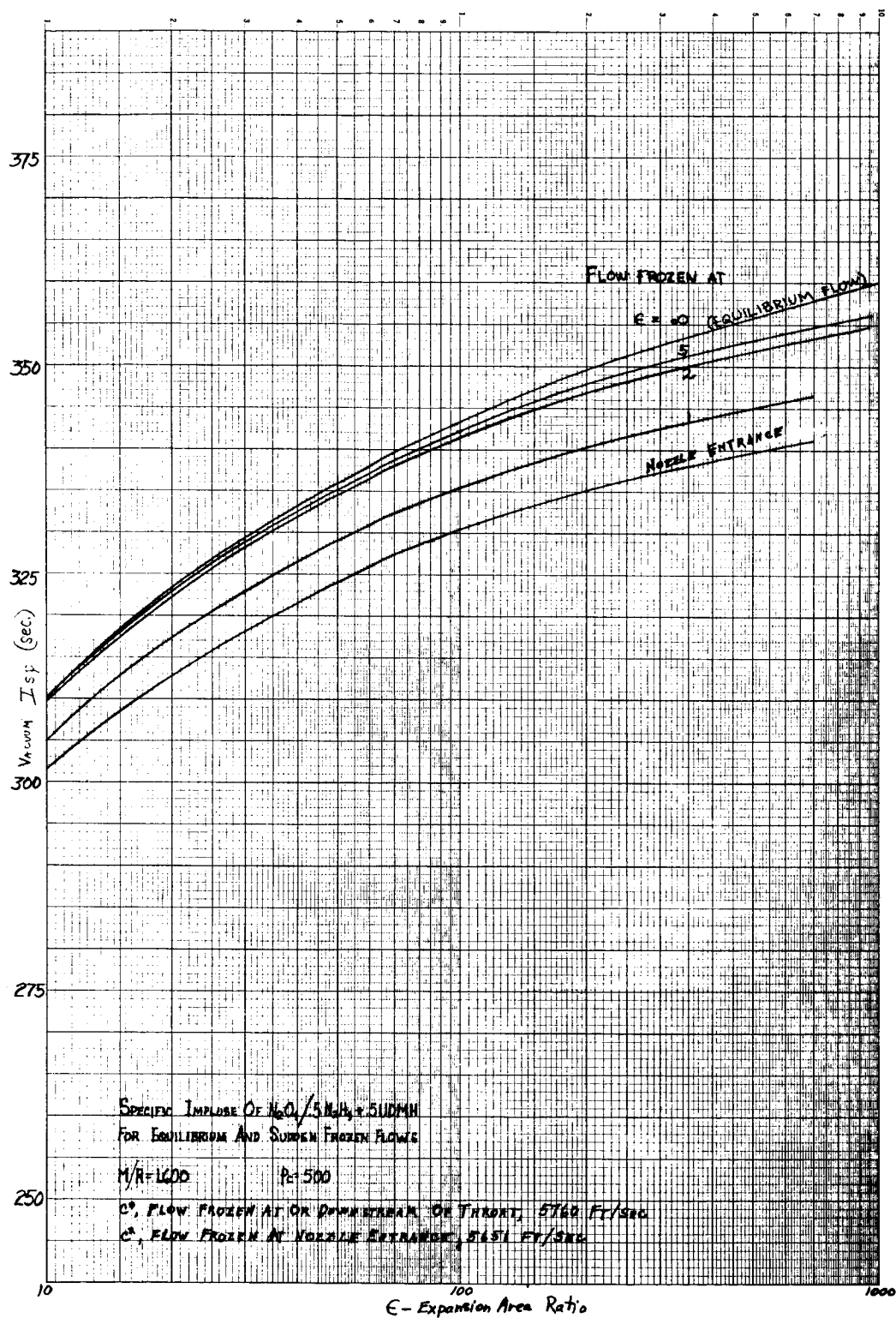
Specific Impulse of F_2/H_2 , $MR = 13.0$, $P_c = 100$ psi

Figure 19



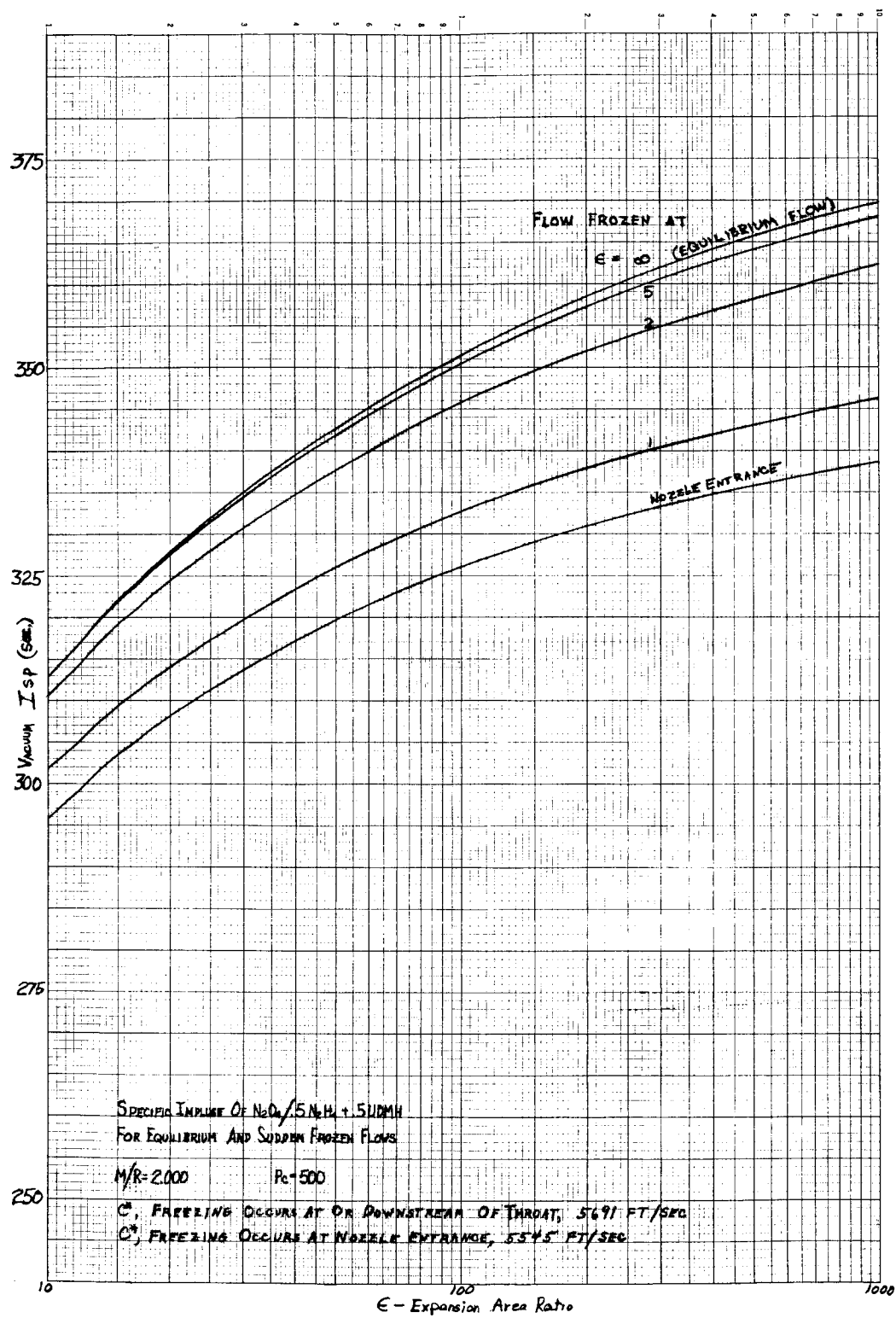
Specific Impulse of F_2/H_2 , $MR = 16.0$, $P_c = 100$ psi

Figure 20



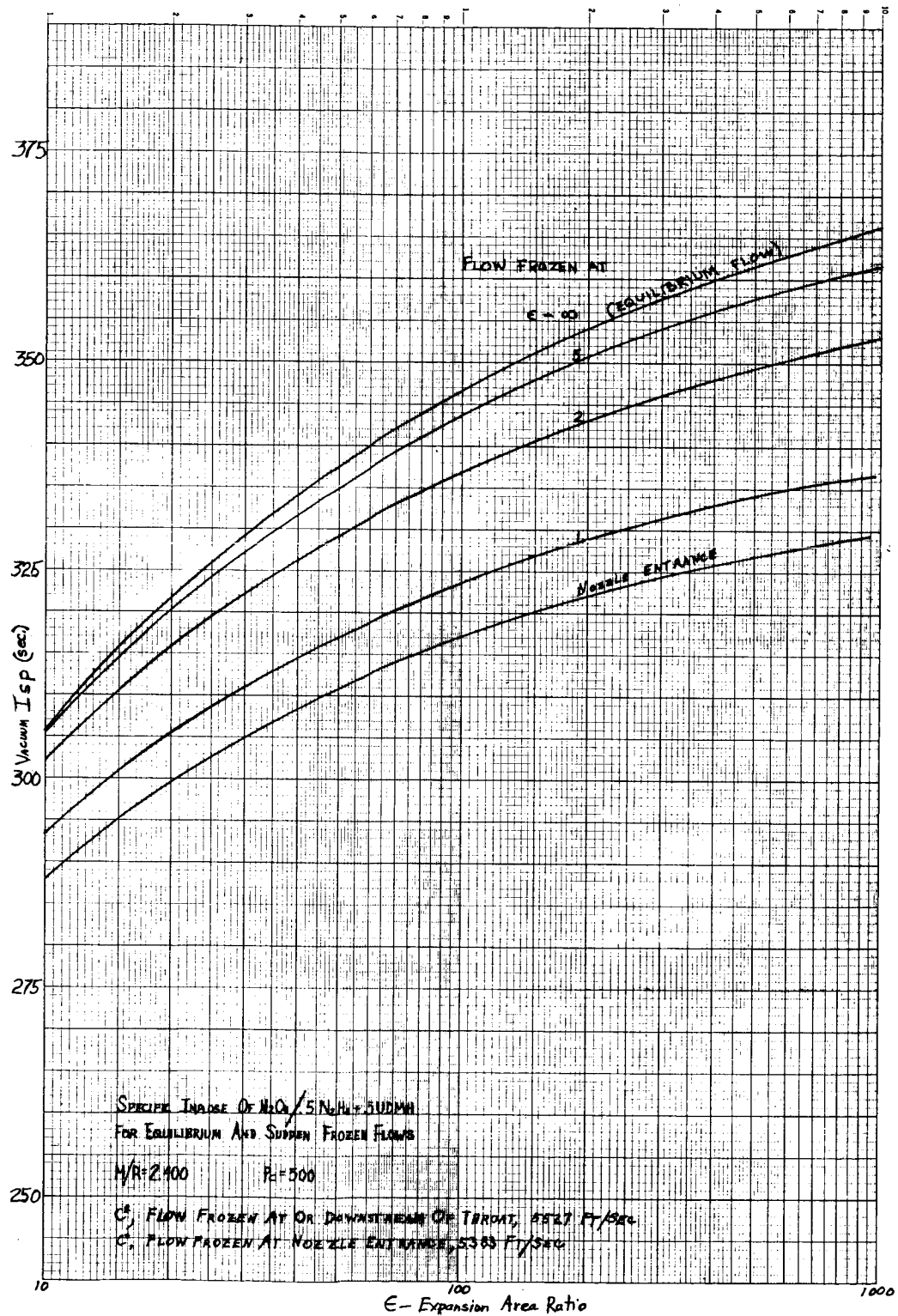
Specific Impulse of N_2O_4 /Aerozine 50, $MR = 1.6$, $P_c = 500$ psi

Figure 21



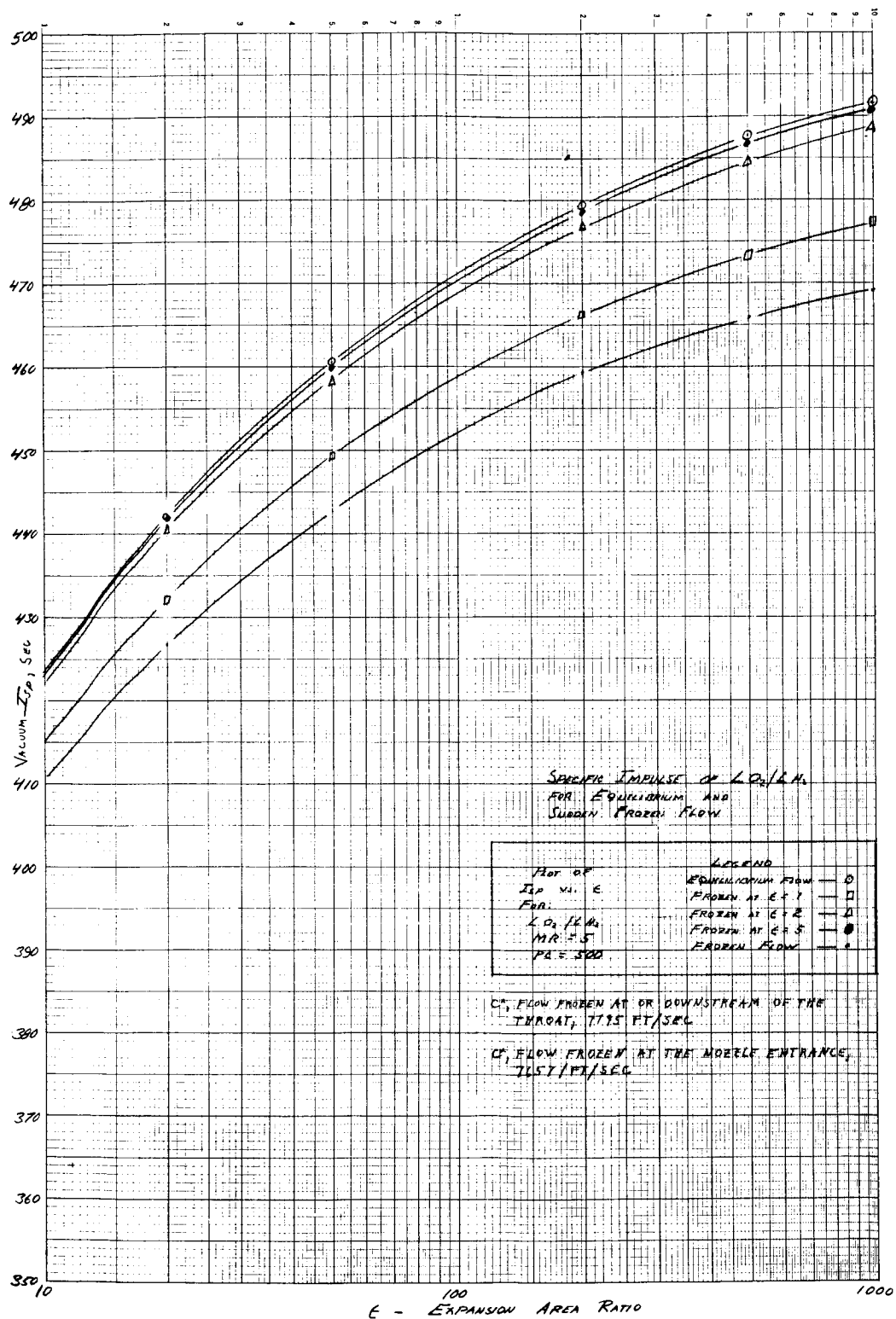
Specific Impulse of N_2O_4 /Aerozine 50, MR = 2.0, $P_c = 500$ psi

Figure 22



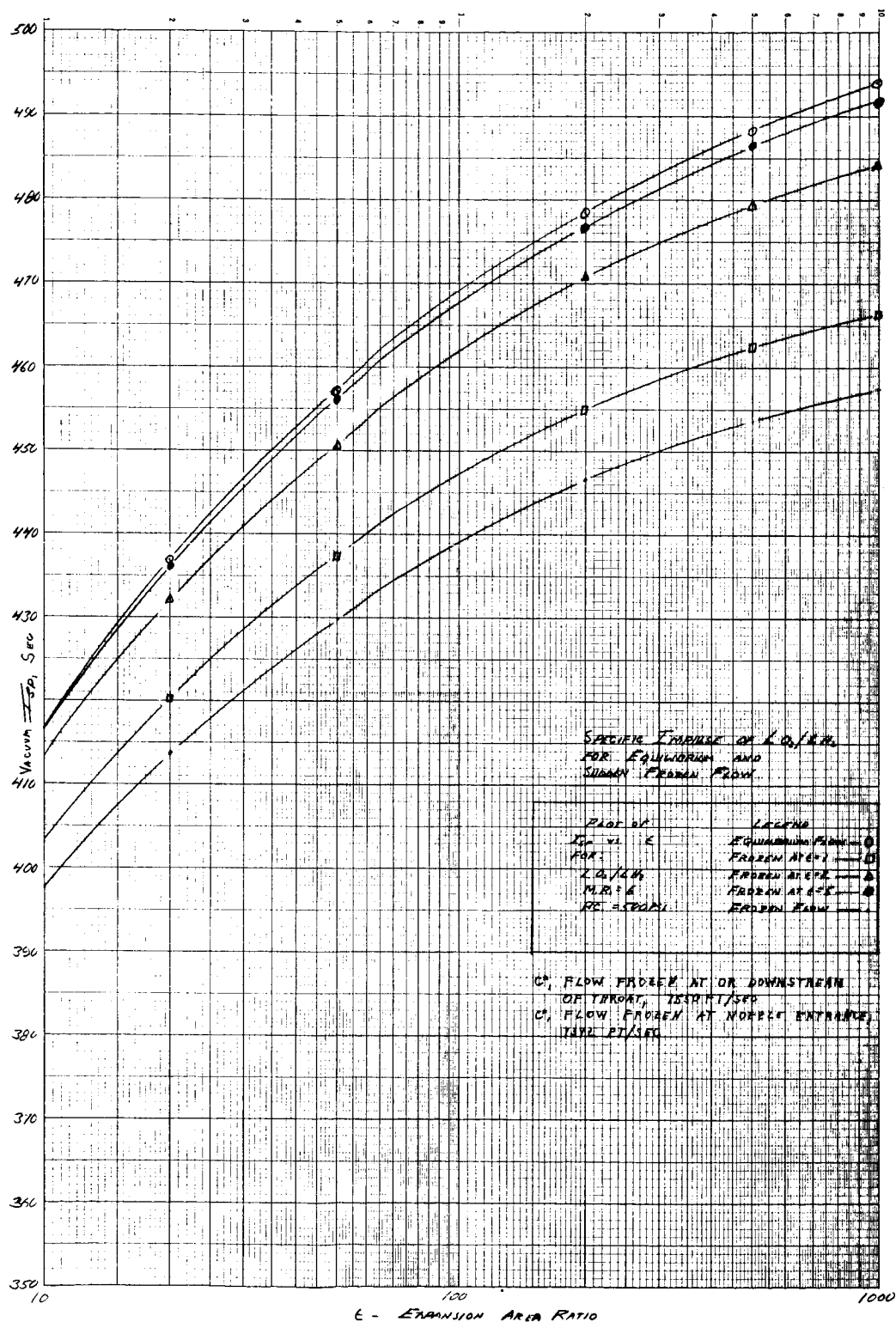
Specific Impulse of N_2O_4 /Aerazine 50, MR = 2.4, $P_c = 500$ psi

Figure 23



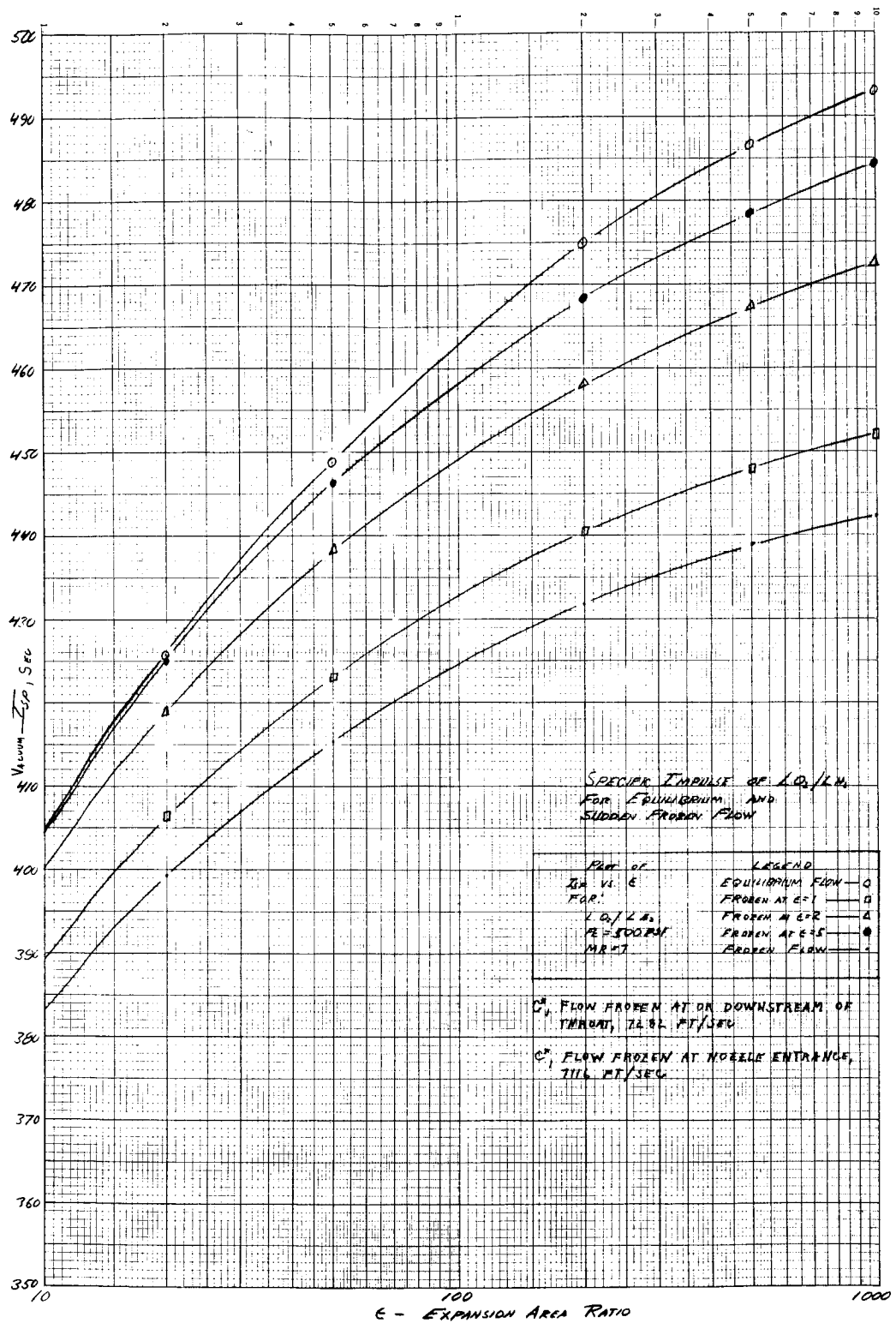
Specific Impulse of LO_2/LH_2 , $MR = 5.0$, $P_c = 500$ psi

Figure 24



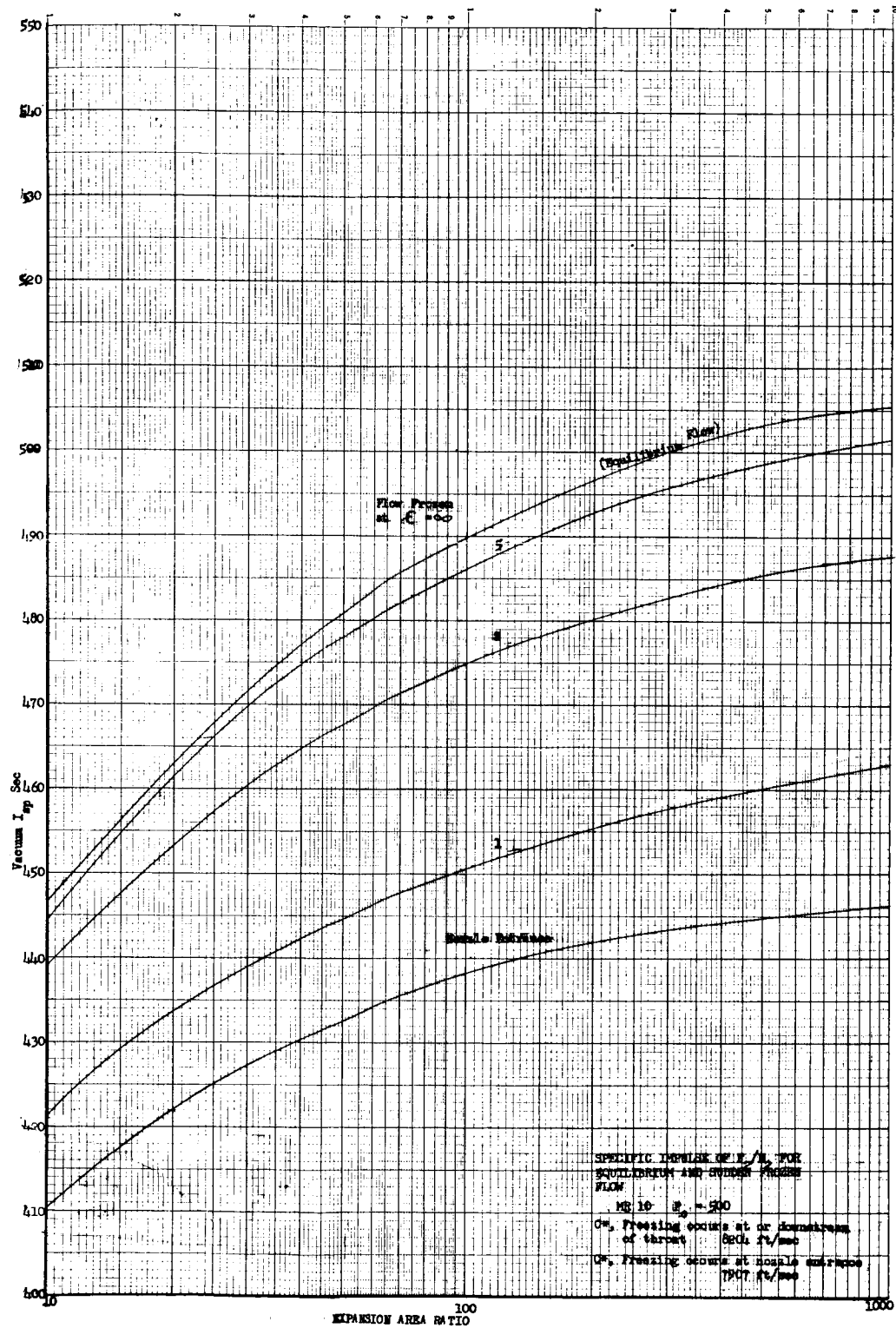
Specific Impulse of LO_2/LH_2 , $MR = 6.0$, $P_c = 500$ psi

Figure 25



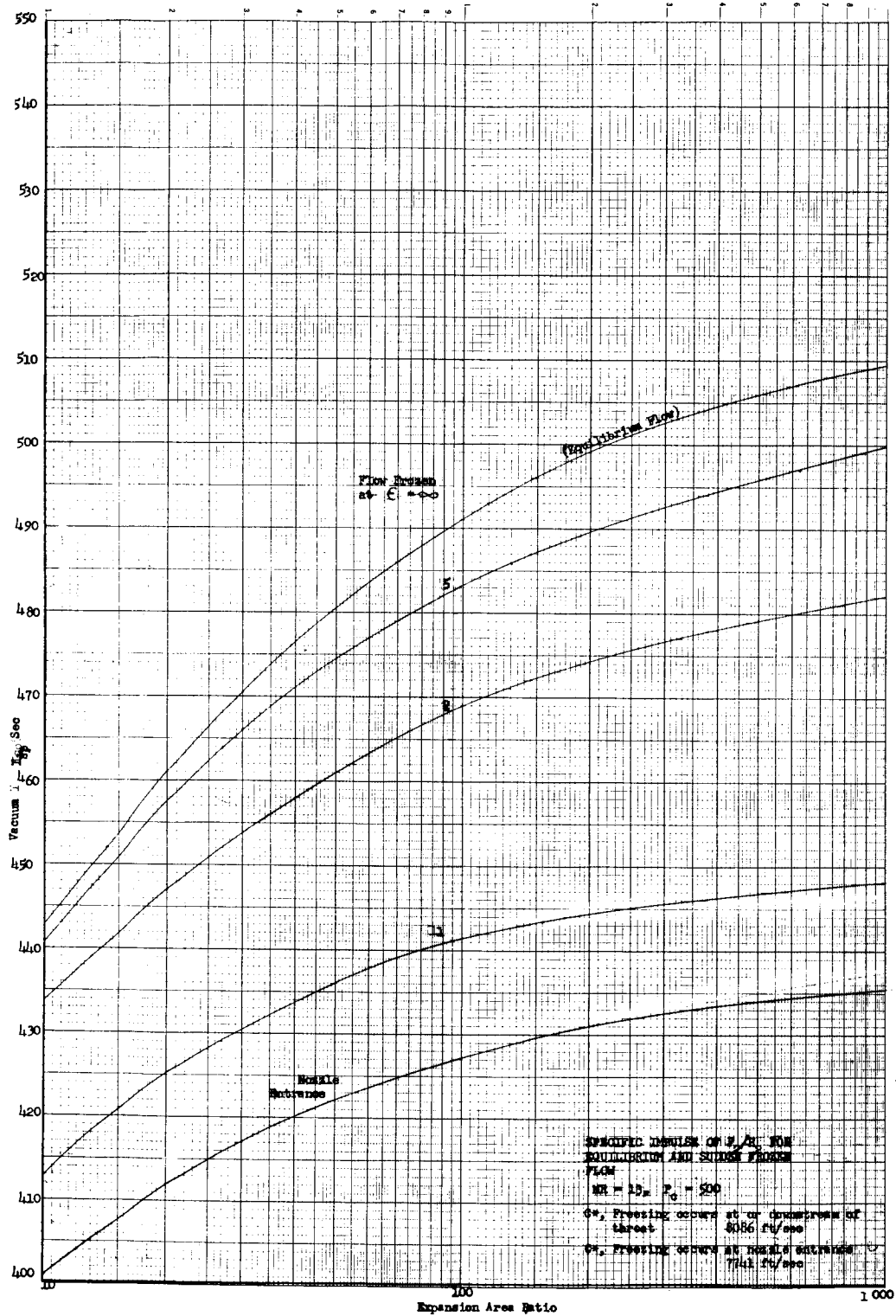
Specific Impulse of LO_2/LH_2 , $MR = 7.0$, $P_c = 500$ psi

Figure 26



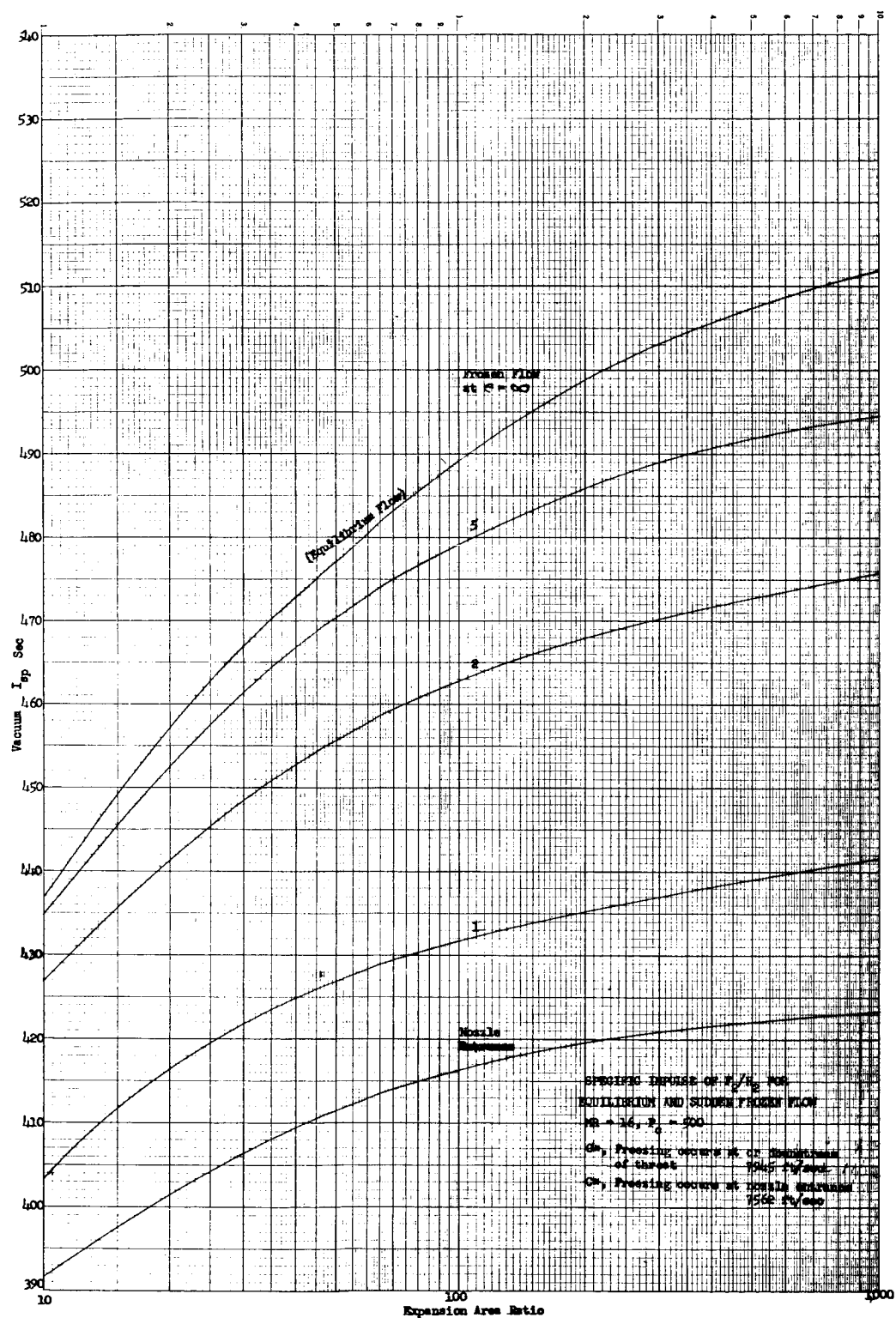
Specific Impulse of F_2/H_2 , MR = 10.0, $P_c = 500$ psi

Figure 27

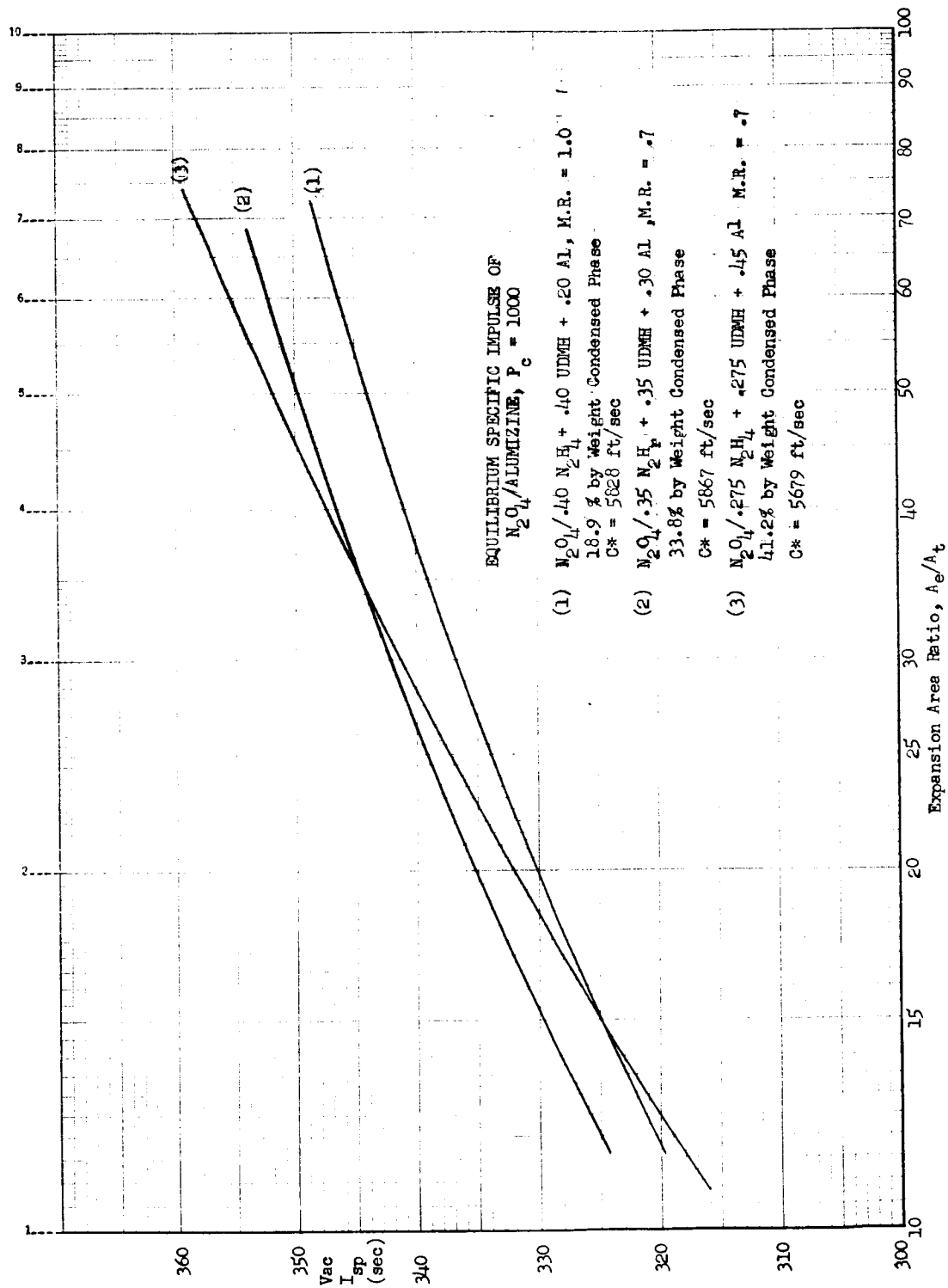


Specific Impulse of F_2/H_2 , MR = 13.0, $P_c = 500$ psi

Figure 28



Specific Impulse of F_2/H_2 , $MR = 16.0$, $P_c = 500$ psi



Equilibrium Impulse of N_2O_4 /Alumizine, $P_c = 1000$ psi

Figure 30

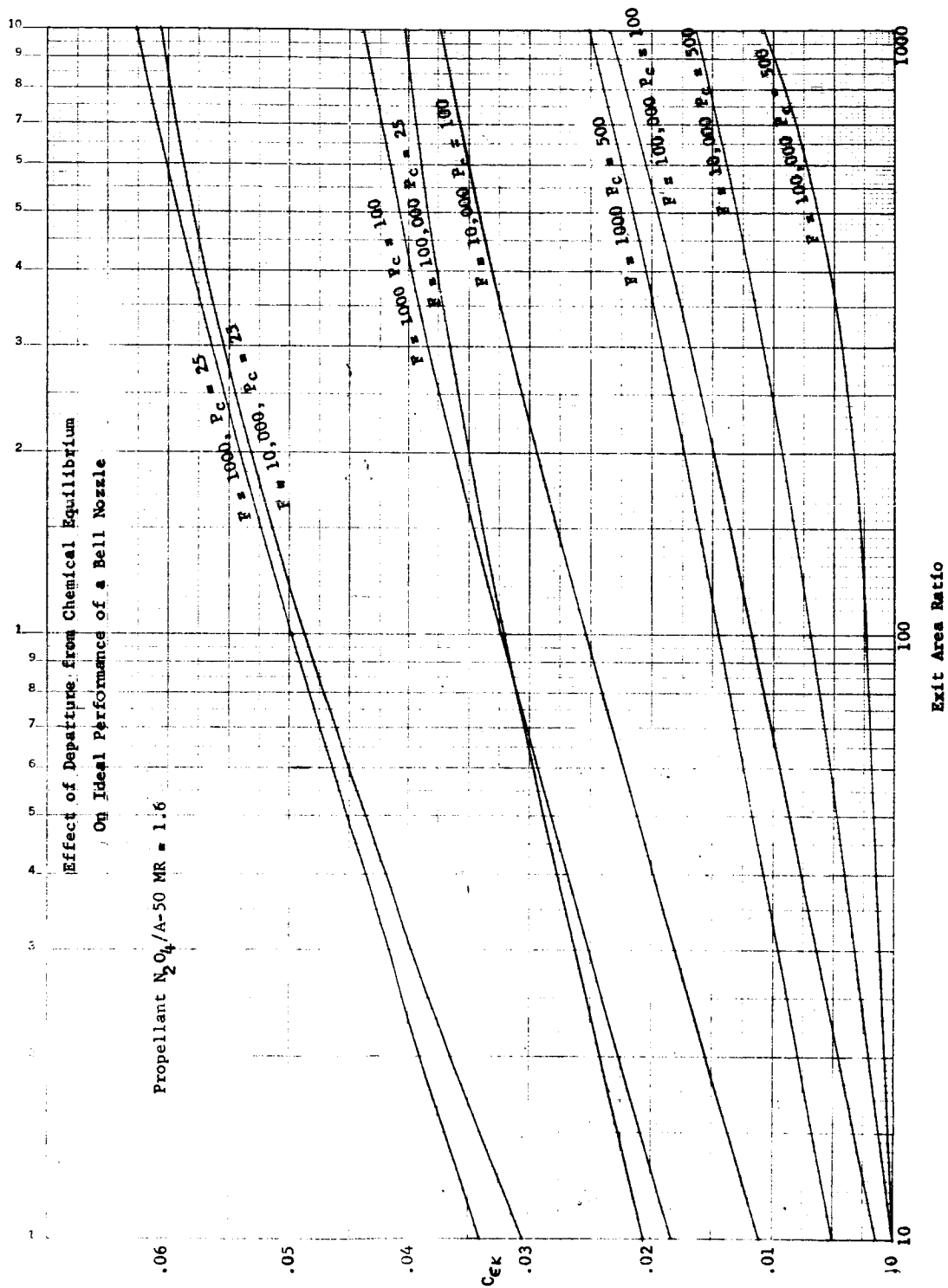


Figure 31

Kinetic Effects for Bell Nozzle, N_2O_4 /Aerozine 50, $MR = 1.6$, $R_d/R_t = .2$

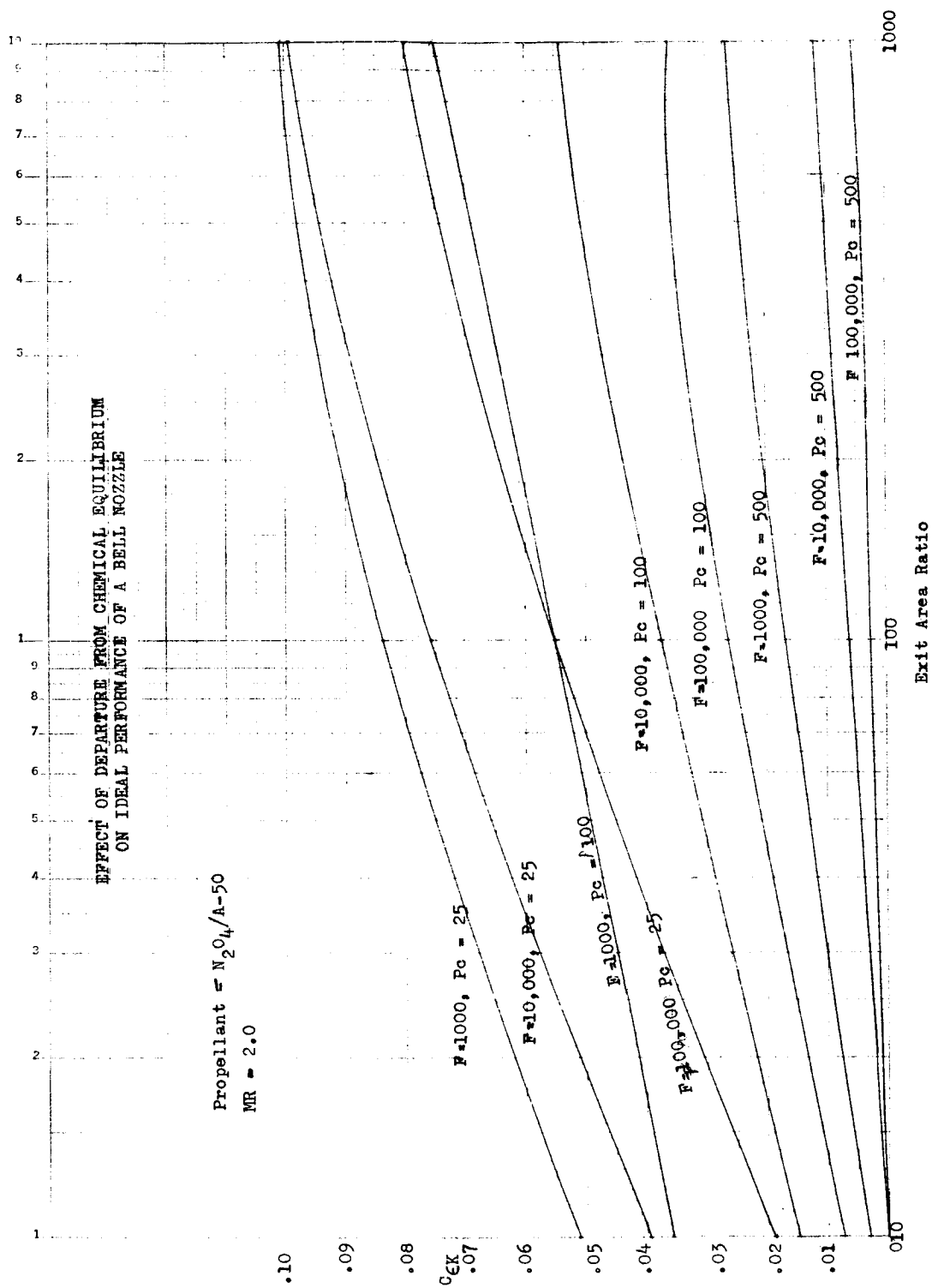


Figure 32

Kinetic Effects for Bell Nozzle, $N_2O_4/Aerozine\ 50$, MR = 2.0, $R_d/R_t = .2$

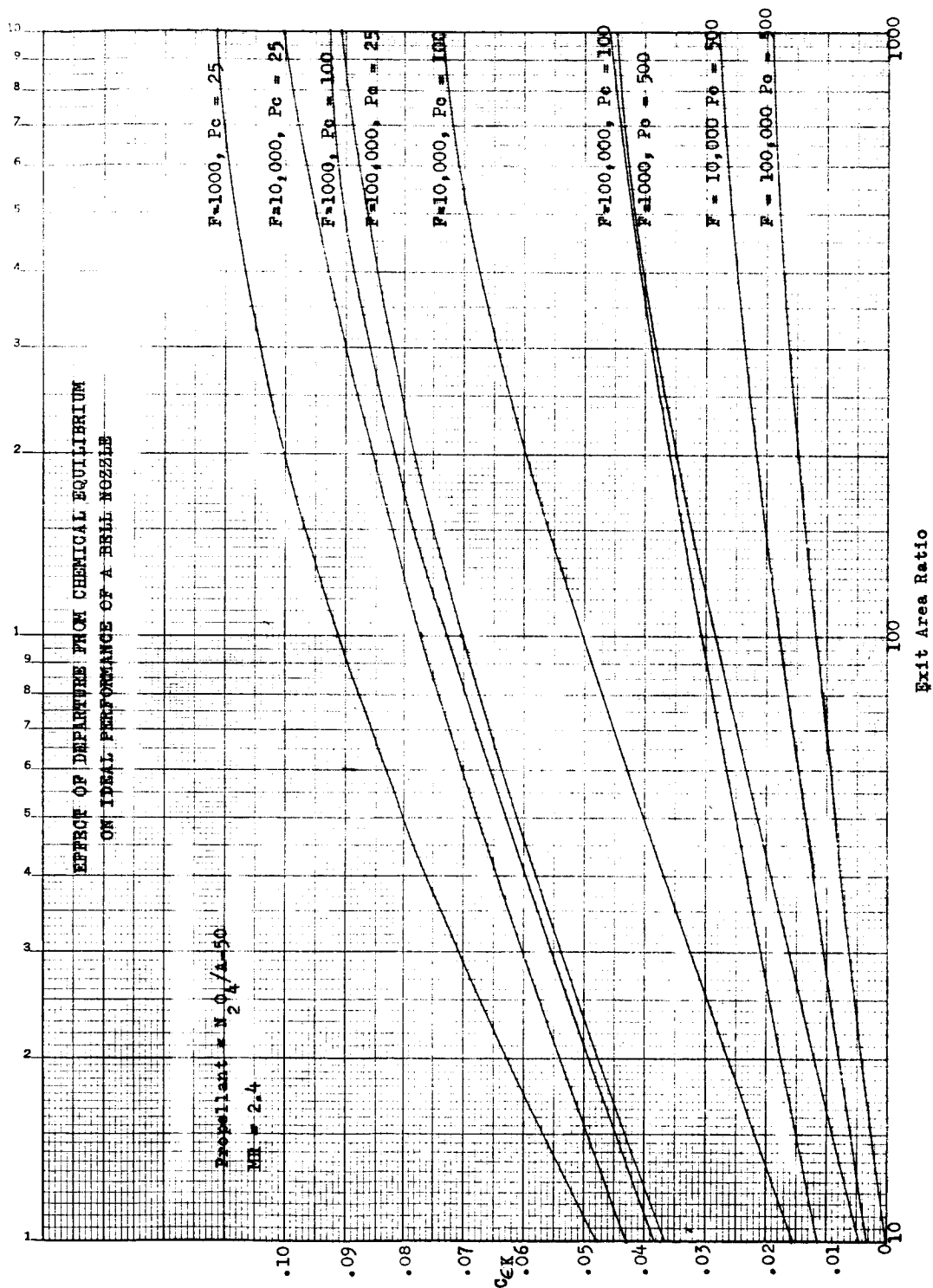


Figure 33

ic Effects for Bell Nozzle, $N_2O_4/Aerozine\ 50$, MR = 2.4, R_d/R .

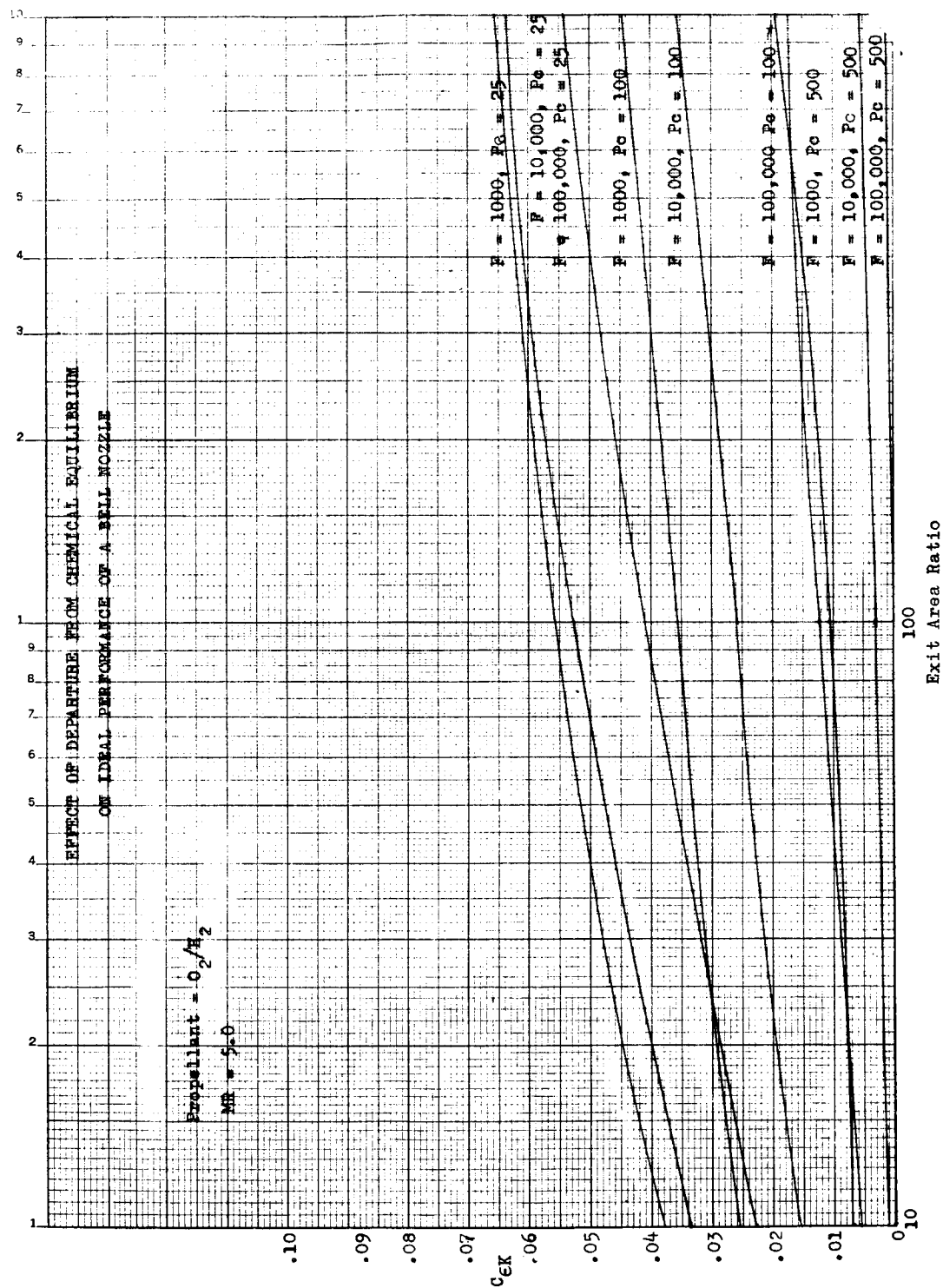


Figure 34

Kinetic Effects for Bell Nozzle, O_2/H_2 , MR = 5.0, $R_d/R_t = .2$

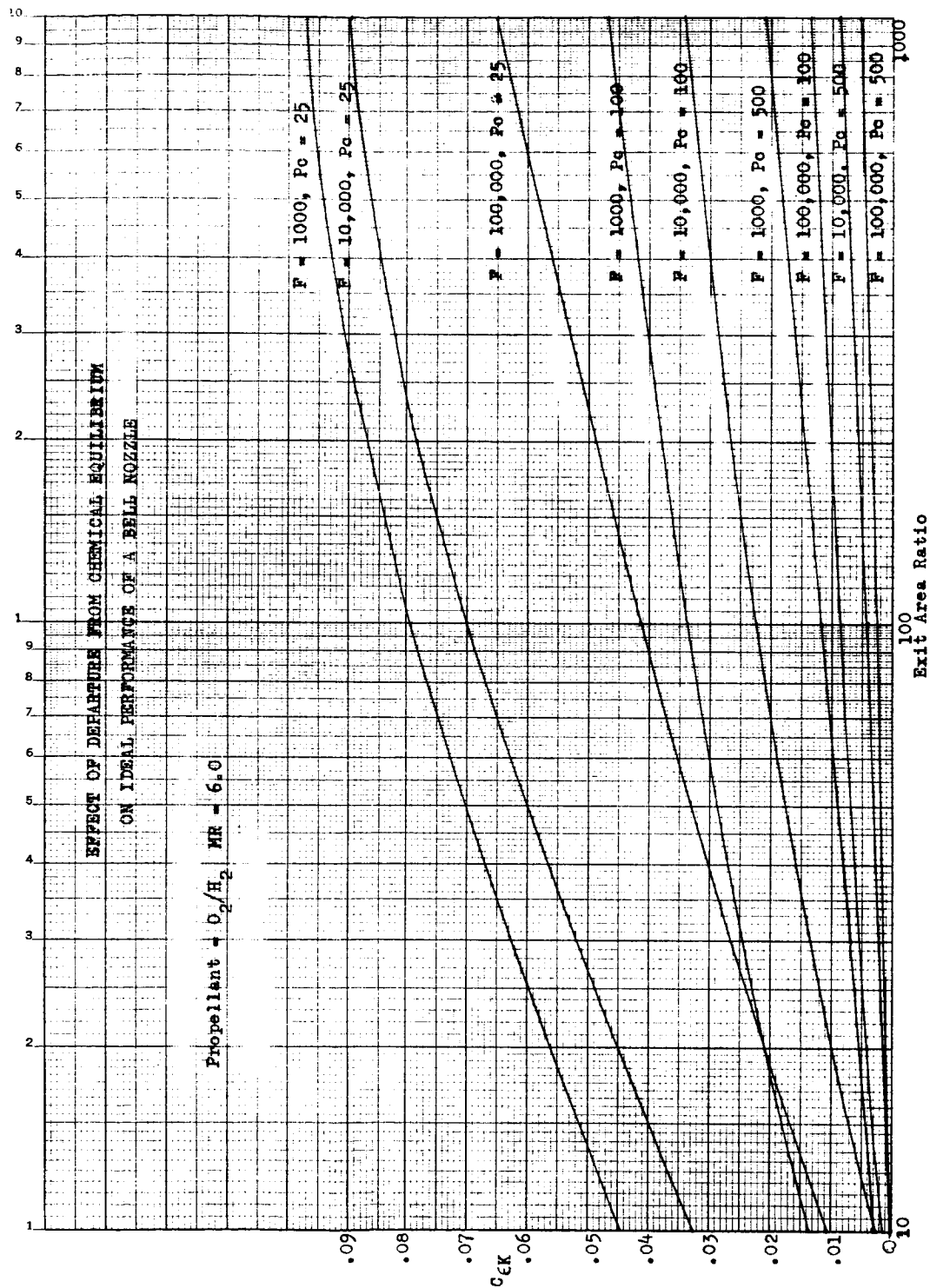


Figure 35

Kinetic Effects for Bell Nozzle, O_2/H_2 , $MR = 6.0$, $R_d/R_t = .2$

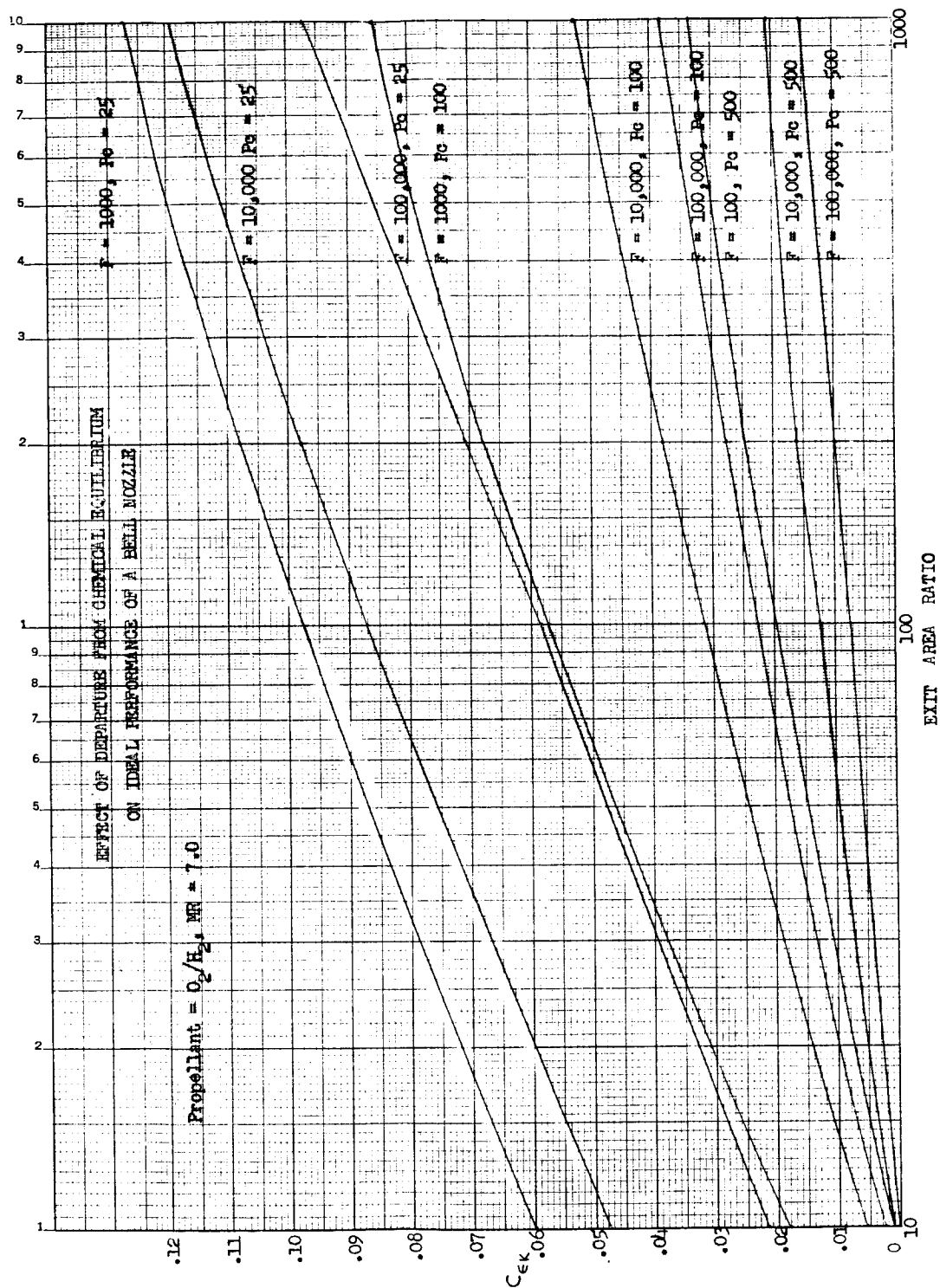


Figure 36

Kinetic Effects for Bell Nozzle, O_2/H_2 , $MR = 7.0$, $R_d/R_t = .2$

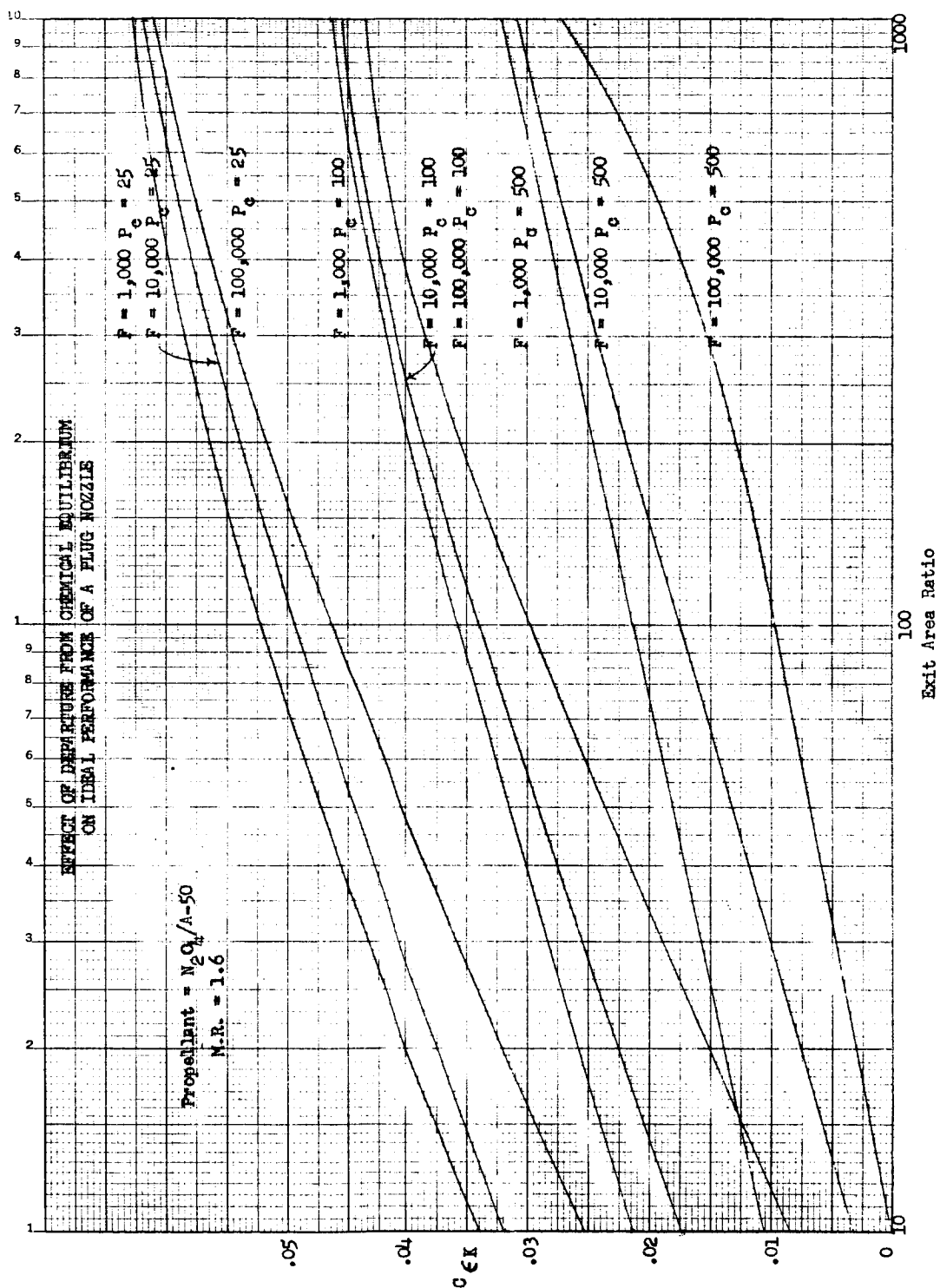


Figure 37

Kinetic Effects for Plug Nozzle, $N_2O_4/Aerozine\ 50$, $MR = 1.6$, $R_d/R_t = .2$

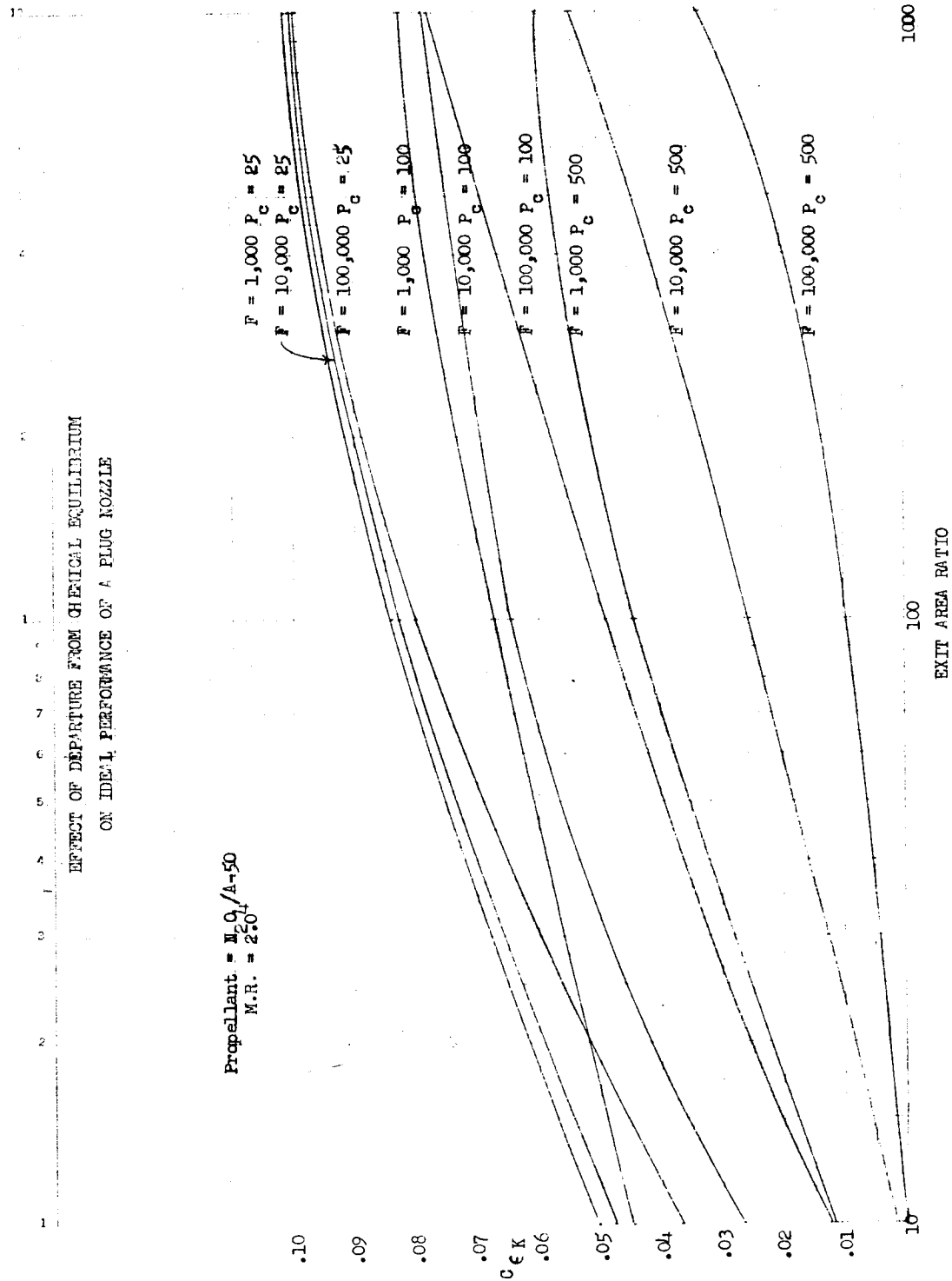


Figure 38

Kinetic Effects for Plug Nozzle, $\text{N}_2\text{O}_4/\text{Aerzine 50}$, $\text{MR} = 2.0$, $R_d/R_t = .2$

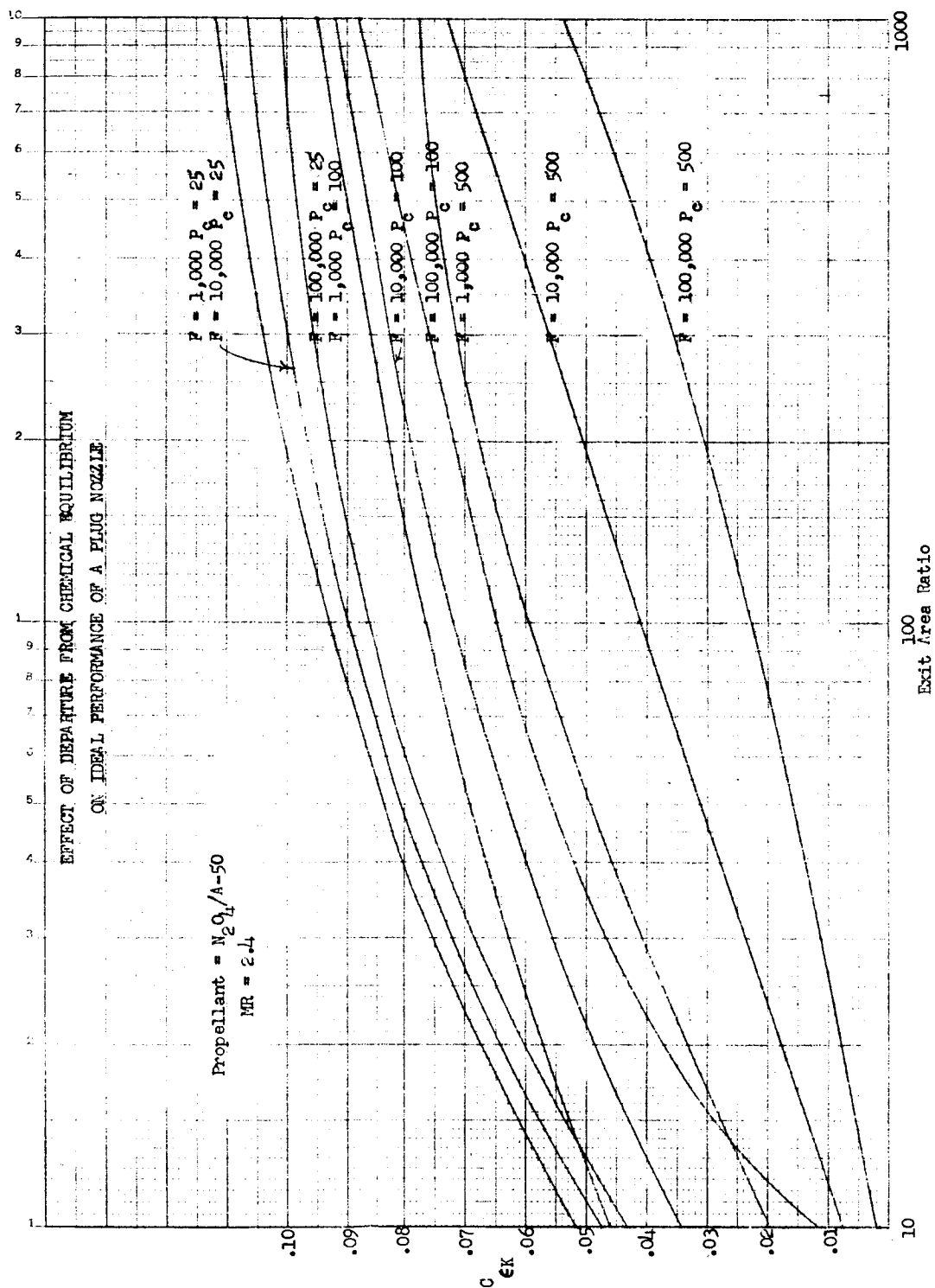


Figure 39

Kinetic Effects for Plug Nozzle, $N_2O_4/Aerozine\ 50$, $MR = 2.4$, $R_d/R_t = .2$

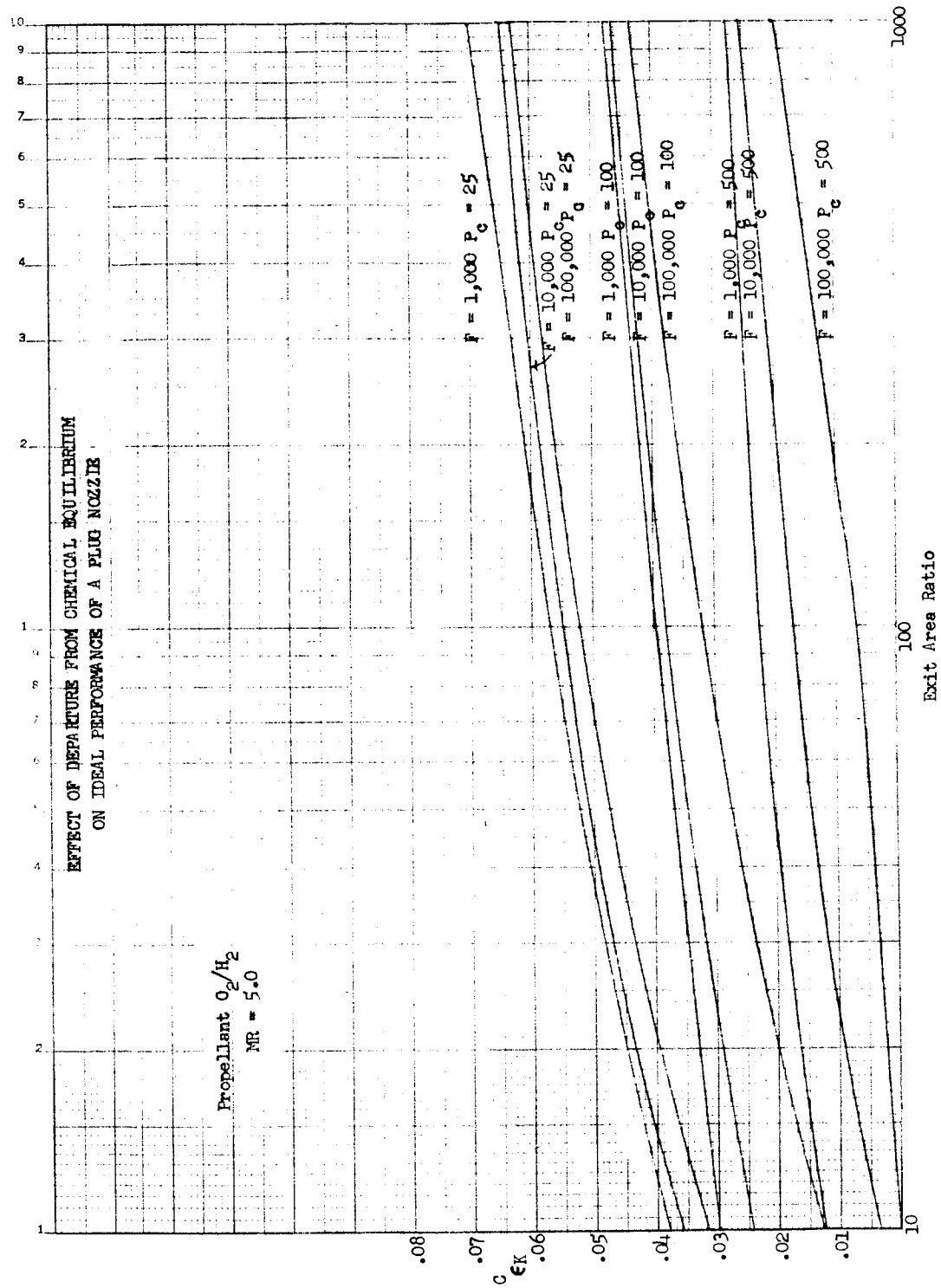


Figure 40

Kinetic Effects for Plug Nozzle, O_2/H_2 , MR = 5.0, $R_d/R_t = .2$

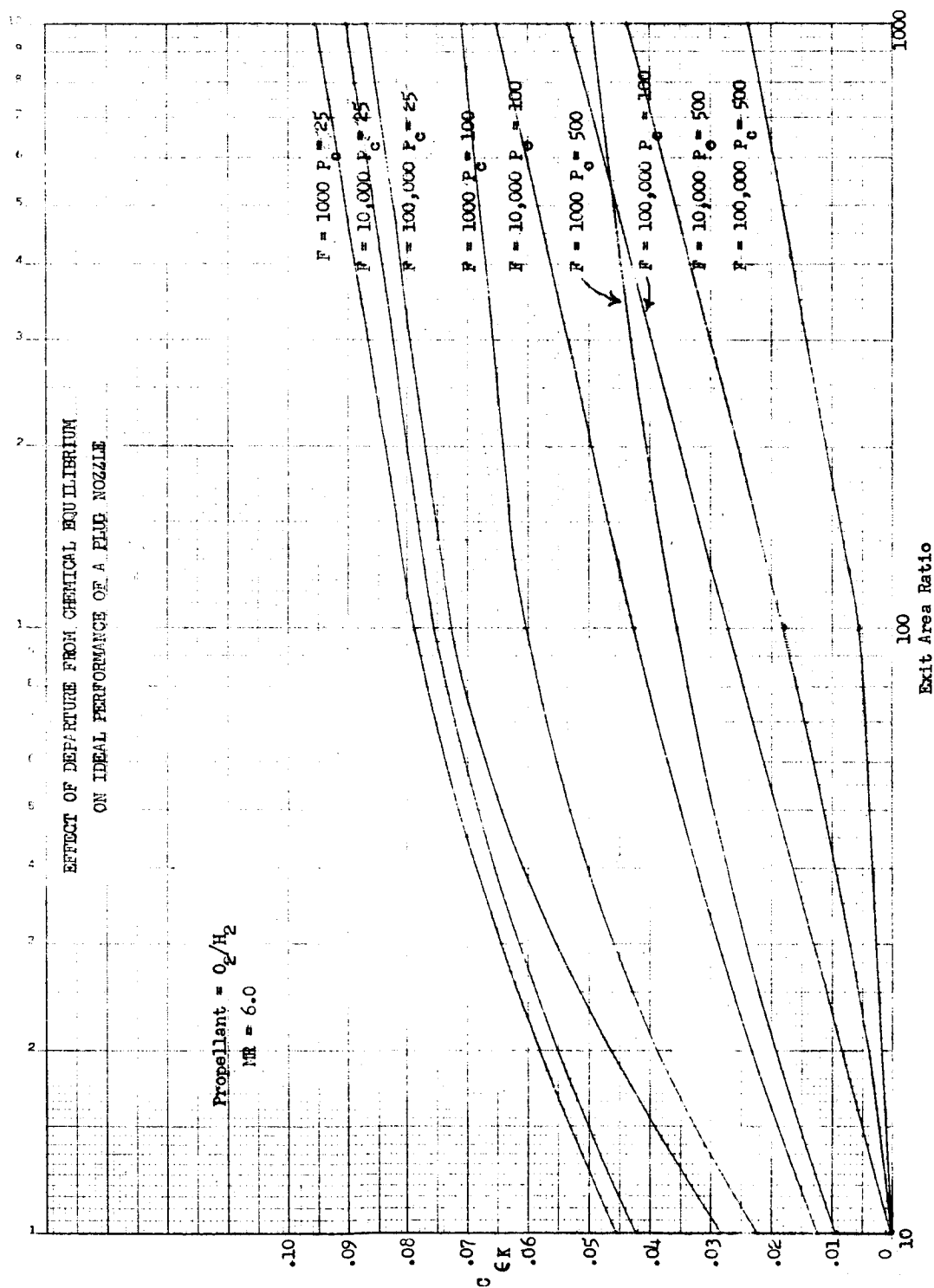
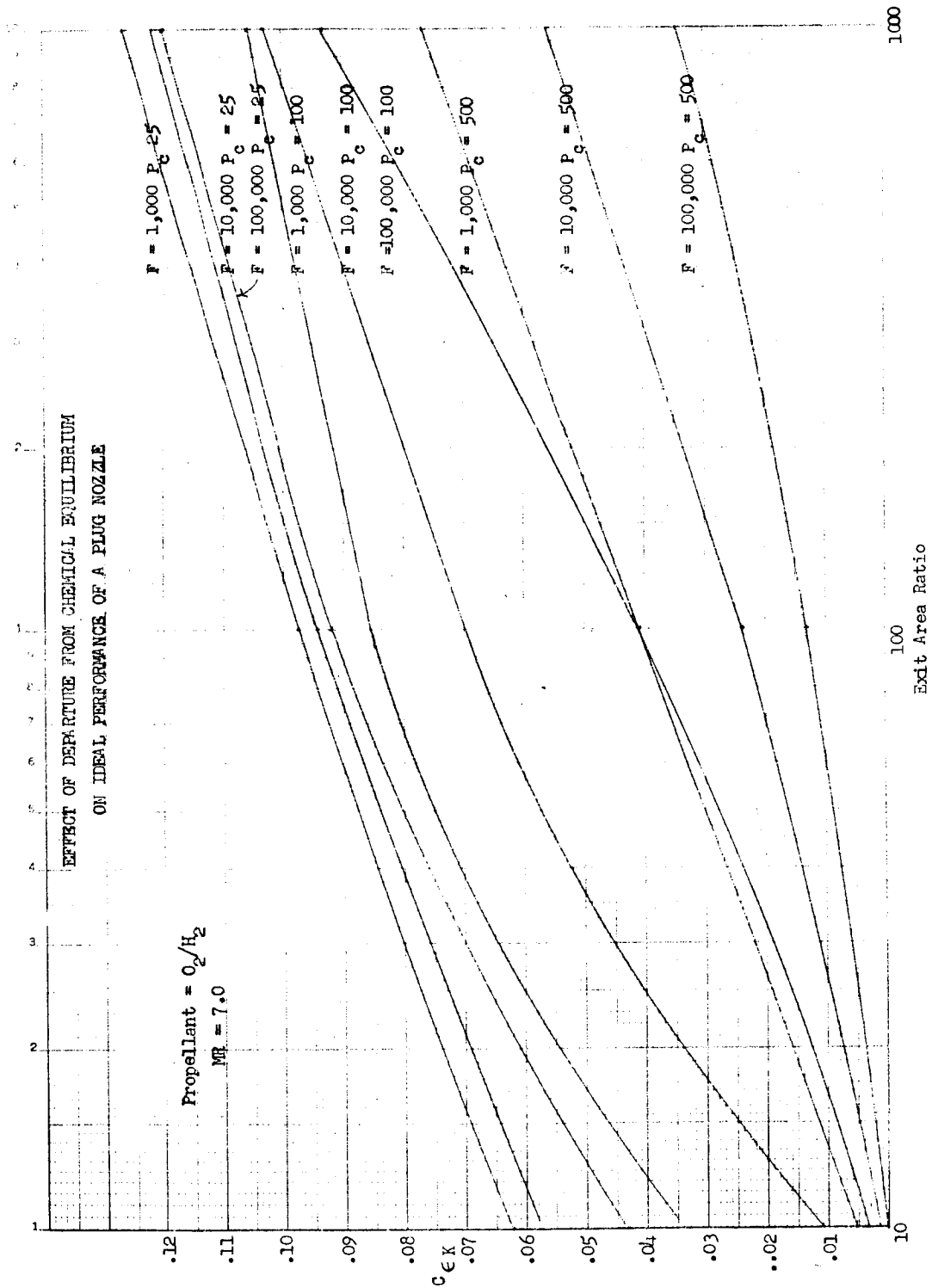


Figure 41

Kinetic Effects for Plug Nozzle, O_2/H_2 , $MR = 6.0$, $R_d/R_t = .2$



Kinetic Effects for Plug Nozzle, O_2/H_2 , MR = 7.0, $R_d/R_t = .2$

Figure 42

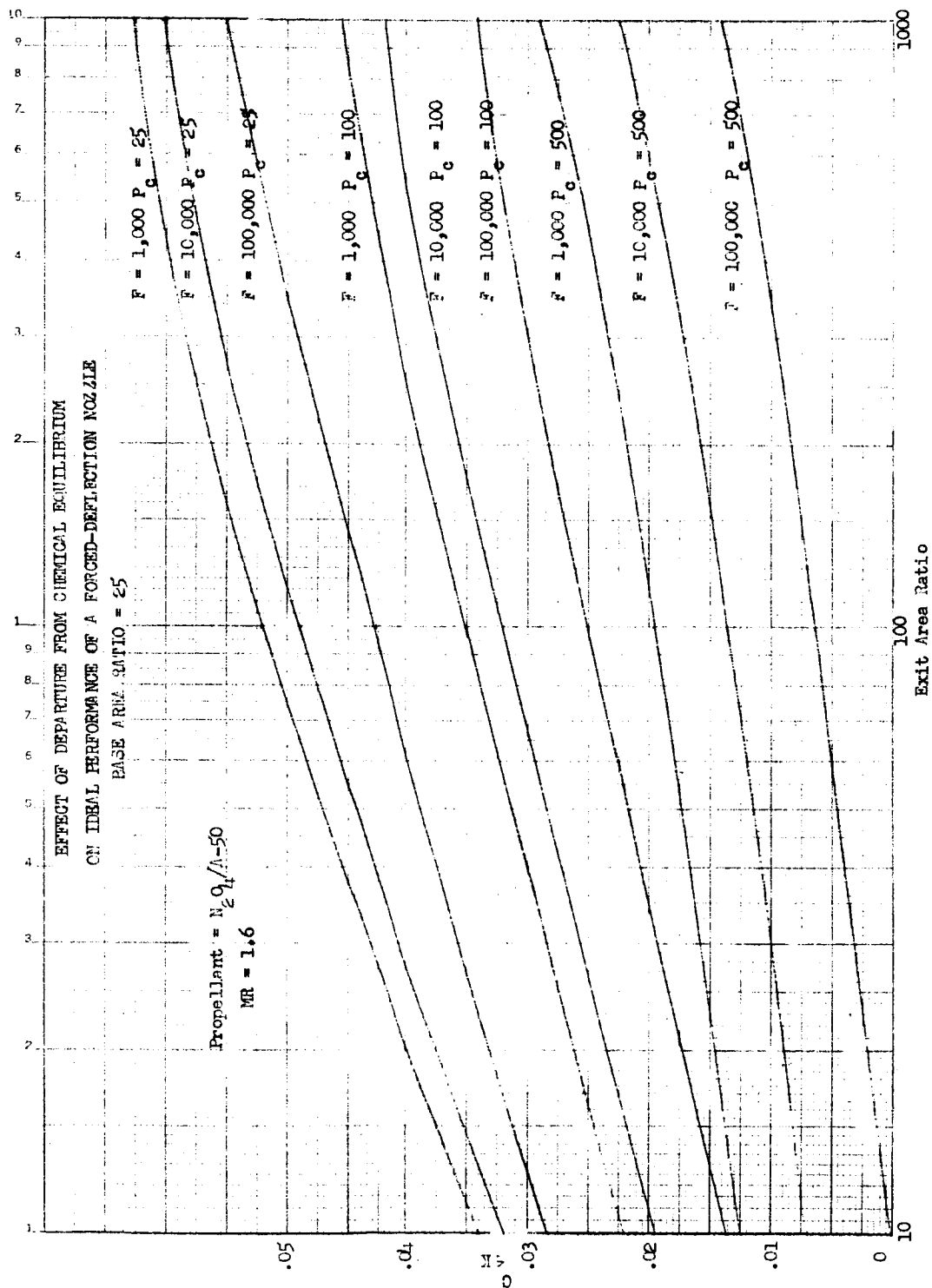


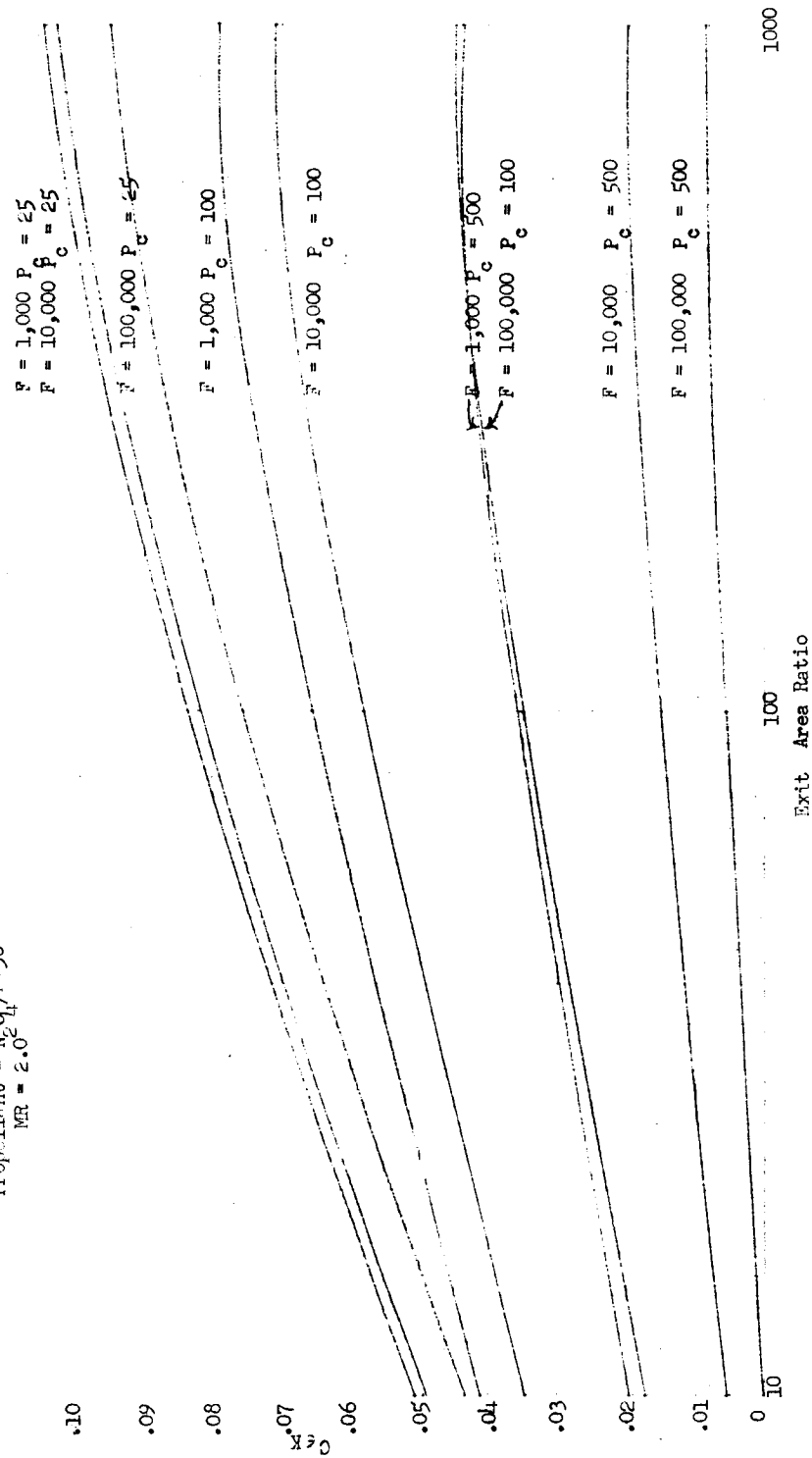
Figure 43

Kinetic Effects for Forced-Deflection Nozzle, $N_2O_4/Aerozine\ 50$, $MR = 1.6$, $R_d/R_t = .2$

EFFECT OF DEPARTURE FROM CHEMICAL EQUILIBRIUM
ON IDEAL PERFORMANCE OF A FORCED-DEFLECTION NOZZLE

BASE AREA RATIO = 25

Propellant = $N_2O_4/H-50$
MR = 2.0



c Effects for Forced-Deflection Nozzle, N_2O_4 /Aerozine 50, MR = 2.0, $R_d/R_+ =$

Figure 44

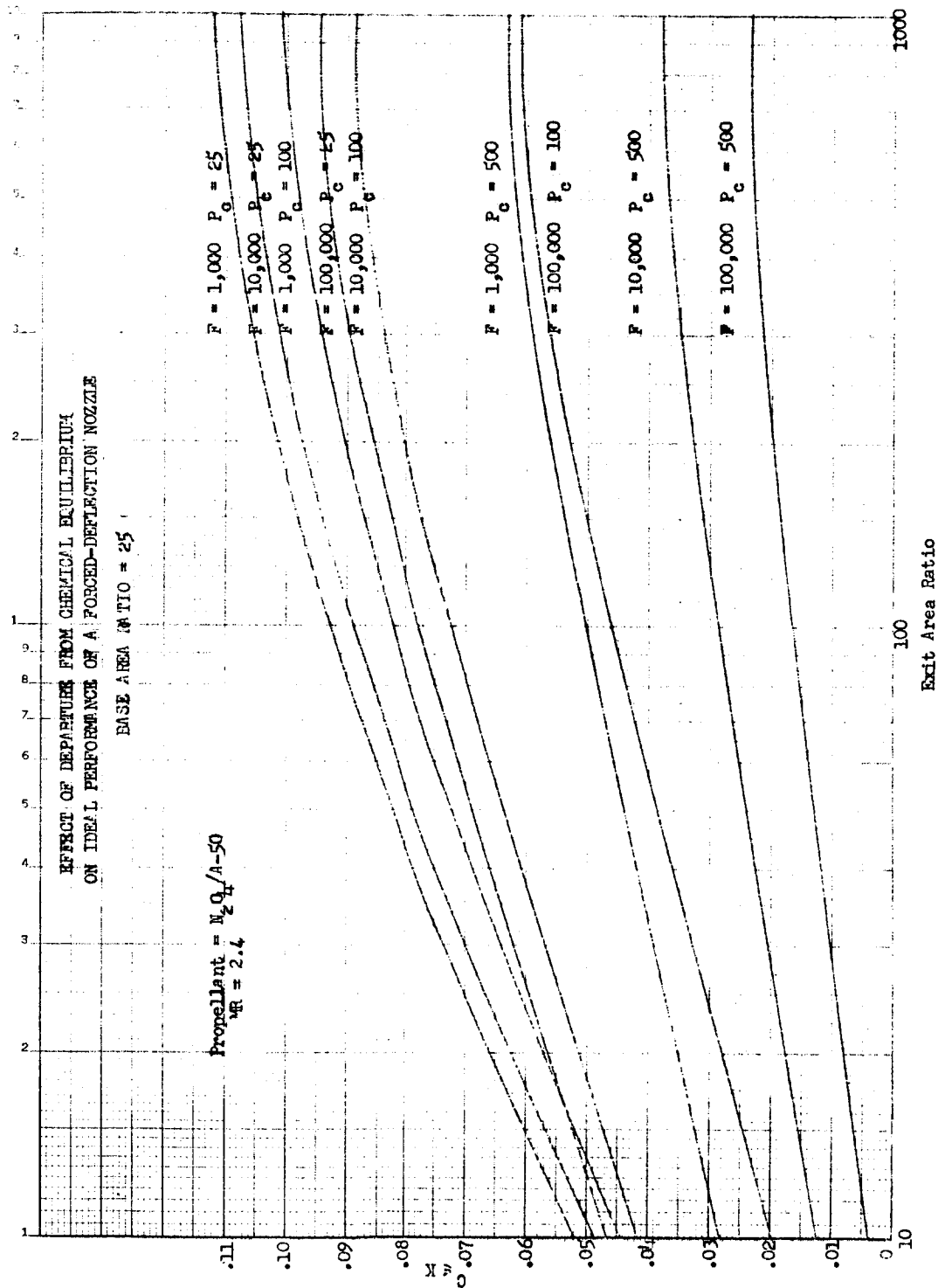
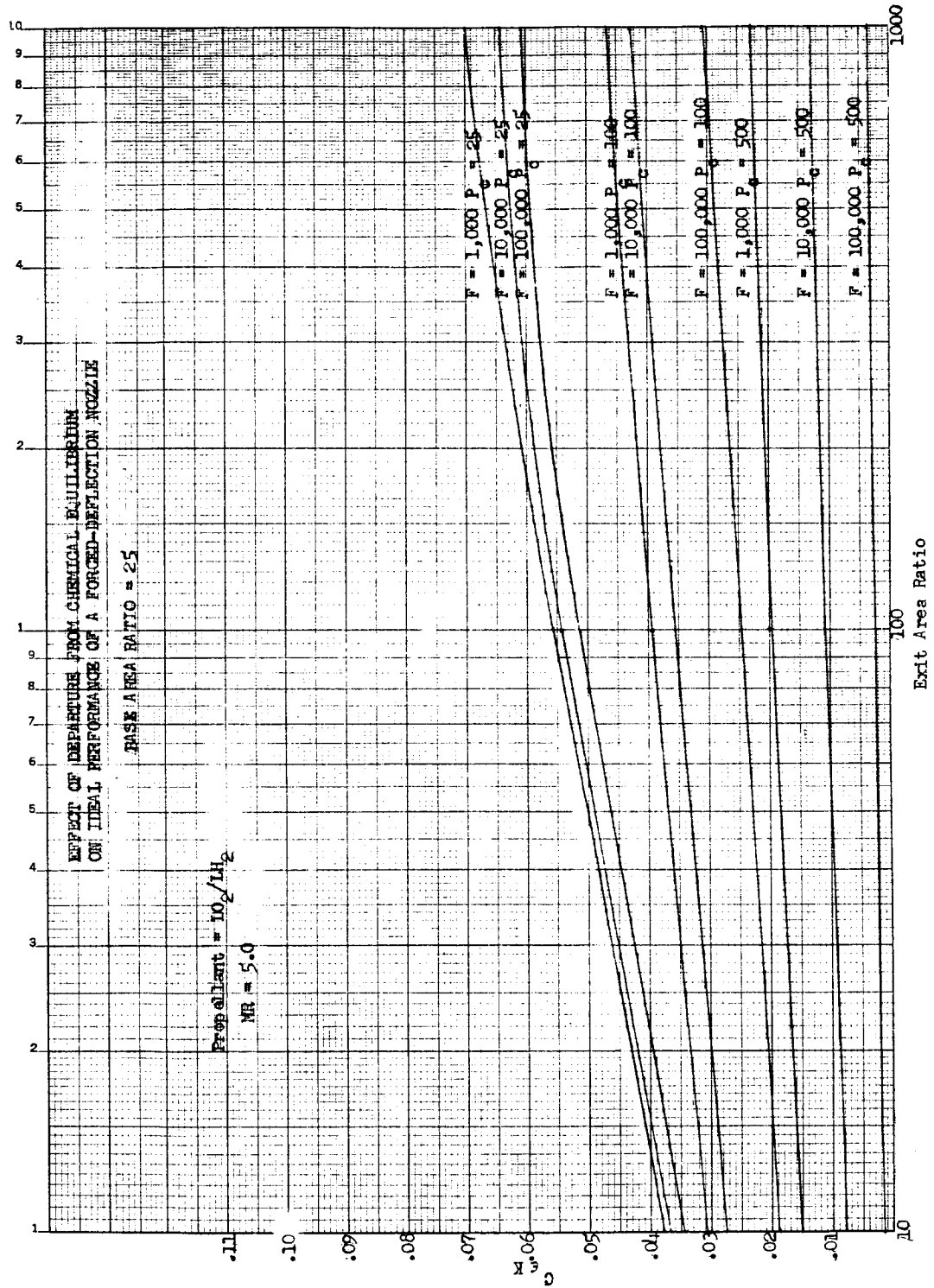


Figure 45

Kinetic Effects for Forced-Deflection Nozzle, $N_2O_4/Aerozine\ 50$, $M_R = 2.4$, $R_d/R_t = .2$



Kinetic Effects for Forced-Deflection Nozzle, LO_2/LH_2 , MR = 5.0, $R_d/R_t = .2$

Figure 46

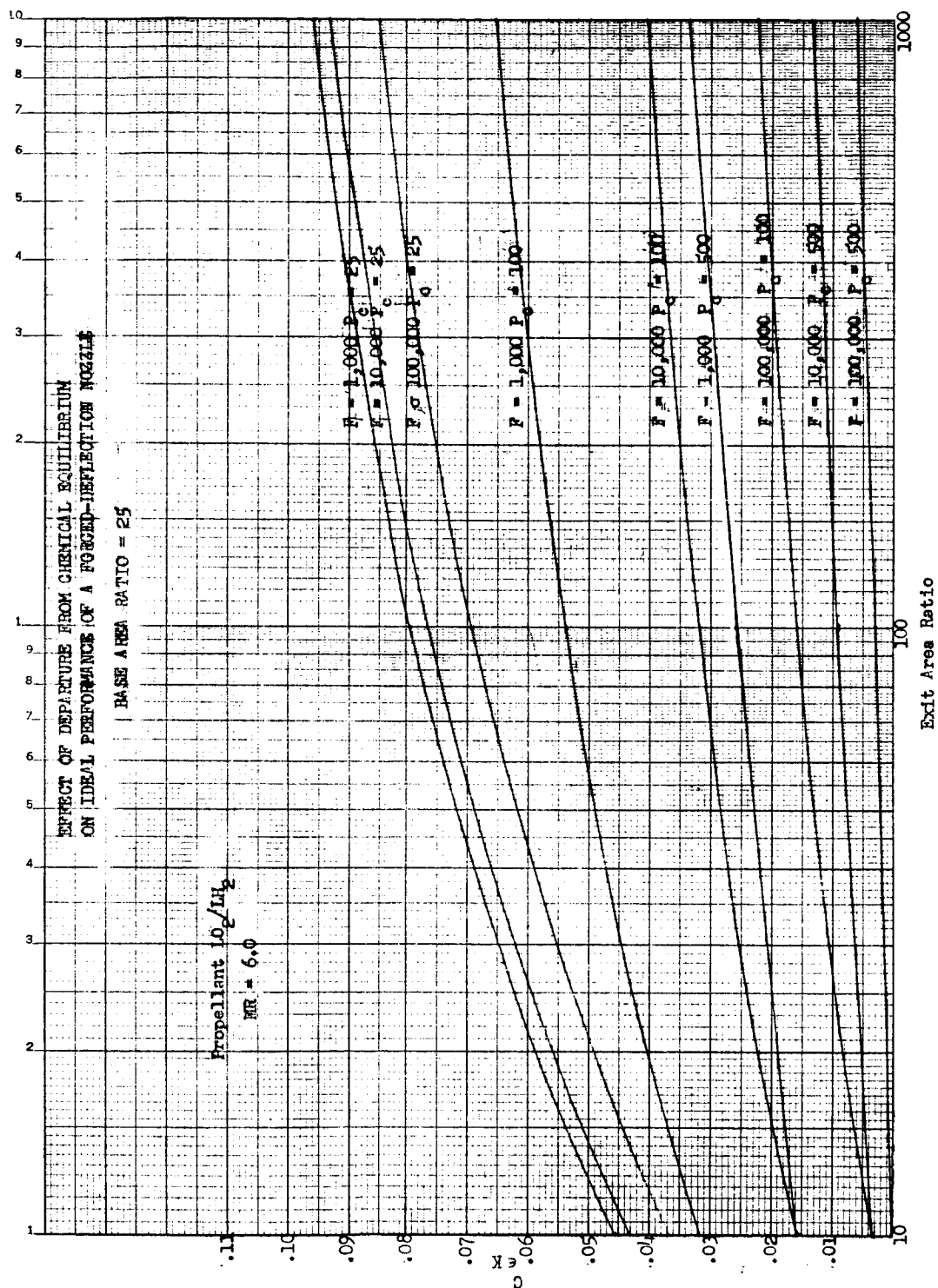


Figure 47

Kinetic Effects for Forced-Deflection Nozzle, LO_2/LH_2 , MR = 6.0, $R_d/R_t = .2$

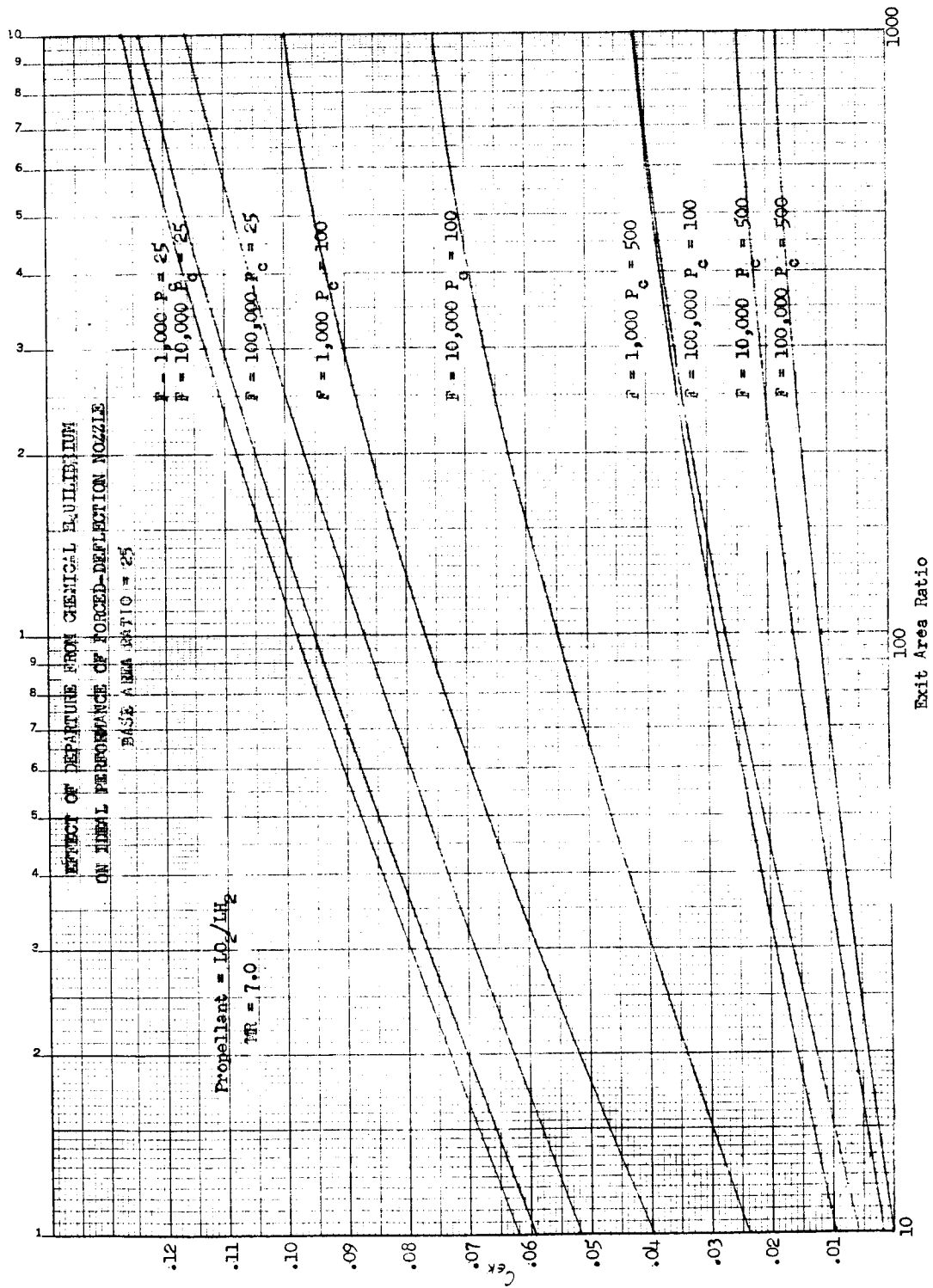


Figure 48

Kinetic Effects for Forced-Deflection Nozzle LO_2/LH_2 , $\text{MR} = 7.0$, $R_d/R_t = .2$

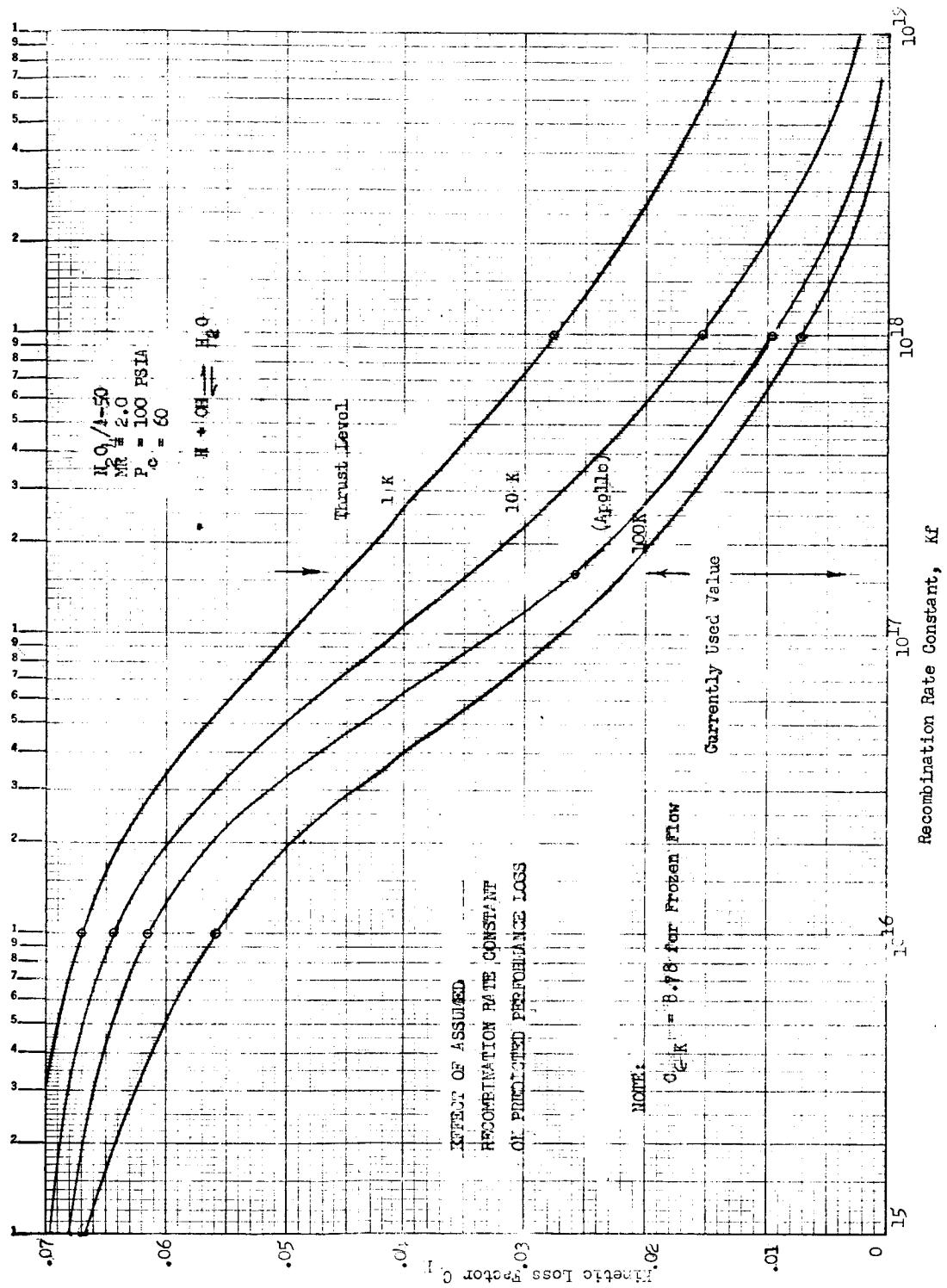


Figure 49

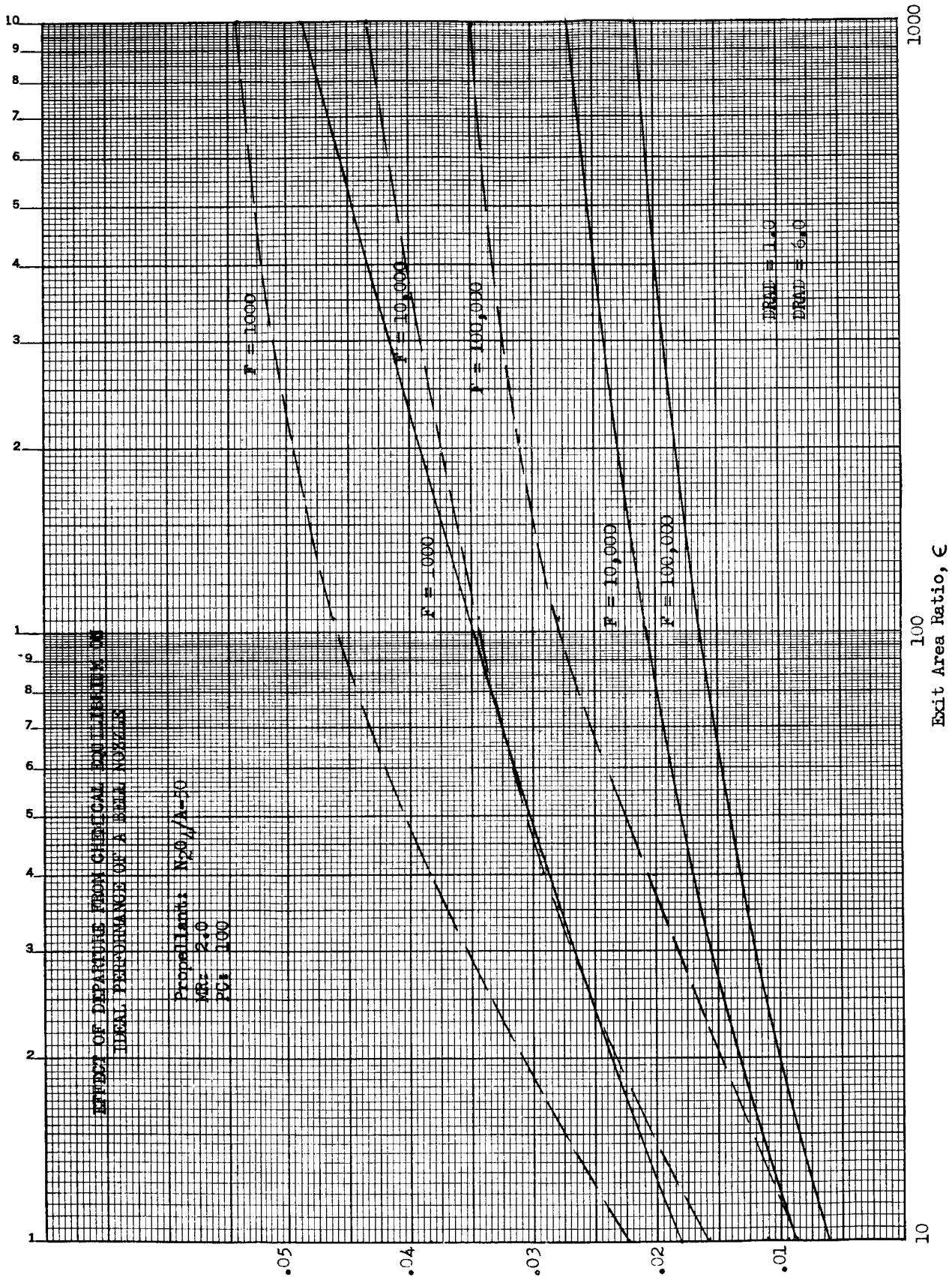


Figure 50

Effect of Departure from Chemical Equilibrium on Ideal Performance
of a Bell Nozzle, $R_D/R_T = 1.0, 6.0$

APPENDIX B

PART 1 SHEAR DRAG LOSSES

PART 2 REDUCTION OF SHEAR DRAG LOSSES

FIGURE LISTFIGURE

PART 1

Exponent N in Boundary-Layer-Velocity Profile	1
Viscosity of LO_2/LH_2 Combustion Products, Equilibrium Flow	2
Viscosity of LO_2/LH_2 Combustion Products, Frozen Flow	3
Variation of Boundary-Layer Thickness with Viscosity Exponent	4
Sonic Velocity in LO_2/LH_2 Combustion Gases	5
Boundary-Layer Displacement Thickness	6
Turbulent Flow Boundary-Layer Growth for Contoured Nozzles	7
Turbulent Flow Boundary-Layer Growth for Truncated Plug Nozzle	8
Turbulent Flow Boundary-Layer Growth for Contoured Nozzle	9
Turbulent Flow Boundary-Layer Scale Effect	10
Turbulent Flow Shear-Drag Loss for Bell (Rao) Nozzles	11
Turbulent Flow Shear-Drag Loss for Conical Nozzles	12
Turbulent Flow Shear-Drag Loss for Full Isentropic Plug Length	13
Turbulent Flow Shear-Drag Loss for 30% of Full Isentropic Plug System	14
Turbulent Flow Shear-Drag Loss for 20% of Full Isentropic Plug Length	15
Turbulent Flow Shear-Drag Loss for 10% of Full Isentropic Plug Length	16
Turbulent Flow Shear-Drag Loss for Forced-Deflection Nozzles, Base Area Ratio = 15	17
Turbulent Flow Shear-Drag Loss for Forced-Deflection Nozzles, Base Area Ratio = 25	18
Turbulent Flow Shear-Drag Loss for Forced-Deflection Nozzles, Base Area Ratio = 50	19
Turbulent Flow Shear-Drag Loss for Forced-Deflection Nozzles, Base Area Ratio = 100	20
Turbulent Flow Shear-Drag Loss for Swirling-Flow Nozzles	21
Turbulent Flow Shear-Drag Loss for Aerodynamic Nozzles, Primary Expansion-Area Ratio = 2	22
Turbulent Flow Shear-Drag Loss for Aerodynamic Nozzles, Primary Expansion-Area Ratio = 5	23
Turbulent Flow Shear-Drag Loss for Aerodynamic Nozzles, Primary Expansion-Area Ratio = 10	24
Turbulent Flow Shear-Drag Loss for Annular Nozzles	25

PART 1 SHEAR DRAG LOSSES

I. INTRODUCTION

The investigation of losses occurring in rocket nozzles due to viscous effects between the nozzle wall and the gaseous boundary layer must be undertaken before the performance of any nozzle can be accurately predicted. There are two possible methods of calculating this shear drag, the name commonly given these viscous effects: (a) momentum considerations of the viscous and inviscid portions of the nozzle gas flow, and (b) empirically derived expressions which correlate drag values with specific variables of the flow, i.e., Reynolds number, Mach number, chamber pressure, etc. The methods were applied to both high and low area ratio nozzles. Cold flow thrust data for a convergent-divergent conical nozzle having an area ratio of 18.2 was available* and a comparison of this data with the results of the drag computation using the two methods described was made. The difference between theoretical and measured thrust was 0.7%. The loss predicted by the extended Frankl-Voishel analysis considering only that portion of the nozzle downstream of the throat was 0.5%. The loss predicted by the boundary layer analysis, also considering only that portion of the nozzle downstream of the throat, was 0.8%.

Initially, it appeared that either of the methods would provide adequate shear drag values. As drag prediction was attempted for the large area ratio nozzles, a major problem was encountered. The problem arose because the nozzle contours were calculated using inviscid flow relations, and the actual Mach number was therefore less than predicted. For the low area ratio nozzles where the boundary layer is quite thin, the predicted Mach number is very nearly equal to the actual Mach number. This is not the case for high area ratio nozzles where the boundary layer is quite thick and occupies a major portion of the flow field. The boundary layer analysis was therefore of questionable value at the higher area ratios, not because the method of analysis was incorrect. The problem was that the input, (Mach number), could not be determined with sufficient accuracy.

*"Model Tests of Several Rocket Exhaust Nozzle Configurations including Thrust Vector Control Devices," R. G. Brasket and C. W. Landgraff, Fluidyne Engineering Corporation Report on Project 0160, November, 1960.

I, Introduction (cont.)

The extended Frankl-Voishel analysis was chosen as the method by which shear drag would be predicted, because it was based upon actual shear drag measurements, was simpler to use, and provided consistent drag data that appeared to be of the correct order of magnitude. Both methods of predicting shear drag losses were examined in some detail, and the main features of each are presented on the following pages.

II. BOUNDARY-LAYER CONSIDERATIONS

Skin friction drag can be predicted by means of momentum considerations, provided one has knowledge of both the velocity profile through the boundary layer, as well as the velocity of the main-stream flow at the interface between the boundary layer and the main stream.

The boundary-layer thickness was calculated using the integral momentum equation for axisymmetric flow in terms of the displacement and momentum thicknesses. The equation was simplified by several assumptions to obtain a differential equation amenable to numerical solution by Adams integration rule. The assumptions made in the program were: (1) Prandtl number equal to one, (2) $\frac{\mu}{\mu_c} = \left(\frac{T}{T_c}\right)^{\omega}$, (3) perfect gas, (4) ratio of specific heats, γ , equal to a constant, (5) gas constant, R , equal to a constant, (6) $u/u_1 = (y/\delta)^{1/7}$, and (7) $\tau_w/\rho_{am} u_1^2 = \frac{.0131}{(Re_{am})^{1/7}}$.

Figure 1 compares the equation for N with the results obtained by six investigators (1) through (6) who experimentally determined the values of N . The figure indicates that a constant value of N adequately describes the boundary layer flow field.

-
- (1) Cole, J. K., Preliminary Investigation of the Interaction of an Oblique Shock Wave and a Turbulent Boundary Layer, Master Thesis, University of New Mexico, 1961.
 - (2) Brinich, P. F., and Diaconis, N. S., "Boundary Layer Development and Skin Friction at Mach Number 3.05," NACA TN 2742, 1952.
 - (3) O'Donnell, R. M., "Experimental Investigation at Mach Number of 2.41 of Average Skin Friction Coefficients and Velocity Profiles for Laminar and Turbulent Boundary Layers and Assessment of Probe Effects," NACA TM 3122, 1954.
 - (4) Rubensin, M. W., Maydew, R. C., and Varga, S. A., "An Analytical and Experimental Investigation of the Skin Friction of the Turbulent Boundary Layer on a Flat Plate at Supersonic Speeds," NACA TN 2305, 1951.
 - (5) Wilson, R. E., "Turbulent Boundary Layer Characteristics at Supersonic Speeds - Theory and Experiment," Journal of Aeronautical Sciences, Vol. 17, No. 9, 1950.
 - (6) Schubauer, G. B., and Klebanoff, P. S., Contributions on the Boundary Layer Transition, NACA Report No. 1289, 1956.

II, Boundary Layer Considerations (cont.)

Figure 2 shows the variation in viscosity with temperature for liquid oxygen/liquid hydrogen, mixture ratio of 5, chamber pressures of 100 psia and 500 psia, under the conditions of equilibrium flow. Figure 3 is the same except that it represents viscosity versus temperature for frozen flow conditions. As can be seen from the figures, the exponent ω , used in the viscosity-temperature relation $(\frac{\mu}{\mu_c}) = (\frac{T}{T_c})^\omega$, can be considered constant for a specified flow condition and chamber pressure. The viscosity data was obtained from an Aerojet computer program using the transport properties subroutine of the thermochemical performance computer program (See Appendix A). The exponent ω was also determined for N_2O_4 /Aerozine 50 and liquid hydrogen/liquid fluorine. The effect of the viscosity exponent on the boundary layer thickness was investigated; the results are shown in Figure 4 for a nozzle having an area ratio of 200. A 10% change in viscosity exponent leads to a corresponding 1% change in boundary layer thickness. It was estimated that the viscosity exponent can be determined to within 2% and that this effect on boundary layer thickness is negligible.

Constant values of γ , ratio of specific heats, and R, gas constant, were assumed in the program. In order to determine the validity of this assumption, the sonic velocities were calculated using $a = \sqrt{\gamma gRT}$ and from an Aerojet-General program which is based on the definition of sonic velocity $a = (\frac{\partial p}{\partial \rho})^{1/2}$, and is therefore free of the assumption of constant γ and R. The results are shown in Figure B-5. The sonic velocity as determined from $a = \sqrt{\gamma gRT}$ is based upon average, constant values of γ and R for liquid oxygen/liquid hydrogen. As can be seen from Figure 5 the agreement between the two is within 2% over a temperature range of 6000°R. Constant values of γ and R were used in the program as the simplifications brought about by this assumption more than compensate for the small error introduced.

Shown in Figure 6 is displacement thickness versus distance along the contour for a bell nozzle having a throat radius of 2.167 in., an area ratio of approximately 18, and an exit Mach number of 3.433. The displacement thickness predicted at the exit by the present analysis is 5.6% greater than that predicted

II, Boundary Layer Considerations (cont.)

by the empirical relation by Monoghan and Johnson.(7) This relation relates boundary layer thickness to Mach number, Reynolds number, and distance along the contour.

Results obtained from the boundary layer program are of general interest and are presented in Figures 7 through 10. Figure 7 shows the boundary layer growth in nozzles having area ratios ranging from 10 to 200 for the LO_2/LH_2 propellant combination. Figures 8 and 9 indicate the comparison of boundary layer growth for contoured convergent-divergent nozzles and plug nozzles. Comparison indicates that the boundary layer growth is greater for external expansion nozzles than for comparable internal expansion nozzles. The plug nozzles of Figure 8 are truncated to approximately 40% of their full isentropic length. The reason for this procedure was that the plug nozzles of interest would likely be truncated to reduce weight while still retaining a high percentage of the design thrust value.

The effect of geometrically scaling nozzles on the boundary layer thickness was investigated. Figure B-10 shows the boundary layer growth in two nozzles, one of which is approximately five times as large as the other. There is definite scale effect.

(7) Monoghan, R. J., and Johnson, J. E., British ALC CP 64, 1949.

III. EMPIRICAL CONSIDERATIONS

The particular empirical relation used for predicting skin friction drag was the extended Frankl-Voishel analysis of Rubesin, Mayden, and Varga.(8) The original analysis was performed by Frankl and Voishel in 1937.(9) In their derivation, the solution to the Von Karman momentum integral could not be solved in a closed form so they performed the integration by using a power series in terms of Mach numbers. In the extended Frankl-Voishel analysis of Rubesin, Maydew, and Varga, the authors numerically integrated the Von Karman momentum integral and thereby avoided the restriction to low free stream Mach numbers.

The extended Frankl-Voishel expression for skin friction is,

$$C_{\text{FRICT}} = \frac{0.472}{(\text{LOG}_{10} \text{Re})^{2.58} \left(1 + \frac{\gamma - 1}{2} M^2\right)^{0.467}} \quad (\text{Eq 1})$$

by definition,

$$C_{\text{FRICT}} = \frac{\gamma_w}{1/2 \rho v^2} \quad (\text{Eq 2})$$

$$\gamma_w = \frac{F_w}{A} \quad (\text{Eq 3})$$

then the final expression for shear drag is,

$$dF_w = \frac{0.472 \rho v^2 dA}{2(\text{LOG}_{10} \text{Re})^{2.58} \left(1 + \frac{\gamma - 1}{2} M^2\right)^{0.467}} \quad (\text{Eq 4})$$

-
- (8) Rubesin, M. W., Maydew, R. C., and Varga, S. A., "An Experimental and Analytical Investigation of the Skin Friction of the Turbulent Boundary Layer on a Flat Plate at Supersonic Speeds," NACA TN 2305, February 1951.
- (9) Frankl, F., and Voishel, V., "Friction in the Turbulent Boundary Layer of a Compressible Gas at High Speeds," NACA TM 1032, 1942.

III, Empirical Considerations (cont.)

and the shear drag loss, C_{ED} is,

$$C_{ED} = \frac{\text{shear drag} = F_w}{\text{ideal one-dimensional thrust} = C_{F_{1-D}} P_c A_t C_d} \quad (\text{Eq 5})$$

Equation 4 was numerically integrated by means of a computer. By using the correct expression for area, a series of eight different types of nozzles were studied.

The viscosity term appearing in the Reynolds number was calculated from the equation $\mu = \mu_o (T/T_o)^w$ where the value of w for each propellant studied was determined from chemical composition data as explained in the boundary-layer analysis. The Reynolds number was based upon distance along the contour using properties evaluated at an arithmetic mean temperature which was an averaged value of wall and free-stream temperature.

The shear-drag losses, C_{ED} , have been calculated for the contoured (Rao), conical, plug, forced-deflection, swirling-flow, annular, shrouded, and clustered nozzles. The losses are shown in Figure 11 through 25. The plug-nozzle losses shown are for the full isentropic plug, as well as for plug nozzles truncated to 10, 20, and 30% for the full isentropic plug length. The forced-deflection nozzle losses are calculated for base area ratios of 15, 25, 50, and 100. The shear-drag curves show the drag loss as a function of area ratio for four values of $F P_c$ (Thrust x Chamber Pressure): 1, 10, 100, and 1,000 $\frac{(\text{lbs})^2}{\text{in}}$

During the analysis of the shear-drag data, it was necessary to plot curves of drag loss versus thrust for a specific area ratio and several chamber pressures. This would result in a large number of necessary plots, but if two of the four variables (C_{ED} , ϵ , P_c , F) could be combined, presentation of the data could be simplified. The drag loss parameter C_{ED} is a function of the parameter $F P_c$ only for a fixed area ratio nozzle. This may be shown by means of the following argument:

III, Empirical Considerations (cont.)

For a fixed area ratio nozzle

$$D = \frac{\rho \mu^2 (0.472) A_{\text{surface}}}{2 \left[\log \frac{\rho V X}{\mu} \right]^{2.58} \left[1 + \frac{\gamma-1}{2} M^2 \right]^{0.467}}$$

and since $\rho \propto P_c$ and $X \propto \sqrt{A_t}$,

$$\frac{D}{F} \propto \frac{P_c A_t}{\left[\log_{10} (P_c \sqrt{A_t}) \right]^{2.58} P_c A_t}$$

where

$$F \propto P_c A_t$$

$$\frac{D}{F} \propto \frac{1}{\left[\log_{10} P_c \sqrt{\frac{F}{P_c}} \right]^{2.58}}$$

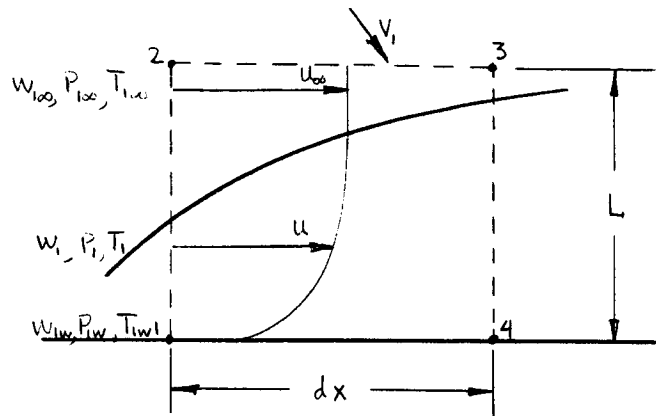
$$\frac{D}{F} = C_{\epsilon D} \propto \frac{1}{\left[\log_{10} \sqrt{F P_c} \right]^{2.58}}$$

so that $F P_c$ is indeed a parameter by which geometrically similar nozzles can be compared.

By plotting the curves for each of the propellants and nozzle types, it was observed that the curves were parallel and that they could all be represented by a single curve to which suitable scaling could be applied (β factor). The effect of propellant variation upon drag loss could then be easily calculated. The factor was determined by plotting the drag loss versus area ratio for a few nozzle types, (bell, plug, and forced-deflection), and then manually shifting the curves an amount, β , so that the curves for several propellants could be represented by a single curve. The factor β was found to be a constant that is independent of nozzle type.

III, Empirical Considerations (cont.)

PART 2 -- REDUCTION OF SHEAR DRAG LOSSES



The following is a derivation of the expression for shear stress with mass injection:

mass flow through plane 1-2

$$\dot{m}_{1-2} = \int_0^L \rho u dy$$

Mass flow through plane 3-4

$$\dot{m}_{3-4} = \int_0^L \rho u dy + \frac{d}{dx} \left[\int_0^L \rho u dy \right] dx$$

Mass flow through plane 2-3

$$\dot{m}_{2-3} = \rho_\infty V_1 dx$$

Mass flow through plane 1-4

$$\dot{m}_{1-4} = \int w_w V_w dx$$

III, Empirical Considerations (cont.)

Applying the conservation of mass principle

$$\dot{m}_{3-4} = \dot{m}_{1-2} + \dot{m}_{1-4} + \dot{m}_{2-3}$$

$$\int_0^L \rho u dy + \frac{d}{dx} \left[\int_0^L \rho u dy \right] dx = \int_0^L \rho u dy + \rho_w V_w dx + \rho_w V_1 dx$$

$$\frac{d}{dx} \int_0^L \rho u dy = \rho_w V_w + \rho_w V_1$$

Momentum through plane 1-2

$$\int_0^L \rho u^2 dy$$

Momentum through plane 3-4

$$\int_0^L \rho u^2 dy + \frac{d}{dx} \left[\int_0^L \rho u^2 dy \right] dx$$

Momentum through plane 2-3

$$\rho_w V_1 U_\infty dx$$

Momentum through plane 1-4

$$\rho_w V_w U_\infty dx$$

Applying the momentum principle: change in momentum through control volume equals the sum forces acting on the control volume.

III, Empirical Considerations (cont.)

$$\Delta \text{momentum} = \Delta(\dot{m}v) = \gamma_w + PL - \left[PL + \frac{d}{dx} (PL) dx \right]$$

$$\Delta(\dot{m}v) = \gamma_w + \frac{d}{dx} (PL) dx$$

$$(\dot{m}v)_{1-2} + (\dot{m}v)_{2-3} + (\dot{m}v)_{1-4} - (\dot{m}v)_{3-4} = \gamma_w + \frac{d}{dx} (PL) dx$$

$$\int_0^L \rho u^2 dy + \rho_\infty V_1 U_\infty dx + \rho_w V_w U_w dx - \int_0^L \rho u^2 dy - \frac{d}{dx} \left[\int_0^L \rho u^2 dy \right] dx = \gamma_w + \frac{d}{dx} (PL) dx$$

Since $U_w = 0$

$$\frac{d}{dx} \int_0^L \rho u^2 dy - \rho_\infty V_1 U_\infty = - \gamma_w - L \frac{dP}{dx}$$

The free stream velocity can be related to the axial pressure gradient by using Bernoulli's equation,

$$\frac{dP}{dx} = - \rho_\infty U_\infty \frac{du_\infty}{dx}$$

Substituting Eq's. 7 and 18 into Eq. 17

$$\frac{d}{dx} \int_0^L \rho u^2 dy + \rho_w V_w U_\infty - U_\infty \frac{d}{dx} \int_0^L \rho u dy = - \gamma_w + \rho_\infty U_\infty L \frac{du_\infty}{dx}$$

since U_∞ does not depend on Y

$$\rho_s U_s L \frac{du_s}{dx} = \rho \frac{du_s}{dx} \int_0^L U_s dy$$

Substituting Eq. (20) into Eq. (19)

$$\gamma_w = \frac{d}{dx} \int_0^L \rho u (u_\infty - u) dy + \frac{du_s}{dx} \int_0^L (\rho_\infty U_\infty - \rho u) dy - \rho_w V_w U_\infty$$

III, Empirical Considerations (cont.)

By definition of displacement and momentum thickness

$$\delta^* = \int_0^\delta \left(1 - \frac{\rho u}{\rho_\infty u_\infty}\right) dy$$

$$\theta = \int_0^\delta \left(\frac{\rho u}{\rho_\infty u_\infty} - \frac{\rho u^2}{\rho_\infty u_\infty^2}\right) dy$$

Substituting Eq. (22) and (23) into Eq. (21)

$$\frac{\gamma_w}{\rho_\infty u_\infty^2} = \frac{d\theta}{dx} + \frac{\theta}{u_\infty} \frac{du_\infty}{dx} \left[2 - M_\infty^2 + \frac{\delta^*}{\theta} - \frac{\rho_w V_w}{\rho_\infty u_\infty} \right]$$

Effect on performance of injecting through nozzle wall rather than through nozzle throat:

Equivalence of thrust and specific impulse for injection through the experimental nozzle walls versus injection through the nozzle throat:

$$\frac{(I_s)_w}{(I_s)_t} = \frac{\frac{F_i}{\dot{w}_s + \dot{w}_p}}{\frac{F_s + F_p}{\dot{w}_s + \dot{w}_p}} = \frac{F_i}{F_s + F_p}$$

The method used to compute this ratio is described below. The flow rate through a sonic nozzle may be computed from:

$$\dot{w} = \rho V A = \frac{M P_c A_t \left(1 + \frac{\gamma-1}{2} M^2\right)^{\frac{1}{2}}}{\sqrt{RT_c}}$$

III, Empirical Considerations (cont.)

since $M = 1.0$ at the throat

$$\dot{w} = P_c A_t \sqrt{\frac{\gamma g}{RT_c}} \left(\frac{2}{\gamma+1} \right)^{\frac{\gamma+1}{2(\gamma-1)}}$$

By definition $F = C_F P_c A_t$

$$\frac{(I_s)_w}{(I_s)_t} = \frac{(C_F P_c A_t)_i}{(C_F P_c A_t)_s + (C_F P_c A_t)_p}$$

Assume the primary and secondary nozzles have the same area ratio and chamber pressure, and that the primary nozzle has the same throat area as the nozzle utilizing injection through the wall.

$$\frac{(I_s)_w}{(I_s)_t} = \frac{C_{Fi} A_{tp}}{(C_F A_t)_s + (C_F A_t)_p}$$

$$\frac{\dot{w}_s}{\dot{w}_p} = \frac{\left[P_c A_t \sqrt{\frac{\gamma g}{RT_c}} \left(\frac{2}{\gamma+1} \right)^{\frac{\gamma+1}{2(\gamma-1)}} \right]_s}{\left[P_c A_t \sqrt{\frac{\gamma g}{RT_c}} \left(\frac{2}{\gamma+1} \right)^{\frac{\gamma+1}{2(\gamma-1)}} \right]_p}$$

$$A_{ts} = \frac{\dot{w}_s}{\dot{w}_p} \frac{\left[P_c A_t \sqrt{\frac{\gamma g}{RT_c}} \left(\frac{2}{\gamma+1} \right)^{\frac{\gamma+1}{2(\gamma-1)}} \right]_p}{\left[P_c \sqrt{\frac{\gamma g}{RT_c}} \left(\frac{2}{\gamma+1} \right)^{\frac{\gamma+1}{2(\gamma-1)}} \right]_s}$$

or

$$A_{ts} = \frac{\dot{w}_s}{\dot{w}_p} \frac{K_p A_{tp}}{K_s} \frac{P_{cp}}{P_{cs}}$$

III, Empirical Considerations (cont.)

Where K is a constant which depends upon the properties of the primary and secondary gases.

Substituting Equation (9) into Equation (6)

$$\frac{(I_s)_w}{(I_s)_t} = \frac{C_{Fi}}{C_{Fs} \frac{\dot{w}_s}{\dot{w}_p} \frac{K_p}{K_s} + C_{FP}}$$

$$\frac{(I_s)_w}{(I_s)_t} = \frac{C_{Fi}}{C_{FP} \frac{C_{Fs}}{C_{FP}} \frac{\dot{w}_s}{\dot{w}_p} \frac{K_p}{K_s} + 1}$$

$$\frac{(I_s)_w}{(I_s)_t} = \frac{F_i P_{ci} A_{tp}}{P_{ci} A_{tp} F_p \left[\frac{C_{Fs}}{C_{FP}} \frac{\dot{w}_s}{\dot{w}_p} \frac{K_p}{K_s} + 1 \right]}$$

For air with Helium injection

$$\frac{C_{Fs}}{C_{FP}} \frac{K_p}{K_s} = 2.27$$

$$\frac{(I_s)_w}{(I_s)_t} = \frac{F_i P_{ci}}{F_o P_{ci} (1 + 2.27 \frac{\dot{w}_s}{\dot{w}_p})}$$

For air with nitrogen injection

$$\frac{C_{Fs}}{C_{FP}} \frac{K_p}{K_s} = 1.017$$

$$\frac{(I_s)_w}{(I_s)_t} = \frac{F_i P_{ci}}{F_o P_{ci} (1 + 1.017 \frac{\dot{w}_s}{\dot{w}_p})}$$

SYMBOLS LIST

A	Surface area, ft^2
a	Sonic velocity, ft/sec
A_t	Throat cross sectional area, ft
C_{frict}	Skin friction coefficient
C_{ED}	Shear drag loss
F	Rocket thrust, lbs
F_w	Shear drag, lbs
g	Gravitational acceleration, ft/sec^2
M	Mach number
N	Exponent in velocity profile
P	Pressure, lbs/ft^2
R	Gas constant, $\text{ft}\cdot\text{lb}_f/\text{lb}_m\cdot^\circ\text{R}$
r	Nozzle radius, ft
Re	Reynolds number
S	Entropy
T	Absolute temperature, degrees rankine
u	Velocity component in axial direction, ft/sec
v	Velocity component normal to wall, ft/sec
x	Distance from nozzle throat measured along nozzle contour
Y	Distance normal to wall, ft
δ	Boundary layer thickness, ft
δ^*	Boundary layer displacement thickness, ft
γ	Ratio of specific heats
ρ	Density, lbs/ft^3
μ	Dynamic viscosity $\text{lb}_m/\text{ft}\cdot\text{sec}$
ω	Viscosity exponent
τ	shearing stress, lbs/ft^2
θ	Nozzle wall angle and momentum thickness, degrees and ft

SYMBOLS LIST (cont.)

Subscripts

AM	Conditions evaluated at arithmetic mean temperature $T_{am} = \frac{T_w + T_1}{2}$
C	Conditions at the chamber
p	Primary
s	Secondary
w	Conditions at the wall
l	Conditions at the edge of the boundary layer
t	Throat conditions
∞	Free stream conditions

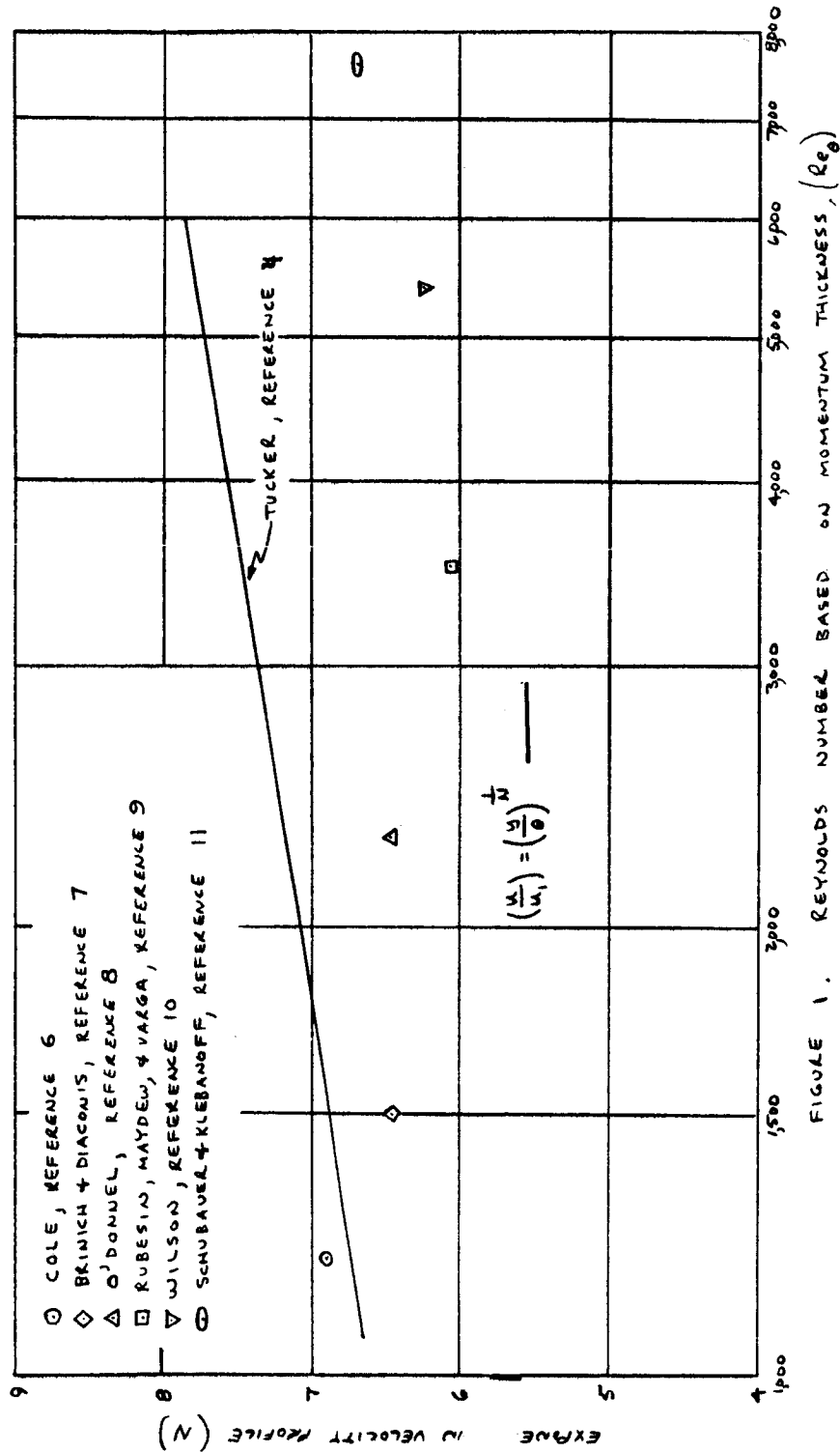
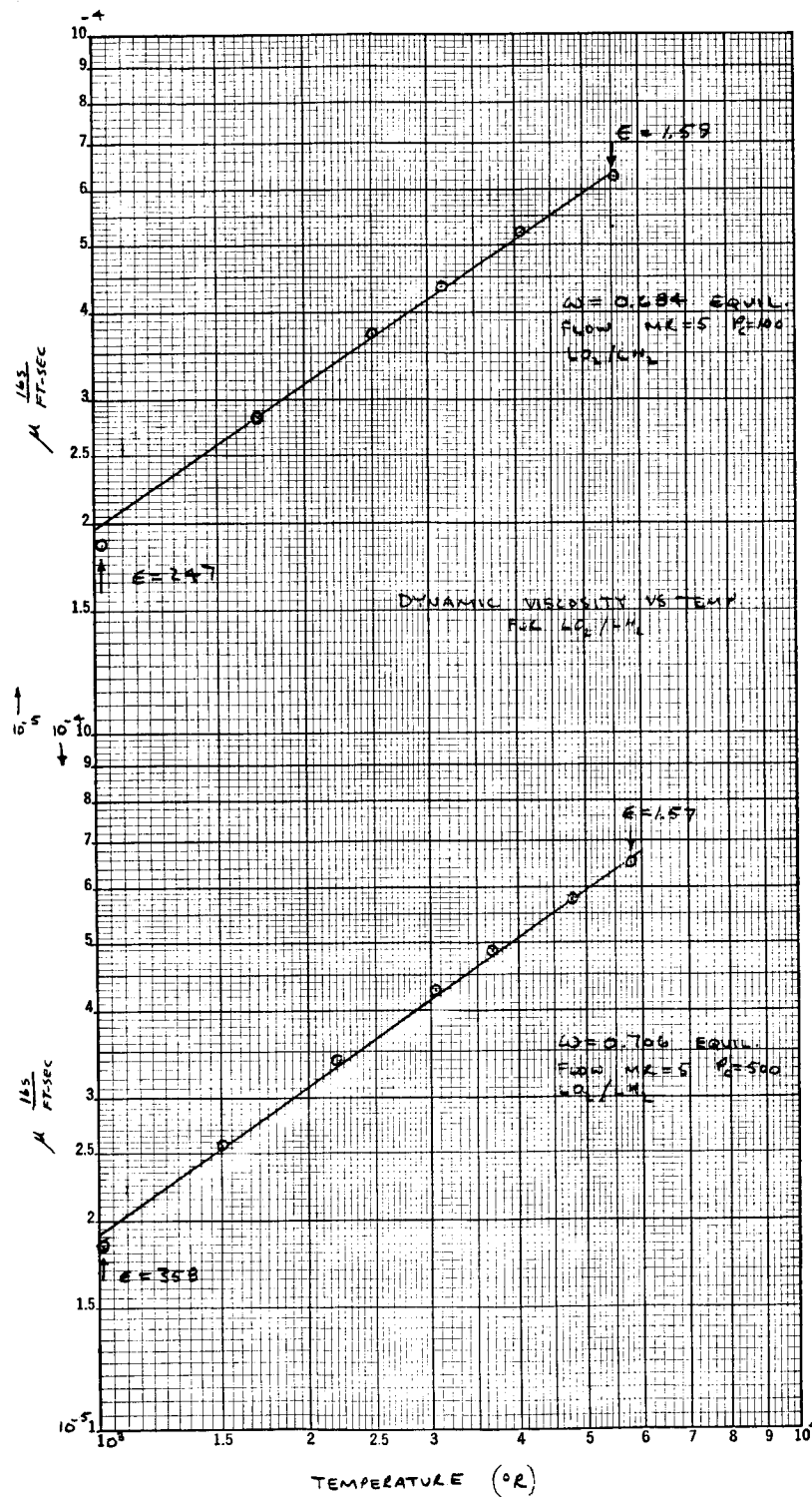


FIGURE 1. REYNOLDS NUMBER BASED ON MOMENTUM THICKNESS, (Re_0)

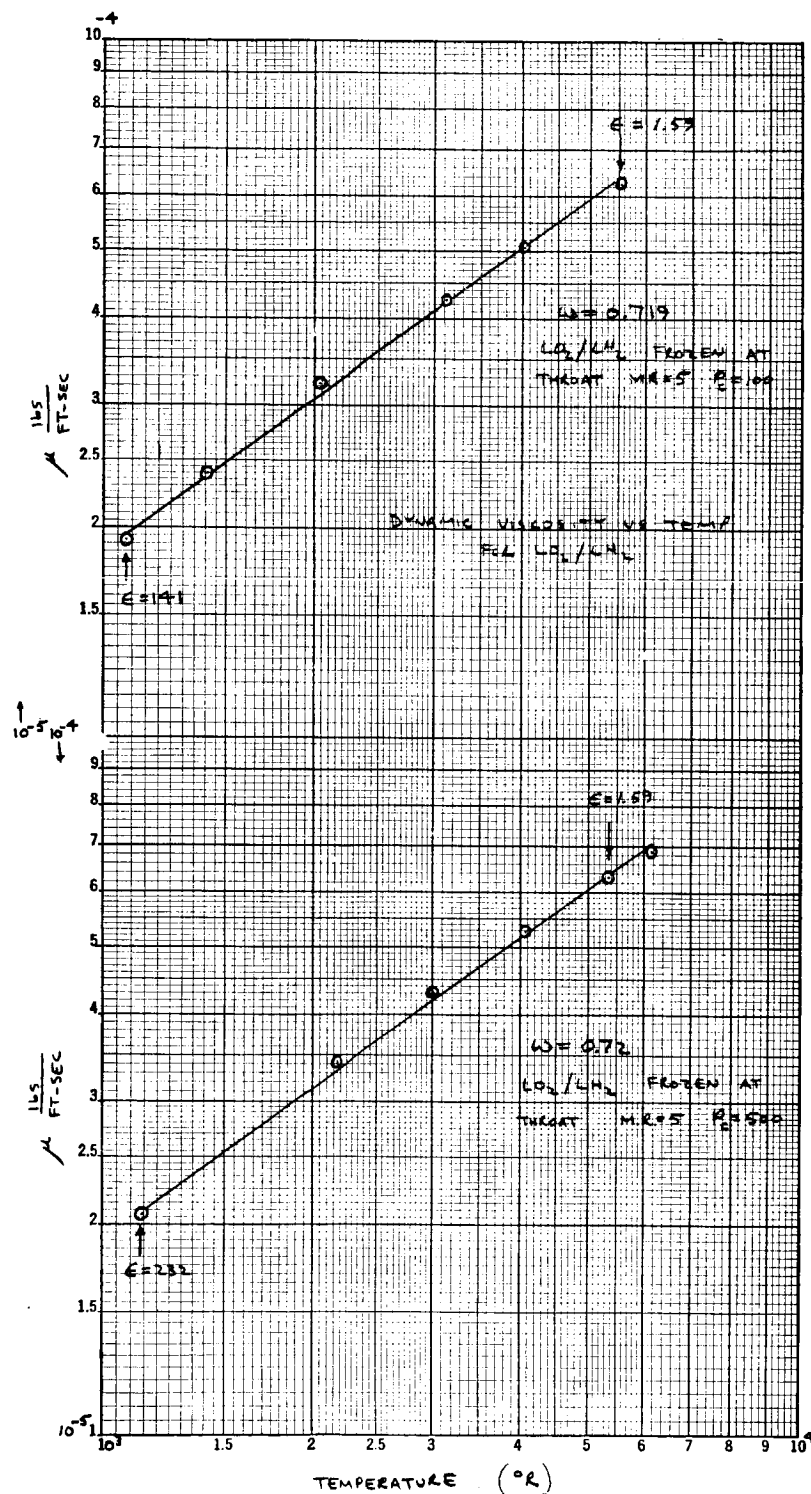
VARIATION OF VELOCITY PROFILE EXPONENT WITH REYNOLDS NUMBER

Figure 1



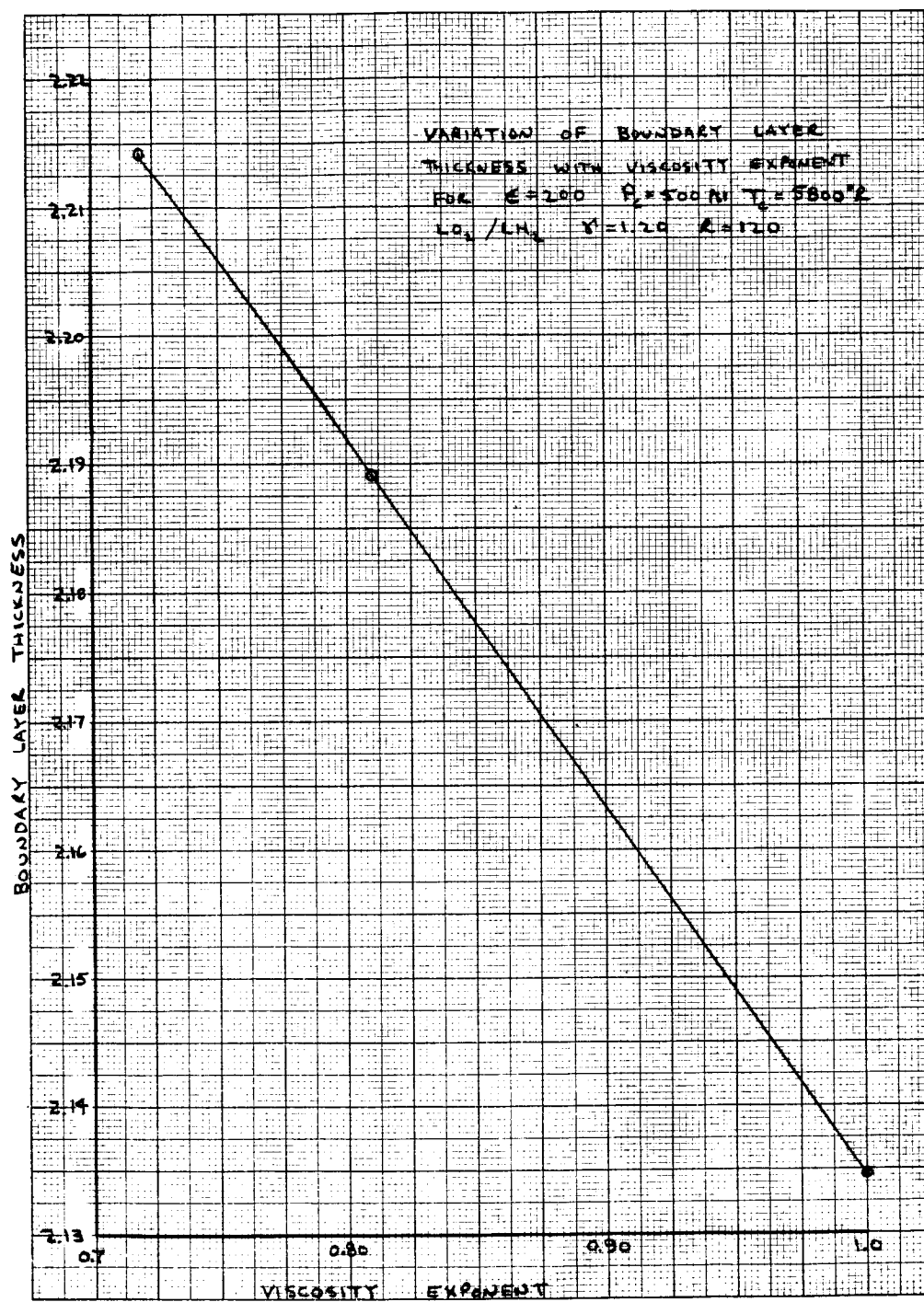
Viscosity of LO_2/LH_2 Combustion Products, Equilibrium Flow

Figure 2



Viscosity of LO_2/LH_2 Combustion Products, Frozen Flow

Figure 3



Variation of Boundary-Layer Thickness with Viscosity Exponent

Figure 4

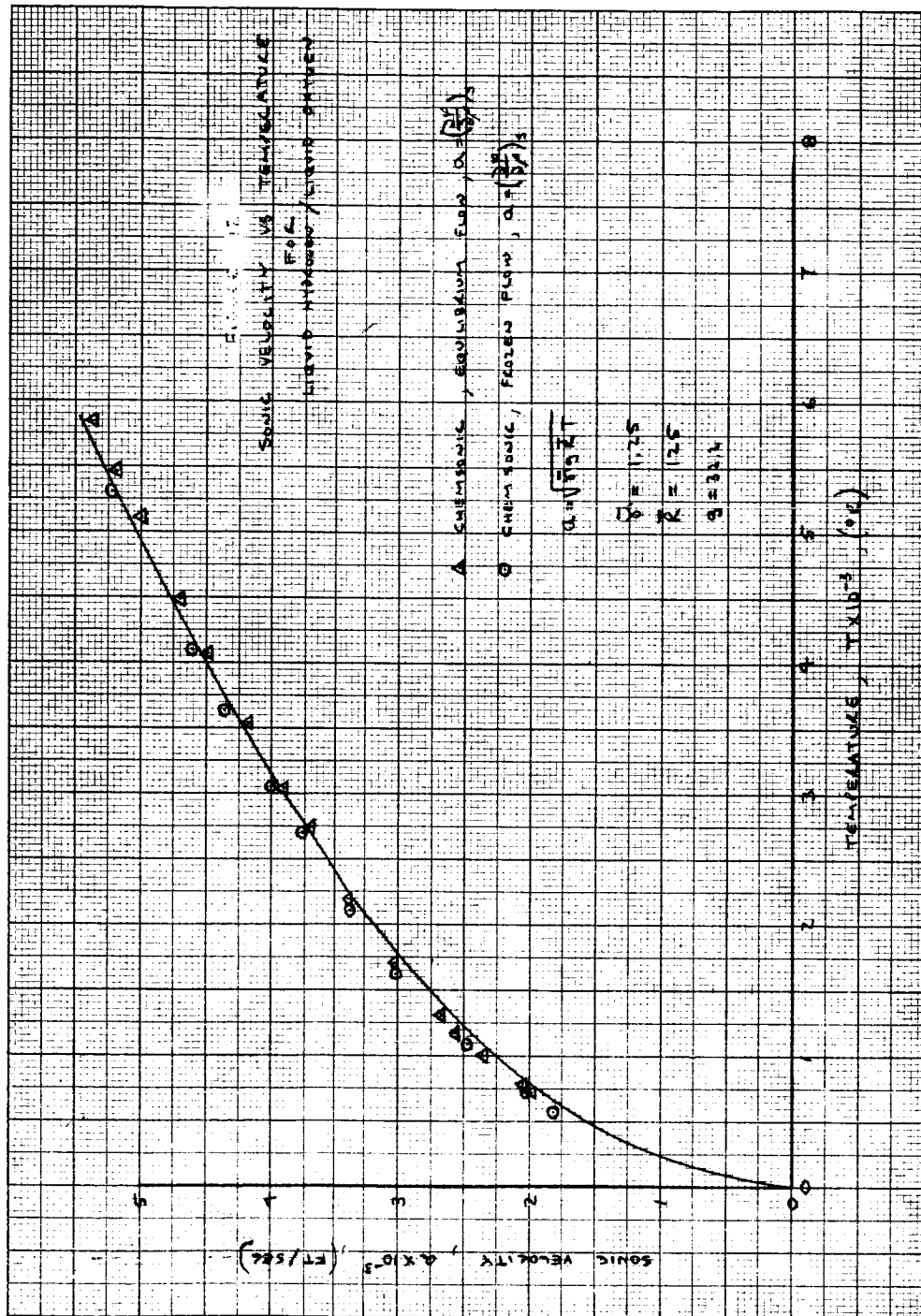


Figure 5

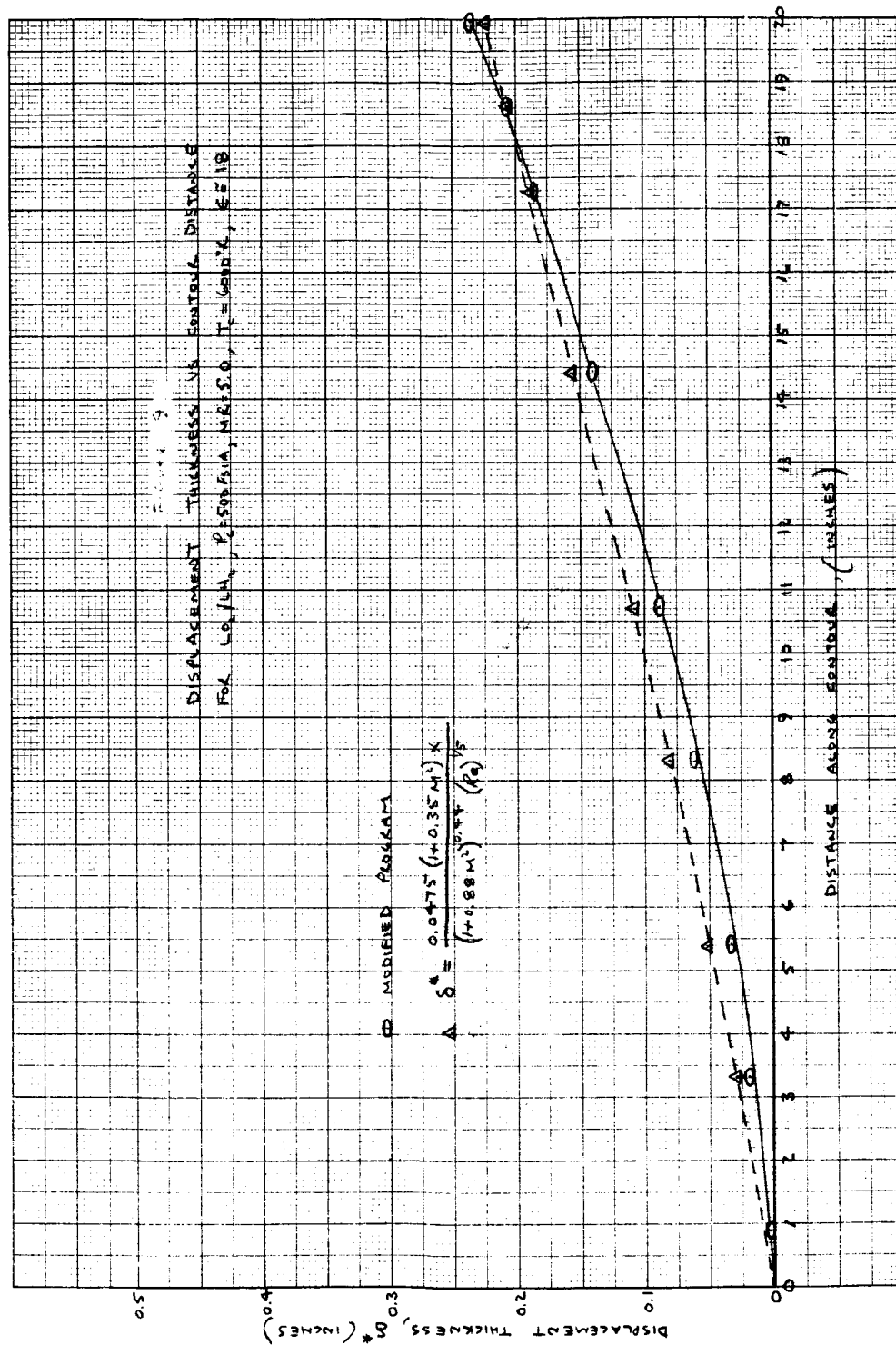


Figure 6

Boundary-Layer Displacement Thickness

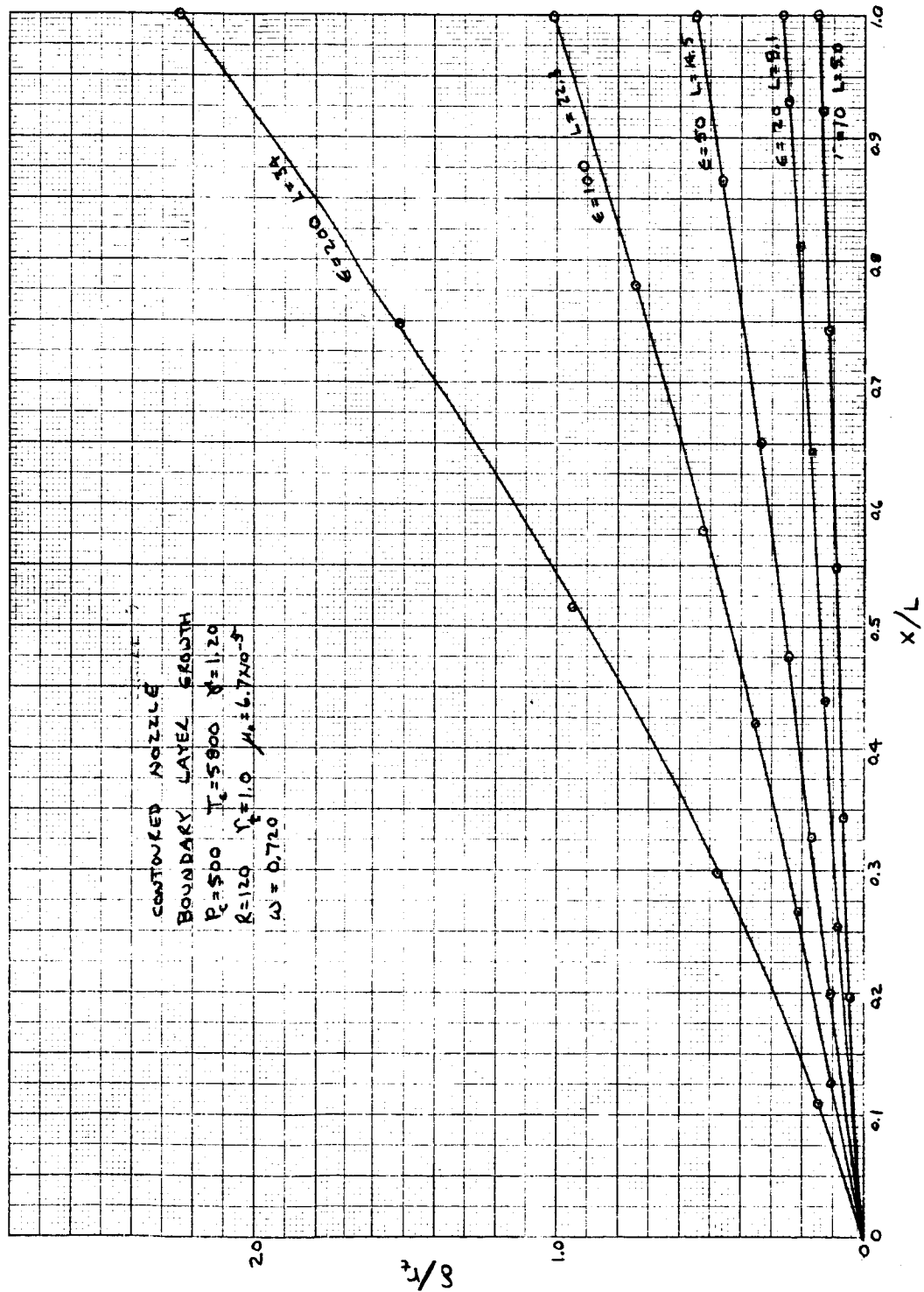


Figure 7

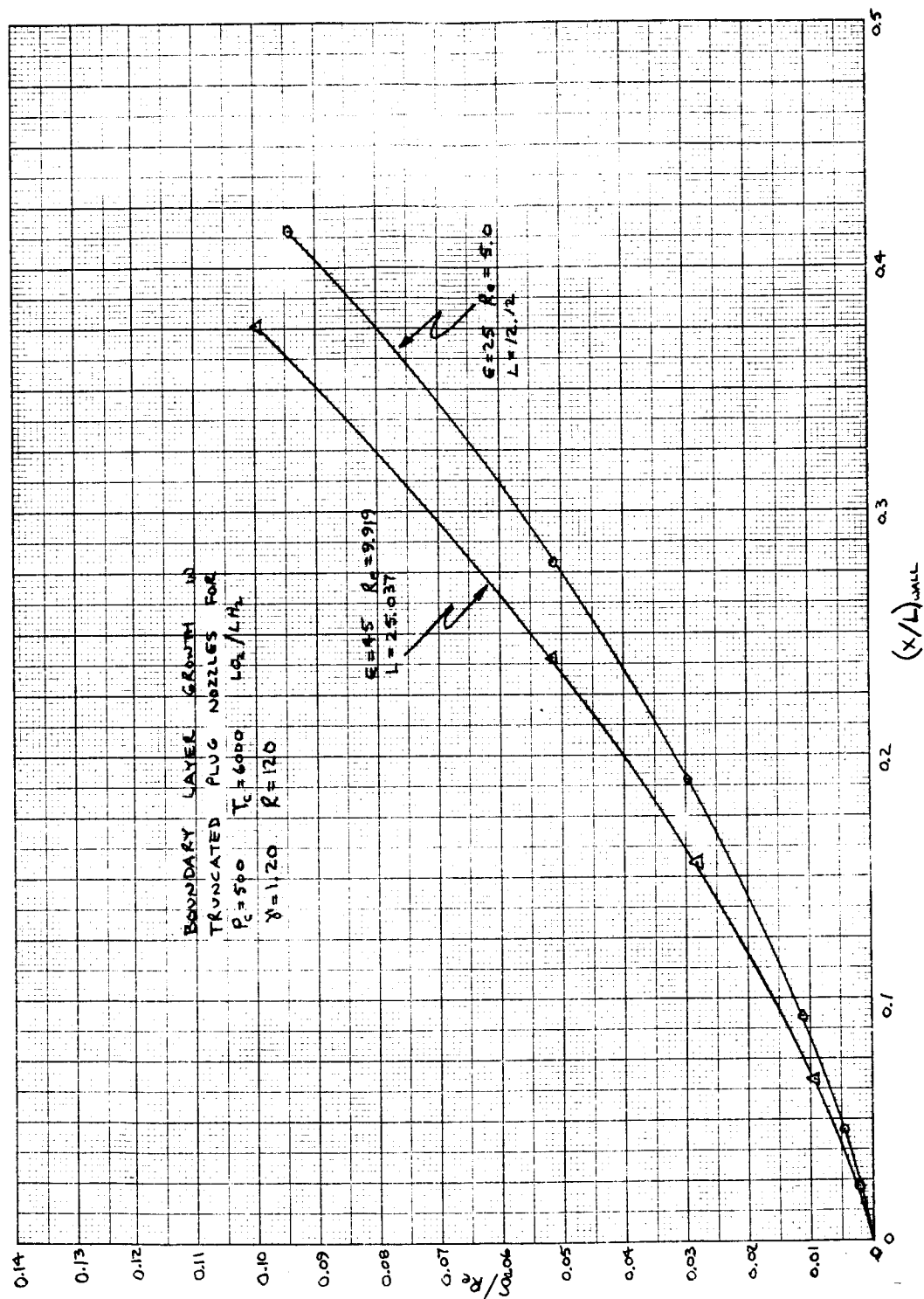


Figure 8

Turbulent Flow Boundary-Layer Growth for Truncated Plug Nozzle

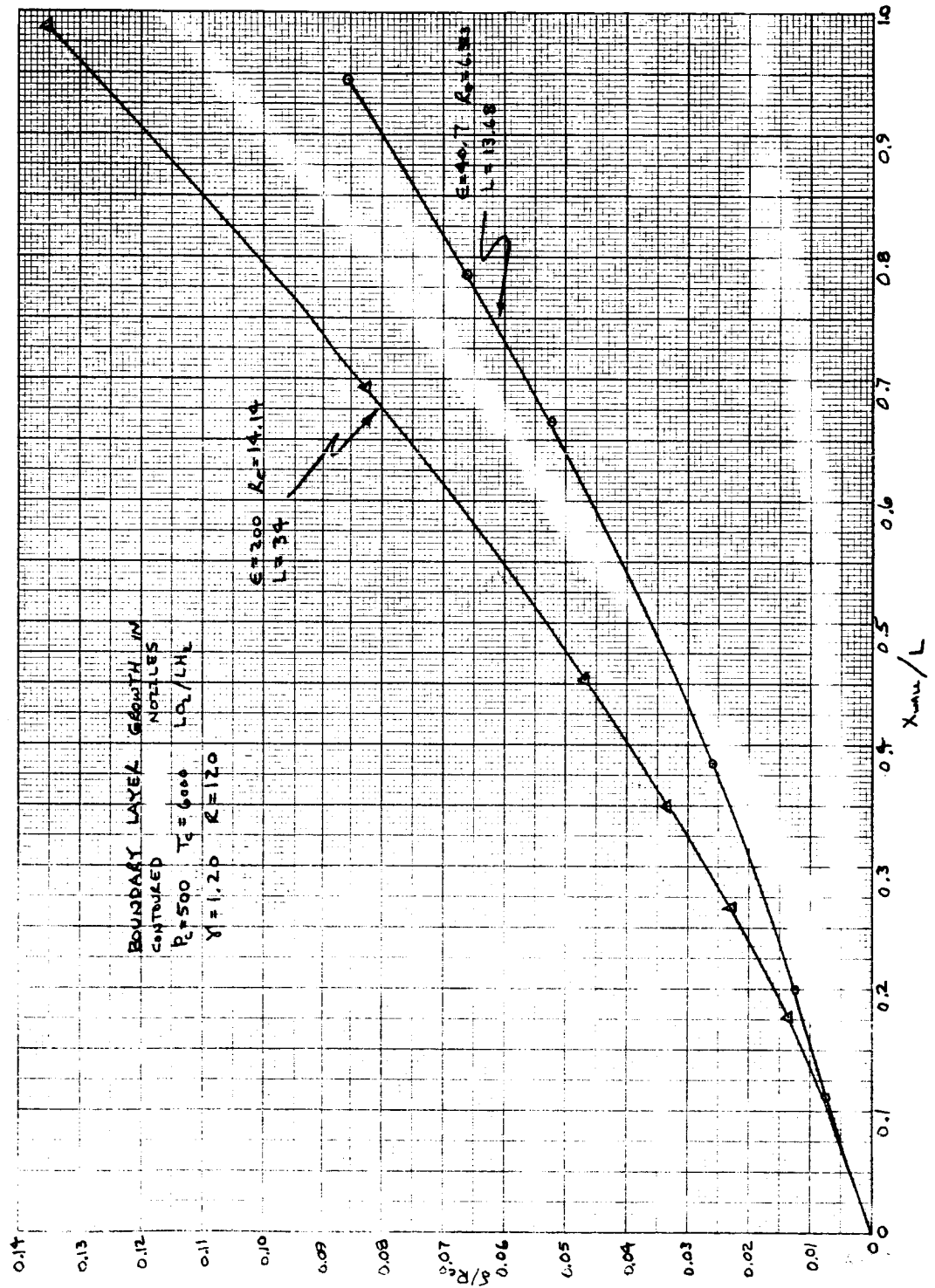
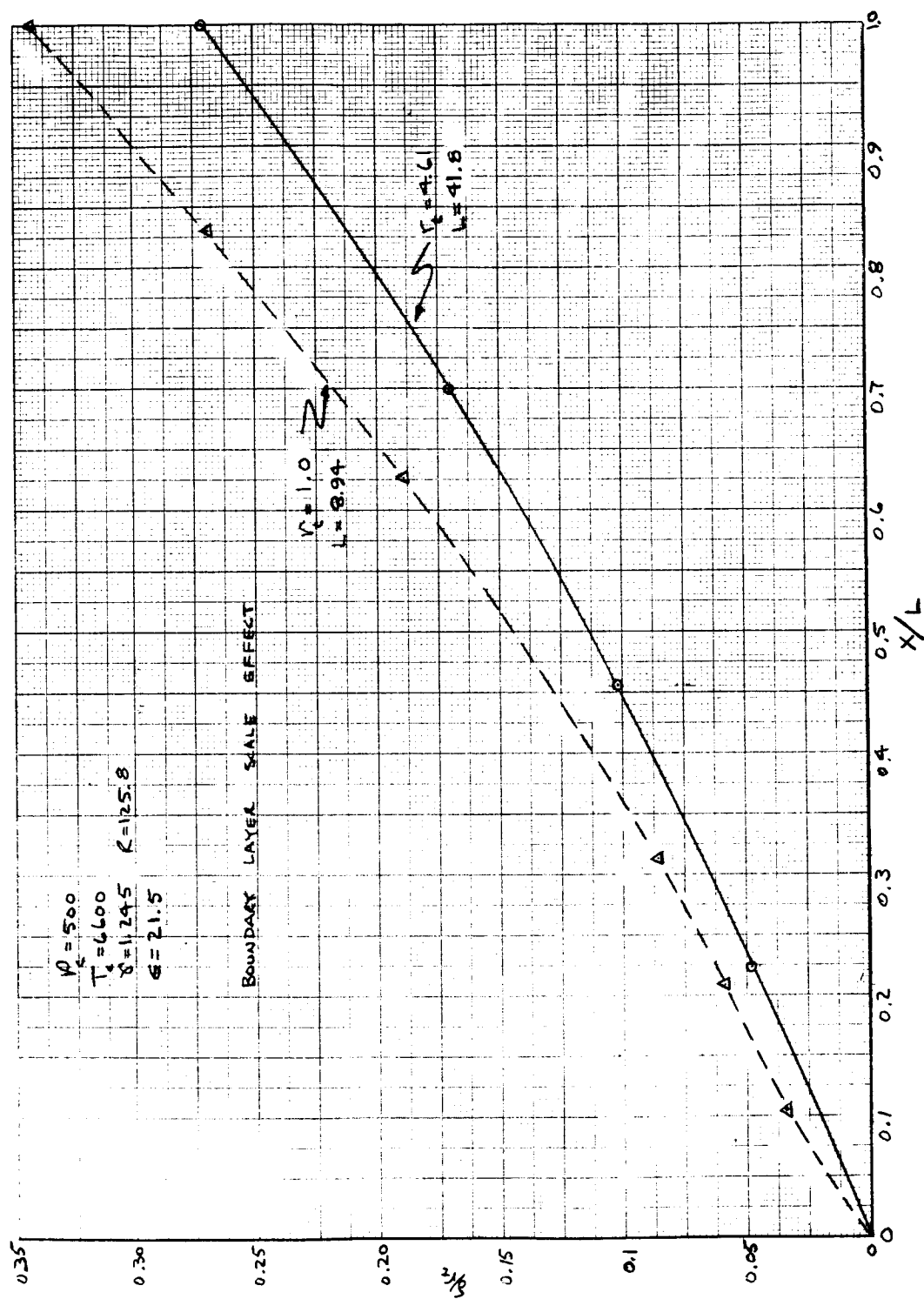
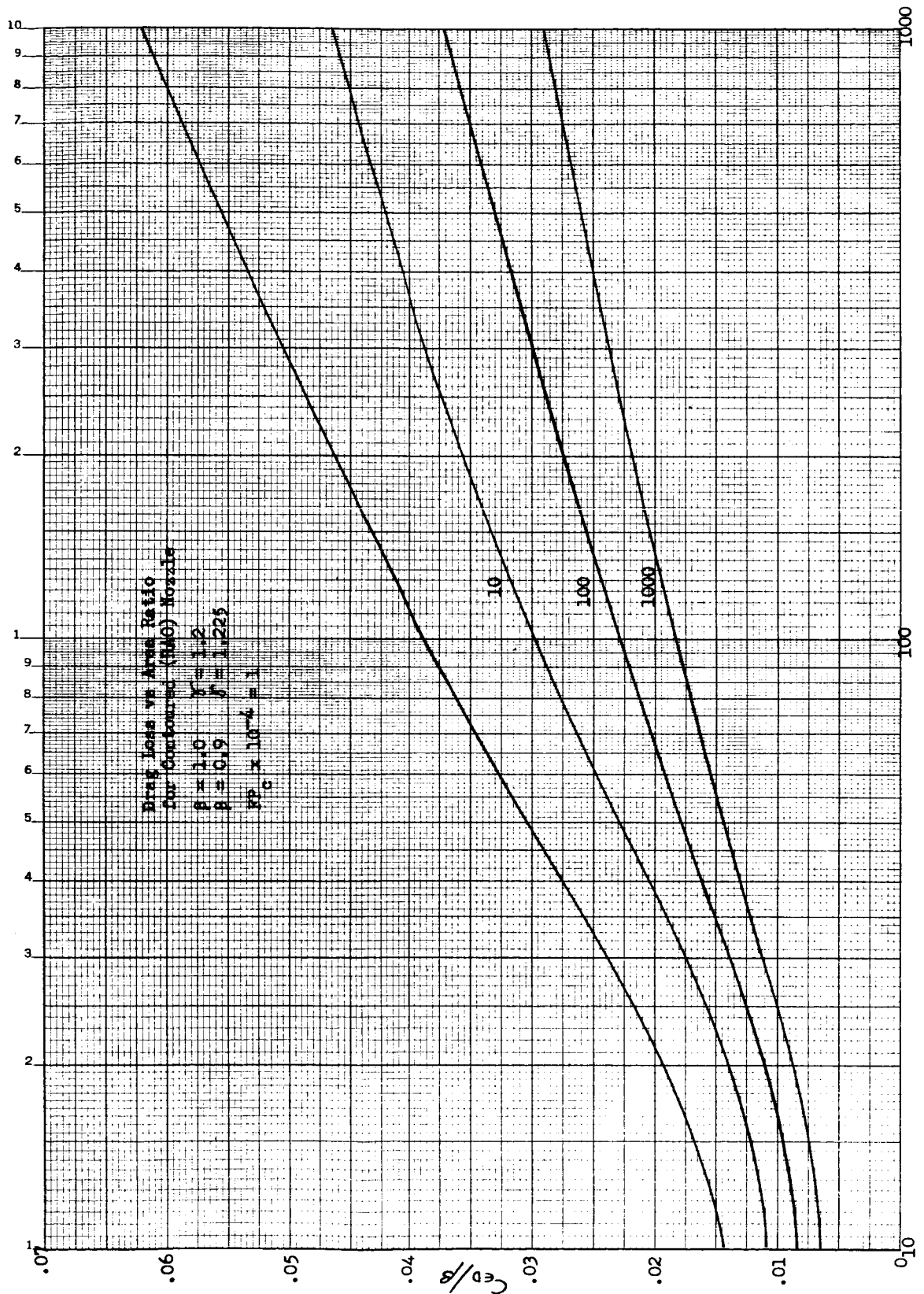


Figure 9



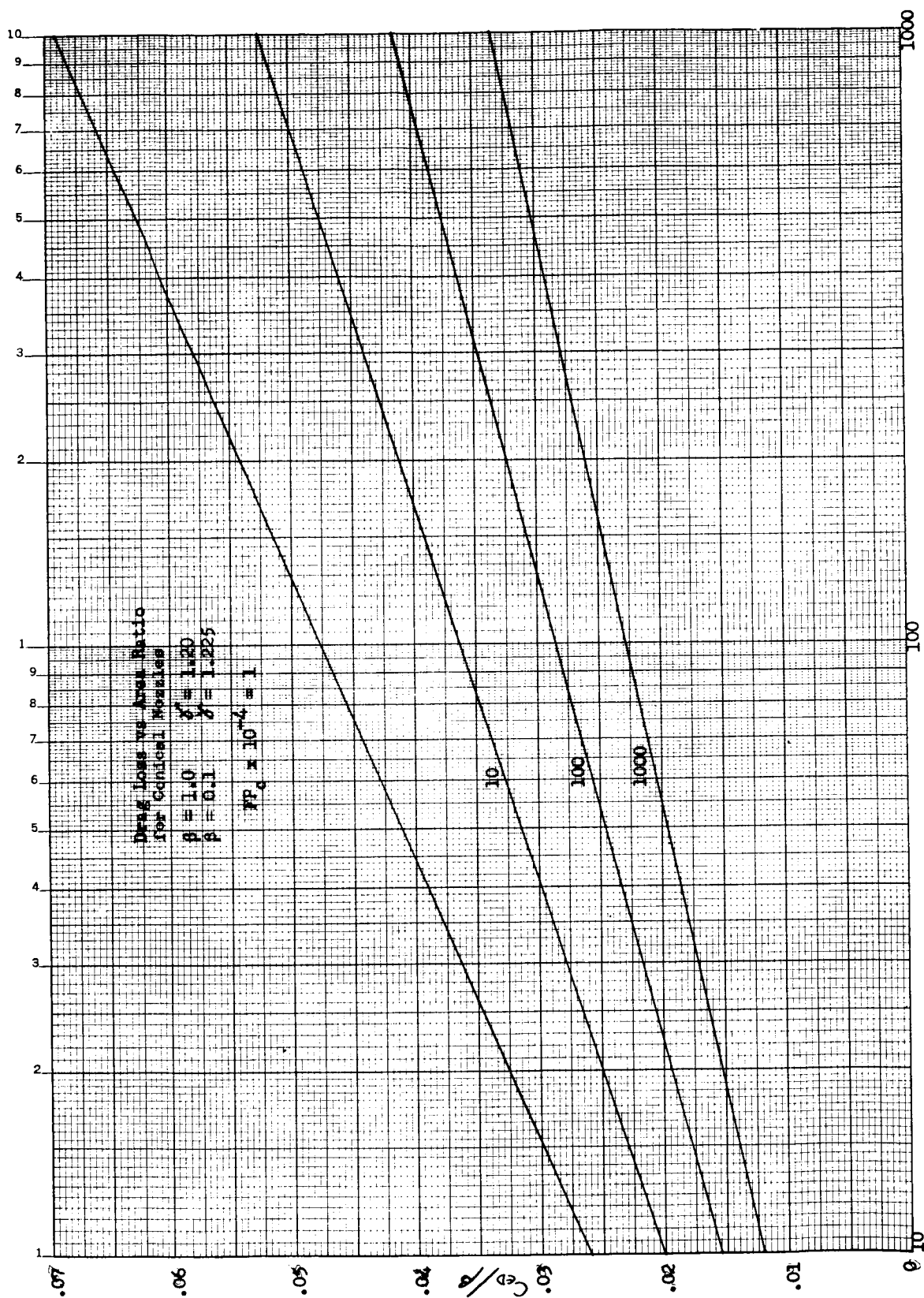
Turbulent Flow Boundary-Layer Scale Effect

Figure 10



Turbulent Flow Shear-Drag Loss for Bell (Rao) Nozzles

Figure 11



Turbulent Flow Shear-Drag Loss for Conical Nozzles

Figure 12

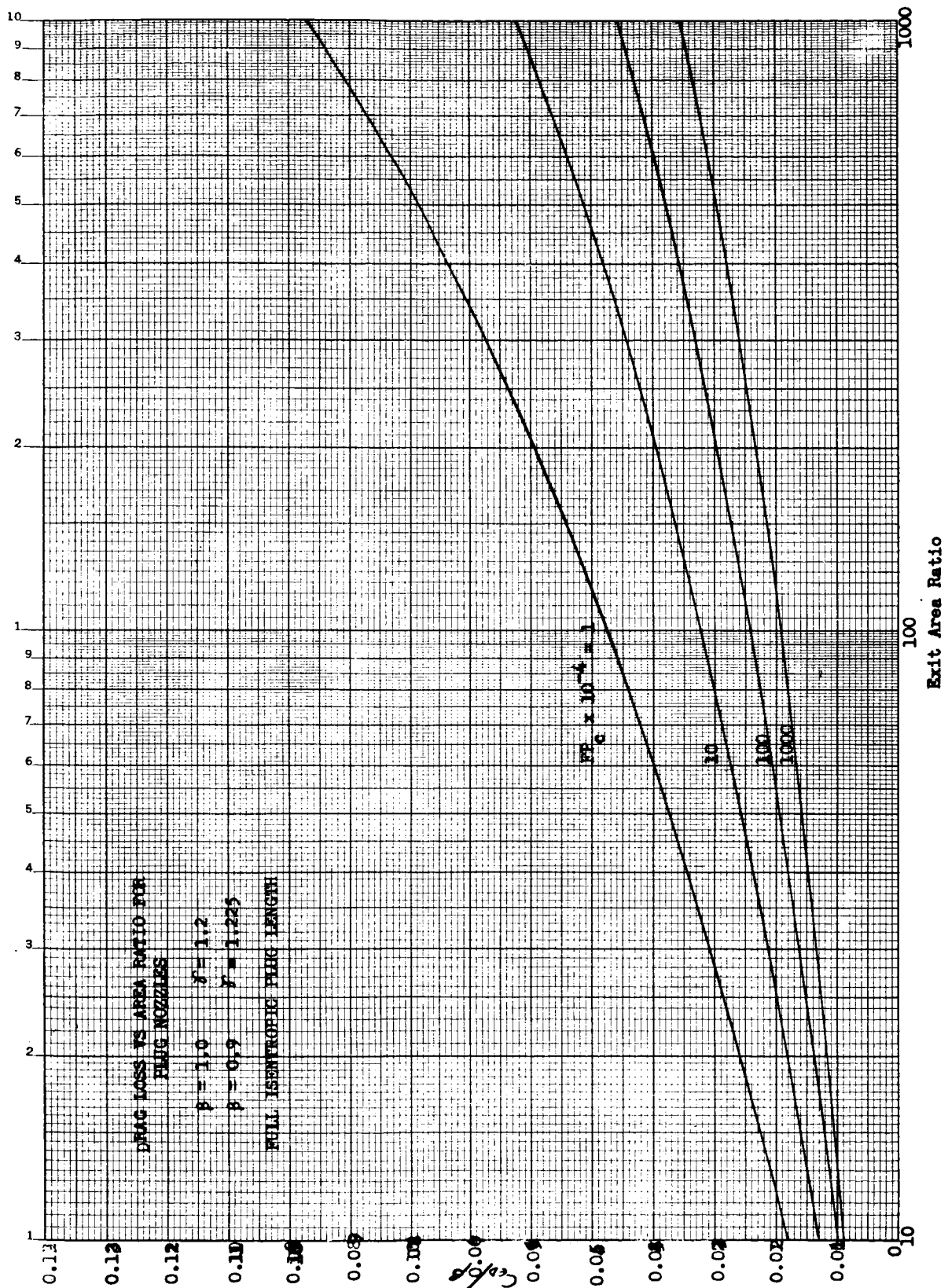


Figure 13

Turbulent Flow Shear-Drag Loss for Full Isentropic Plug Length

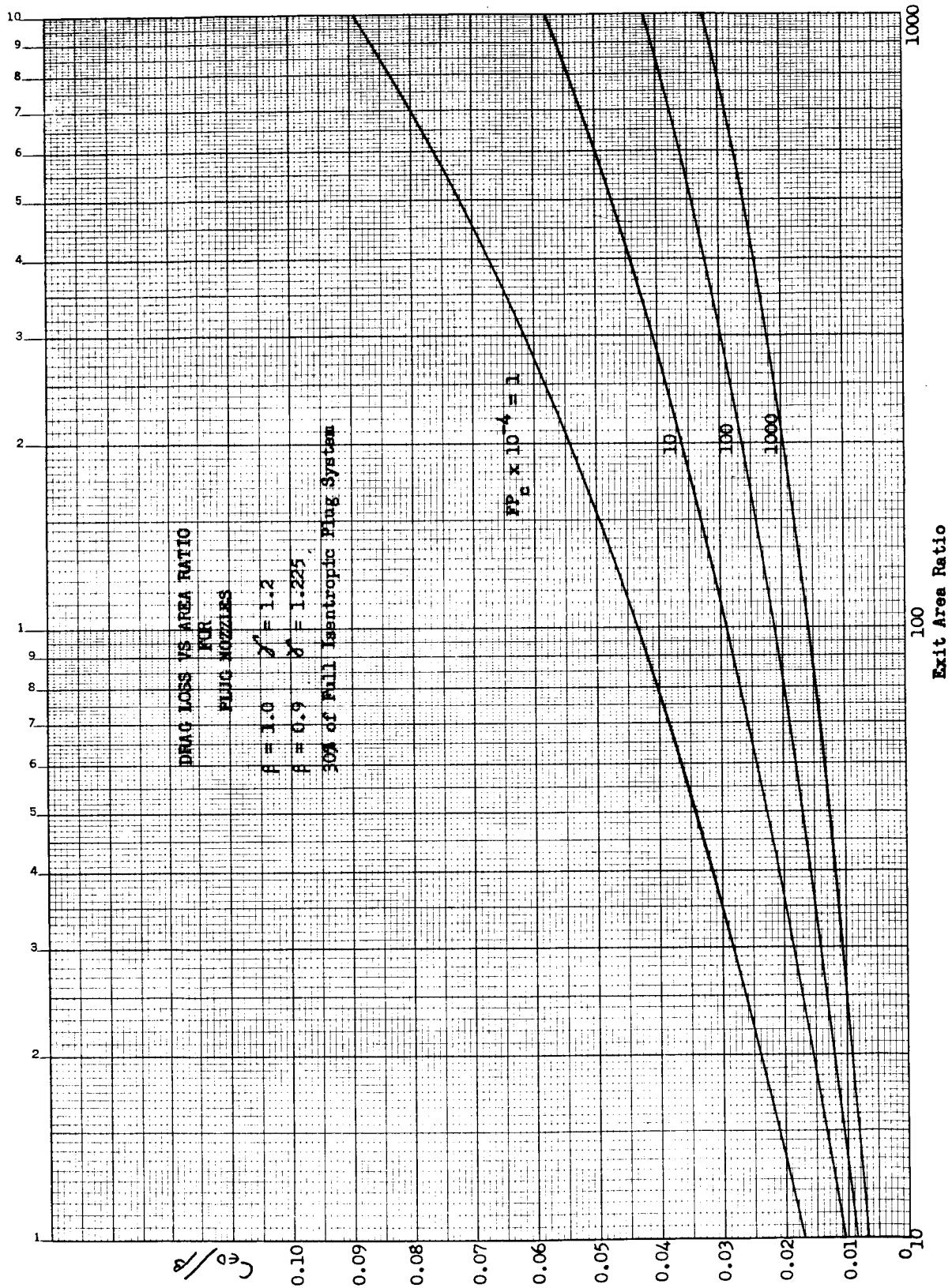
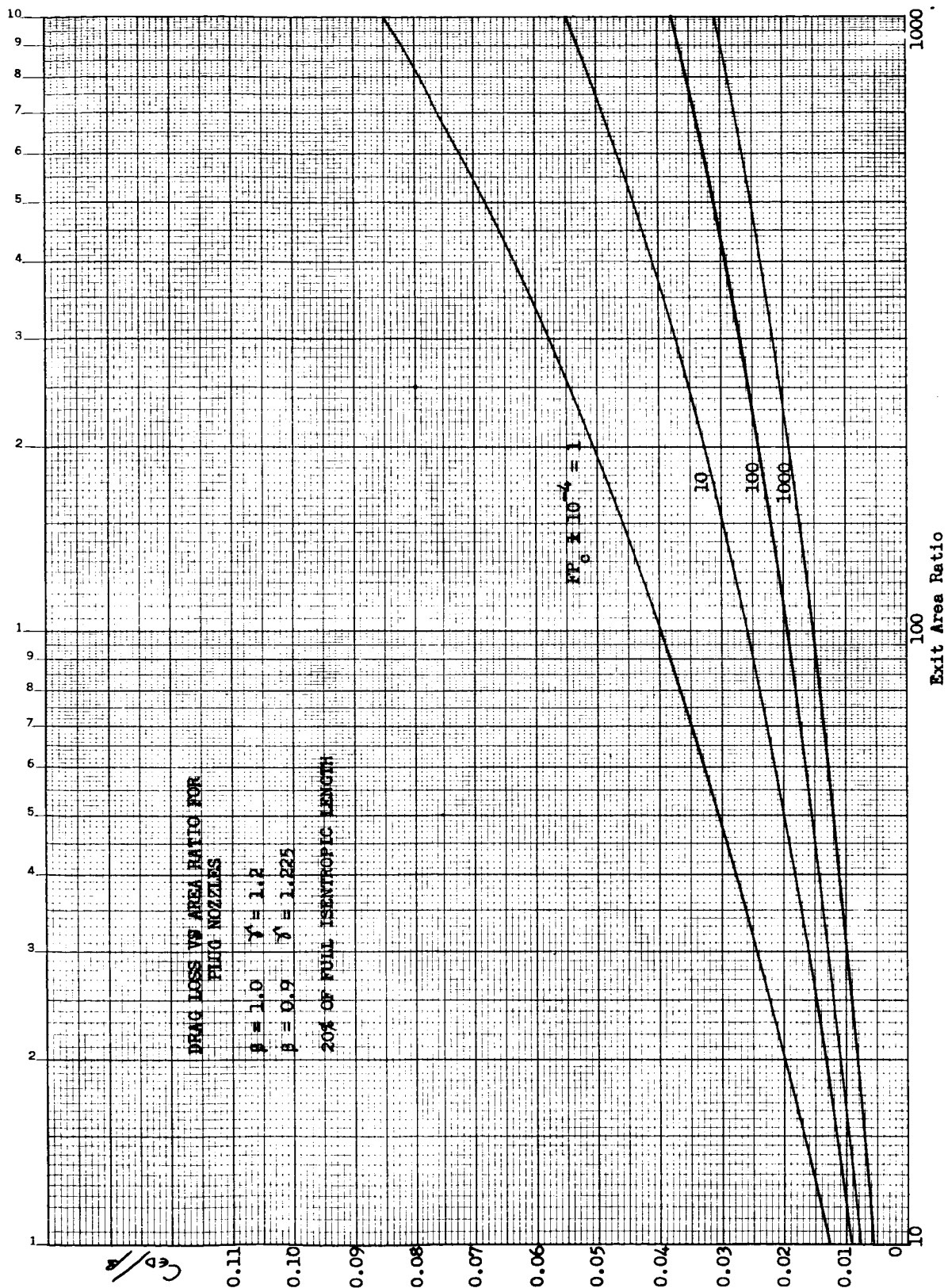


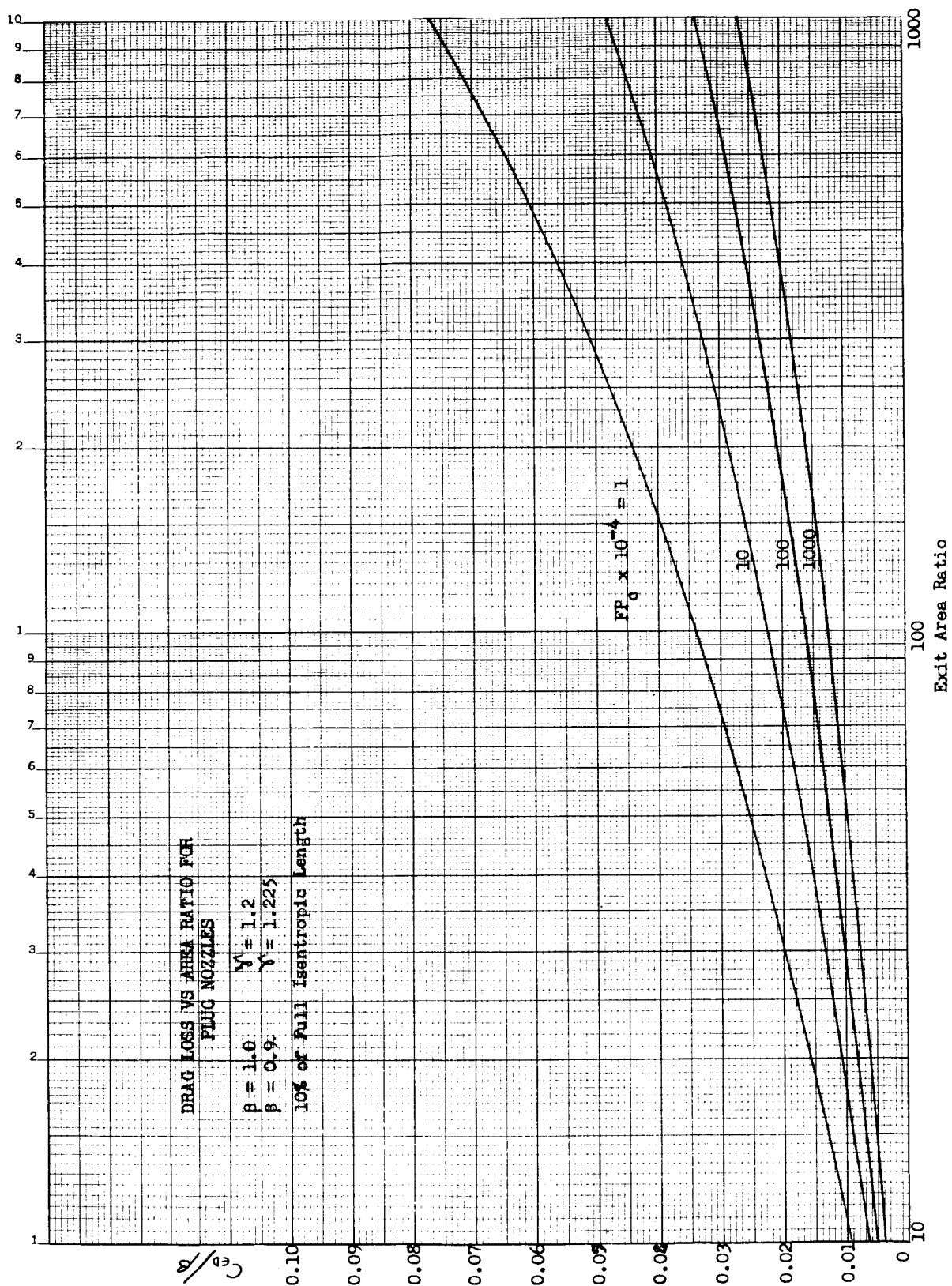
Figure 14

Turbulent Flow Shear-Drag Loss for 30% of Full Isentropic Plug System



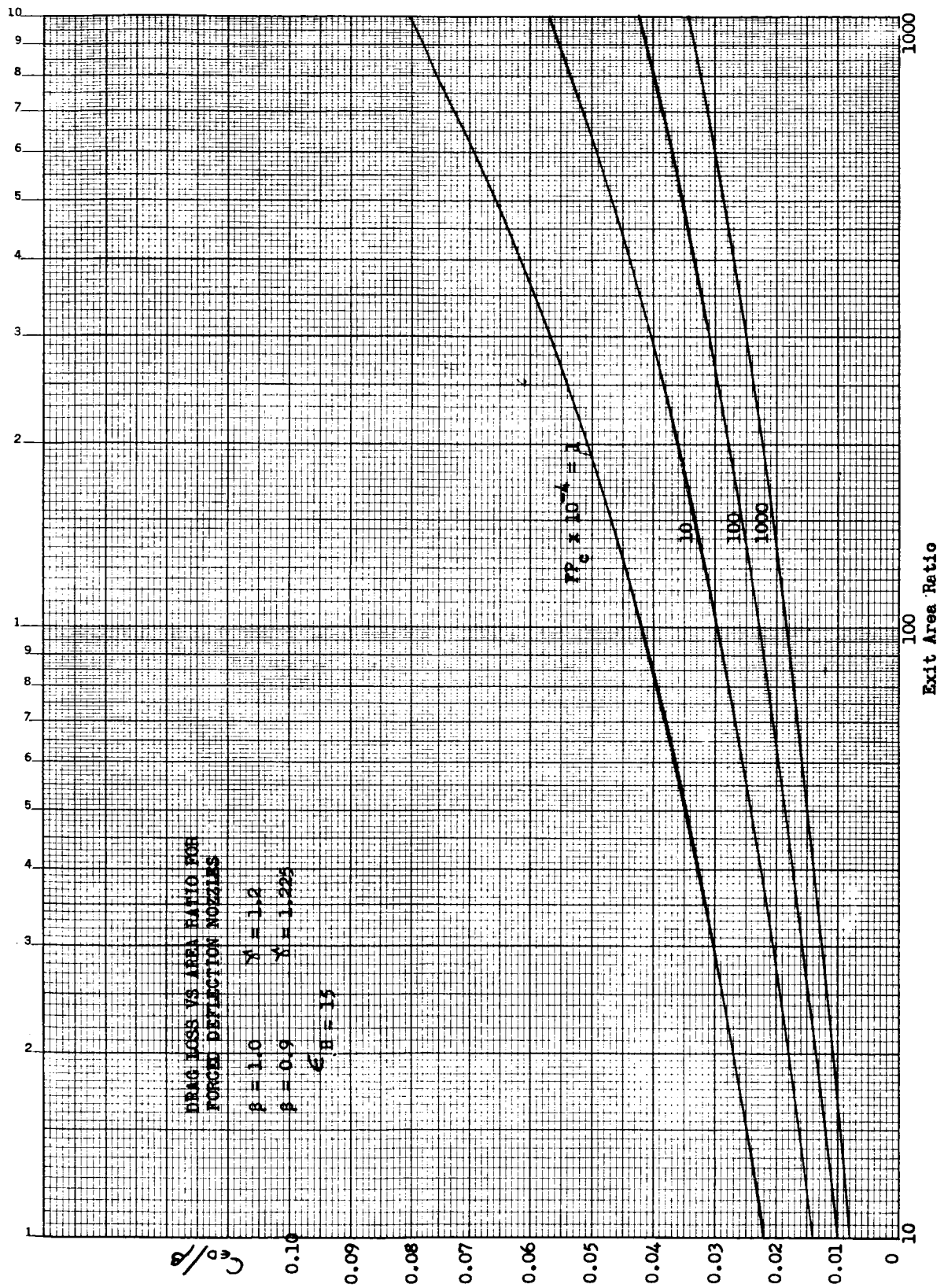
Turbulent Flow Shear-Drag Loss for 20% of Full Isentropic Plug Length

Figure 15



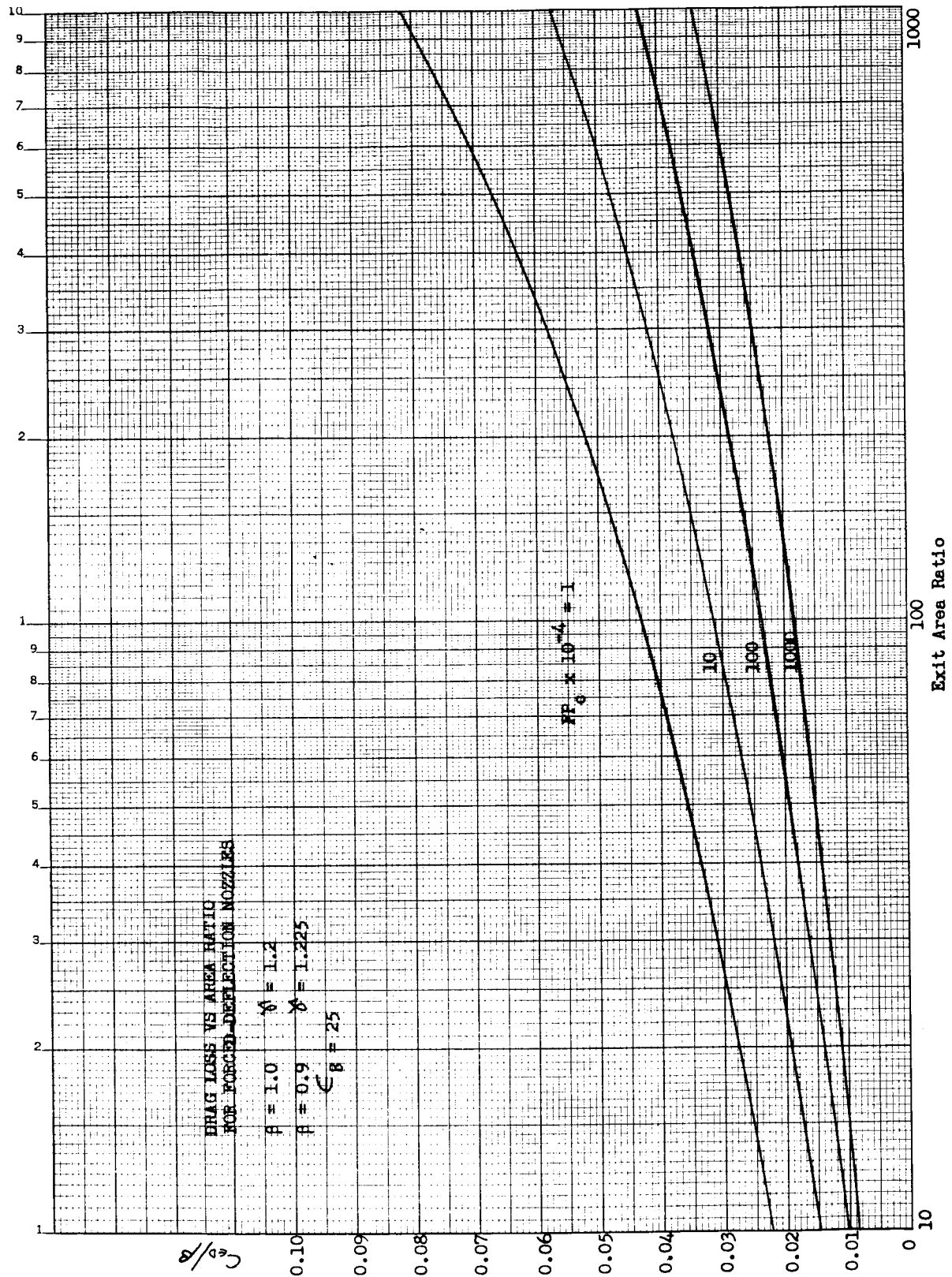
Turbulent Flow Shear-Drag Loss for 10% of Full Isentropic Plug Length

Figure 16



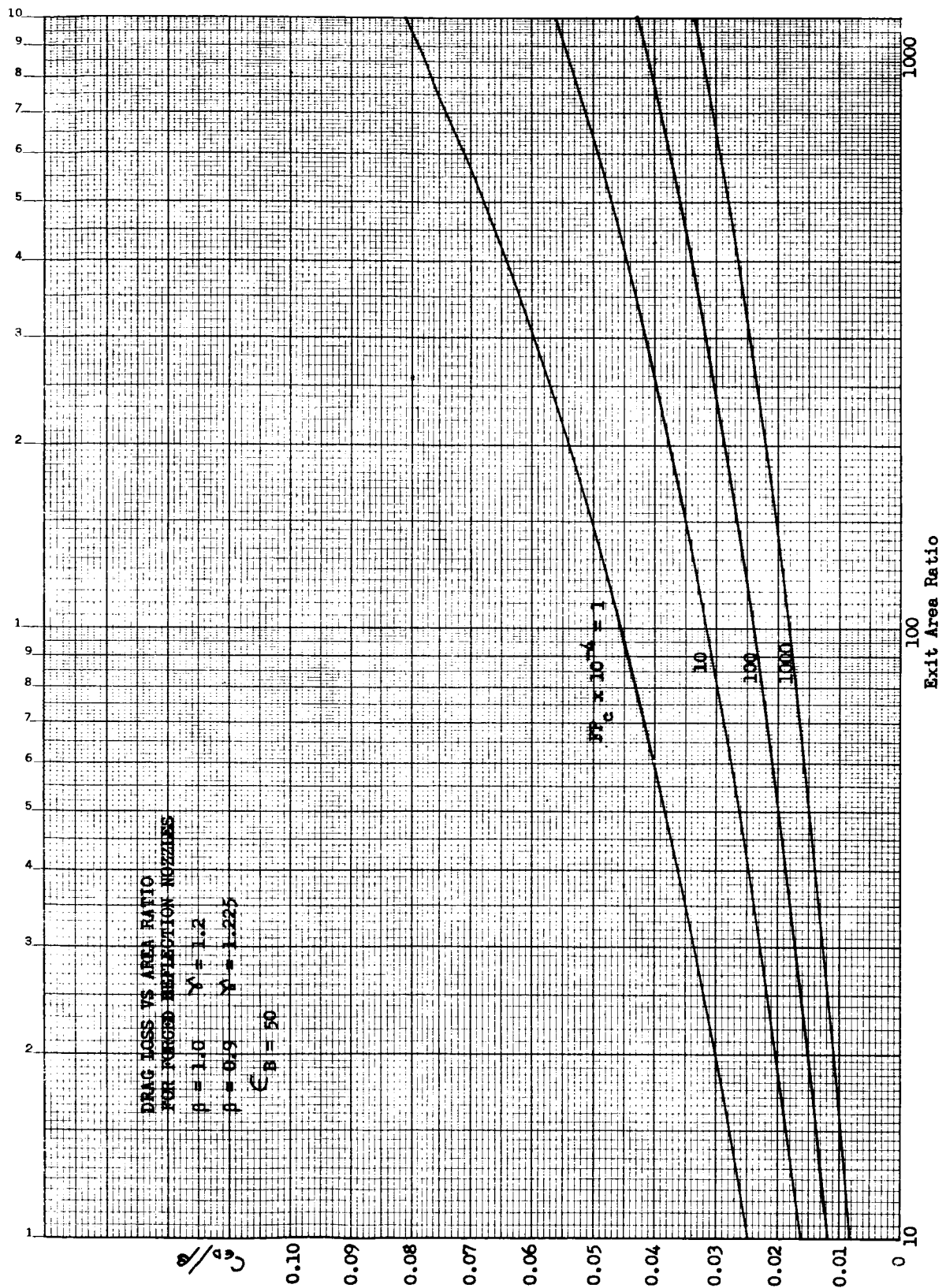
Turbulent Flow Shear-Drag Loss for Forced-Deflection Nozzles,
Base Area Ratio = 15

Figure 17



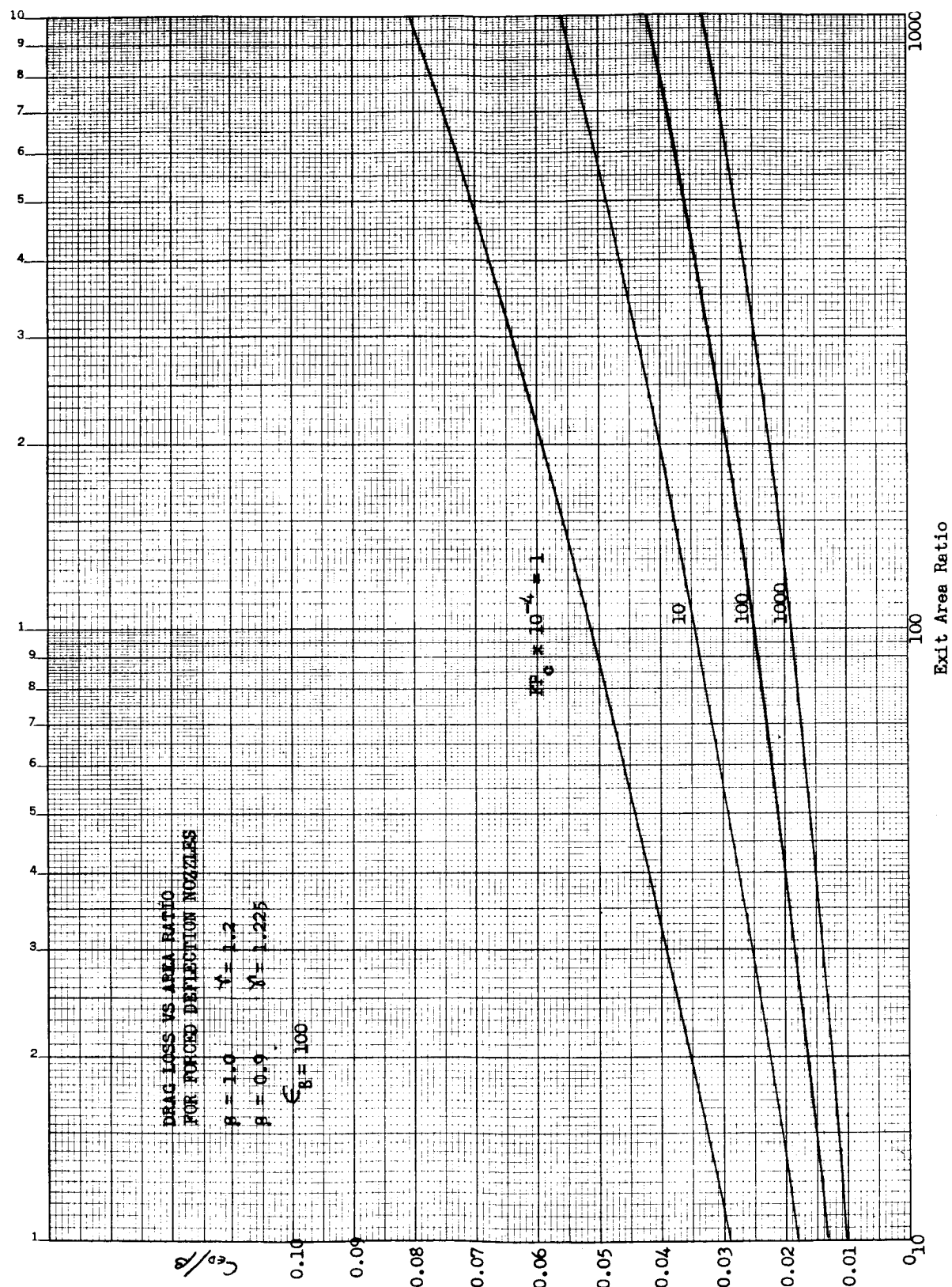
Turbulent Flow Shear-Drag Loss for Forced-Deflection Nozzles,
Base Area Ratio = 25

Figure 18



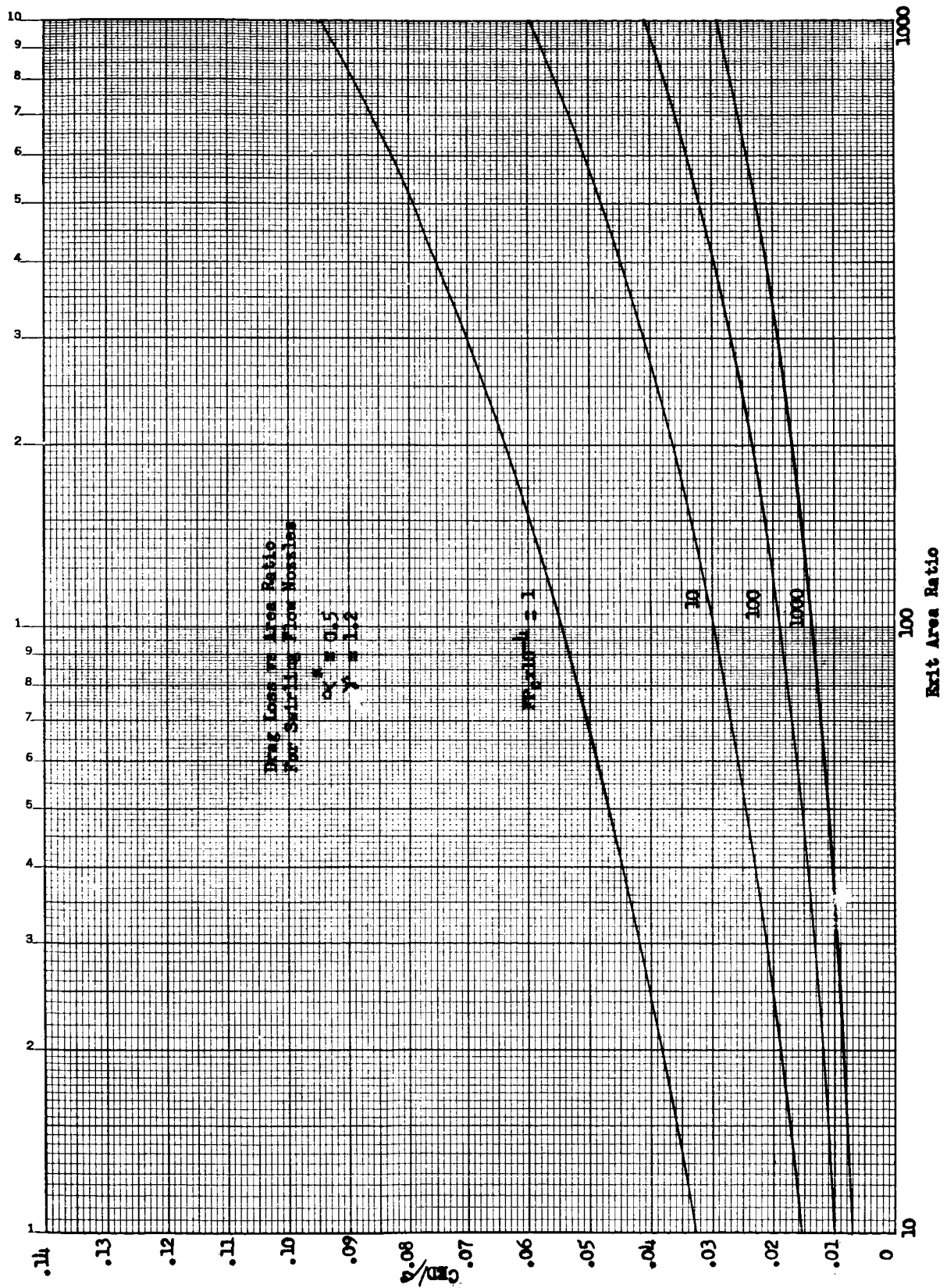
Turbulent Flow Shear-Drag Loss for Forced-Deflection Nozzles,
Base Area Ratio = 50

Figure 19



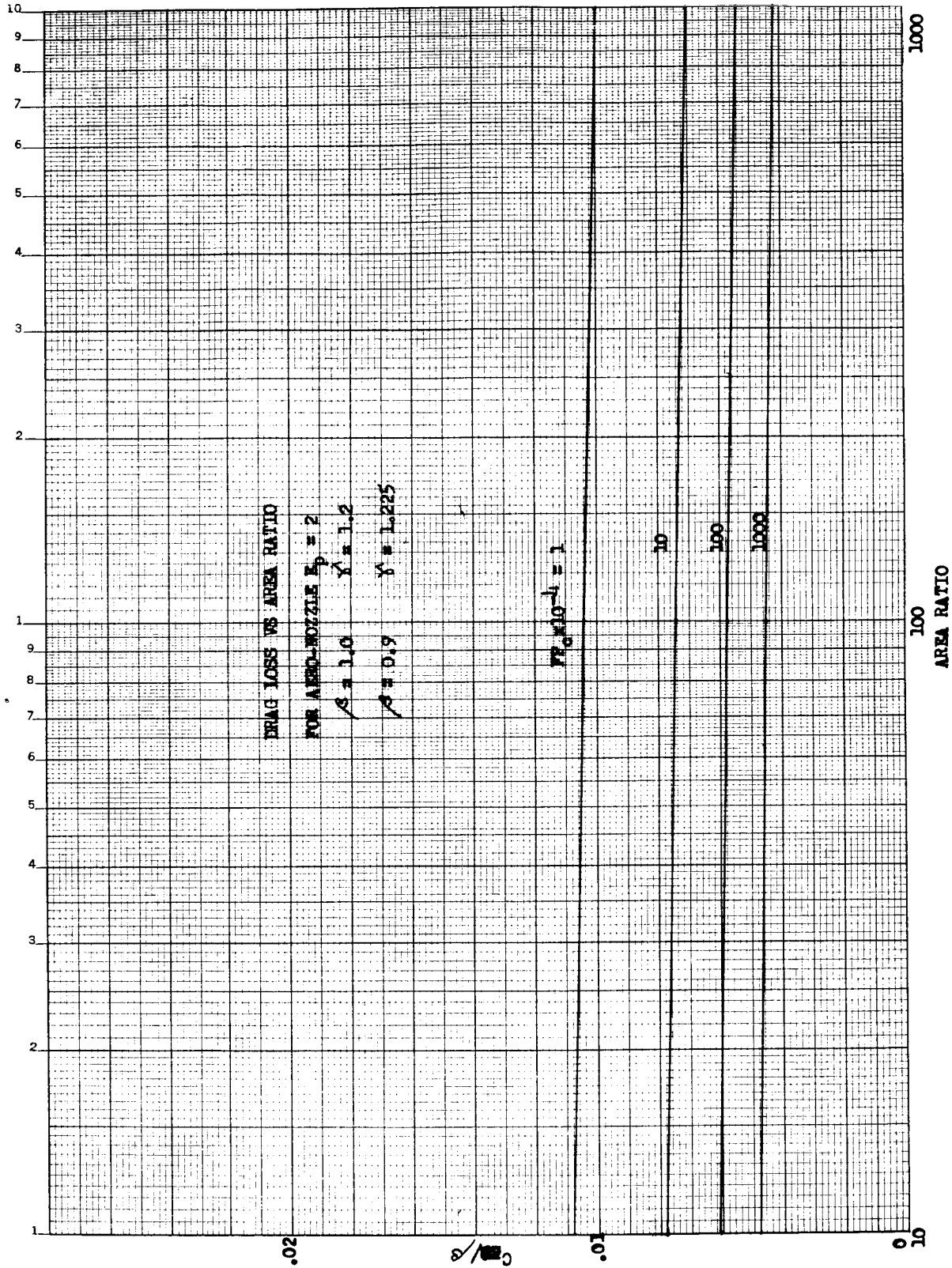
Turbulent Flow Shear-Drag Loss for Forced-Deflection Nozzles,
Base Area Ratio = 100

Figure 20



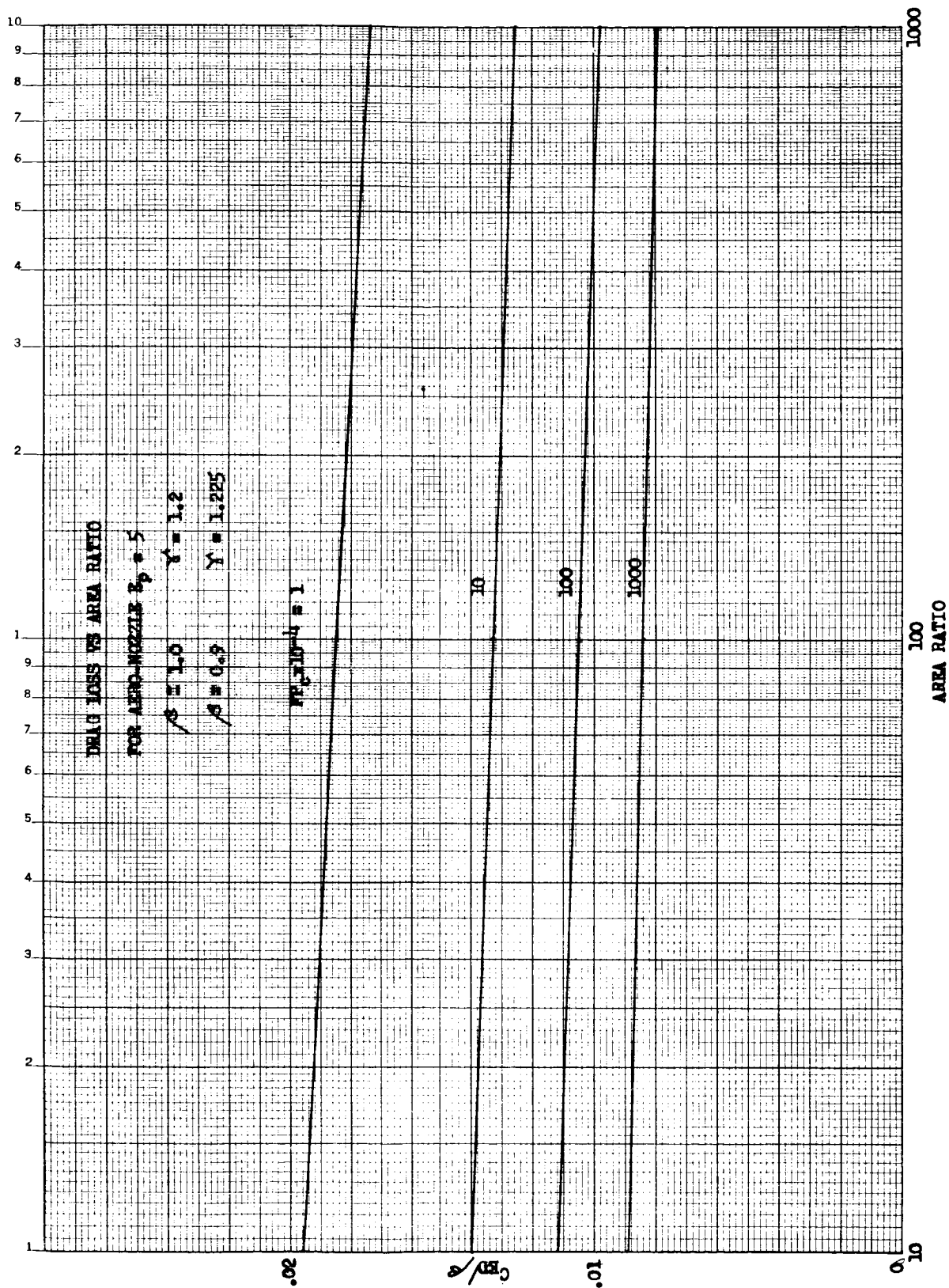
Turbulent Flow Shear-Drag Loss for Swirling-Flow Nozzles

Figure 21



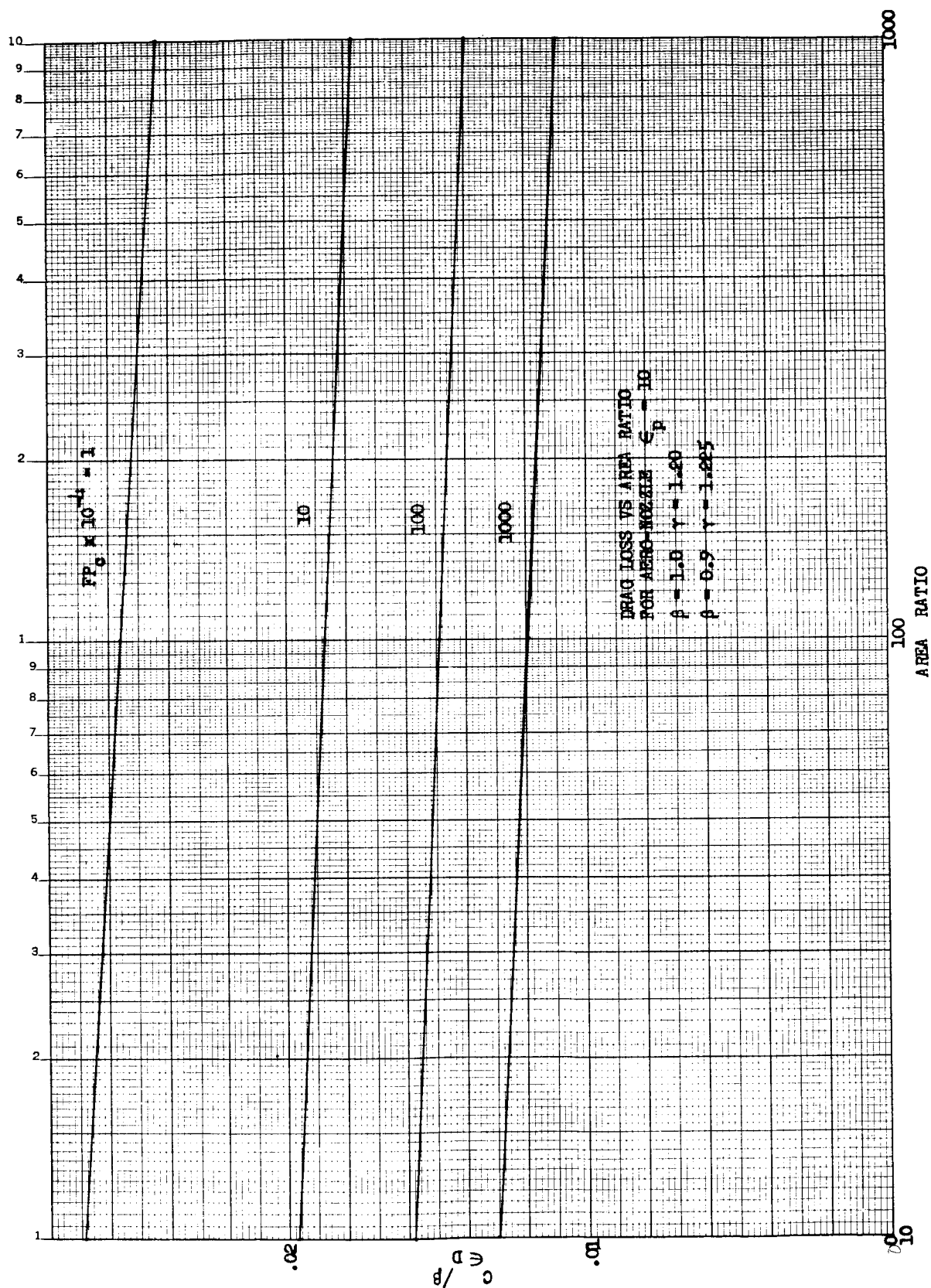
Turbulent Flow Shear-Drag Loss for Aerodynamic Nozzles, Primary
Expansion-Area Ratio = 2

Figure 22



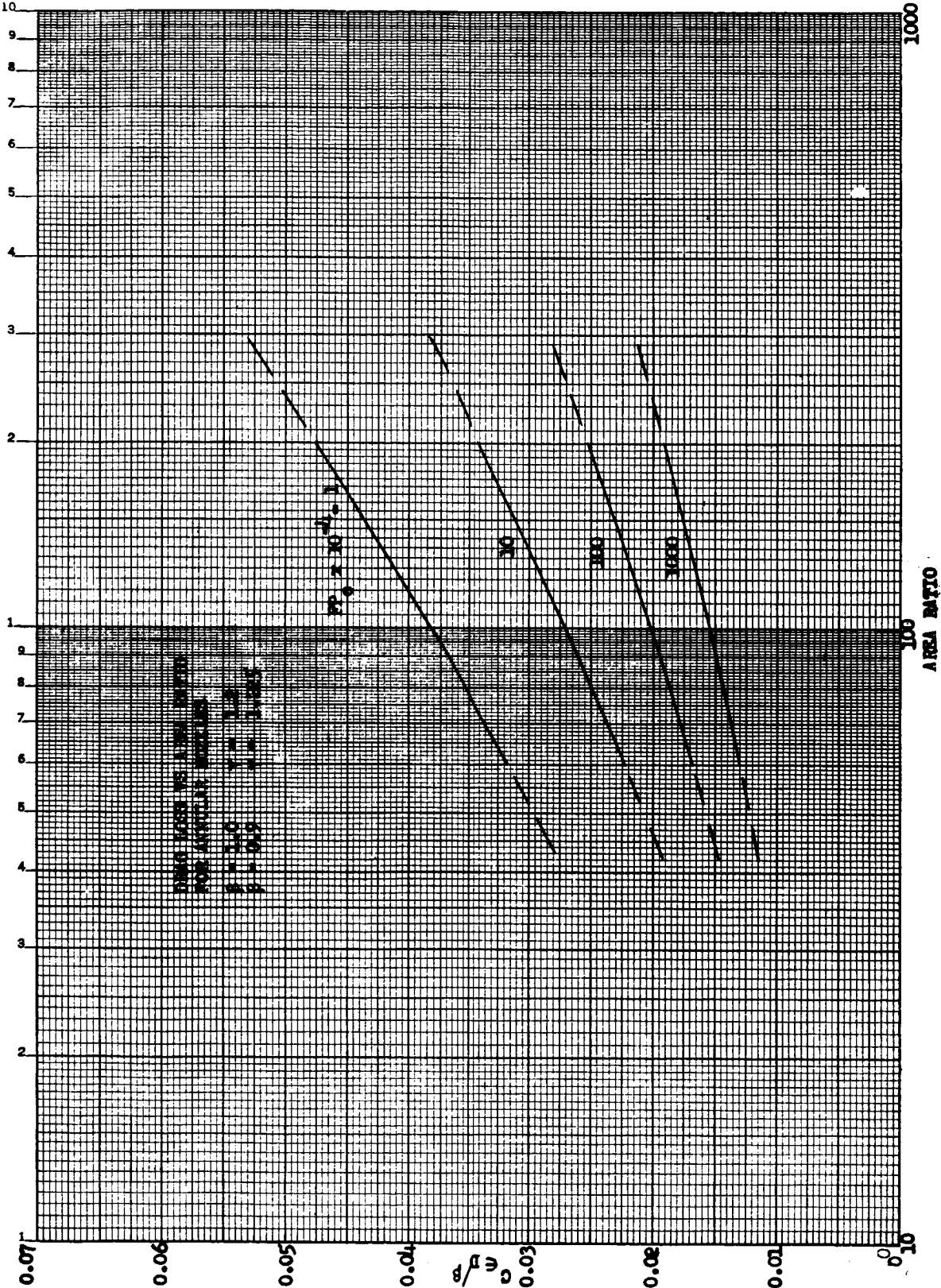
Turbulent Flow Shear-Drag Loss for Aerodynamic Nozzles, Primary
Expansion-Area Ratio = 5

Figure 23



Turbulent Flow Shear-Drag Loss for Aerodynamic Nozzles, Primary
Expansion-Area Ratio = 10

Figure 24



Turbulent Flow Shear-Drag Loss for Annular Nozzles

Figure 25

APPENDIX C

GEOMETRICAL THRUST LOSSES AND OPTIMUM NOZZLE CONTOUR DESIGN

Part 1 Perfect Gas

Part 2 Equilibrium Flow for Bell Nozzle

FIGURE LIST

	<u>FIGURE</u>
Geometric Losses for Cone, Bell, Forced-Deflection, Plug, and Two-Dimensional Wedge Nozzles	1
Geometric Losses for Disk Nozzle	2
Performance of a Conical Nozzle	3
Nozzle Control Surfaces and Parameter for Performance and Design Analysis	4
Geometric Losses for a Plug Nozzle as a Function of Plug-Length Truncation	5

PART I -- PERFECT GAS

I. INTRODUCTION

Geometrical losses in a rocket nozzle are a result of the gases leaving the nozzle exit plane in a non-axial direction and with non-uniform velocity. They are a function of the nozzle contour as well as its area ratio. The losses have been computed for each of the nozzles investigated, and are shown on Figures 1 and 2. The basic definition of the thrust loss parameter $C_{\epsilon G}$ is

$$C_{\epsilon G} = 1 - \frac{C_F'}{C_{F1-D}}$$

where C_F' is the maximum vacuum thrust coefficient for a given nozzle length, derived by taking into account only the geometric losses. C_{F1-D} is the vacuum thrust coefficient obtained by expanding the gas one-dimensionally to the area ratio of the nozzle. The one-dimensional vacuum thrust coefficient C_{F1-D} may be computed as a function of area ratio and ratio of specific heats from the following two equations:*

$$C_{F1-D} = \sqrt{\frac{2\gamma^2}{\gamma-1} \left(\frac{2}{\gamma+1}\right)^{\frac{\gamma+1}{\gamma-1}} \left[1 - \left(\frac{P_e}{P_c}\right)^{\frac{\gamma-1}{\gamma}}\right]} + \frac{P_e}{P_c} \epsilon$$

and

$$\epsilon = \frac{\left(\frac{2}{\gamma+1}\right)^{\frac{\gamma+1}{\gamma-1}}}{\left(\frac{P_e}{P_c}\right)^{\frac{1}{\gamma}} \sqrt{\frac{2}{\gamma-1} \left[1 - \left(\frac{P_e}{P_c}\right)^{\frac{\gamma-1}{\gamma}}\right]}}$$

*Tables of C_{F1-D} are presented as a function of γ and P_e/P_c in H. S. Seifert and J. Crum, Thrust Coefficient and Expansion Ratio Tables, Guided Missile Research Division, The Ramo-Wooldridge Corporation, 29 Feb 1956.

I, Introduction (cont.)

The method used to compute C_F' is discussed under each of the separate nozzle headings below.

II. CONICAL NOZZLE

The ratio of $C_F'/C_{F_{1-D}}$ may be computed directly for the conical nozzle, by assuming source flow and a spherical constant mach distribution at the nozzle exit. The resulting loss factor is

$$C_{EG} = \frac{1 - \cos \alpha}{2}$$

where α is the optimum half-angle of the cone. The optimum half-angle is that angle which results in a maximum thrust coefficient for a given nozzle length. It is determined graphically as shown on Figure 3.

III. BELL NOZZLE

The contour of the bell nozzle used for the mission analysis was determined for a perfect gas with a fixed ratio of specific heats using a computer program employing the method of characteristics. A Sauer* start line was used, and the contour was optimized using the method of Rao.** The Sauer start line has a parabolic velocity distribution which allows less mass flow through the throat than predicted by one dimensional theory. The discharge coefficient (Sauer mass flow/one dimensional mass flow) is shown on Figure III-2. The thrust coefficient calculated in the program includes the effect of this discharge coefficient, and was divided by the discharge coefficient to remove this effect. The geometric loss factor shown on Figure C-1 is, therefore, independent of discharge coefficient. The nozzles designed have a toroidal section immediately downstream of the throat with a radius of two-tenths of the nozzle throat radius. Increasing the downstream radius has very little effect on the nozzle losses for the same area ratio nozzle, and so the larger radii were not considered in this study. The performance of this nozzle and its optimum contour were also calculated for equilibrium flow of the gas, as described in Part 2 of Appendix C.

*Sauer, R., "General Characteristics of the Flow Through Nozzles at Near Critical Speeds," NACA TM 1147, 1946.

**Rao, G.V.R., "Exhaust Nozzle Contour for Optimum Thrust, "Jet Propulsion, Vol 28, No. 6, June 1958

IV. FORCED-DEFLECTION NOZZLE

The expansion process in the forced-deflection nozzle originates as a Prandtl-Meyer expansion about the plug lip. The entire flow field is asymmetric with respect to the direction of flow, and the gas streamlines are monotonic curves from the throat to the nozzle exit. Exact solution of the gas dynamic equations has shown that the following assumptions may be made:

a. The family of characteristics or Mach lines associated with the Prandtl-Meyer expansion may be assumed to lie straight and with uniform flow properties, V and θ .

b. The flow properties may be determined by the two-dimensional Prandtl-Meyer relationship.

Using these assumptions, the nozzle contour may be determined from continuity and axisymmetric, geometric considerations. To apply these principles, it is necessary to properly select a control surface, S , which completely encloses the rocket system.

continuity

$$\dot{m} = \int_S \rho \vec{V} \cdot \vec{n} \, ds \quad (\text{Eq 1})$$

momentum

$$F = \int_S \left[\frac{(\rho \vec{V} \cdot \vec{n})}{g} (-\vec{V}) - p \vec{n} \right] dS \quad (\text{Eq 2})$$

When Equations 1 and 2 are applied to specific control surfaces, S , for a forced-deflection nozzle, the following relationships exist:

$$\dot{m} = \int_{R_p}^{R_e} \rho_e V_e \frac{\sin \mu_e}{\sin (\theta_e + \mu_e)} 2\pi R \, dR \quad (\text{Eq 3})$$

IV, Forced-Deflection Nozzle (cont.)

$$F = \int_{R_p}^{R_e} \left[\rho_e \frac{V_e^2}{g} \frac{\sin \mu_e \cos \theta_e}{\sin (\theta_e + \mu_e)} + P_e \right] 2\pi R dR \quad (\text{Eq 4})$$

The geometric relations are shown on Figure 4. Equation 3 may be used for computation of the nozzle contour by equating the mass flow through the control surface to the mass flow through the throat. The following relationships result:

$$\left(\frac{R_i}{r_t} \right)^2 - \left(\frac{R_p}{r_t} \right)^2 = \left[\left(\frac{2}{\gamma + 1} \right) \left(1 + \frac{\gamma - 1}{2} M^2 \right) \right]^{\frac{\gamma + 1}{2(\gamma - 1)}} \sin (\theta_i + \mu_i) \quad (\text{Eq 5})$$

The flow properties along the i^{th} control surface are found from the two-dimensional Prandtl-Meyer relationship

$$\theta_i = \theta_e + \nu_e - \nu_i \quad (\text{Eq 6})$$

where

$$\nu = \sqrt{\frac{\gamma + 1}{\gamma - 1}} \left[\tan^{-1} \sqrt{\frac{\gamma - 1}{\gamma + 1} (M^2 - 1)} \right] - \tan^{-1} \sqrt{M^2 - 1} \quad (\text{Eq 7})$$

Thus, once the nozzle exit conditions and lip radius are known, the entire contour may be found through successive application of Equation 5 with the flow properties determined by Equations 6 and 7. The lip radius in dimensionless form is R_p/r_t , and this quantity squared is the ratio of the base area to the throat area. It is referred to throughout this report as the base ratio, and is selected as an independent parameter. The nozzle exit angle, θ_e , was computed using Rao's optimum angle:

$$\theta_e = \frac{1}{2} \sin^{-1} \left[\frac{2 \sqrt{M_e^2 - 1}}{\gamma M_e^2} \right] \quad (\text{Eq 8})$$

IV, Forced-Deflection Nozzle (cont.)

and the nozzle length from the relation

$$\frac{L}{r_t} = \frac{\frac{R_e}{r_t} - \frac{R_p}{r_t}}{\tan(\theta_e + \mu_e)} \quad (\text{Eq 9})$$

The nozzle performance is found from Equation 4. After some manipulation, it may be written in the form

$$C_F' = \frac{P_e}{P_c} \epsilon_e \left[\frac{\gamma M_e \cos \theta_e}{\sin(\theta_e + \mu_e)} + 1 \right] \quad (\text{Eq 10})$$

where

$$\epsilon_e = \left(\frac{R_e}{r_t} \right)^2 - \left(\frac{R_b}{r_t} \right)^2 \quad (\text{Eq 11})$$

The pressure on the base of the nozzle is approximately one thousandth of the chamber pressure and has been neglected in this analysis.

V. PLUG NOZZLE

An efficient plug-nozzle design results if an isentropic plug is designed to give uniform parallel flow at the exit. This is commonly referred to as the "isentropic spike," and may be truncated considerably with low performance losses. The calculation of the contour and performance of the truncated isentropic plug nozzle was similar to that for the forced-deflection nozzle.

The resulting equations for the plug nozzle (Figure 4), corresponding to Equations 5, 6, 9, 10, and 11 for the forced-deflection nozzle are:

$$\left(\frac{R_L}{r_t} \right)^2 - \left(\frac{R_i}{r_t} \right)^2 = \left[\frac{2}{\gamma + 1} \left(1 + \frac{\gamma - 1}{2} M^2 \right) \right]^{\frac{\gamma + 1}{2(\gamma - 1)}} \sin(-\theta_i + \mu_i)$$

V, Plug Nozzle (cont.)

where

$$\theta_i = \theta_e - \nu_e + \nu_i$$

$$\frac{L_i}{r_t} = \frac{\frac{R_L}{r_t} - \frac{R_i}{r_t}}{\tan(-\theta_i + \mu_i)}$$

$$C_F' = \frac{P_e}{P_c} \in_e \left[\frac{\gamma M_e \cos \theta_e}{\sin(-\theta_e + \mu_e)} + 1 \right]$$

$$\epsilon_e = \left(\frac{R_L}{r_t} \right)^2 - \left(\frac{R_e}{r_t} \right)^2$$

An isentropic spike results when R_e and θ_e are zero.

Experimental data taken from plug nozzles with an area ratio of 30:1 and truncated from 6 to 33% of their isentropic length indicates that about 70% of the thrust which would have been produced by the portion of the isentropic spike which was removed by truncation is recovered by the pressure on the base. This factor establishes the basis for the geometrical loss factor $C_{\epsilon G}$ shown on Figure 5. The factor was computed from

$$C_{\epsilon G} = .3 \left(1 - \frac{C_F'}{C_{F_{isen}}} \right)$$

where $C_{F_{isen}}$ is the thrust coefficient of an isentropic spike, and C_F' is the thrust coefficient of the truncated isentropic spike with no thrust recovery caused by pressure on the base area.

VI. ANNULAR NOZZLE

The outer contour of the annular nozzle was designed with a computer program.* The inner contour is a mirror image of the outer contour, with the base ratio of the nozzle selected such that the inner contour meets at a point in the exit plane of the nozzle. This does not result in an optimum nozzle. It is expected that an optimum contour has a steeper inner contour. Increasing the base ratio such that the inner boundary does not come to a point will also increase the performance of this nozzle due to the pressure on the base.

The performance of the annular nozzle was estimated from the performance of a two-dimensional wedge. The losses of the wedge nozzle (Figure 1) were computed by a method similar to the cone, except that

$$C_{EG} = 1 - \frac{\sin \alpha}{\alpha}$$

These wedge nozzle losses were multiplied by the ratio of the bell nozzle losses of the cone nozzle losses at the area ratio of the wedge, to correct for the effect of lowering the exit angle by contouring. The losses thus calculated are thought to be low.

VII. STAR NOZZLE

A three-dimensional analysis is required for an exact calculation of optimum contour and performance of the star nozzle. Since this was not available, a crude approximation of two-dimensional flow in a wedge nozzle was used. A number of sections similar to the section shown in Figure II-9 were arranged as shown to form a polygon exit plane, with throats extending to the same diameter as the exit. From the figure it may be seen that the wedge nozzles at the center polygon have an area

* Rao, G.V.R., "Analysis of a New Concept Rocket Nozzle," Liquid Rockets and Propellants Progress on Astronautics and Rocketry, Vol. 2, M. Summerfield, Academic Press, New York, 1960.

VII, Star Nozzle (cont.)

ratio of 1, and the wedges at the outer periphery of the nozzle have a very high area ratio. The effective area ratio of the unit is related to the maximum area ratio by the relation

$$= \frac{1 + \epsilon_{\max}}{2}$$

The length of the nozzle may be computed from geometrical considerations:

$$\frac{L}{r_t} = \frac{1}{\tan \alpha_{\min}} \sqrt{\frac{\pi (\epsilon - 1) \tan \left(\frac{180}{n} \right)}{n}}$$

This is the length shown on Figure II-6 for a nozzle with eight throats. For comparison with other nozzles, the length is also presented as a function of hydraulic radius ratio on Figure II-7. The hydraulic radius ratio is defined as

$$\frac{R}{r_t} = \frac{2A_t}{P_t r_t}$$

which, after substitution of geometric relations, is

$$\frac{R}{r_t} = \frac{1}{1 + \frac{\epsilon - 1}{\tan \theta}} \sqrt{\frac{\pi (\epsilon - 1)}{n \tan \theta}}$$

A real star nozzle might have throats that do not extend all the way to the exit radius. If the throat area is kept constant and the length of the throat reduced, its hydraulic radius increases and its shape approaches (in the limit) a circular throat. Therefore, a curve may be drawn from the star nozzle to the circular throat on Figure II-7 representing all star nozzles with throats ranging from lengths equal to the exit radius to a single circular throat. The curve between the star nozzle with throat length equal to exit radius and the circular throat was assumed linear. This established a L/r_t of 15.7 for the design nozzle. The length was

VII, Star Nozzle (cont.)

further reduced by 12% to account for the effect of contoured, rather than wedge sections. The performance of a star nozzle was assumed to be identical with the annular nozzle, since they may both be approximated with a two-dimensional wedge.

VIII. AERODYNAMIC NOZZLE

The method of calculation of the geometric losses in the aerodynamic nozzle is described in Appendix F.

IX. SWIRL NOZZLE

The basic procedure for calculating the one-dimensional performance of a swirling flow nozzle is given by Mager.* This analysis was programed on the computer, and the results are discussed in Section II, D, 6. The geometric losses were assumed to be identical to the bell nozzle losses at the geometric area ratio of the swirling flow nozzle. For example, a swirling flow nozzle with an effective area ratio of 100:1 and a swirl magnitude of 0.5 has a geometric area ratio of 25 (Figure II-10). The geometric losses may be obtained from the Figure 1 bell nozzle curve, and are 2.19%.

A two-dimensional analysis was conducted and is described in Appendix E. Sufficient time was not available to program this analysis for Phase II.

X. DISK NOZZLE

The disk nozzle was analyzed using an existing computer program in which contour is input, and performance is calculated using the method of characteristics. The high losses of this nozzle are shown in Figure 2.

* Mager, A., "Approximate solution of isentropic swirling flow through a nozzle," ARS Journal, 31:1140-1141, Aug., 1961.

PART 2 -- GEOMETRIC LOSSES AND OPTIMUM NOZZLE DESIGN OF A BILL NOZZLE WITH
EQUILIBRIUM AND FROZEN FLOW

I. SUPERSONIC FLOW OF A GAS IN CHEMICAL EQUILIBRIUM: DYNAMIC AND THERMODYNAMIC
RELATIONS

A better model of two-dimensional and axisymmetric flow is obtained when the effects of change in chemical composition as the gas flows through the nozzle are taken into account.

The assumptions made for the equilibrium composition analysis are as follows:

- (a) Equilibrium composition is maintained in the combustion gases throughout the nozzle expansion.
- (b) The flow is isentropic.
- (c) The gases behave as ideal gases.
- (d) The propellants burn completely in an ideal plenum chamber at one pressure.
- (e) The gases are homogeneous and at zero velocity in the plenum chamber.

In the numerical computation the pressure is taken as the independent variable and the other thermodynamic variables are obtained as functions of pressure.

We have from thermodynamics that the change in entropy is given by

$$dS = \frac{dQ}{T} = \frac{dE}{T} + \frac{p}{T} d\left(\frac{1}{\rho}\right) - \frac{\sum \mu_i dn^i}{T} \quad (\text{Eq 1})$$

with summation on the i .

The first law yields

$$- d\left(\frac{v^2}{2}\right) = dH \quad (\text{Eq 2})$$

with H defined as

$$H = E + \frac{p}{\rho} \quad (\text{Eq 3})$$

I, Supersonic Flow of a Gas in Chemical Equilibrium: Dynamic and Thermodynamic Relations (cont.)

combining Equation 2 and 3 we have

$$- d\left(\frac{V^2}{2}\right) = dE + \frac{1}{\rho} dp + p d\left(\frac{1}{\rho}\right) \quad (\text{Eq 4})$$

Assuming an isentropic flow

$$dS = 0 \quad (\text{Eq 5})$$

and Equation 1 becomes

$$dE + p d\left(\frac{1}{\rho}\right) = 0 \quad (\text{Eq 6})$$

(It can be shown for constant entropy, equilibrium flow that $\mu_i dn^i = 0$.)

Combining Equation 4 and 6

$$- d\left(\frac{V^2}{2}\right) = \frac{1}{\rho} dp \quad (\text{Eq 7})$$

The sound velocity is defined as

$$c^2 = \left(\frac{\partial p}{\partial \rho}\right)_{S = \text{constant}} \quad (\text{Eq 8})$$

With isentropic flow this may be written in differential form

$$c^2 = \frac{dp}{d\rho} \quad (\text{Eq 9})$$

or

$$dp = c^2 d\rho \quad (\text{Eq 10})$$

Combining Equations 10 and 7

$$- d\left(\frac{V^2}{2}\right) = \frac{c^2}{\rho} d\rho \quad (\text{Eq 11})$$

I, Supersonic Flow of a Gas in Chemical Equilibrium: Dynamic and Thermodynamic Relations (cont.)

Assuming irrotational flow

$$\frac{\partial u}{\partial y} - \frac{\partial v}{\partial x} = 0. \quad (\text{Eq 12})$$

This enables us to define a potential function ϕ which satisfies Equation 12 identically

$$u = \frac{\partial \phi}{\partial x} = \phi_x, \quad v = \frac{\partial \phi}{\partial y} = \phi_y \quad (\text{Eq 13})$$

The continuity equation written in general two-dimensional form is

$$\frac{\partial}{\partial x}(\rho y^\sigma u) + \frac{\partial}{\partial y}(\rho v y^\sigma) = 0 \quad (\text{Eq 14})$$

with

$$\begin{aligned} \sigma &= 0 && \text{2-dimensional plane flow} \\ &= 1 && \text{3-dimensional axi-symmetric flow} \end{aligned}$$

Using Equation 11, with $V^2 = u^2 + v^2$, eliminate ρ from Equation (Eq 14). First note that from (Eq 11)

$$\frac{\partial \rho}{\partial x} = -\frac{\rho}{c^2}(\phi_x \phi_{xx} + \phi_y \phi_{yx}) \quad (\text{Eq 15})$$

$$\frac{\partial \rho}{\partial y} = -\frac{\rho}{c^2}(\phi_x \phi_{xy} + \phi_y \phi_{yy}) \quad (\text{Eq 16})$$

Equation 14 becomes

$$\left(1 - \frac{\phi_x^2}{c^2}\right)\phi_{xx} - 2\frac{\phi_x \phi_y}{c^2}\phi_{xy} + \left(1 - \frac{\phi_y^2}{c^2}\right)\phi_{yy} + \frac{\sigma \phi_y}{y} = 0 \quad (\text{Eq 17})$$

$$c^2 = c^2(V) \quad (\text{Eq 18})$$

I, Supersonic Flow of a Gas in Chemical Equilibrium: Dynamic and Thermodynamic Relations (cont.)

If we set θ = flow angle, then

$$\begin{aligned} u &= V \cos \theta \\ v &= V \sin \theta \end{aligned} \quad (\text{Eq 19})$$

and with the Mach angle α defined by

$$\sin \alpha = \frac{c}{V} = \frac{1}{M} \quad (\text{Eq 20})$$

then the method of characteristics applied to equation (1-17) yields the following expressions:

$$\frac{dy}{dx} = \tan(\theta - \alpha) \quad \text{Characteristic I} \quad (\text{Eq 21})$$

$$\frac{dy}{dx} = \tan(\theta + \alpha) \quad \text{Characteristic II} \quad (\text{Eq 22})$$

$$\frac{1}{V} \left(\frac{dV}{d\theta} \right)_I = -\tan \alpha + \sigma \cdot \frac{\sin \alpha \tan \alpha \sin \theta}{y \sin(\theta - \alpha)} \left(\frac{dy}{d\theta} \right)_I \quad (\text{Eq 23})$$

$$\frac{1}{V} \left(\frac{dV}{d\theta} \right)_{II} = \tan \alpha + \sigma \cdot \frac{\sin \alpha \tan \alpha \sin \theta}{y \sin(\theta + \alpha)} \left(\frac{dy}{d\theta} \right)_{II} \quad (\text{Eq 24})$$

$$\text{I: } \frac{dy}{dx} = \frac{\sqrt{M^2 - 1} \sin \theta - \cos \theta}{\sqrt{M^2 - 1} \cos \theta + \sin \theta} \quad (\text{Eq 25})$$

$$\text{II: } \frac{dy}{dx} = \frac{\sqrt{M^2 - 1} \sin \theta + \cos \theta}{\sqrt{M^2 - 1} \cos \theta - \sin \theta} \quad (\text{Eq 26})$$

$$\text{I: } \frac{1}{M} \left(1 + \frac{M}{c} \frac{dc}{dM} \right) \frac{dM}{d\theta} = -\frac{1}{\sqrt{M^2 - 1}} + \sigma \frac{\sin \theta}{y \sqrt{M^2 - 1} (\sqrt{M^2 - 1} \sin \theta - \cos \theta)} \left(\frac{dy}{d\theta} \right) \quad (\text{Eq 27})$$

$$\text{II: } \frac{1}{M} \left(1 + \frac{M}{c} \frac{dc}{dM} \right) \frac{dM}{d\theta} = \frac{1}{\sqrt{M^2 - 1}} + \sigma \frac{\sin \theta}{y \sqrt{M^2 - 1} (\sqrt{M^2 - 1} \sin \theta + \cos \theta)} \frac{dy}{d\theta} \quad (\text{Eq 28})$$

I, Supersonic Flow of a Gas in Chemical Equilibrium: Dynamic and Thermodynamic Relations (cont.)

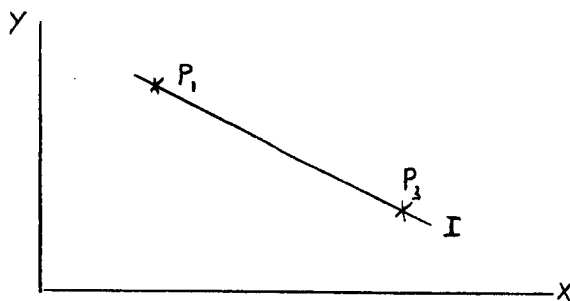
The presence of the sound velocity (c) in the equations is the main effect of including the shifting equilibrium. This adds no great complication to the computation since c can be obtained as a function of Mach number using an existing program that computes the sonic velocity in a reacting gas mixture.*

* G. Gruber, Calculating the Equilibrium Sonic Velocity in a Reacting Gas Mixture, Report RM 7345, Aerojet-General Corporation, 26 July 1961.

II. NUMERICAL SOLUTION OF CHARACTERISTIC EQUATIONS

A. FINITE DIFFERENCE APPROXIMATIONS

The numerical solution of the problem using the method of characteristics consists of building up a network of points using Equations 25 through 28 Section I. Consider a I characteristic passing through the points $P_1(x_1, y_1, M_1, \theta_3)$ with the flow at P_1 known as illustrated below:



and the flow at P_3 to be determined.

To integrate Equation 25, Section I, along $P_1 P_3$

$$\int_{y_1}^{y_3} dy = \int_{x_1}^{x_3} \frac{\sqrt{m^2 - 1} \sin \theta - \cos \theta}{\sqrt{m^2 - 1} \cos \theta + \sin \theta} dx \quad (\text{Eq 29})$$

choose the finite difference form:

$$\text{I:} \quad \frac{y_3 - y_1}{x_3 - x_1} = \frac{\sqrt{M_{13}^2 - 1} \sin \theta_{13} - \cos \theta_{13}}{\sqrt{M_{13}^2 - 1} \cos \theta_{13} + \sin \theta_{13}} \quad (\text{Eq 30})$$

$$\text{with} \quad M_{13} = \frac{M_1 + M_3}{2}$$

$$\text{and} \quad \theta_{13} = \frac{\theta_1 + \theta_3}{2}$$

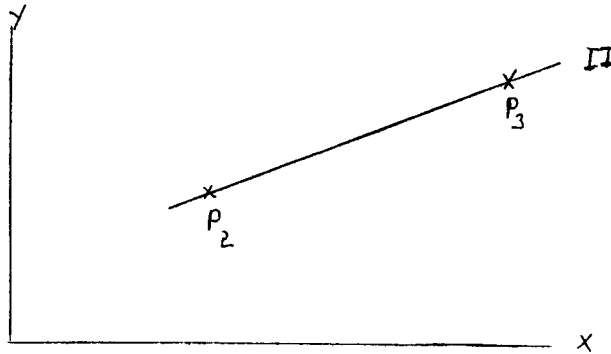
II, A, Finite Difference Approximations (cont.)

Similarly, Equation 27 is approximated by

$$I: \frac{\sqrt{M_{13}^2 - 1}}{M_{13}} \left(1 + \frac{M_{13}}{C_{13}} \left(\frac{dC}{dM} \right)_{13} \frac{M_3 - M_1}{\theta_3 - \theta_1} \right) = -1 + \frac{\sigma \sin \theta_{13}}{y_{13} (\sqrt{M_{13}^2 - 1} \sin \theta_{13} + \cos \theta_{13})} \cdot \frac{(y_3 - y_1)}{(\theta_3 - \theta_1)} \quad (\text{Eq 31})$$

with C_{13} and $\left(\frac{dC}{dM} \right)_{13}$ obtained from the table of C versus M.

Now consider a II characteristic passing through the points $P_2(x_2, y_2, M_2, \theta_2)$ and $P_3(x_3, y_3, M_3, \theta_3)$ with the flow at P_2 known and the flow at P_3 to be determined as shown below:



The finite difference forms for Equations 26 and 28 along $P_2 P_3$ are

$$II: \frac{y_3 - y_2}{x_3 - x_2} = \frac{\sqrt{M_{23}^2 - 1} \sin \theta_{23} + \cos \theta_{23}}{\sqrt{M_{23}^2 - 1} \cos \theta_{23} - \sin \theta_{23}} \quad (\text{Eq 32})$$

$$II: \frac{\sqrt{M_{23}^2 - 1}}{M_{23}} \left(1 + \frac{M_{23}}{C_{23}} \left(\frac{dC}{dM} \right)_{23} \frac{M_3 - M_2}{\theta_3 - \theta_2} \right) = \frac{\sigma \sin \theta_{23}}{y_{23} (\sqrt{M_{23}^2 - 1} \sin \theta_{23} + \cos \theta_{23})} \cdot \frac{(y_3 - y_2)}{(\theta_3 - \theta_2)} \quad (\text{Eq 33})$$

II, A, Finite Difference Approximations (cont.)

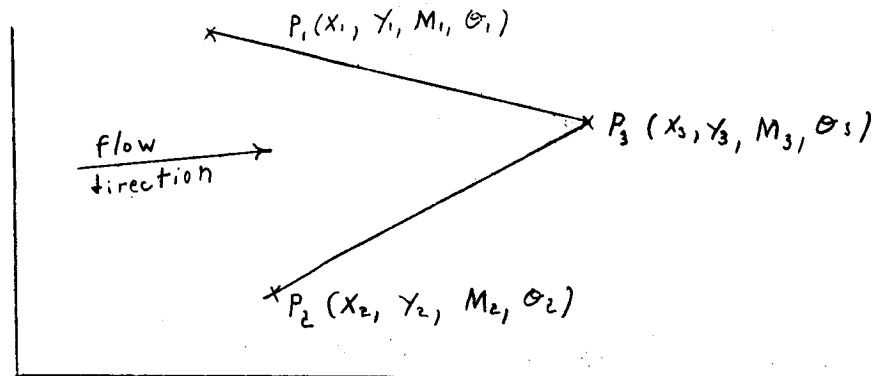
with

$$M_{23} = \frac{M_2 + M_3}{2}, \quad \theta_{23} = \frac{\theta_2 + \theta_3}{2},$$

and C_{23} and $\left(\frac{dC}{dM}\right)_{23}$ obtained from the table of C versus M .

B. CALCULATING AN INTERIOR POINT

In this section the calculation of a single interior network point is examined as illustrated below.



In the figure above, assume that the flow conditions at points P_1 and P_2 are known and the flow at P_3 is to be determined. At point P_1 the direction of the I characteristic is given by Equation 30 and the change of M, θ along this characteristic is given by Equation 31. Similarly, at point P_2 the direction of the II characteristic is given by Equation 32 and the change in M and θ along it by Equation 33, thus yielding four equations in the four unknowns x_3, y_3, M_3 and θ_3 .

The slope of the characteristic is a function of the average Mach number and average flow angle which in turn depend upon M_3 and θ_3 . Therefore, assume an initial guess and gradually converge on the correct average.

II, B, Calculating an Interior Point (cont.)

Define

$$\begin{aligned}
 K_1 &= \sqrt{M_{13}^2 - 1} \cos \theta_{13} + \sin \theta_{13} \\
 K_2 &= \sqrt{M_{13}^2 - 1} \sin \theta_{13} - \cos \theta_{13} \\
 K_3 &= \sqrt{M_{23}^2 - 1} \cos \theta_{23} - \sin \theta_{23} \\
 K_4 &= \sqrt{M_{23}^2 - 1} \sin \theta_{23} + \cos \theta_{23}
 \end{aligned}
 \tag{Eq 34}$$

then Equations 30 and 32 become

$$(y_3 - y_1)(K_1) = (x_3 - x_1)(K_2) \tag{Eq 35}$$

$$(y_3 - y_2)(K_3) = (x_3 - x_2)(K_4) \tag{Eq 36}$$

or

$$K_1 y_3 - K_2 x_3 = K_1 y_1 - K_2 x_1 = K_5$$

$$K_3 y_3 - K_4 x_3 = K_3 y_2 - K_4 x_2 = K_6$$

Thus

$$y_3 = \frac{\begin{vmatrix} K_5 & -K_2 \\ K_6 & -K_4 \end{vmatrix}}{\begin{vmatrix} K_1 & -K_2 \\ K_3 & -K_4 \end{vmatrix}} = \frac{K_2 K_6 - K_4 K_5}{K_2 K_3 - K_1 K_4} \tag{Eq 37}$$

$$x_3 = \frac{K_2 K_6 - K_4 K_5}{K_2 K_3 - K_1 K_4} \tag{Eq 38}$$

II, B, Calculating an Interior Point (cont.)

To solve Equations 31 and 33 for M_3 and θ_3 , define

$$\left. \begin{aligned} G_1 &= \sqrt{M_{13}^2 - 1} / M_{13} \\ G_2 &= \sqrt{M_{23}^2 - 1} / M_{23} \\ H_1 &= \left(1 + \frac{M_{13}}{C_{13}} \left(\frac{dC}{dM}\right)_{13}\right) \\ H_2 &= \left(1 + \frac{M_{23}}{C_{23}} \left(\frac{dC}{dM}\right)_{23}\right) \end{aligned} \right\} \quad (\text{Eq 39})$$

$$\left. \begin{aligned} F_1 &= \sigma \left(\frac{y_3 - y_1}{K_2} \right) = \sigma \left(\frac{x_3 - x_1}{K_1} \right) \\ F_2 &= \sigma \left(\frac{y_3 - y_2}{K_4} \right) = \sigma \left(\frac{x_3 - x_2}{K_3} \right) \end{aligned} \right\} \quad (\text{Eq 40})$$

then Equations 31 and 33 become

$$H_1 G_1 (M_3 - M_1) = -(\theta_3 - \theta_1) + \frac{\sin \theta_{13}}{y_{13}} F_1 \quad (\text{Eq 41})$$

$$H_2 G_2 (M_3 - M_2) = (\theta_3 - \theta_2) + \frac{\sin \theta_{23}}{y_{23}} F_2 \quad (\text{Eq 42})$$

from which

$$H_1 G_1 M_3 + \theta_3 = H_1 G_1 M_1 + \theta_1 + \frac{\sin \theta_{13}}{y_{13}} F_1 = L_1$$

$$H_2 G_2 M_3 - \theta_3 = H_2 G_2 M_2 - \theta_2 + \frac{\sin \theta_{23}}{y_{23}} F_2 = L_2$$

II, B, Calculating an Interior Point (cont.)

Solving for M_3 and θ_3 :

$$M_3 = \frac{L_1 + L_2}{H_1 G_1 + H_2 G_2} \quad (\text{Eq 43})$$

$$\theta_3 = \frac{H_2 G_2 L_1 - H_1 G_1 L_2}{H_1 G_1 + H_2 G_2} \quad (\text{Eq 44})$$

To start the iteration, assume $M_{13} = M_1$, $M_{23} = M_2$, $\theta_{13} = \theta_1$, $\theta_{23} = \theta_2$, and

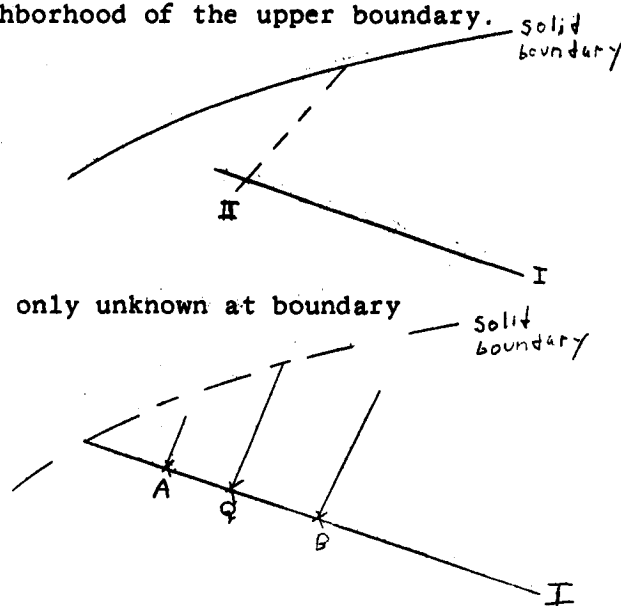
- a. Compute $C_{13} = f(M_{13})$ and $C_{23} = f(M_{23})$.
- b. Calculate K_1 , K_2 , K_3 , K_4 , G_1 , G_2 , H_1 , and H_2 using Equations 34 and 39.
- c. Calculate x_3 and y_3 using Equations 37 and 38.
- d. Calculate F_1 and F_2 (Equation 40) choosing that form which has the largest denominator
 e.g., if $|K_2| > |K_1|$ then $F_1 = \frac{y_3 - y_1}{K_2} \sigma$
 or if $|K_1| > |K_2|$ then $F_1 = \frac{x_3 - x_1}{K_1} \sigma$
- e. Calculate M_3 and θ_3 using Equations 43 and 44.
- f. Compare the new M_3 with the previously computed M_3 .
- g. Return to step a if the change in M_3 is too large (i.e., $> 10^{-5}$).

When the change in M_3 is sufficiently small, the iteration has converged giving the flow at, and location of, P_3 . Using this procedure, a complete flow field is constructed point by point.

II, Numerical Solution of Characteristic Equations (cont.)

C. BOUNDARY POINT

Consider a characteristic point in the neighborhood of the upper boundary. If the boundary is defined by a continuous function, it would be necessary to find the intersection of the II characteristic through P with the upper boundary. However, in practice, the boundaries are specified by discrete points with the slope of the boundary at each point given (x, y, θ specified). The only unknown at boundary points is the Mach number.



As can be seen from the figure, the II characteristics passing through A and B do not necessarily intersect the boundary at the point P. The II characteristic passing through P intersects the I characteristic through A, B, at Q. Since the flow at points A and B is known, interpolation yields the flow data at Q. Also, Q and P must satisfy the II characteristic Equations 36 and 42. The basic method consists of assuming values of M_P , M_Q and θ_Q , and intersecting the II characteristic passing through P with the line joining A and B. This intersection gives x_Q and y_Q , which can then be used for linear interpolation between A and B to obtain M_Q and θ_Q . The variation of M along the II characteristic from Q to P as given by Equation 36 is used to obtain M_P . The new M_P is compared with the previously computed M_P . Convergence is obtained when the successive values are sufficiently close together (i.e., $\Delta M_P < 10^{-5}$).

The II characteristic passing through Q and P satisfies Equations 36 and 42;

$$(y_P - y_Q)(K_3) = (x_P - x_Q)(K_4) \quad (\text{Eq 36})$$

$$H_2 G_2 (M_P - M_Q) = (\theta_P - \theta_Q) + \frac{\sin \theta_{PQ}}{y_{PQ}} F_2 \quad (\text{Eq 42})$$

II, C, Boundary Point (cont.)

with

$$K_3 = \sqrt{M_{PQ}^2 - 1} \cos \theta_{PQ} - \sin \theta_{PQ}$$

$$K_4 = \sqrt{M_{PQ}^2 - 1} \sin \theta_{PQ} + \cos \theta_{PQ}$$

$$\theta_{PQ} = \frac{(\theta_P + \theta_Q)}{2}$$

$$M_{PQ} = \frac{(M_P + M_Q)}{2}$$

$$G_2 = \frac{\sqrt{M_{PQ}^2 - 1}}{M_{PQ}}$$

(Eq 45)

$$H_2 = \left[\left(1 + \frac{M_{PQ}}{C_{PQ}} \left(\frac{dC}{dM} \right) \right) \right]_{PQ}$$

$$F_2 = \sigma \frac{y_P - y_Q}{K_4} = \sigma \frac{x_P - x_Q}{K_3}$$

(Eq 46)

The equation of the line joining A, B, evaluated at Q is:

$$y_Q = y_B + \frac{y_A - y_B}{x_A - x_B} (x_Q - x_B)$$

(Eq 47)

With x_P and y_P known, solve Equations 36 and 44 for x_Q and y_Q .

$$y_Q = y_P (x_Q - x_P) \frac{K_4}{K_3} = y_B + \frac{y_A - y_B}{x_A - x_B} (x_Q - x_B)$$

II, C, Boundary Point (cont.)

$$x_Q \left(\frac{K_4}{K_3} - \frac{y_A - y_B}{x_A - x_B} \right) = y_B - x_B \left(\frac{y_A - y_B}{x_A - x_B} \right) - y_P + x_P \frac{K_4}{K_3}$$

$$x_Q = \frac{1}{\left(\frac{K_4}{K_3} - \frac{y_A - y_B}{x_A - x_B} \right)} \left[y_B - y_P + x_P \frac{K_4}{K_3} - x_B \left(\frac{y_A - y_B}{x_A - x_B} \right) \right] \quad (\text{Eq 48})$$

with x_Q and y_Q determined, interpolate for M_Q and θ_Q

$$M_Q = M_B + \left(\frac{x_Q - x_B}{x_A - x_B} \right) (M_A - M_B) \quad (\text{Eq 49})$$

$$\theta_Q = \theta_B + \left(\frac{x_Q - x_B}{x_A - x_B} \right) (\theta_A - \theta_B)$$

The iteration can be started by assuming $M_Q = M_P = \frac{(M_B + M_A)}{2}$.

- a. Compute $C_Q(M_Q)$ and $C_P(M_P)$.
- b. Calculate quantities given in Equation 31.
- c. Calculate x_Q using Equation 48 and y_Q from Equation 33 unless $x_A = x_B$, in which case $x_Q = x_A = x_B$ and y_Q is calculated using Equation 36.
- d. Calculate M_Q and θ_Q using equations 49.
- e. Calculate F_2 using that form of Equation 46 having the largest magnitude denominator.
- f. Calculate a new value for M_P using Equation 43.

II, C, Boundary Point (cont.)

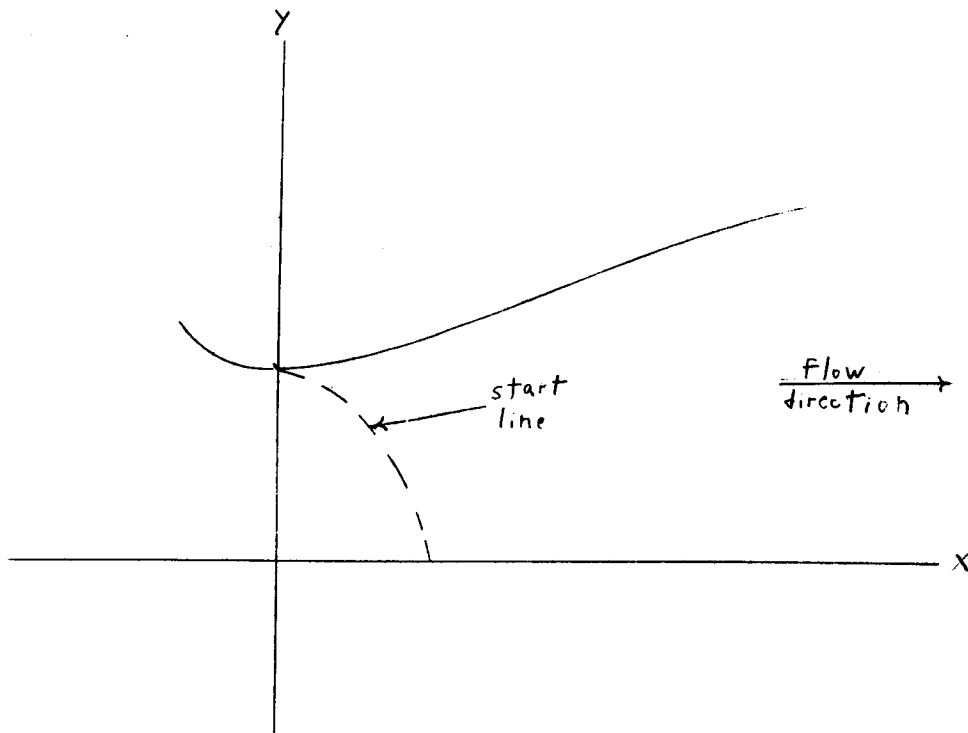
$$M_P = M_Q + \frac{1}{H_2 G_2} \left[(\theta_P - \theta_Q) + (F_2) \left(\frac{\sin \theta_{PQ}}{y_{PQ}} \right) \right]$$

g. Compare the new M_P with the previous M_P . If they are too far apart (i.e., greater than 10^{-5}), return to a. Using Equation 35 and 42, similar equations can be developed for a characteristic point in the neighborhood of the lower boundary.

II, Numerical Solution of Characteristic Equations (cont.)

D. THE START LINE

The methods for solving for interior and boundary points gives the means for developing the complete flow through the nozzle if the flow along a start line immediately downstream of the nozzle throat is known. This start line can be obtained by using the method presented by R. Sauer*.



The only problem encountered in using this method in shifting equilibrium problems is that it requires the ratio of specific heats (γ). However, in the neighborhood of the throat, the Mach number is 1, hence pressure and density are nearly constant. Therefore, assuming a constant γ along the start line should be a good approximation.

* R. Sauer, General Characteristic of flow through nozzles at near critical speeds, NACA JM1147, 1947

II, Numerical Solution of Characteristic Equations (cont.)

E. MASS FLOW AND THRUST

Using the equations in sections 2, and 3 the characteristic network representing the flow through any axisymmetric nozzle for equilibrium or frozen flow can be constructed. Other useful quantities are the mass flow and the total axial thrust which is composed of the axial momentum flux of the gas and the pressure x area in the axial direction on the boundaries of the nozzle.

The momentum flux is obtained from

$$\frac{\dot{m}V}{g} = \frac{\dot{m}MC}{g}$$

with the mass flow rate (\dot{m}) given by:

$$\dot{m} = \frac{\rho AV}{144} = \frac{\rho AMC}{144} \text{ lb/sec}$$

For an elemental area dA

$$d\dot{m} = \frac{\rho MC}{144} dA$$

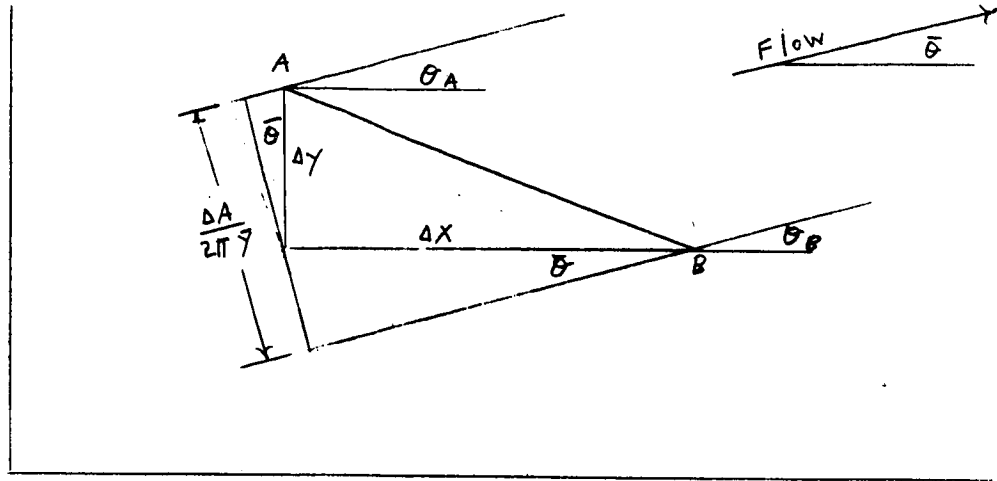
which in finite difference form becomes:

$$\Delta\dot{m} + \frac{\bar{\rho}\bar{M}\bar{C}}{144} \Delta A$$

with the bars denoting the average value across the incremental area ΔA .

ΔA can be described in terms of the component of area normal to the direction of flow between two points. The effective flow area between the points A B is shown below.

II, E, Mass Flow and Thrust (cont.)



$$\Delta A = (\Delta y \cos \bar{\theta} - \Delta x \sin \bar{\theta}) 2\pi \bar{y}$$

$$= [(y_B - y_A) \cos \bar{\theta} - (x_B - x_A) \sin \bar{\theta}] [\pi(y_B + y_A)]$$

with $\bar{\theta} = (\theta_A + \theta_B)/2$ and $\bar{y} = (y_B + y_A)/2$

Hence $\Delta \dot{m} = \pi \frac{\bar{\rho} \bar{M} \bar{C}}{144} (y_B + y_A) [(y_B - y_A) \cos \bar{\theta} - (x_B - x_A) \sin \bar{\theta}]$ (Eq 50)

The axial component of the momentum at point B is obtained from

$$\text{Mom.}_{\text{axial B}} = \text{Mom.}_{\text{axial A}} + \Delta \text{Mom.}_{\text{axial AB}}$$

with

$$\Delta \text{Mom.}_{\text{axial AB/sec}} = \frac{MC}{g} \Delta \dot{m} \cos(\bar{\theta})$$

Substituting from Equation (50) gives:

$$\Delta \text{Mom.}_{\text{axial AB/sec}} = \frac{\bar{\rho} \bar{M}^2 \bar{C}^2}{144g} (y_B + y_A) [(y_B - y_A) \cos \bar{\theta} - (x_B - x_A) \sin \bar{\theta}] \cos \bar{\theta}$$
 (Eq 51)

II, E, Mass Flow and Thrust (cont.)

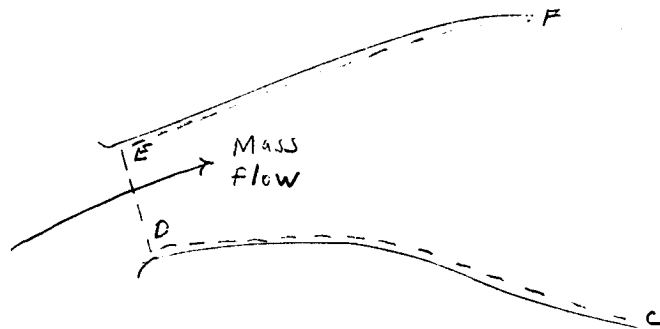
The thrust because of the pressure of the gas acting on the solid boundary wall can also be written in terms of radial and axial components.

The axial component

$$\begin{aligned}
 F_{\text{axial}} &= \text{Press.} \cdot \text{Area axial} \\
 &= P \cdot A \cos \theta \\
 \Delta F_{\text{axial}} &= \bar{P} \cdot \Delta A \cos \bar{\theta} \\
 &= \pi \bar{P} (y_B^2 - y_A^2) \quad (\text{Eq 52})
 \end{aligned}$$

Note that P is obtained at each boundary point from a table of P verses M , with M known at each point.

In obtaining the total thrust of a given nozzle, it is necessary to integrate the momentum flux and pressure thrust over a suitable control surface. A control surface often used consists of a curve going along a solid boundary across the flow in the neighborhood of the throat and along the other solid boundary.



In the figure, integrate $P \cdot \Delta A$ along CD , DE and EF , and the momentum flux along DE . The sum of these gives the total thrust of the nozzle. The total mass flow is obtained from integrating mass flow along DE .

The divergence loss for a nozzle then may be calculated from

$$\lambda = 1 - \frac{F}{F_{1\text{-Dimensional}}}$$

III. THE OPTIMUM THRUST NOZZLE

A. INTRODUCTION

G.V.R. Rao gives a method for designing the nozzle contour to yield the optimum thrust.* The governing conditions are the nozzle length, the ambient pressure, and the flow conditions in the neighborhood of the throat. The ratio of specific heats was assumed constant. The mathematical method employed is the calculus of variation. Lagrangean multipliers are determined and the control surface ascertained to be a surface generated by a left running characteristic. The method of characteristics is then used to compute the contour.

Later, Rao presented a method** that takes care of the varying gas properties associated with chemical reaction occurring downstream of the nozzle. Because γ is no longer constant, the original method of deriving the Lagrangean constants as well as the identification of the control surface should be re-examined. In the following we shall show that the equations as given in Rao's earlier paper are still valid, except that a method to compute c through thermal chemical considerations is needed. The method is attributed to Gruber and appears in the work cited earlier.

B. THE VARIATION INTEGRAL

We want to optimize the thrust

$$\text{Thrust} = \int_{y_C}^{y_E} \left[(p - p_a) + \frac{\rho V^2 \sin(\phi - \theta) \cos \theta}{\sin \phi} \right] 2\pi y \, dy$$

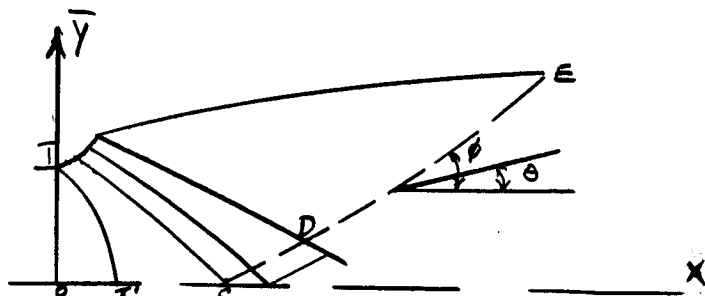
with

p = flow pressure

p_a = ambient pressure

θ = flow direction angle

ϕ = direction of control surface (not to be confused with potential function mentioned in Section I.)



* G.V.R. Rao, "Exhaust Nozzle Contour for Optimum Thrust," Jet Propulsion, June 1958, 377 to 382

** G.V.R. Rao, "Contoured Rocket Nozzle," Ninth Congress of the International Astronautical Federation, Amsterdam, 1958.

III, B, The Variation Integral (cont.)

The constraints are

$$\text{Mass flow (known)} = \int_{y_C}^{y_E} \rho v \frac{\sin(\phi - \theta)}{\sin \phi} 2 \pi y \, dy$$

and

$$\text{Length (known)} = x_C + \int_{y_C}^{y_E} \cot \phi \, dy$$

or

$$\int_{y_C}^{y_E} \cot \phi \, dy = \text{constant}$$

Of the five variables ρ , V , ϕ , θ , p , we shall take ϕ , θ and the Mach number M as dependent variables and y as the independent variable.

Letting

$$f_1 = \left[p - p_a + \rho v^2 \cdot \frac{\sin(\phi - \theta) \cos \theta}{\sin \phi} \right] y$$

$$f_2 = \rho \cdot v \frac{\sin(\theta - \phi)}{\sin \phi} y$$

$$f_3 = \cot \phi$$

and introducing Lagrangean multipliers λ_2 , λ_3 , we have the integral

$$I = \int_{y_C}^{y_E} (f_1 + \lambda_2 f_2 + \lambda_3 f_3) \, dy$$

III, B, The Variation Integral (cont.)

to optimize. From this we get three equations from the three coefficients of $\delta M, \delta \phi, \delta \theta$:

$$f_{1M} + \lambda_2 f_{2M} + \lambda_3 f_{3M} = 0 \quad (\text{Eq 52})$$

$$f_1 + \lambda_2 f_2 \phi + \lambda_3 f_3 \phi = 0 \quad (\text{Eq 53})$$

$$f_{1\theta} + \lambda_2 f_{2\theta} + \lambda_3 f_{3\theta} = 0 \quad (\text{Eq 54})$$

These equations are valid for points on DE. In addition, we have the equation

$$f_1 + \lambda_2 f_2 + \lambda_3 f_3 = 0, \text{ at E.} \quad (\text{Eq 55})$$

As $f_{3M} = f_{3\theta} = 0$, we have from Equations (52) and (53)

$$\lambda_2 = f_{1M}/f_{2M} = -f_{1\theta}/f_{2\theta} \quad (\text{Eq 56})$$

Let

$$\ell = \frac{\sin(\phi - \theta) \cos \theta}{\sin \phi}$$

then

$$\begin{aligned} \frac{f_{1M}}{f_{2M}} &= \frac{\frac{dp}{dM} + \ell \frac{dp V^2}{dM}}{\frac{\ell}{\cos \theta} \frac{dp V}{dM}} = \frac{\cos \theta}{\ell} \frac{dp}{dp V} + \frac{dp V^2}{dp V} \cos \theta \\ &= \frac{\cos \theta}{\ell} \frac{V}{\frac{V^2}{C^2} + \rho V \frac{dV}{d\rho}} + V \cos \theta + \rho V \cos \theta \frac{dV}{d\rho V} \end{aligned} \quad (\text{Eq 57})$$

III, B, The Variation Integral (cont.)

Now

$$VdV = -\frac{1}{\rho} dp$$

Hence

$$\rho V \frac{dV}{dp} = -1 \quad (\text{Eq 58})$$

Next,

$$d\phi = -\frac{\rho}{c^2} VdV, \quad \text{or} \quad V \frac{d\phi}{dV} = -\frac{\rho V^2}{c^2}$$

$$\frac{dV}{d\rho V} = \frac{1}{\rho + V \frac{d\rho}{dV}} = \frac{1}{\rho - \rho \frac{V^2}{c^2}}$$

$$= \frac{1}{\rho (1 - M^2)} \quad (\text{Eq 59})$$

Substituting Equations 58 and 59 in 57, we have

$$\frac{f_{1M}}{f_{2M}} = \frac{V \cos \theta}{M^2 - 1} \frac{1 - \ell}{\ell} + V \cos \theta \quad (\text{Eq 60})$$

On the other hand

$$\frac{f_{1\theta}}{f_{2\theta}} = V \cos \theta + V \tan (\phi - \theta) \sin \theta \quad (\text{Eq 61})$$

Hence, from Equations (60) and (61), we have

$$\frac{\cos \theta}{M^2 - 1} \left(1 - \frac{\sin \phi}{\sin (\phi - \theta) \cos \theta} \right) = \tan (\phi - \theta) \sin \theta \quad (\text{Eq 62})$$

III, B, The Variation Integral (cont.)

By definition,

$$\sin \alpha = \frac{1}{M}, \quad M^2 - 1 = \cot^2 \alpha$$

Therefore Equation 62 reduces to

$$\tan(\phi - \theta) = \tan \pm \alpha$$

or

$$- \theta = \pm \alpha$$

As CDE is crossed by streamline, $\phi > \theta$,

$$\phi = \theta + \alpha \quad (\text{Eq 63})$$

This says that DE is a left running characteristic.

Now by Equations 61 and 63, we have

$$\lambda_2 = -v \frac{\cos(\theta - \alpha)}{\cos \alpha} \quad (\text{Eq 64})$$

and this is valid for points on DE.

From Equation 53 we obtain

$$\lambda_3 = -\rho v^2 y \tan \alpha \sin^2 \theta$$

III, The Optimum Thrust Nozzle (cont.)

C. THE COMPATIBILITY EQUATION

In Rao's paper published in June 1958 in Jet Propulsion, the compatibility equation for constant γ is

$$\frac{d\theta}{dy} - \frac{dM}{dy} \frac{\sqrt{M^2 - 1}}{M \left[\frac{\gamma - 1}{2} M^2 - 1 \right]} + \frac{\sin \alpha \sin \theta}{y \sin (\theta + \alpha)} = 0$$

In his Amsterdam presentation, this becomes

$$\frac{d\theta}{dy} - \frac{\cot \alpha}{V} \frac{dV}{dy} + \frac{\sin \alpha \sin \theta}{y \sin (\theta + \alpha)} = 0 \quad (\text{Eq 66})$$

where no γ appears.

This form can be derived from

$$\frac{dp}{\rho V^2 \tan \alpha} + d\theta + \frac{\sin \alpha \sin \theta}{\sin (\theta + \alpha)} \frac{dy}{y} = 0$$

given on Page 257 of Rao's work. Our job is now to show that Equation 66 is satisfied for points on DE. We shall start from

$$\lambda_2 = - \frac{V \cos (\theta - \alpha)}{\cos \alpha} \quad (\text{Eq 67})$$

$$\lambda_3 = \rho V^2 y \tan \alpha \sin^2 \theta \quad (\text{Eq 68})$$

Take logarithmic differentiation of (3.3-2)

$$\therefore 0 = d \ln V + \left[\tan \alpha + \tan (\theta - \alpha) \right] d\alpha - \tan (\theta - \alpha) d\theta \quad (\text{Eq 69})$$

III, C, The Compatibility Equation (cont.)

Now

$$\tan \alpha + \tan (\theta - \alpha) = \frac{\sin \theta}{\cos \alpha \cos (\theta - \alpha)}$$

Equation 69 becomes

$$\frac{\cos(\theta - \alpha)}{\sin \theta} d \ln V = \frac{d \alpha}{\cos \alpha} - \frac{\sin (\theta - \alpha)}{\sin \theta} d \theta = 0 \quad (\text{Eq 70})$$

Taking the log differentiation of Equation 68

$$0 = d \ln \rho + 2 d \ln V + d \ln y + \frac{d \alpha}{\sin \alpha \cos \alpha} + 2 \cot \theta d \theta \quad (\text{Eq 71})$$

Now

$$d \frac{V^2}{2} = - \frac{1}{\rho} d \rho \quad \text{Bernoulli's equation.}$$

∴

$$V dV = - \frac{1}{\rho} \frac{d \rho}{d \rho} d \rho = - C^2 d \ln \rho$$

or

$$V^2 d \ln V = - C^2 d \ln \rho$$

∴

$$M^2 d \ln V = - d \ln \rho$$

Substituting in Equation 71

$$0 = M^2 d \ln V + 2 d \ln V + d \ln y + \frac{d \alpha}{\sin \alpha \cos \alpha} + 2 \cot \theta d \theta$$

or

$$(2 - M^2) d \ln V + d \ln y + \frac{d \alpha}{\sin \alpha \cos \alpha} + 2 \cot \theta d \theta = 0$$

III, C, The Compatibility Equation (cont.)

Now $2 - M^2 = \frac{\sin^2 \alpha - \cos^2 \alpha}{\sin^2 \alpha}$, we have

$$\frac{\sin^2 \alpha - \cos^2 \alpha}{\sin^2 \alpha} d \ln V + d \ln y + \frac{d \alpha}{\sin \alpha \cos \alpha} + 2 \cot \theta d \theta = 0$$

$$\therefore \frac{\sin^2 \alpha - \cos^2 \alpha}{\sin \alpha} d \ln V + \sin \alpha d \ln y + \frac{d \alpha}{\cos \alpha} + 2 \sin \alpha \cot \theta d \theta = 0 \quad (\text{Eq 72})$$

Equations 70 to 72:

$$\left(\frac{\cos (\theta - \alpha)}{\sin \theta} - \frac{\sin^2 \alpha - \cos^2 \alpha}{\sin \alpha} \right) d \ln V - \sin \alpha d \ln y - \left[\frac{\sin (\theta - \alpha)}{\sin \theta} + 2 \sin \alpha \cot \theta \right] d \theta = 0 \quad (\text{Eq 73})$$

Now

$$\frac{\cos (\theta - \alpha)}{\sin \theta} - \frac{\sin^2 \alpha - \cos^2 \alpha}{\sin \alpha} = \frac{\cos \alpha}{\sin \alpha} \cdot \frac{\sin (\theta + \alpha)}{\sin \theta}$$

Next,

$$\frac{\sin (\theta - \alpha) + 2 \sin \alpha \cos \theta}{\sin \theta} = \frac{\sin (\theta + \alpha)}{\sin \theta}$$

74 is then reduced to

$$\cot \alpha \frac{\sin (\theta + \alpha)}{\sin \theta} d \ln V - \sin \alpha d \ln y - \frac{\sin (\theta + \alpha)}{\sin \theta} d \theta = 0$$

III, C, The compatibility Equation (cont.)

or
$$d\theta - \cot \alpha d \ln V + \frac{\sin \alpha \sin \theta}{\sin (\theta + \alpha)} d \ln y = 0$$

i.e.

$$d\theta - \cot \alpha \frac{dV}{V} + \frac{\sin \alpha \sin \theta}{\sin (\theta + \alpha)} \frac{dy}{y} = 0. \quad (\text{Eq 74})$$

The possibility of deriving Equation 74 from the constancy of λ_2, λ_3 along DE gives us the assurance that the assumption of constancy of λ_2, λ_3 is mathematically sound and physically compatible.

IV. COMPUTATION OF THE OPTIMUM THRUST NOZZLE

A. INTRODUCTION

The following is concerned with implementing the optimum thrust nozzle design equations given by G.V.R. Rao. The equations are modified to place them in a form more suitable for computation.

Equation 67, Section III, can be written as

$$\begin{aligned} -\lambda_2 &= \frac{MC \cos(\theta - \alpha)}{\cos \alpha} \\ &= \frac{MC [\cos \theta \cos \alpha + \sin \theta \sin \alpha]}{\cos \alpha} \end{aligned}$$

which is further simplified by using $\sin \alpha = 1/M$ from which

$$\begin{aligned} \cos \alpha &= \frac{\sqrt{M^2 - 1}}{M} \\ -\lambda_2 &= \frac{MC}{\sqrt{M^2 - 1}} \left[\sqrt{M^2 - 1} \cos \theta + \sin \theta \right] \end{aligned} \quad (\text{Eq 75})$$

Equation 68 becomes

$$\begin{aligned} -\lambda_3 &= y \rho V^2 \sin^2 \theta \tan \alpha \\ &= \frac{y \rho M^2 C^2 \sin^2 \theta}{\sqrt{M^2 - 1}} \end{aligned} \quad (\text{Eq 76})$$

Equation 14 of Rao's paper on the contoured rocket nozzle is

$$\sin 2\theta = \frac{P_e - P_a}{\frac{1}{2} \rho V^2} \cot \alpha \quad \text{at E} \quad (\text{Eq 77})$$

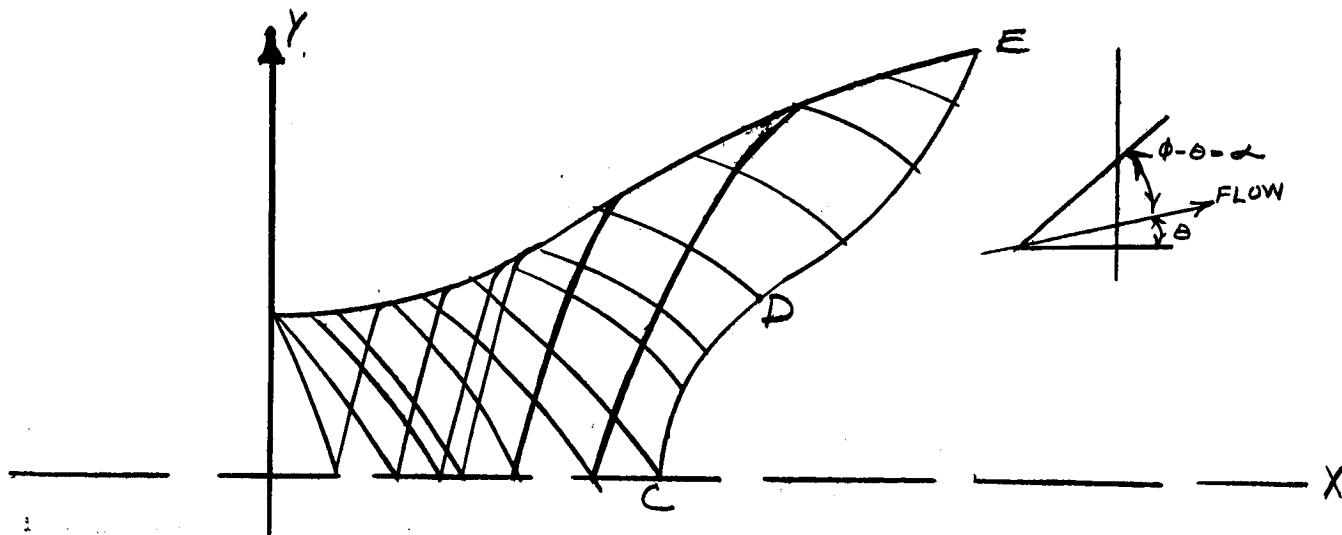
or

$$\sin 2\theta = \frac{2(P_e - P_a)}{\rho M^2 C^2} \cot \alpha$$

IV, A, Introduction (cont.)

Equation 3 of Rao's paper gives the length of the diverging section:

$$\begin{aligned}
 L &= x_C + \int_C^E \cot \theta \, dy \\
 &= x_C + \int_C^E \cot(\theta + \alpha) \, dy \\
 &= x_C + \int_{y_C}^{y_E} \frac{\cot \theta \cot \alpha - 1}{\cot \theta + \cot \alpha} \, dy \\
 &= x_C + \int_{y_C}^{y_E} \frac{\sqrt{M^2 - 1} \cot \theta - 1}{\cot \theta + \sqrt{M^2 - 1}} \, dy
 \end{aligned}
 \tag{Eq 78}$$



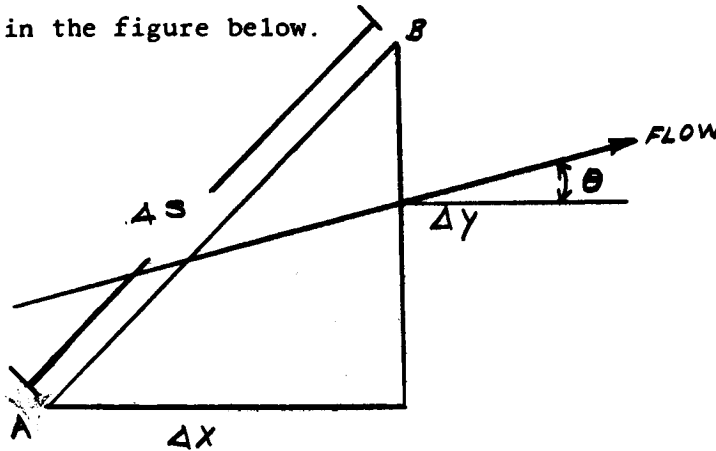
If Equations 75 and 76 could be solved for M and θ ; they would be expressed as functions of y and hence could be substituted into Equation 78, which in turn could then be integrated to determine L . Unfortunately, solving Equations 75 and 76 for M and θ analytically is difficult because of the tabular functions p and C . They are therefore solved pointwise by using a numerical iteration scheme. This requires that a numerical scheme also be used for integrating Equation 78.

IV, Computation of the Optimum Thrust Nozzle (cont.)

B. THE NOZZLE LENGTH

At each interior point C the values of λ_2 , λ_3 can be computed using Equations 75 and 76. These values of λ_2 , λ_3 then determine a control surface as λ_2 , λ_3 are constant along a control surface. Equations 77 and 78 with conservation of mass additionally define an unique optimum thrust nozzle.

L is computed using Equation 78 with the initial point of integration (x_C, y_C) known. The integral is computed by subdividing the interval C-E into small subintervals and accumulating the contribution in each subinterval. Let a subinterval be between the point A, B as in the figure below.



From the figure, the length of the nozzle to B, by Equation 78, becomes:

$$x_B = x_A + \int_A^B \frac{\sqrt{M^2-1} \cot \theta - 1}{\cot \theta + \sqrt{M^2-1}} dy$$

Using average values of the variables across the interval AB gives

$$x_B = x_A + \left(\frac{\sqrt{M_{AB}^2-1} \cot(\theta_{AB}) - 1}{\cot(\theta_{AB}) + \sqrt{M_{AB}^2-1}} \right) (y_B - y_A) \quad (\text{Eq 78})$$

IV, B, The Nozzle Length (cont.)

Choosing $\Delta y = Y_B - Y_A = \text{constant}$, determined from the size of the nozzle, we can solve Equations 75 and 76 for θ_B and M_B using the Newton-Raphson Method for use in Equation 78 and hence obtain x_B . This process of incrementing y , solving Equations 75 and 76, and integrating Equation 78 forward one step is continued until $y = y_e$.

C. M AND θ ON THE CONTROL SURFACE OR EXIT CHARACTERISTIC

The Newton-Raphson iteration method is used for solving Equations 75 and 76. This method is used because it converges rapidly when good first guesses are used for the variables. In this case, with fine spacing, M and θ at the previously determined point will be close to the desired M and θ .

The Newton-Raphson method is derived from the Taylor's Series expansion of a function of two variables.

$$0 = f(x, y) = f(x_k, y_k) + (x - x_k) \frac{\partial f(x_k, y_k)}{\partial x} + (y - y_k) \frac{\partial f(x_k, y_k)}{\partial y} + \dots$$

$$0 = g(x, y) = g(x_R, y_R) + (x - x_R) \frac{\partial g(x_k, y_k)}{\partial x} + (y - y_k) \frac{\partial g(x_k, y_k)}{\partial y} + \dots$$

$f(x, y)$ and $g(x, y)$ are set equal to zero since we desire the x and y which satisfy the equations.

Truncating the series and letting

$$\Delta x = x_{k+1} - x_k \text{ and } \Delta y = y_{k+1} - y_k,$$

we have

$$f(x_k, y_k) + \Delta x f_x(x_k, y_k) + \Delta y f_y(x_k, y_k) = 0$$

$$g(x_k, y_k) + \Delta x g_x(x_k, y_k) + \Delta y g_y(x_k, y_k) = 0$$

which is a pair of linear equations in the unknowns Δx and Δy .

$$\Delta x f_x + \Delta y f_y = -f$$

$$\Delta x g_x + \Delta y g_y = -g$$

f, g, f_x, \dots all evaluated

at x_k, y_k .

IV, C, M and θ on the Control Surface or Exit Characteristic (cont.)

which upon solving gives

$$\left. \begin{aligned} \Delta y &= \frac{gf_x - fg_x}{f_y g_x - g_y f_x} \\ \Delta x &= \frac{fg_y - gf_y}{f_y g_x - g_y f_x} \\ y_{k+1} &= y_k + \Delta y \\ x_{k+1} &= x_k + \Delta x \end{aligned} \right\} \quad (\text{Eq 79})$$

Thus in our case, let

$$g(M, \theta) = \lambda_2 + MC \left[\cos \theta + \frac{\sin \theta}{\sqrt{M^2 - 1}} \right] \quad (\text{Eq 80})$$

$$f(M, \theta) = \lambda_3 + \frac{\gamma \rho M^2 C^2 \sin^2 \theta}{\sqrt{M^2 - 1}} \quad (\text{Eq 81})$$

differentiating with respect to M and θ ;

$$g_\theta = \frac{\partial g}{\partial \theta} = -MC \left[\sin \theta - \frac{\cos \theta}{\sqrt{M^2 - 1}} \right] \quad (\text{Eq 82})$$

$$f_\theta = \frac{\partial f}{\partial \theta} = \frac{\gamma \rho M^2 C^2 \sin 2\theta}{\sqrt{M^2 - 1}} \quad (\text{Eq 83})$$

$$\begin{aligned} g_M &= \frac{\partial g}{\partial M} = C \left[\cos \theta + \frac{\sin \theta}{\sqrt{M^2 - 1}} \right] + M \left[\cos \theta + \frac{\sin \theta}{\sqrt{M^2 - 1}} \right] \left(\frac{dC}{dM} \right) - \frac{M^2 C \sin \theta}{(M^2 - 1)^{3/2}} \\ &= \frac{1}{(M^2 - 1)^{3/2}} \left\{ (C + M \frac{dC}{dM}) (M^2 - 1) (\sqrt{M^2 - 1} \cos \theta + \sin \theta) - M^2 C \sin \theta \right\} \end{aligned} \quad (\text{Eq 84})$$

$$\begin{aligned} f_M &= \frac{\partial f}{\partial M} = \frac{\gamma \sin^2 \theta}{\sqrt{M^2 - 1}} M^2 C^2 \frac{d\rho}{dM} + 2\rho C^2 M + 2\rho M^2 C \frac{dC}{dM} - \frac{\gamma \rho M^3 C^2 \sin^2 \theta}{(M^2 - 1)^{3/2}} \\ &= \frac{MC \gamma \sin^2 \theta}{\sqrt{M^2 - 1}} \left\{ MC \left(\frac{d\rho}{dM} \right) + 2\rho \left(\frac{dC}{dM} \right) + \rho C \left(\frac{M^2 - 2}{M^2 - 1} \right) \right\} \end{aligned} \quad (\text{Eq 85})$$

IV, C, M and θ on the Control Surface or Exit Characteristic (cont.)

Note that $\frac{dp}{dM}$ and $\frac{dC}{dM}$ are obtained from the tables $p(M)$, $C(M)$ using numerical differentiation.

$$\Delta \theta = \frac{gf_M - fg_M}{f_{\theta}g_M - g_{\theta}f_M}$$

$$\Delta M = \frac{fg_{\theta} - gf_{\theta}}{f_{\theta}g_M - g_{\theta}f_M}$$

$$\theta_{k+1} = \theta_k + \Delta \theta$$

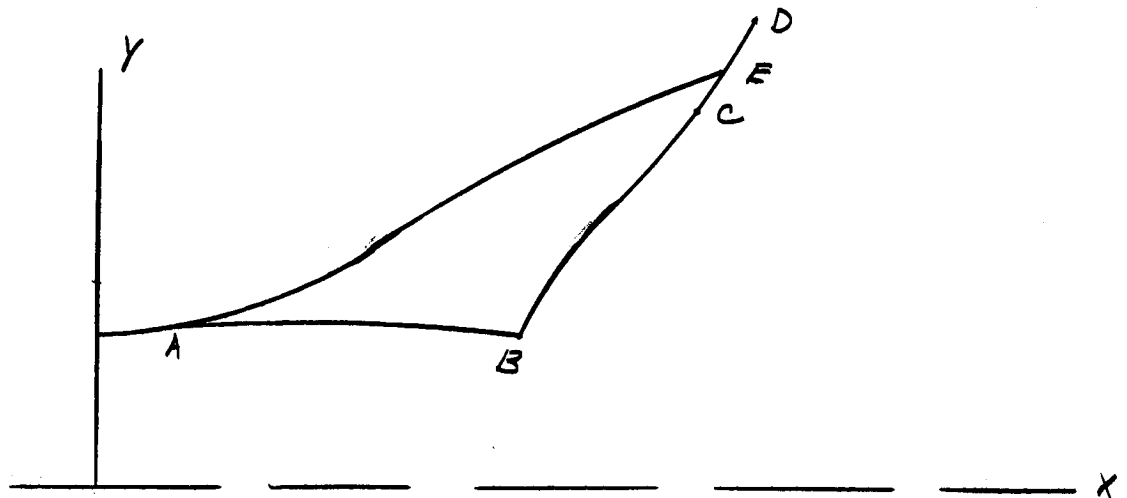
$$M_{k+1} = M_k + \Delta M$$

(Eq 86)

From given first guesses for M and θ , calculate f , g , f_{θ} , g_{θ} , f_M and g_M . With these values calculate $\Delta \theta$ and ΔM from which are obtained new values for M and θ . This process is repeated until the change in M and θ is negligible.

D. FINDING THE EXIT POINT

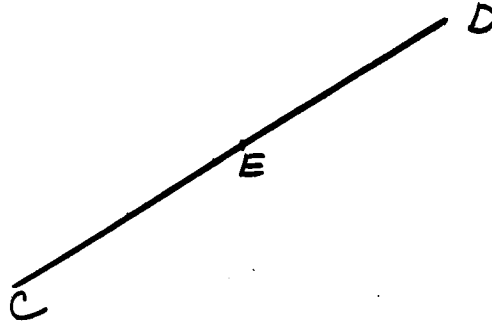
The integral for nozzle length is computed until the exit point is reached. The exit point is determined from conservation of mass flow.



According to the above figure, the total mass flow through the area from A to B must also pass through the area from B to E. Because we have built the characteristic network, point by point, to get to point B, we can integrate the mass flow between

IV, D, Finding the Exit Point (cont.)

A and B by summing repeated applications of Equation 50. The mass flowing between B and E can be obtained by the same method. In integrating the mass flow, we have to interpolate on x and y to obtain the true exit point.

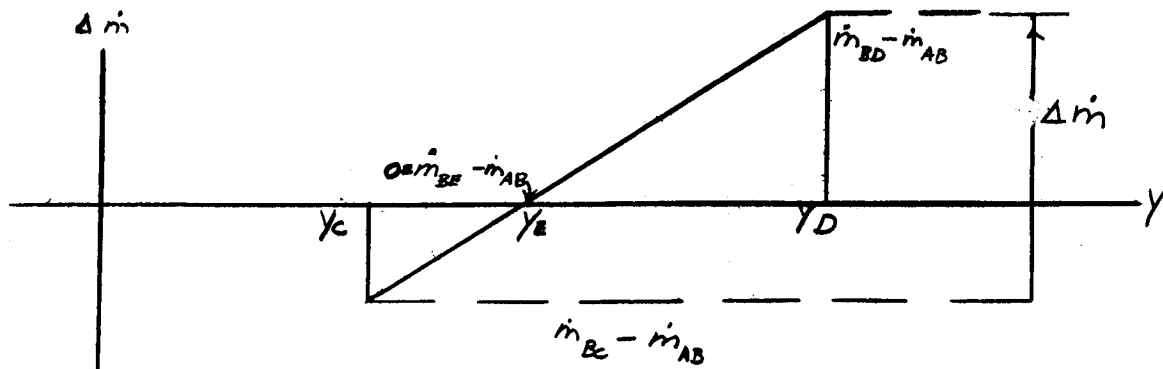


Assume that in integrating from C to D we pass over the mass balance point E, then denote the mass-flow rate between A and B by \dot{m}_{AB} , between B and E by \dot{m}_{BE} , etc. Then

$$\dot{m}_{BD} = \dot{m}_{BC} + \Delta \dot{m}_{CD} \quad \Delta \dot{m} \text{ from Eq 50}$$

$$\dot{m}_{AB} < \dot{m}_{BD} \quad \text{therefore} \quad \dot{m}_{BD} - \dot{m}_{AB} > 0$$

$$\dot{m}_{AB} > \dot{m}_{BC} \quad \text{therefore} \quad \dot{m}_{BC} - \dot{m}_{AB} < 0$$



Then from the figure

$$\frac{y_D - y_C}{\Delta \dot{m}} = \frac{y_D - y_E}{\dot{m}_{BD} - \dot{m}_{BE}} = \frac{y_E - y_D}{\dot{m}_{BE} - \dot{m}_{BD}} = \frac{y_E - y_D}{\dot{m}_{AB} - \dot{m}_{BD}}$$

IV, D, Finding the Exit Point (cont.)

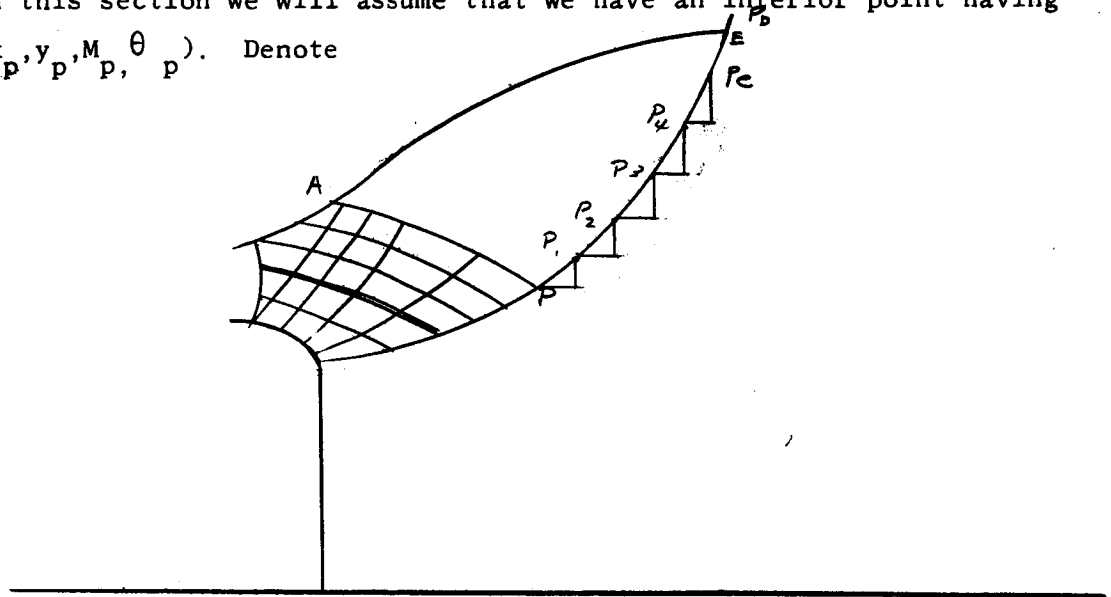
$$\text{Therefore } y_E = y_D + \frac{\dot{m}_{AB} - \dot{m}_{BD}}{\Delta \dot{m}} (y_D - y_C) \quad (\text{Eq 87})$$

$$\text{and } x_E = x_D + \frac{\dot{m}_{AB} - \dot{m}_{BD}}{\Delta \dot{m}} (y_D - y_C)$$

Iteration is necessary to obtain the correct x_E, y_E as the mass flow does not vary linearly from C to D.

E. COMPUTATIONAL PROCEDURE (Summary)

In this section we will assume that we have an interior point having coordinates $(x_p, y_p, M_p, \theta_p)$. Denote



the integrated mass flow from A to P by \dot{m}_{AP} . NOTE: $\dot{m}_{AP} < 0$. At the point P the values of x_p, y_p, M_p, θ_p are known and therefore interpolating in the tables for C, ρ , $\frac{dp}{dM}$ and $\frac{dC}{dM}$, yields the values at point P.

$$\text{Compute } \lambda_2 = -M_P C \left[\cos \theta_P + \frac{\sin \theta_P}{\sqrt{M_P^2 - 1}} \right]$$

$$\lambda_3 = - \frac{y_P \rho M_P^2 C^2 \sin^2 \theta_P}{\sqrt{M_P^2 - 1}}$$

IV, E, Computational Procedure (Summary) (cont.)

Choose Δy such that it is approximately one-fourth the average Δy used in computing the grid upstream of point P; then

$$y_{P1} = y_P + \Delta y$$

Now we can compute M_{P1} and θ_{P1} using Equations 80 through 86. Use M_P and θ_P as first guesses for $M_{P1}^{(0)}$ and $\theta_{P1}^{(0)}$:

$$g = \lambda_2 + M_{P1} C \left[\cos \theta_{P1} + \frac{\sin \theta_{P1}}{\sqrt{M_{P1}^2 - 1}} \right]$$

$$f = \lambda_3 + \frac{y_{P1} \rho M_{P1}^2 C^2 \sin^2 \theta_{P1}}{\sqrt{M_{P1}^2 - 1}}$$

$$g_\theta = -M_{P1} C \left[\sin \theta_{P1} - \frac{\cos \theta_{P1}}{\sqrt{M_{P1}^2 - 1}} \right]$$

$$f_\theta = \frac{y_{P1} \rho M_{P1}^2 \sin 2\theta_{P1}}{\sqrt{M_{P1}^2 - 1}}$$

$$g_M = \frac{1}{(M_{P1}^2 - 1)^{3/2}} \left\{ (C + M_{P1}) \left(\frac{dC}{dN} \right) (M_{P1}^2 - 1) (\sqrt{M_{P1}^2 - 1} \cos \theta_{P1} + \sin \theta_{P1}) - M_{P1}^2 C \sin \theta_{P1} \right\}$$

$$f_M = \frac{M_{P1} C y_{P1} \sin^2 \theta_{P1}}{\sqrt{M_{P1}^2 - 1}} \left[M_{P1} C \left(\frac{d\rho}{dM} \right) + 2\rho \frac{dC}{dM} + \rho C \left(\frac{M_{P1}^2 - 2}{M_{P1}^2 - 1} \right) \right]$$

where C_1 , ρ , $\frac{d\rho}{dM}$ and $\frac{dC}{dM}$ are all taken from our tables at $M = M_{P1}$; then

$$\Delta \theta = \frac{g_M^f - f_M g_\theta}{f_\theta g_M - g_\theta f_M}$$

$$\Delta M = \frac{f_\theta g_\theta - g_\theta^f}{f_\theta g_M - g_\theta f_M}$$

$$M_{P1}^{(1)} = M_{P1}^{(0)} + \Delta M$$

$$\theta_{P1}^{(1)} = \theta_{P1}^{(0)} + \Delta \theta$$

IV, E, Computational Procedure (Summary) (cont.)

Return and calculate g , f , etc. until ΔM and $\Delta \theta$ are less than some predetermined allowable error.

Now that y_{P1} , θ_{P1} and M_{P1} are known, we can calculate x_{P1} using Equation 73.

$$x_{P1} = x_P + (\Delta y) \left(\frac{M_{PP1}^2 \cot(\theta_{PP1}) - 1}{\cot(\theta_{PP1}) + M_{PP1}^2} \right)$$

with

$$M_{PP1} = \frac{M_P + M_{P1}}{2}$$

$$\theta_{PP1} = \frac{\theta_P + \theta_{P1}}{2}$$

The mass flowing between P and $P1$ is given by Equation 50

$$\Delta \dot{m} = \frac{\pi}{144} \bar{\rho} \bar{C} M_{PP1} (y_{P1} + y_P) \left[\Delta Y \cos \theta_{PP1} - (x_{P1} - x_P) \sin \theta_{PP1} \right]$$

with

$$\bar{\rho} = \frac{\rho_P + \rho_{P1}}{2} \quad \text{and} \quad \bar{C} = \frac{C_P + C_{P1}}{2}$$

Therefore, the mass flowing between $P1$ and the upper boundary is

$$-\dot{m} = -(\Delta \dot{m} + \dot{m}_{AP})$$

Increasing y by Δy and repeating the above process for P_2 , P_3 , P_4 will eventually make $\dot{m} > 0$. At that point we have passed the exit point and hence must interpolate for the coordinates of the point which makes $\dot{m} = 0$. There are obtained from Equation 87

$$y_E = y_D + \frac{\dot{m}_{AB} - \dot{m}_{BD}}{\Delta \dot{m}} (y_D - y_C)$$

$$x_E = x_D + \frac{\dot{m}_{AB} - \dot{m}_{BD}}{\Delta \dot{m}} (y_D - y_C)$$

IV, E, Computational Procedure (Summary) (cont.)

Once points on the exit characteristic are known, along with the total mass flow passing through the area AP and PE, it becomes a simple matter to generate the nozzle contour itself. By repeated applications of the equations for generating interior points, we can generate the characteristic network in the region AP and PE. Points on the nozzle contour are obtained by integrating the mass flow along each characteristic and interpolating for the point where the total mass flow between P and the point is a constant.

SYMBOL LIST, PART 1

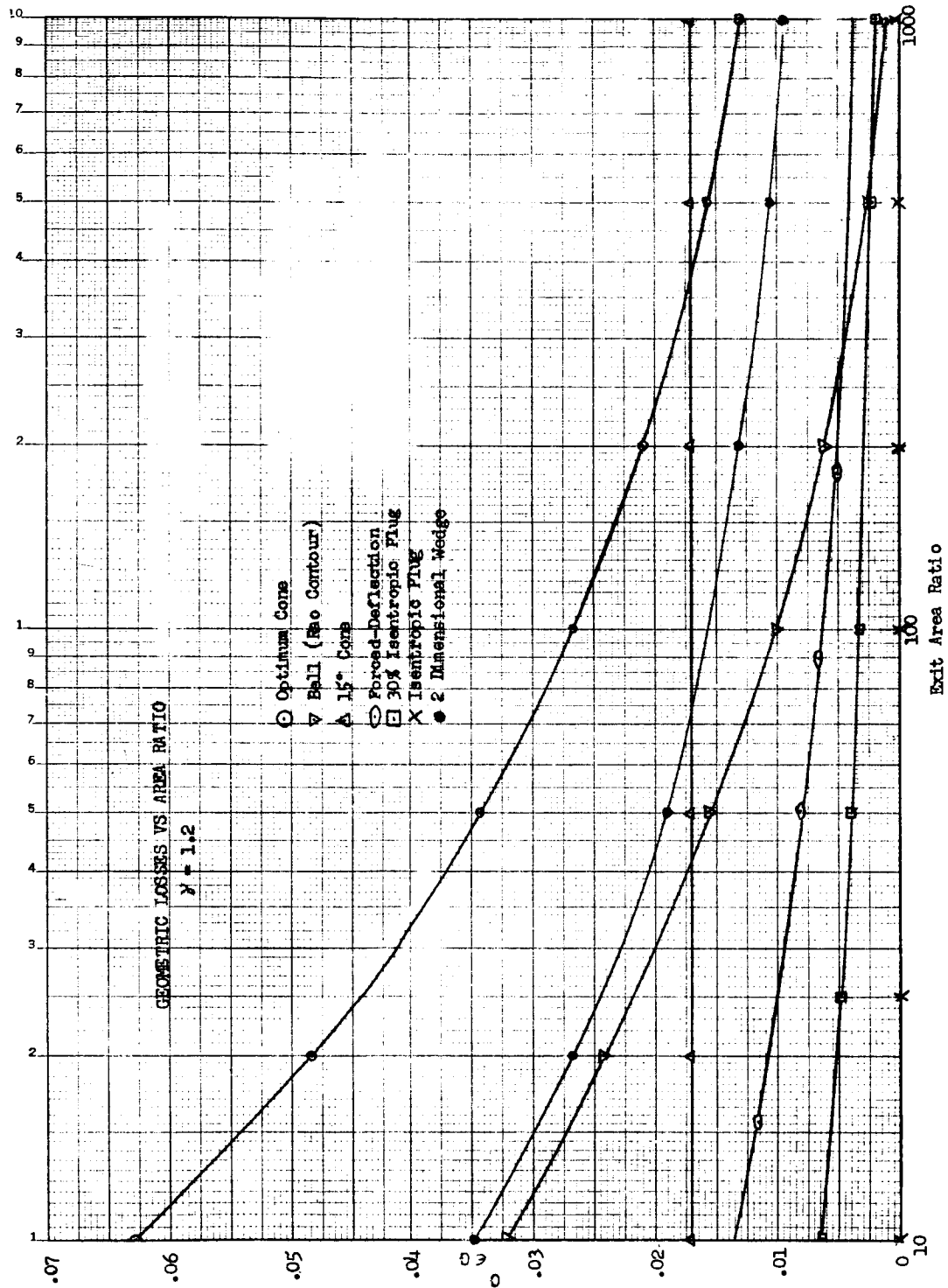
A_t	throat area, in. ²
$C_{\epsilon G}$	geometric loss parameter
C_F	vacuum thrust coefficient of a nozzle with geometric losses only
C_{Fl-D}	one-dimensional vacuum thrust coefficient
g	gravitational constant, 32.2 ft/sec ²
L	length, in.
M	Mach number
\dot{m}	weight flow rate, lb/sec
n	unit vector, outer normal to S, number of throats
P	pressure, psia
r_t	radius of equivalent circular throat = $\sqrt{A_t/\pi}$
R	radius, ft
S	control surface
V	gas velocity, ft/sec
α	half-angle of cone and wedge nozzles,°
ϵ	area ratio
γ	ratio of specific heats
ρ	density of gas, lb/ft ³
μ	Mach angle, $\sin^{-1} 1/M$
ν	Prandtl-Meyer angle

Subscripts

c	chamber
e	exit
i	designates i^{th} control surface
p	lip of base

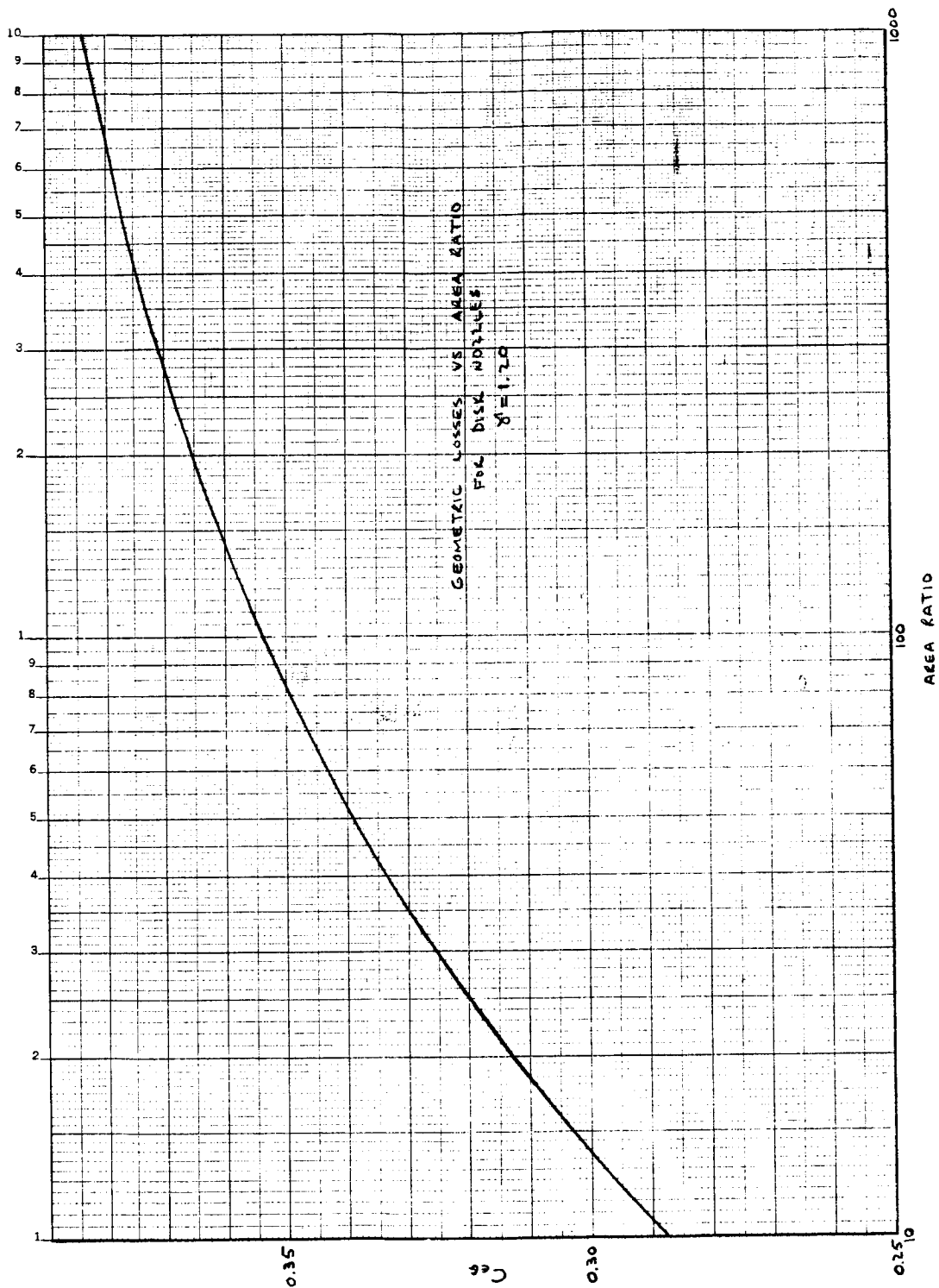
SYMBOL LIST, PART 2

c, C	sound velocity, ft/sec
E	internal energy, Btu/lb
F	thrust, lb
H	enthalpy, Btu/lb
\dot{m}	mass-flow rate, lb/sec
M	Mach number = $\frac{V}{C}$, (-)
n_i	number of moles i'th constituent
p	pressure, lb/in ²
S	entropy, Btu/lb
u, v	component velocities in x, y directions, ft/sec
V	flow velocity, ft/sec
x, y	cylindrical coordinates x = axial, y = radial, in.
α	Mach angle : $\sin \alpha = \frac{C}{V}$, (-)
γ	ratio of specific heats, (-)
θ	flow angle $u = V \cos \theta$, $v = V \sin \theta$, (-)
ρ_i	partial molar free energy i'th constituent
ρ	density, lb/ft ³
ρ_s	wall radius upstream of throat, in.
σ	= 0, 2 dim plane, = 1, axi-symmetric flow, (-)
ϕ	potential function, ft ² /sec
Subscripts	
a	ambient
e	exit
p	value of variable at point p
PQ	average of value at P and at Q
t	throat



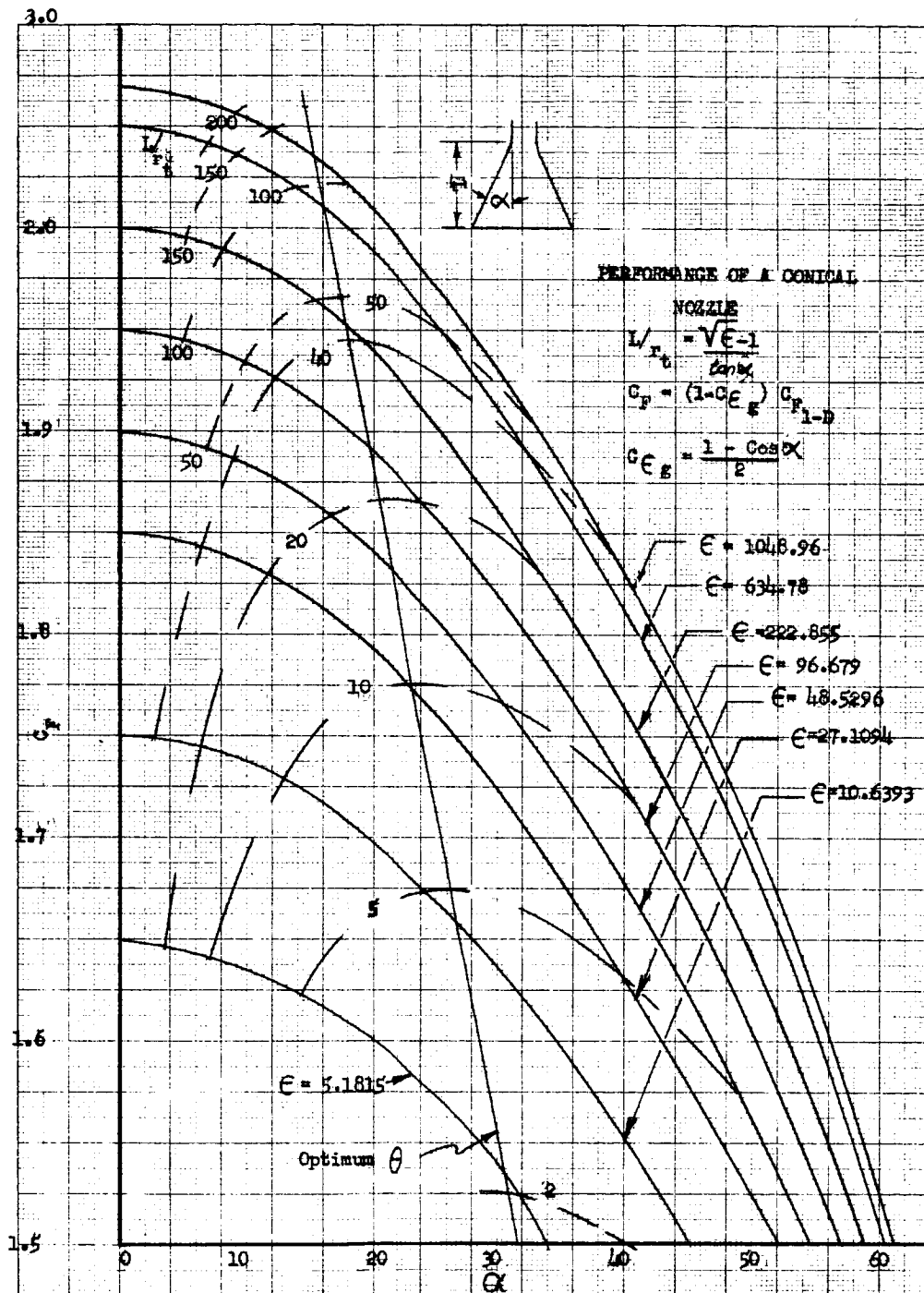
Geometric Losses for Cone, Bell, Forced-Deflection, Plug, and Two-Dimensional Wedge Nozzles

Figure 1



Geometric Losses for Disk Nozzle

Figure 2



Performance of a Conical Nozzle

Figure 3

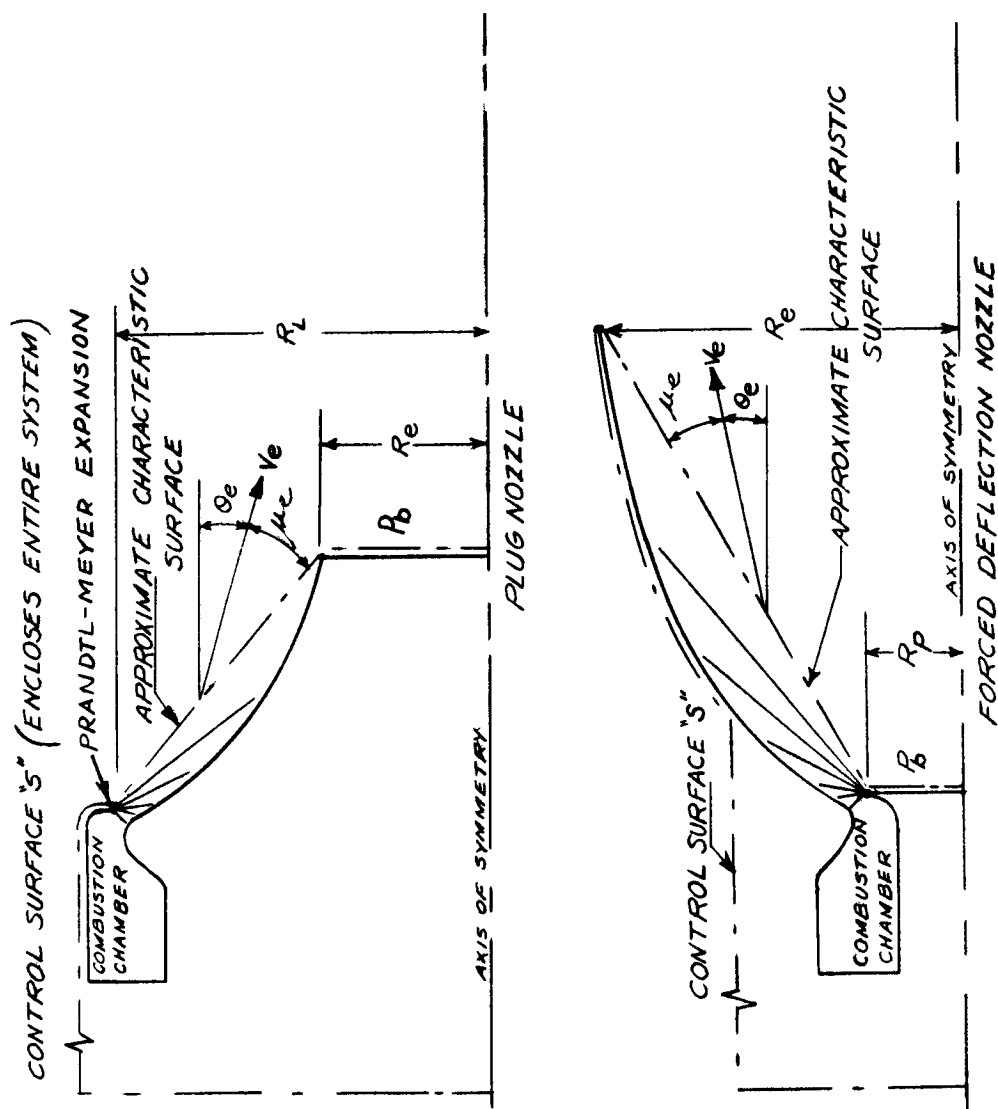


Figure 4

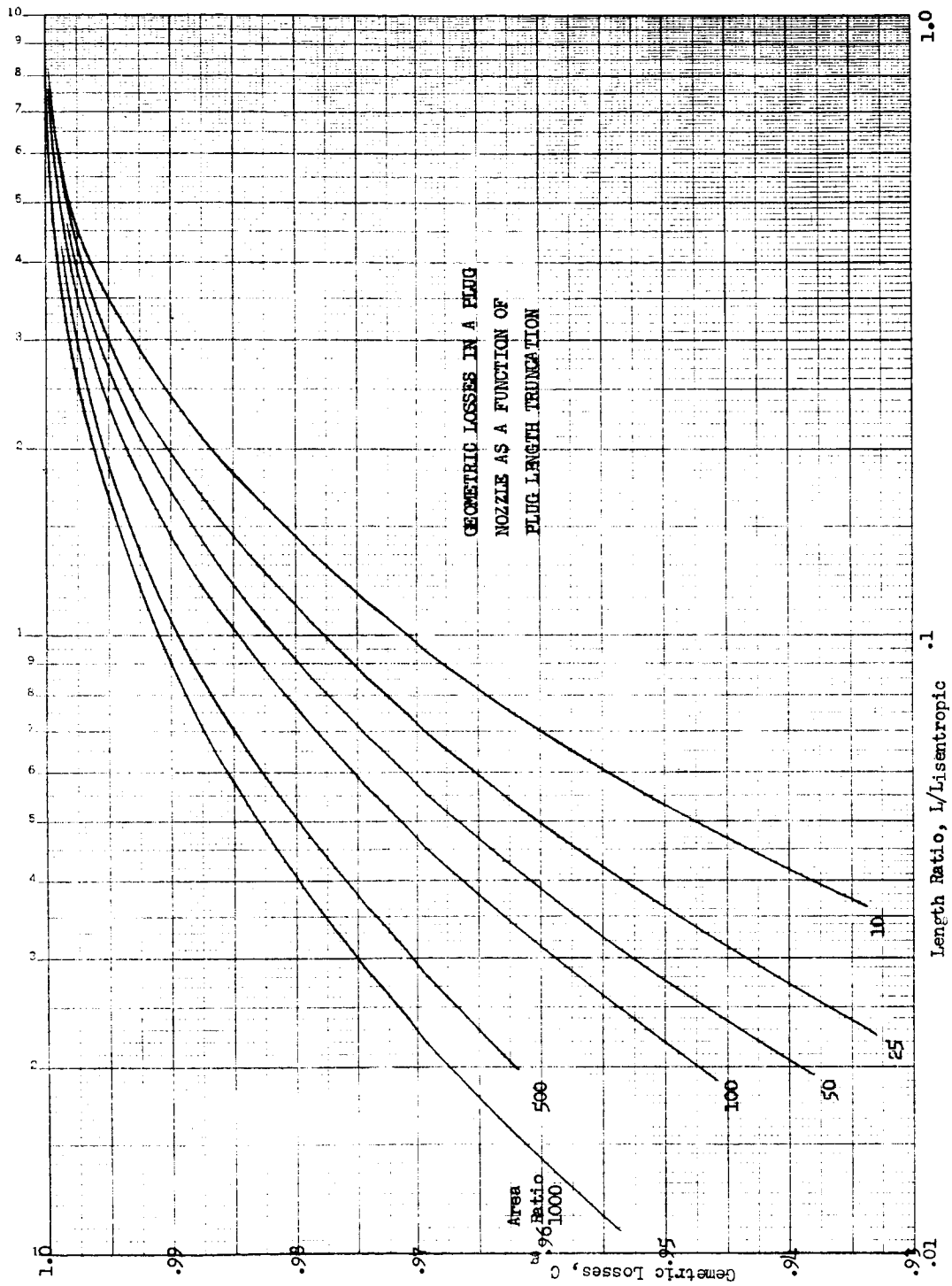


Figure 5

Geometric Losses for a Plug Nozzle as a Function of Plug-Length Truncation

Report NAS 7-136-F

APPENDIX D

TWO-PHASE FLOW LOSSES

FIGURE LIST

FIGURE

Effect of Expansion Ratio on Performance Loss $P_c = 1000$ psi

1

I. PROPELLANT SYSTEM

Propellant systems that contain a metal additive such as aluminum have solid or liquid particles or both in the exhaust products. The specific composition of the particles will usually vary. This variation is not of significance in an aluminum system except at particle contents above 30 to 35% (by weight) of the exhaust flow. In this slope range of particle content, the aluminum system will usually tend to increase its particle content through condensation or by chemical reactions of other species which do not appear in significant quantities at lower initial concentrations of aluminum (Al, Al/liquid, Al₂O and AlN/solid). The propellant system investigated was N₂O₄/Aerozine 50 and an aluminum additive. The amount of aluminum introduced into the Aerozine 50 produced weight percents of particles in the exhaust products of 18.9%, 33.8% and 41.2%. The identity of the oxidizer and fuel components is important only as the oxidizer and fuel affect the ratio of specific heats of the gas. For a specific particle content, size, composition, and nozzle, the net vacuum performance loss is affected only by the ratio of specific heats for the gas. By varying the initial particle content with no change in the overall oxidizer to fuel mixture ratio, the effective mixture ratio changes considerably. Consequently, the effective ratio of specific heats of the gas can vary significantly. This variation in effective ratio of specific heats leads to some anomalies in the data presented in Figure 1.

II. PARTICLE LAG ANALYSIS

The magnitude of the thermal and velocity lags in the gas particle exhaust system and the resultant performance degradation are functions of the specific nozzle to be used as well as the inherent properties of the particles and gases.* A one-dimensional flow of a thermally perfect gas and constant gas viscosity is assumed in this program.

The assumed mathematical behavior of the particles in the analysis program is that the particles: (1) have negligible volume, (2) have no partial pressure, (3) become a supercooled liquid below their fusion temperature, (4) are not permeable or porous, (5) do not change their chemical identity, (6) have a heat transfer coefficient that is a function of the gas Reynolds number:

$$h = \frac{K_g}{D_p} \left[2 + 0.37 (R_e^{0.6}) \left(\mu_{g,p_g} / K_g \right)^{0.33} \right] \quad (\text{Eq 1})$$

and (7) a drag coefficient, C_D , that is a function of the Reynolds number:

$$\begin{aligned} 0 \leq R_e \leq 0.1, \quad C_D &= 24/R_e \\ 0.1 \leq R_e \leq 2000, \quad C_D &= 3.271 - 0.8893 \ln(R_e) \\ &\quad + 0.034117 \ln^2(R_e) + 0.001443 \ln^3(R_e) \end{aligned} \quad (\text{Eq 2})$$

In addition to these general assumptions, the program is limited by restrictions that: (a) do not permit consideration of a particle size distribution, and (b) allow only one particle substance of constant properties. Also, the nature of the mathematical formulation prevents the evaluation of performance with particles of zero diameter. This latter restriction affects the validity of computer program results as the particle size becomes very small in relation to the nozzle size; in fact, Equation 1 becomes indeterminate at zero particle diameter. Since the

* The mathematical formulation of the two-phase flow analysis program is presented in Glauz, R. D., "Combined Subsonic Supersonic Gas - Particle Flow," ARS Preprint No. 1717-61, April 26, 1961

II, Particle Lag Analysis (cont.)

definition of ideal performance is equated to performance with particles of zero diameter, it becomes necessary to use an independent approach to evaluate the ideal performance, which is defined as that performance value realized when no velocity or thermal lag exists.

III. IDEAL PERFORMANCE

The method used to obtain ideal performance is that presented by M. F. Diels.* This method makes use of the same assumptions as the two-phase flow analysis program, and within these assumptions of one-dimensional, frozen flow (constant ratio of specific heats), this method makes no approximations, and is exact. Basically the method presented by Diels involves determining an effective ratio of specific heats (Equation 3) from which the Mach number of the gas may be computed by employing one-dimensional, isentropic flow relationships.

$$\gamma \text{ (effective)} = N = \left[1 - \frac{Z}{WY} \frac{(\gamma-1)}{(\gamma)} \right]^{-1} \quad (\text{Eq 3})$$

$$\text{where } Z = \text{velocity lag} = 1 + \left(\frac{\dot{m}_p}{\dot{m}_g} \right) \left(\frac{V_p}{V} \right)^2$$

$$Y = \text{velocity lag constant} = 1 + \left(\frac{\dot{m}_p}{\dot{m}_g} \right) \left(\frac{V_p}{V_g} \right)$$

$$\text{and, } W = \text{temperature lag constant} = 1 + \left(\frac{\dot{m}_p}{\dot{m}_g} \right) \left(\frac{C_{pp}}{C_{pg}} \right) \frac{(T_{oc} - T_p)}{(T_{oc} - T_g)}$$

In calculating the ideal performance (no thermal or velocity lags), these expressions reduce to:

$$N = \left[1 - \frac{1}{W} \frac{(\gamma-1)}{(\gamma)} \right]^{-1}$$

$$Z = 1 + \frac{\dot{m}_p}{\dot{m}_g} = y$$

* Diels, M. F., "Performance of Rocket Nozzles with Gas-Particle Flow," Aerojet-General Corporation Technical Memorandum No. 136SRP, 20 May 1960

III, Ideal Performance (cont.)

$$\text{and } W = 1 + \left(\frac{\dot{m}_p}{\dot{m}_g} \right) \left(\frac{C_{pp}}{C_{pg}} \right)$$

Sonic velocity at the throat is calculated in Equation 4.

$$(V_t)_g = \left[\left(\frac{N}{N+1} \right) \left(\frac{1}{y} \right) (2 R_g T_{oc}) \right]^{1/2} \quad (\text{Eq 4})$$

Gas-particle velocity at the exit plane is found by Equation 5,

$$(V_{gp})_e = V_{tg} M^* \quad (\text{Eq 5})$$

and specific impulse may then be computed by Equation 6

$$I_s = Y \dot{m}_g (V_{gp})_e + A_e (P_e - P_a) / (\dot{m}_p + \dot{m}_g) \quad (\text{Eq 6})$$

IV. RELATIVE PERFORMANCE

The simplifying assumptions made in the computer analysis program and ideal performance formulations concerning the nature of flow result in absolute values of performance and performance loss that are not a realistic approach to the problem of making quantitative performance predictions. Data resulting from this investigation has been prepared primarily in the form of proportionate loss factors. These factors may then be applied directly to equilibrium-flow, thermochemical predictions of vacuum specific impulse to compute absolute performance.

The assumption of constant particle identity is, of course, not made in using the thermochemical calculations, because it is assumed that there is chemical equilibrium. However, the difficulty is minimized by assuming the particle composition and content that are predicted for the throat region using the thermochemical calculations exist throughout the nozzle, because this is the area where particle effects are most severe. This approach is used in lieu of a more exact method of analysis, which would involve the direct use of equilibrium-thermochemical procedures in the particle flow analysis. Computations of this nature are presently beyond the state of the art.

V. PROPELLANT AND NOZZLE PARAMETERS

The ratio of specific heats of the gaseous components of the gas and particle system investigated was approximately 1.2:1. All calculations were made with a chamber pressure of 1,000 psia and vacuum exit conditions with a conical nozzle having a 15° divergence angle. Upstream and downstream blend radii were $2r_t$ and $0.2r_t$, respectively. Several particle sizes were investigated: primarily 2 and 5 micron dia, but the 41.8% particle content case was investigated also at 8 and 11 micron particle dia. The effects of nozzle size and expansion ratio were also investigated. Three discrete nozzle sizes were used to give a wide range of information. Throat radii of 1.0, 7.5 and 15.0 in., and expansion ratios of 12:1, 20:1, 30:1, 40:1, and 50:1 were selected for specific investigation.

VI. GENERAL DISCUSSION

The most difficult factor in the prediction of performance degradation caused by two-phase flow is the selection of an effective particle diameter. Since the resultant loss factors are extremely sensitive to the particle size assumed, this selection is critical. Numerous attempts to make an accurate determination of particle sizes and their distribution have been generally unsatisfactory. Information concerning solid rocket motors indicates that the size of the particles in the exhaust stream may not depend on either the initial size of the metal additive or motor size, although there is evidence of some size dependence on chamber pressure. The primary controlling function of particle size appears to be the propellant system itself rather than any engine parameter. Experiments on the pentaborane/hydrazine system, for example, resulted in particle diameters of 0.03 to 0.1 microns.* Particle diameters of this magnitude produce no discernible lag effects and the system behaves essentially as an ideal gas.

It is not clear whether or not particle size changes along the nozzle axis or whether the change is an increase or decrease in size. Measurement devices have generally been some physical collection technique downstream of the exit plane. A technique of this type disturbs the system being sampled. The extent of this disturbance and its effect on the results is not known. The result of these attempts is that accumulations of particles have been sampled whose mass mean diameters are about 2 microns (in systems which utilize aluminum as an additive). The aspect that makes the particle growth factor important is that the performance loss is most sensitive to particle size in the throat region. Consequently, even knowing the particle size distribution at the exit plane or beyond, does not necessarily tell us accurately about particle size in the throat region. The size of the particles to be expected from a liquid rocket engine is also unknown. However, it has been assumed that a 2-micron particle dia will adequately describe a system whose particles are primarily aluminum oxide. The data presented in Figure 1 makes this assumption.

* Hoglund, R. F., Saalars, "Expansion Nozzles for Gas-Particle Flows,"
Aeroneutronic Technical Report C-1232, 20 April 1961

VI, General Discussion (cont.)

Evidence also exists that the particles may be porous. Such porosity would tend to compromise the validity of the lag calculations. There is little evidence to support the belief that such porosity exists in the throat region if it exists at all. If evidence sufficient to warrant a revision of the data appears, the difficulty could be easily circumvented by assuming a different effective particle diameter, or by a recalculation using a modified particle density.

Generally, performance efficiency decreases with increasing particle diameter, decreasing expansion ratio, decreasing throat area, and increasing particle content to some minimum point. It has been established that contraction ratio, convergence angle, blend radii and effective divergence angle will also influence the losses from two-phase flow. Previous works* have indicated that an effective divergence angle between 20° and 25° , and blend radii of about $3x r_t$ are about optimum to maximize specific impulse for a 5K-lb thrust solid rocket motor. These values are approximate and depend upon the propellant and nozzle parameters used.

The specific contour of the nozzle to be used is a significant factor in determining the losses caused by a two-phase flow. These losses can be classified into two distinct areas: (1) losses caused by particle size and quantity that result in thermal and velocity lags, and (2) losses caused by the contour of the nozzle. This second group of losses should not be confused with losses normally referred to as "geometry losses" that is, divergence loss. Two-phase geometry losses are incurred in addition to the normal divergence losses. A conical nozzle of the same length and expansion ratio as a bell-shaped nozzle will generally experience less two-phase loss than the bell nozzle. This is because the initial divergence angle of the bell nozzle is greater than the conical nozzle, which

* *ibid.*, Hogland, R. F., and Saalars

Ditore, M. J., Haigh, "Minuteman Nozzle Contour Development Program Phase I and Phase II," Aerojet-General Corporation, Technical Memorandum No. 158 SRP, 27 February 1961

Kliegel, J. R. Nickerson, "Flow of Gas-Particle Mixtures Through Axially Symmetrical Nozzles," Space Technology Laboratories, TR-60-000-19286

VI, General Discussion (cont.)

by the ratio F/P_c . There is some question as to the validity of F/P_c as an exact theoretical parameter that can be used to describe the relationship of particle size and nozzle size to performance, because F/P_c varies as a function of expansion ratio and is not a measure of throat size alone. However, the effect of this inexactness is slight in view of the indeterminacy of the particle diameters. Until such time as an effective particle size is definitely known, the use of F/P_c as a relative size parameter should be adequate.

LIST OF SYMBOLS

A	Area (in. ²)
C _D	Drag Coefficient
C _p	Specific heat at constant pressure (ft ² /sec ² °R)
D _p	Particle diameter (microns, ft)
F	Thrust (lb)
G	Particle content, %
h	heat transfer coefficient ($\frac{\text{ft-lb}}{\text{sec-ft}^2\text{°R}}$)
I _s	Specific impulse (sec)
K _g	thermal conductivity ($\frac{\text{ft-lb}}{\text{ft - sec°R}}$)
\dot{m}	mass flow (lb/sec)
M*	Mach No. referred to throat conditions
N	effective ratio of specific heats
P	Pressure (lb/in. ²)
R	gas content (ft ² /sec ² °R)
r _t	throat radius (in.)
Re	Reynolds Number
T _o	temperature (°R)
V	velocity (ft/sec)

Greek Notation

γ	ratio of specific heats
ϵ	expansion ratio
ρ	density (slugs/ft ³)
μ_g	gas viscosity (lb-sec/ft ²)

LIST OF SYMBOLS (cont.)

Subscripts

a	ambient
c	chamber
e	exit plane
g	gas
p	particle
t	throat

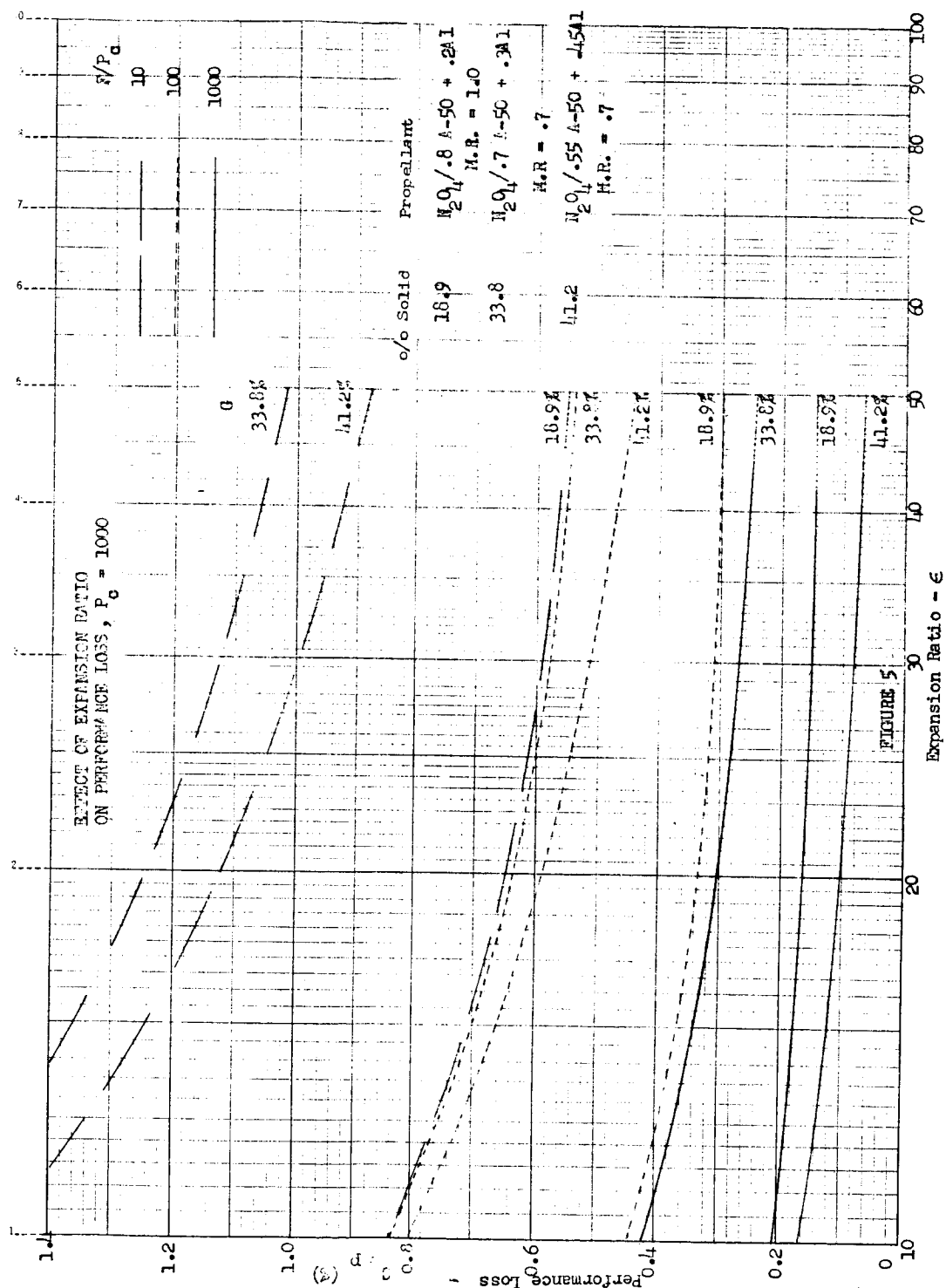


Figure 1

Effect of Expansion Ratio on Performance Loss $P_c = 1000$ psi

Report NAS 7-136-F

APPENDIX E

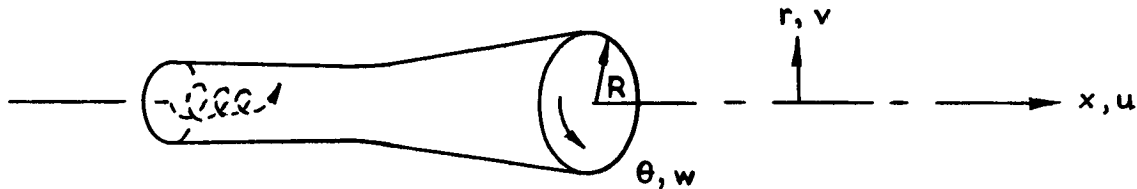
ANALYSIS OF A SWIRLING-FLOW NOZZLE

I. SUPERSONIC REGION

The swirling flow nozzle, as applied, is relatively new, and unlike the plug and expansion-deflection nozzles, adequate analytical techniques for treating it have apparently not yet been developed. Mager* has analyzed this type of flow for one dimensional axial flow, neglecting the radial component of velocity. The problem has been reformulated to include the radial velocity component and to develop the characteristic equations to permit a better performance estimate to be made. The analysis is summarized below.

A. THE POTENTIAL

We shall assume an irrotational flow through a nozzle with swirling flow. Cylindrical coordinates are of course most appropriate in this case.



Define a potential function so that:

$$v = \phi_r = \frac{\partial \phi}{\partial r}, \quad w = \frac{\partial \phi}{r \partial \theta} = \frac{\phi_\theta}{r}, \quad u = \frac{\partial \phi}{\partial x}$$

Irrotationality:

$$\nabla \times \bar{V} = 0 : \frac{\partial u}{\partial \theta} - \frac{\partial wr}{\partial x} = 0, \quad \frac{\partial u}{\partial r} - \frac{\partial v}{\partial x} = 0, \quad \frac{\partial v}{\partial \theta} - \frac{\partial wr}{\partial \theta} = 0$$

* Mager, A., "Approximate Solution of Isentropic Swirling Flow Through a Nozzle"
ARS Journal, August 1961

I, A, The Potential (cont.)

$$\nabla \rho \cdot \bar{V} = 0, r \frac{\partial \rho u}{\partial x} + \frac{\partial \rho v r}{\partial r} + \frac{\partial \rho w}{\partial \theta} = 0$$

Euler's equation:

$$dp = - \frac{\rho}{2} d(u^2 + v^2 + w^2)$$

From these we obtain the differential equation of the flow:

$$\left(1 - \frac{\phi_x^2}{a^2}\right) \phi_{xx} + \left(1 - \frac{\phi_r^2}{a^2}\right) \phi_{rr} + \left(1 - \frac{\phi_\theta^2}{r^2 a^2}\right) \frac{\phi_{\theta\theta}}{r} - 2 \frac{\phi_r \phi_\theta}{r a^2} \phi_{r\theta} - 2 \frac{\phi_\theta \phi_x}{r a^2} \phi_{\theta x} - 2 \frac{\phi_x \phi_r}{a^2} \phi_{xr} + \frac{\phi_r}{r} \left(1 + \frac{\phi_\theta^2}{r^2 a^2}\right) = 0$$

where

$$a^2 = a_t^2 - \frac{\gamma-1}{2} \left(\phi_r^2 + \frac{\phi_\theta^2}{r^2} + \phi_x^2 \right)$$

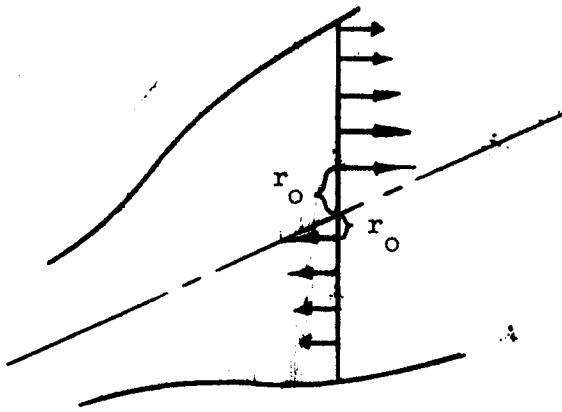
If the flow is such that ϕ_θ , ϕ_x , and ϕ_r do not change with θ , then $\phi_{\theta\theta} = \phi_{x\theta} = \phi_{r\theta} = 0$, and the equations of flow reduce to

$$\frac{\left(1 - \frac{\phi_x^2}{a^2}\right)}{a^2} \phi_{xx} + \left(1 - \frac{\phi_r^2}{a^2}\right) \phi_{rr} - \frac{2 \phi_x \phi_r}{a^2} \phi_{xr} + \frac{\phi_r}{r} \left(1 + \frac{\phi_\theta^2}{r^2 a^2}\right) = 0 \quad (\text{Eq 1})$$

This flow has a circumferential velocity $\frac{1}{r} \phi_\theta = \omega$ besides the axial $\phi_x = u$ and the radial $\phi_r = V$. In the so-called axially symmetric flow, the flow properties are the same in all meridian planes passing through the axis of symmetry. In each of these meridian planes the flow is two-dimensional, and there is no flow crossing the meridian plane (i.e., $\phi_\theta = 0$).

In our case, as described by Eq 1, there is for each meridian plane a component flow velocity normal to the plane.

I, A, The Potential (cont.)



A typical velocity profile for one station of the axis is shown in the sketch to the left. The flow is not axially symmetric in the usual sense.

As far as speed is concerned, there is no difference caused by θ , so our flow may be called a scalarly axial-symmetric flow.

Let us now obtain a preliminary determination of ϕ . First because

$$\phi_{\theta\theta} = 0,$$

$$\phi_{\theta} = f(x, r) \text{ and } \phi = \theta f(x, r) + g(x, r).$$

Next,

$$0 = \phi_{x\theta} = \phi_{\theta x} = f_x(x, r)$$

$$\therefore f(x, r) = h(r), \text{ no } x \text{ appearing}$$

Finally,

$$0 = \phi_{r\theta} = \phi_{\theta r} = h_r(r)$$

$$\therefore h(r) = K_1 = \text{a constant}$$

and

$$\phi = K_1 \theta + g(x, r) \quad (\text{Eq 2})$$

I, Supersonic Region (cont.)

B. THE SIGNIFICANCE OF K_1

Our flow is different from the usual axial-symmetric flow simply because of the presence of K_1 .

Since

$$w = \frac{1}{r} \frac{\partial \phi}{\partial \theta} = \frac{K_1}{r},$$

we have

$$wr = K_1$$

Let us confine our attention to a nozzle. Let $R(x)$ be the wall radius at Station x . Then the corresponding circumferential velocity at the wall is $K_1/R(x)$ and we can denote it by $w(x)$.

$$w(x)R(x) = K_1$$

In particular, at the throat area,

$$K_1 = w^*(x)R^*(x) = \bar{w}_{\max} R_{\min}.$$

This gives us a method to determine the constant K_1 . K_1 is called the swirling magnitude of the flow.

The velocity of the flow is given by

$$V^2 = u^2 + v^2 + \frac{K_1^2}{r^2} = U^2 + \frac{K_1^2}{r^2}, \quad U^2 \equiv u^2 + v^2.$$

Now

$$\rho = \rho_t \left[1 - \frac{\gamma-1}{2} \left(\frac{V}{a_t} \right)^2 \right]^{\frac{1}{\gamma-1}} = \rho_t \left\{ 1 - \frac{\gamma-1}{2a_t^2} \left(U^2 + \frac{K_1^2}{r^2} \right) \right\}^{\frac{1}{\gamma-1}}$$

It follows that r can not be arbitrarily small as

$$\rho \geq 0 \iff 1 \geq \frac{\gamma-1}{2a_t^2} \left(U^2 + \frac{K_1^2}{r^2} \right).$$

I, B, The Significance of K_1 (cont.)

Hence, there exists a void of radius r_0 in the flow.

$$r_0^2 = \frac{\frac{\gamma-1}{2} K_1^2}{a_t^2 - \frac{\gamma-1}{2} (u^2 + v^2)} \quad (\text{Eq 3})$$

Note that

$$a_t^2 - \frac{\gamma-1}{2} (u^2 + v^2) = a^2 + \frac{\gamma-1}{2} w^2 \geq a^2,$$

so $r_0(x)$ is real, and exists as long as K_1 exists.

C. EQUATIONS OF CHARACTERISTICS

Because $\phi = K_1 \theta + g(x, r)$,

$$\phi_x = g_x, \quad \phi_r = g_r, \quad \phi_{xx} = g_{xx}, \quad \phi_{rr} = g_{rr},$$

$$\phi_{xr} = g_{xr}, \quad \phi_\theta = K_1$$

Eq 1 becomes

$$\left(1 - \frac{g_x^2}{a^2}\right) g_{xx} - \frac{2 g_x g_r}{a^2} g_{xr} + \left(\frac{1 - g_r^2}{a^2}\right) g_{rr} + \frac{g_r}{r} \left(1 + \frac{K_1^2}{r^2 a^2}\right) = 0 \quad (\text{Eq 4})$$

If we let

$$A = 1 - \frac{g_x^2}{a^2}, \quad B = \frac{-g_x g_r}{a^2}, \quad C = 1 - \frac{g_r^2}{a^2},$$

$$D = \frac{-g_r}{r} \left(1 + \frac{K_1^2}{r^2 a^2}\right),$$

then Eq 4 becomes

$$A g_{xx} + 2B g_{xr} + C g_{rr} = D$$

we have also

$$dx g_{xx} + dr g_{xr} = dg_x$$

$$dx g_{xr} + dr g_{rr} = dg_r$$

I, C, Equations of Characteristics (cont.)

Solving for g_{xx} , g_{xr} , g_{rr} :

$$g_{xx} = \frac{\begin{vmatrix} D & 2B & C \\ dg_x & dr & 0 \\ dg_r & dx & dr \end{vmatrix}}{\begin{vmatrix} A & 2B & C \\ dx & dr & 0 \\ 0 & dx & dr \end{vmatrix}}, \quad g_{xr} = \frac{\begin{vmatrix} A & D & C \\ dx & dg_x & 0 \\ 0 & dg_r & dr \end{vmatrix}}{D}, \quad g_{rr} = \frac{\begin{vmatrix} A & 2B & D \\ dx & dr & dg_x \\ 0 & dx & dg_r \end{vmatrix}}{D}$$

Putting the numerator and the denominator of g_{xr} at zero,

$$A(dr)^2 - 2Bdxdr + C(dx)^2 = 0 \quad (\text{Eq 5})$$

$$A dr dg_x - D dx dr + C dx dg_r = 0 \quad (\text{Eq 6})$$

If we eliminate A from Eq 5 and Eq 6, we obtain

$$- 2B dr dg_x + D(dr)^2 + C(dx dg_x - dr dg_r) = 0,$$

which is the numerator of g_{xx} . Next, if we eliminate C from Eq 5 and Eq 6, we obtain:

$$A(dr dg_x - dx dg_r) - 2B dx dg_r + D dx^2 = 0,$$

which is the numerator of g_{rr} . So, along the characteristics given by Eq 5 and Eq 6, there may be discontinuity of g_x and g_r , but g_{xx} , g_{xr} , and g_{rr} are in general finite.

I, C, Equations of Characteristics (cont.)

From Eq 5,

$$\begin{aligned} \left(\frac{dr}{dx} \right)_{I,II} &= \frac{B \pm \sqrt{B^2 - AC}}{A} \\ &= \frac{\frac{-g_x g_r}{a^2} \pm \sqrt{\frac{g_x^2 g_r^2}{a^4} - \left(1 - \frac{g_x^2}{a^2} - \frac{g_r^2}{a^2} + \frac{g_x^2 g_r^2}{a^4} \right)}}{1 - \frac{g_x^2}{a^2}} \\ &= \frac{\frac{-g_x g_r}{a^2} \pm a \sqrt{g_x^2 + g_r^2 - a^2}}{a^2 - g_x^2} \end{aligned}$$

Therefore,

$$\left(\frac{dr}{dx} \right)_{I,II} = \frac{-uv \pm a \sqrt{u^2 + v^2 - a^2}}{a^2 - u^2} \quad (\text{Eq } 5')$$

This on the surface involves only u, v, but actually we have the velocity of sound

$$a^2 = a_t^2 - \frac{\gamma-1}{2} (u^2 + v^2 + w^2),$$

and thus $w = \frac{K_1}{r}$ enters into the picture.

Next, from Eq 6 we have

$$\begin{aligned} \frac{dv}{du} \bigg|_{I,II} &= \frac{uv \pm a \sqrt{u^2 + v^2 - a^2}}{a^2 - v^2} - \frac{a^2 v}{r(a^2 - v^2)} \left(1 + \frac{K_1^2}{r^2 a^2} \right) \left(\frac{dr}{du} \right)_{I,II}. \end{aligned} \quad (\text{Eq } 6')$$

We derived Eq 5' and Eq 6' on the supposition that

$$B^2 - AC > 0,$$

I, C, Equations of Characteristics (cont.)

or that Eq 5 is hyperbolic. This in terms of u, v is

$$u^2 + v^2 - a^2 > 0.$$

In case of axial symmetric flow, $u^2 + v^2$ is the square of total velocity, and if the flow is supersonic this condition must be satisfied. In our present case, it is not necessary that

$$u^2 + v^2 + w^2 - a^2 > 0 \rightarrow u^2 + v^2 - a^2 > 0$$

(i.e., even though the flow is supersonic, $u^2 + v^2 - a^2$ may be less than zero).

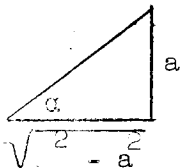
If $u^2 + v^2 - a^2 > 0$, then Eq 5' and Eq 6' give real characteristics. That is, each equation offers two distinct directions.

D. METHOD OF CHARACTERISTICS IN A SUFFICIENTLY SUPERSONIC REGION

If now $v^2 - w^2 = U^2 = u^2 + v^2 > a^2$ we can establish

$$u = U \cos \beta \text{ and } v = U \sin \beta,$$

where B is the projected flow direction in a meridian plane. Defining



$$\frac{1}{M} \equiv \sin \alpha \equiv \frac{a}{U} < 1, U = Ma$$

then

$$\frac{-uv \pm a \sqrt{U^2 - a^2}}{a^2 - u^2} = \frac{-U^2 \sin \beta \cos \beta \pm a^2 \sqrt{U^2 - a^2}}{U^2 \sin^2 \alpha - U^2 \cos^2 \beta}$$

$$= \frac{-\sin \beta \cos \beta \pm \sin^2 \alpha \cot \alpha}{\sin^2 \alpha - \cos^2 \beta} = \frac{-\sin \beta \cos \beta \pm \sin \alpha \cos \alpha}{\frac{1 - \cos 2\alpha}{2} - \frac{1 + \cos 2\beta}{2}}$$

I, D, Method of Characteristics in a Sufficiently Supersonic Region (cont.)

$$\begin{aligned}
 &= \frac{-\sin 2\beta \pm \sin 2\alpha}{-(\cos 2\alpha + \cos 2\beta)} = \frac{\sin 2\beta \mp \sin 2\alpha}{\cos 2\alpha + \cos 2\beta} \\
 &= \frac{2 \sin (\beta \mp \alpha) \cos (\beta \pm \alpha)}{2 \cos (\alpha + \beta) \cos (\alpha - \beta)} = \frac{\tan (\beta \mp \alpha)}{1}
 \end{aligned}$$

Therefore Eq 5' becomes

$$\left(\frac{dr}{dx} \right)_{I,II} = \tan (\beta \mp \alpha) \quad (\text{Eq 7})$$

This can also be written as

$$(dr)_{I,II} = \tan (\beta \mp \alpha) (dx)_{I,II}$$

Eq 6' can also be expressed in terms of U, β .

First

$$\begin{aligned}
 \frac{uv \pm a \sqrt{U^2 - a^2}}{a^2 - v^2} &= \frac{U^2 \sin \beta \cos \beta \pm a^2 \cot \alpha}{U^2 (\sin^2 \alpha - \sin^2 \beta)} \\
 &= \frac{\sin 2\beta \mp \sin 2\alpha}{\cos 2\beta - \cos 2\alpha} = \frac{\sin (\beta \mp \alpha) \cos (\beta \pm \alpha)}{\sin (\beta + \alpha) \sin (\beta - \alpha)} \\
 &= -\cot (\beta \pm \alpha).
 \end{aligned}$$

Next,

$$\begin{aligned}
 \frac{-a^2 v}{a^2 - v^2} &= -\frac{(U^2 \sin^2 \alpha - \sin^2 \beta)^2}{U^2 (\cos 2\beta - \cos 2\alpha)} = \frac{-2 U \sin^2 \alpha \sin \beta}{2 \sin (\beta + \alpha) \sin (\alpha - \beta)} \\
 &= \frac{U \sin^2 \alpha \sin \beta}{\sin (\beta + \alpha) \sin (\beta - \alpha)}
 \end{aligned}$$

I, D, Method of Characteristics in Sufficiently Supersonic Region (cont.)

It follows that Eq 6' becomes

$$\left(\frac{dv}{du} \right)_{I, II} = -\cot(\beta \pm \alpha) + \frac{U \sin^2 \alpha \sin \beta}{r \sin(\beta + \alpha) \sin(\beta - \alpha)} S \left(\frac{dr}{du} \right)_{I, II}$$

or

$$\left(\frac{dv}{d\beta} \right)_{I, II} = -\cot(\beta \pm \alpha) \left(\frac{du}{d\beta} \right)_{I, II} + \frac{U \sin^2 \alpha \sin \beta}{r \sin(\beta + \alpha) \sin(\beta - \alpha)} S \left(\frac{dr}{d\beta} \right)_{I, II}$$

Now

$$u = U \cos \beta \quad du = \cos \beta dU - U \sin \beta d\beta$$

$$\frac{du}{d\beta} = \cos \beta \frac{dU}{d\beta} - U \sin \beta$$

$$v = U \sin \beta \quad \frac{dv}{d\beta} = \sin \beta \frac{dU}{d\beta} + U \cos \beta$$

$$\begin{aligned} \sin \beta \left(\frac{dU}{d\beta} \right)_{I, II} + U \cos \beta + \cot(\beta \pm \alpha) \left[\cos \beta \left(\frac{dU}{d\beta} \right)_{I, II} - U \sin \beta \right] \\ = \frac{U \sin^2 \alpha \sin \beta}{r \sin(\beta + \alpha) \sin(\beta - \alpha)} S \left(\frac{dr}{d\beta} \right)_{I, II} \end{aligned}$$

Therefore,

$$\left[\sin \beta + \cot(\beta \pm \alpha) \cos \beta \right] \left(\frac{dU}{d\beta} \right)_{I, II} + U \cos \beta - U \sin \beta \cot(\beta \pm \alpha) = \dots$$

thus

$$\frac{\cos(\beta \pm \alpha - \beta)}{\sin(\beta \pm \alpha)} \left(\frac{dU}{d\beta} \right) + U \frac{\sin(\beta \pm \alpha - \beta)}{\sin(\beta \pm \alpha)} = \dots$$

i.e.,

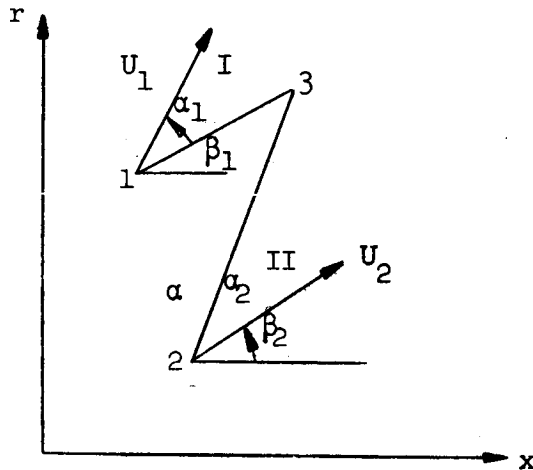
$$\begin{aligned} \frac{1}{U} \left(\frac{dU}{d\beta} \right)_{I, II} + \tan \pm \alpha &= \frac{\sin(\beta \pm \alpha)}{\cos \alpha} \cdot \frac{S}{r} \left(\frac{dr}{d\beta} \right)_{I, II} \frac{\sin^2 \alpha \sin \beta}{\sin(\beta + \alpha) \sin(\beta - \alpha)} \\ &= \frac{S}{r} \left(\frac{dr}{d\beta} \right)_{I, II} \frac{\sin \alpha \tan \alpha \sin \beta}{\sin(\beta \pm \alpha)} \end{aligned}$$

I, D, Method of Characteristics in Sufficiently Supersonic Region (cont.)

or

$$\frac{1}{U} \left(\frac{dU}{d\beta} \right)_{I,II} = \mp \tan \alpha + \frac{S}{r} \frac{\sin \alpha \tan \beta \sin \theta}{\sin (\beta \mp \alpha)} \left(\frac{dr}{d\beta} \right)_{I,II} \quad (\text{Eq 8})$$

$$S = 1 + \frac{K_1^2}{2^2 a^2}$$



We have from Eq 7

$$r_3 - r_1 = \tan (\beta_1 - \alpha_1) (x_3 - x_1)$$

$$r_3 - r_2 = \tan (\beta_2 + \alpha_2) (x_3 - x_2)$$

Conditions at positions 1 and 2 are known; hence

 x_3 and r_3

can be found.

Next, we can rewrite Eq 8 as follows:

$$\frac{1}{U} (dU)_{I,II} = \mp \tan \alpha \cdot (d\beta)_{I,II} + \frac{S}{r} \frac{\sin \alpha \tan \alpha \sin \theta}{\sin (\beta \mp \alpha)} (dr)_{I,II}$$

$$\mp \frac{\cot \alpha}{U} (dU)_{I,II} = (d\beta)_{I,II} \mp \frac{\sin \alpha \tan \alpha \sin \theta}{\sin (\beta \mp \alpha)} \frac{S}{r} \cot \alpha (dr)_{I,II}$$

$$\therefore (d\beta)_{I,II} = \mp \frac{\cot \alpha}{U} (dU)_{I,II} \pm \frac{\sin \alpha \sin \theta}{\sin (\beta \mp \alpha)} \frac{S}{r} (dr)_{I,II}$$

And in difference forms:

$$\beta_3 - \beta_1 = - \frac{\cot \alpha_1}{U_1} (U_3 - U_1) + \frac{\sin \alpha_1 \sin \beta_1}{\sin (\beta_1 - \alpha_1)} \frac{S_1}{r} (r_3 - r_1)$$

$$\beta_3 - \beta_2 = \frac{\cot \alpha_2}{U_2} (U_3 - U_2) + \frac{\sin \alpha_2 \sin \beta_2}{\sin (\beta_2 + \alpha_2)} \frac{S_2}{r_2} (r_3 - r_2)$$

I, D, Method of Characteristics in Sufficiently Supersonic Region (cont.)

From these, β_3 and U_3 can be found.

Thus, we have seen that in the region where

$$U^2 = V^2 - w^2 = u^2 + v^2 > a^2$$

We can apply the method of characteristics for axial symmetric flow, with only slight modification due to the factor

$$S = 1 + \frac{K_1^2}{r^2 a^2}$$

Close to the throat region, the circumferential velocity W is large and the total velocity is nearly equal to a ; hence $U < a$. The potential equation is elliptic as $B^2 - AC < 0$. There is no real characteristic, and the foregoing method cannot be applied. In order to handle the complete flow field from the throat to the exit area, we need a counterpart of Sauer's work of 1944 on throat area.

It is to be recalled that our swirling flow is not axially symmetric, not one-dimensional. Because of the existence of K_1 , the swirling magnitude, there is a core of void described by

$$r_o^2 = \frac{\frac{\gamma-1}{2} K_1^2}{A_t^2 - \frac{\gamma-1}{2} (u^2 + v^2)}$$

II. TRANSONIC REGION

The potential equation of swirling flow is, from Section A, Eq (4),

$$(a^2 - g_x^2) g_{xx} = 2g_x g_r g_{xr} + (a^2 - g_r^2) g_{rr} + \frac{g_r}{r} (a^2 + \frac{K_1^2}{r^2}) = 0 \quad (1)$$

where a = local speed of sound in swirling flow. For isentropic flow of a perfect gas this may be represented from an energy balance as:

$$\left. \begin{aligned} a^2 &= a_t^2 - \frac{\gamma-1}{2} \left\{ g_x^2 + g_r^2 + \left(\frac{K_1}{r} \right)^2 \right\} \\ \text{where } a^{*2} &= \frac{2}{\gamma+1} \left[a_t^2 - \frac{\gamma-1}{2} \left(\frac{K_1}{r} \right)^2 \right] = \frac{2}{\gamma+1} a_t^2 \left[1 - \alpha^{*2} \left(\frac{r_t}{r} \right)^2 \right] \end{aligned} \right\} \quad (2)$$

Note that a^* is not the critical sonic velocity of the swirling flow. It is the critical sonic velocity considering the x and r components of velocity only, or the "axial" sonic velocity. The parameter α^* is defined

$$\alpha^* = \frac{K_1}{r_t a_t} \sqrt{\frac{\gamma-1}{2}}$$

The axial sonic line is given by

$$g_x^2 + g_r^2 = a^{*2}$$

A velocity perturbation potential is now assumed similar to the method used by Sauer* for finding the characteristics of the flow in the vicinity of the axial critical curve:

$$\begin{aligned} g_x &= a^* + g_x^* \\ g_r &= 0 + g_r^* \end{aligned}$$

* R. Sauer, General Characteristics of the Flow through Nozzles at Near Critical Speeds, NACA TM No. 1147, 1946.

II, Transonic Region (cont.)

Substituting (2) and (3) into the coefficient of g_{xx} in Eq (1),

$$a^2 - g_x^2 = -\frac{\gamma+1}{2} \left(g_x^{*2} + 2 a^* g_x^* \right) - \frac{\gamma-1}{2} g_r^{*2}$$

and, ignoring the g_x^{*2} and g_r^{*2} terms,

$$a^2 - g_x^2 \approx -(\gamma+1) a^* g_x^*$$

Similarly, the coefficients of the third and fourth terms of (1) may be evaluated as

$$a^2 - g_r^2 = a^{*2} - \frac{\gamma-1}{2} \left[2 a^* g_x^* + g_x^{*2} \right] - \frac{\gamma+1}{2} g_r^{*2} \approx a^{*2}$$

$$a^2 + \left(\frac{K_1}{r} \right)^2 \approx a^{*2} + \left(\frac{K_1}{r} \right)^2$$

Equation (1) may then be written as

$$-(\gamma+1) a^* g_x^* g_{xx}^* - 2(a^* + g_x^*) g_r^* g_{xr}^* + a^{*2} g_{rr}^* + \frac{g_r^*}{r} \left[a^{*2} + \left(\frac{K_1}{r} \right)^2 \right] = 0 \quad (4)$$

Sauer also ignores the second term of this equation, since g_{xr}^* approaches zero as x and r approach zero for axisymmetric flow. Since the axial sonic line in swirling flow is expected to be closer to the throat plane than for axisymmetric flow, this approximation also applies for swirling flow, and Equation (4) becomes (comparable to Sauer's Eq 8):

$$(\gamma+1) a^* g_x^* g_{xx}^* = a^{*2} g_{rr}^* + \frac{g_r^*}{r} \left[a^{*2} + \left(\frac{K_1}{r} \right)^2 \right] \quad (5)$$

II, Transonic Region (cont.)

Assuming the perturbation potential of the form

$$g^*(x, r) = f_0(x) + r^2 f_2(x) + r^4 f_4(x) + \dots$$

The perturbation velocities g_x^* and g_r^* become

$$g_x^* = f_0' + r^2 f_2' + r^4 f_4' + \dots$$

$$g_r^* = 2r f_2 + 4r^3 f_4 + \dots \quad (6)$$

and Eq (5) becomes, ignoring r^4 and higher powers of r ,

$$\begin{aligned} & (\gamma + 1) a^* \left[f_0' f_0'' + r^2 (f_0' f_2'' + f_2' f_0'') + \dots \right] \\ & = 4 a^{*2} (f_2 + 4 r^2 f_4) + (2 f_2 + 4 r^2 f_4) \left(\frac{K_1}{r} \right)^2 \end{aligned} \quad (7)$$

Now, assume f_0' , f_2 , and f_4'' may be represented by

$$f_0' = c_0 + c_1 x, \quad f_2 = d_0 + d_1 x, \quad f_4'' = f_4' = 0$$

so that (8)

$$f_0'' = c_1, \quad f_2' = d_1, \quad f_2'' = 0$$

Equation (7) is an identity which must hold for all values of r between 0 and r_t . It may therefore be solved by arranging each of the terms in order of powers of r and equating coefficients of the powers of r to zero. However, since a^* is a function of r , it is necessary to square both sides, substitute a^{*2} from Eq (2), and multiply r^4 . This results in

II, Transonic Region (cont.)

$$\begin{aligned}
& 2(\gamma + 1) c_1^2 (a_t^2 r^4 - \frac{\gamma-1}{2} K_1^2 r^2) (f_0'^2 + 2d_1 f_0' r^2 + d_1 r^4) \quad (9) \\
& = \frac{64}{(\gamma + 1)^2} (f_2^2 + 8 f_2 f_4 r^2 + 16 f_4^2 r^4) \left[\left(\frac{\gamma-1}{2} \right)^2 K_1^4 \right. \\
& \quad \left. - (\gamma - 1) a_t^2 K_1^2 r^2 + a_t^4 r^4 \right] \\
& \quad + \frac{32}{\gamma + 1} K_1^2 \left(- \frac{\gamma-1}{2} K_1^2 f_2^2 + a_t^2 f_2^2 r^2 - 3(\gamma - 1) f_2 f_4 K_1^2 r^2 \right. \\
& \quad \left. - 4(\gamma - 1) f_4^2 K_1^2 r^4 + 6 a_t^2 f_2 f_4 r^4 + 8 a_t^2 f_4^2 r^6 \right. \\
& \quad \left. + 4 K_1^4 (f_2^2 + 4 f_2 f_4 r^2 + 4 f_4^2 r^4) \right) \quad (9)
\end{aligned}$$

The coefficients of the r^4 terms result in

$$\begin{aligned}
& 2(\gamma + 1) c_1^2 \left[a_t^2 (c_0 + c_1 x)^2 - (\gamma - 1) K_1^2 d_1 (c_0 + c_1 x) \right] \\
& = \frac{64}{(\gamma + 1)^2} \left[a_t^4 (d_0 + d_1 x)^2 + (11 - 5\gamma) a_t^2 K_1^2 f_4 (d_0 + d_1 x) \right. \\
& \quad \left. + \frac{(3\gamma - 5)^2}{4} f_4^2 K_1^4 \right]
\end{aligned}$$

This is an identity in x . Setting the coefficient of the x^2 terms to zero results in

$$d_1 = \frac{1}{2} \frac{c_1^2}{a_t} \left(\frac{\gamma + 1}{2} \right)^{3/2} \quad (10)$$

II, Transonic Region (cont.)

Equating the sum of the r^6 coefficients to zero,

$$2(\gamma + 1) c_1^2 \left[a_t^2 d_1 f_o' - \frac{\gamma - 1}{2} K_1^2 d_1^2 \right]$$

$$= \frac{64}{(\gamma + 1)^2} 8 f_2 f_4 a_t^4 + \frac{256}{(\gamma + 1)^2} (5 - 3\gamma) f_4^2 a_t^2 K_1^2$$

This is again an identity in x . Considering the coefficients of x' ,

$$4(\gamma + 1) c_1^2 a_t^2 d_1 c_1 = \frac{64}{(\gamma + 1)^2} 8 d_1 f_4 a_t^4$$

and
$$f_4 = \frac{c_1^3}{16 a_t^2} \left(\frac{\gamma + 1}{2} \right)^3 \quad (11)$$

Now at the wall of the throat the flow can have no radial velocity, so that if the origin of the x - axis is selected at the throat,

$$g_r(o, r_t) = 0$$

and
$$g_r^*(o, r_t) = 0$$

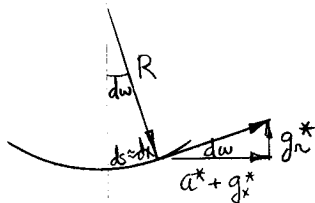
Therefore, from Equations (6), (8), and (11),

$$d_o = - \frac{c_1^3 r_t^2}{8 a_t^2} \left(\frac{\gamma + 1}{2} \right)^3 \quad (12)$$

II, Transonic Region (cont.)

Equations (10), (11), and (12) determine d_1 , f_4 , and d_0 in terms of C_1 . C_1 may be determined by considering the flow at the wall in the vicinity of the throat.

From the figure, it may be seen that



$$\Delta \omega = \frac{g_r^*}{a^* + g_x^*} \approx \tan \omega = \frac{\Delta g_r^*}{a^* + g_x^*} \approx \frac{g_{rx}^* \Delta s}{a^* + g_x^*}$$

The curvature of the wall at T is then

$$\frac{1}{R} = \frac{d\omega}{ds} = \lim_{x \rightarrow 0} \frac{g_{rx}^*}{a^* + g_x^*} = \lim_{x \rightarrow 0} \frac{g_{rx}^* x}{a^* \left(1 + \frac{g_x^*}{a^*}\right)}$$

Using a series approximation of the denominator, ignoring powered terms of g_r^* , and substituting Eq (6),

$$\frac{1}{R} = \lim_{x \rightarrow 0} \frac{g_{rx}^* x}{a^*} \left(1 - \frac{g_x^*}{a^*}\right) = \lim_{x \rightarrow 0} \frac{2r f_2'}{a^*} \left(1 - \frac{2r f_2 + 4r^3 f_4}{a^*}\right)$$

and, substituting from (8), (10), (11), and (12)

$$\frac{1}{R} = \frac{2 r_t d_1}{a^*} = \frac{r_t C_1^2}{a^* (r_t) a_t} \left(\frac{\gamma+1}{2}\right)^{3/2}$$

or, since $a^* (r_t) = a_t \sqrt{\frac{2}{\gamma+1} (1 - \alpha^{*2})}$

$$C_1^2 = \frac{a_t^2 \sqrt{1 - \alpha^{*2}}}{R r_t} \left(\frac{2}{\gamma+1}\right)^2 \quad (13)$$

II, Transonic Region (cont.)

To obtain a formula for C_o , consider the sonic line where $g_x^* \rightarrow 0$, so that, from Eq (6) and (8),

$$C_o + C_1 x + r^2 d_1 = 0$$

$$\text{or, } C_o = -C_1 x - r^2 d_1$$

At the edge of the void, the sonic line and the start (zero angle) line meet each other, for $P_a = 0$. Since at this point $g_r^* = 0$, $C_1 x$ may be obtained by solving Equation (6)

$$f_2 + 2 r^2 f_4 = 0$$

$$\text{or, } d_o + d_1 x + 2 r^2 f_4 = 0$$

and substituting from (10), (11), (12), and (13) yields

$$C_1 x_a = \frac{r_t^2 - r_a^2}{4R r_t} a_t \sqrt{\frac{2}{\gamma+1} (1 - \alpha^{*2})} \quad (15)$$

By noting that at the edge of the void the speed of sound is zero so that, from Equation (2) $r_a = r_t \alpha^*$, Equations (13), (14), (15), and (10) may be solved for C_o to yield

$$C_o = \frac{-(1 + \alpha^{*2}) \sqrt{1 - \alpha^{*2}} a_t r_t}{4R} \sqrt{\frac{2}{\gamma+1}} \quad (16)$$

II, Transonic Region (cont.)

Collection of formulas:

$$C_1^2 = \left(\frac{2a_t}{\gamma + 1} \right)^2 \frac{\sqrt{1 - \alpha^{*2}}}{R r_t} \quad (13)$$

(12) & (13) \rightarrow

$$d_o = - \frac{a_t}{8} \sqrt{\frac{r_t}{R^3}} (1 - \alpha^{*2})^{3/4} \quad (17)$$

(10) & (13)

$$d_1 = \frac{a_t}{2R r_t} \sqrt{\frac{2(1 - \alpha^{*2})}{\gamma + 1}} \quad (18)$$

(11) & (13) \rightarrow

$$f_4 = \frac{a_t}{16} \frac{(1 - \alpha^{*2})^{3/4}}{(R r_t)^{3/2}} \quad (19)$$

$$C_o = \frac{-(1 + \alpha^{*2}) a_t r_t}{R} \sqrt{\frac{1 - \alpha^{*2}}{8(\gamma + 1)}} \quad (16)$$

Equation (15) is not restricted to the edge of the void, and may be used to determine the coordinates of the start line by solving for x and substituting C_1 from Equation (13):

$$x = \frac{1}{8} \sqrt{\frac{2(\gamma + 1)}{R r_t}} (r_t^2 - r^2) (1 - \alpha^{*2}) \quad (20)$$

Note that for $\alpha^* = 0$ (no swirl), this reduces to Sauer's axisymmetric flow start line. The equation for the axial sonic line is

$$x = \sqrt{\frac{\gamma + 1}{8R r_t}} \left(\frac{1 + \alpha^{*2}}{2} r_t^2 - r^2 \right) (1 - \alpha^{*2})^{1/4}$$

These two lines will meet only at $r = r_t$ * with $P_a = 0$.

II, Transonic Region (cont.)

The related Mach number (considering x and r components of velocity only) must also be determined for the start line. A critical mach number is defined as

$$\bar{M}^2 \triangleq \frac{g_x^2 + g_r^2}{a^{*2}} \quad (21)$$

It is used to compute the related mach number \bar{M} :

$$\bar{M} = \left[\frac{\frac{2}{\gamma+1} \bar{M}^2}{1 - \frac{\gamma-1}{\gamma+1} \bar{M}^2} \right]^{1/2}$$

Since $g_r = 0$ on the start line,

$$\bar{M}^* = \frac{g_x}{a^*} = 1 + \frac{g_x^*}{a^*} = 1 + u'$$

Hence

$$u' = \frac{C_0 + C_1 x + r^2 d_1}{a^*}$$

which, when combined with (13), (16), (18), yields

$$u' = \frac{r^2}{4R r_t} \sqrt{\left[1 - \left(\frac{r_t}{r} \right)^2 \alpha^{*2} \right] (1 - \alpha^{*2})}$$

LIST OF SYMBOLS

a	Speed of sound
a_t	Speed of sound at stagnation conditions
K_1	Equal to wr
\bar{M}	Related Mach no., equal to U/a
r	Radial distance
r_o	Void ratio
r_t	Nozzle throat radius
u	Velocity in axial direction
U	Related velocity, equal to $u^2 + v^2$
v	Velocity in radial direction
V	Velocity
w	Velocity in circumferential direction
x	Axial distance
α	Related Mach angle
α^*	Swirl magnitude
β	Angle between U and u
γ	Ratio of specific heats
θ	Angular coordinate
ϕ	Potential function
ρ	Density

Report NAS 7-136-F, Appendix F

APPENDIX F

ANALYSIS OF AN AERODYNAMIC NOZZLE

FIGURE LIST

	<u>Figure</u>
Aerodynamic Nozzles	1
Aerodynamic-Nozzle Length, Primary Contour is a 15° Cone	2
Aerodynamic-Nozzle Length, Primary Contour is a 20° Cone	3
Aerodynamic-Nozzle Loss Factor, Primary Contour is a 15° Cone	4
Aerodynamic-Nozzle Loss Factor, Primary Contour is a 20° Cone	5
Length vs Loss Factor, Primary Contour is a 15° Cone	6
Length vs Loss Factor, Primary Contour is a 20° Cone	7
Conical Primary Nozzle Contours	8

I. INTRODUCTION

The aerodynamic nozzle, illustrated schematically by Figure 1, is unique compared to most other nozzle concepts in that a gas boundary rather than a solid boundary constrains the flow throughout the major portion of the nozzle skirt.

Attainment of high effective area ratios, the ratio of the area of the shroud to the area of the throat, by the aerodynamic nozzle is possible by free expansion of the primary nozzle gases into a cylindrical extension from the vehicle base. This cylindrical extension or shroud is of sufficient length that reattachment of the flow occurs near its exit, resulting in a trapped gas pocket at a finite pressure which results in constant pressure turning of the exhaust gases to the near axial direction. A shock is formed at the shroud reattachment point and the flow deflection angle and corresponding static pressure rise satisfy the conditions for reattachment of a turbulent boundary layer. These reattachment conditions are empirical and have been determined for flow over a rearward facing step and around axial, symmetric bodies with blunt bases. This data has been correlated with forward facing step flow separation data and the latter is used to solve for the static pressure rise, flow deflection angle, and the point on the shroud where reattachment occurs. The flow deflection angle is defined, in this instance, as the angle through which the flow turns, through the reattachment shock, to the axial direction.

The current study was undertaken to determine the relationship between primary nozzle design, shroud length and overall expansion area ratio as well as to define the gas-gas interface and determine the relative performance of the resulting nozzle based upon that for one-dimensional flow.

The design charts and loss factors presented on Figures 2 through 5 allow design and performance analysis of the aerodynamic nozzle. The configurations considered were limited to those with conical primary nozzles having expansion area ratios from 2 through 15. Cross-plotting of the results, however, would possibly allow judicious extrapolation to other conical nozzles of different wall half-angle or larger area ratios.

I, Introduction (cont.)

The loss factors presented in Figures 4 and 5 define only geometric losses and do not include frictional shear drag or other real gas effects, as the calculations were based upon the isentropic flow of a perfect gas. The shroud length determined for each expansion ratio by this procedure offers the best performance for that expansion ratio. Increasing the shroud length does not change the reattachment point and adds shear drag, while decreasing shroud length requires flow over-expansion for reattachment with a consequent decrease in base pressure.

II. PRIMARY NOZZLE AND FLOW FIELD

The eight conical primary nozzles selected (see Figure 6) utilized two skirt wall half-angles: 15 and 20°; and four expansion area ratios: 2, 5, 10 and 15. The flow field within these nozzles was determined by the method of characteristics and points within the field near the nozzle exit then used to determine the constant pressure, constant Mach number free boundary at pressure ratios, $\frac{P_c}{P_b}$, from 100 to 1000.

A representative series of these free boundaries for a 15° half-angle primary nozzle, expansion area ratio of 2, is shown on Figure 7.

III. SHROUD FLOW REATTACHMENT

Conditions for reattachment of the free flow boundary to the shroud were determined by using empirical rocket nozzle flow separation data and the two-dimensional oblique shock relations. The pressure rise coefficient across an oblique shock wave in air, $\frac{\Delta P}{q}$, associated with the boundary layer separation ahead of a forward facing step, and that associated with flow separation in a nozzle, are plotted versus approach Mach number on Figure 8. These curves, No. 1 and 2, are nearly identical and show good enough correlation that the two sets of data could be used interchangeably. Curve No. 3 is a plot of the pressure rise coefficient associated with flow separation in a real rocket nozzle and, from the preceeding statement, may also be considered as boundary layer separation data of a forward facing step for a real rocket gas. This is significant because the pressure rise coefficient experienced during reattachment of the flow behind a rearward facing step is 0.06 greater than that required for boundary layer separation ahead of a forward facing step, Curve No. 3*. Curve No. 3 is therefore uniformly increased 0.06 to obtain Curve No. 4 and data from this curve is used throughout the remaining calculations. Points on the attached aerodynamic nozzle design charts were located by the following procedure:

1. A constant pressure, constant Mach number free boundary was selected for a particular pressure ratio.
2. The oblique shock pressure rise coefficient with reattachment was selected from Curve No. 4, Figure 8, by using the constant, free boundary Mach number.
3. The flow deflection angle associated with this pressure rise coefficient and approach Mach number was found from oblique shock graphs.**

* Love, E. S., Base Pressure at Supersonic Speeds on Two-Dimensional Airfoils and on Bodies of Revolution With and Without Fins Having Turbulent Boundary Layers, NACA Technical Note No. 3819, January 1957.

** Compressible Flow Tables in Aerojet General Corporation Solid Engine Design Handbook, 1958.

III, Shroud Flow Reattachment (cont.)

4. The point on the free boundary where the flow angle equals the above oblique shock flow deflection angle is the point where the shroud should first contact the free boundary to turn the flow to an axial direction through the reattachment shock. Thus the shroud length and overall area ratio are determined as a function of base pressure ratio and primary nozzle configuration and area ratio.

Results of this study, in the form of aerodynamic nozzle design charts, are presented on Figures 2 and 3 and may be used to determine the basic nozzle configuration from the above parameters.

IV. PERFORMANCE

Performance of the aerodynamic nozzle can be examined by reference to a loss factor, ϵ_G , which is a measure of nozzle losses due to geometric factors only.

$1 - \epsilon_G$ is the vacuum thrust efficiency:

$$(1 - \epsilon_G) = \frac{\left(\frac{C_F}{C_F} \right)_{\text{VAC}} \text{AERO NOZZLE}}{\left(\frac{C_F}{C_F} \right)_{\text{VAC}} \text{1-DIM at } \epsilon_o}$$

where

$$C_{F \text{ VAC}}^{\text{AERO NOZZLE}} = C_{F \text{ VAC}}^{\text{PRIMARY}} + \frac{P_b}{P_c} (\epsilon_o - \epsilon_p) \frac{1}{C_D}$$

$$C_{D \text{ AERO NOZZLE}} = C_{D \text{ PRIMARY}} = 0.995 \text{ (for this study only)}$$

$$C_D = \dot{w} \text{ actual} / \dot{w} \text{ ideal}$$

$$\epsilon_o = \text{overall expansion ratio}$$

$$\epsilon_p = \text{primary expansion ratio}$$

$$P_b = \text{base pressure}$$

Loss factors determined by this method are plotted versus aerodynamic nozzle expansion ratio and length on Figures 4 and 5.

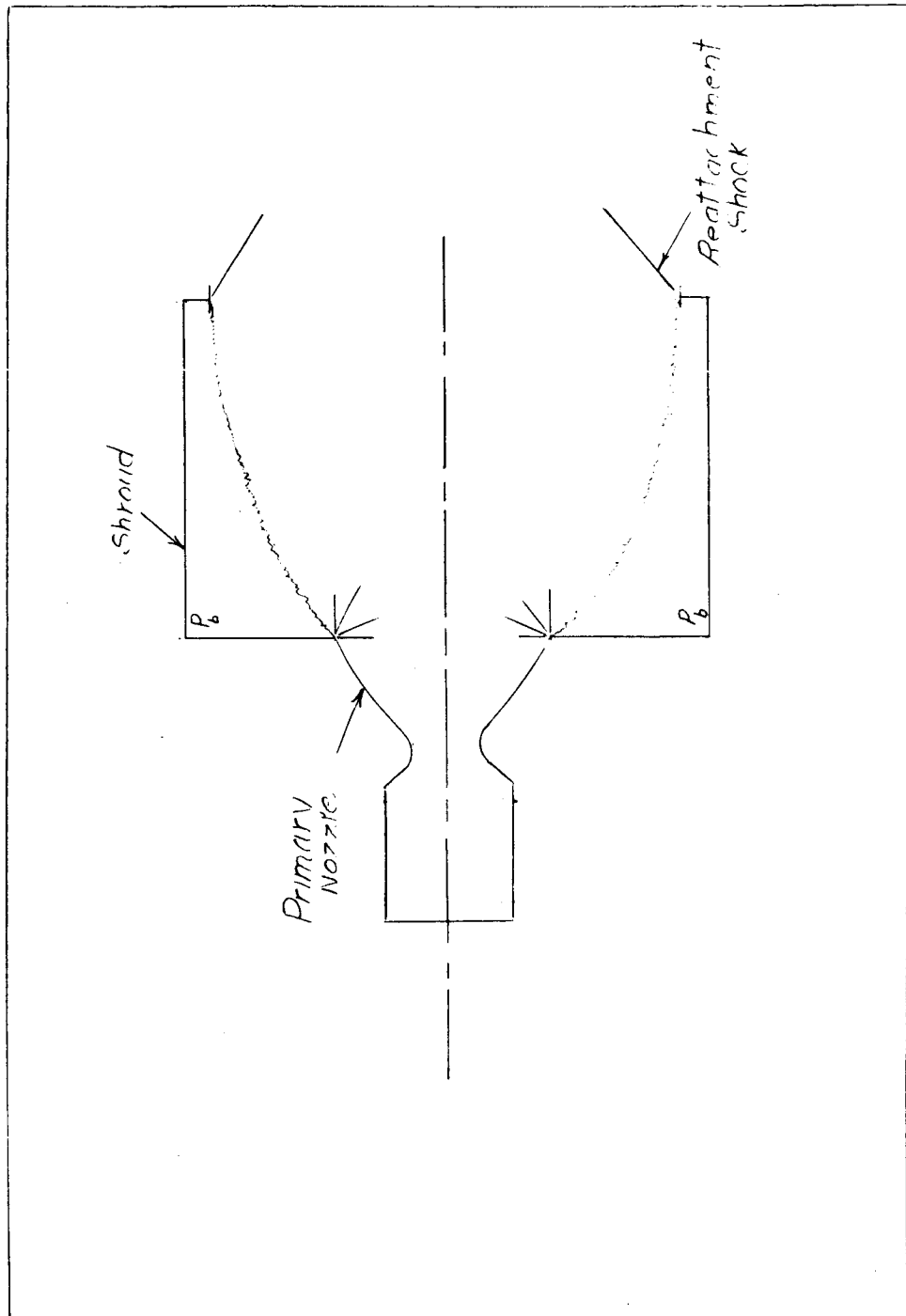


Figure 1

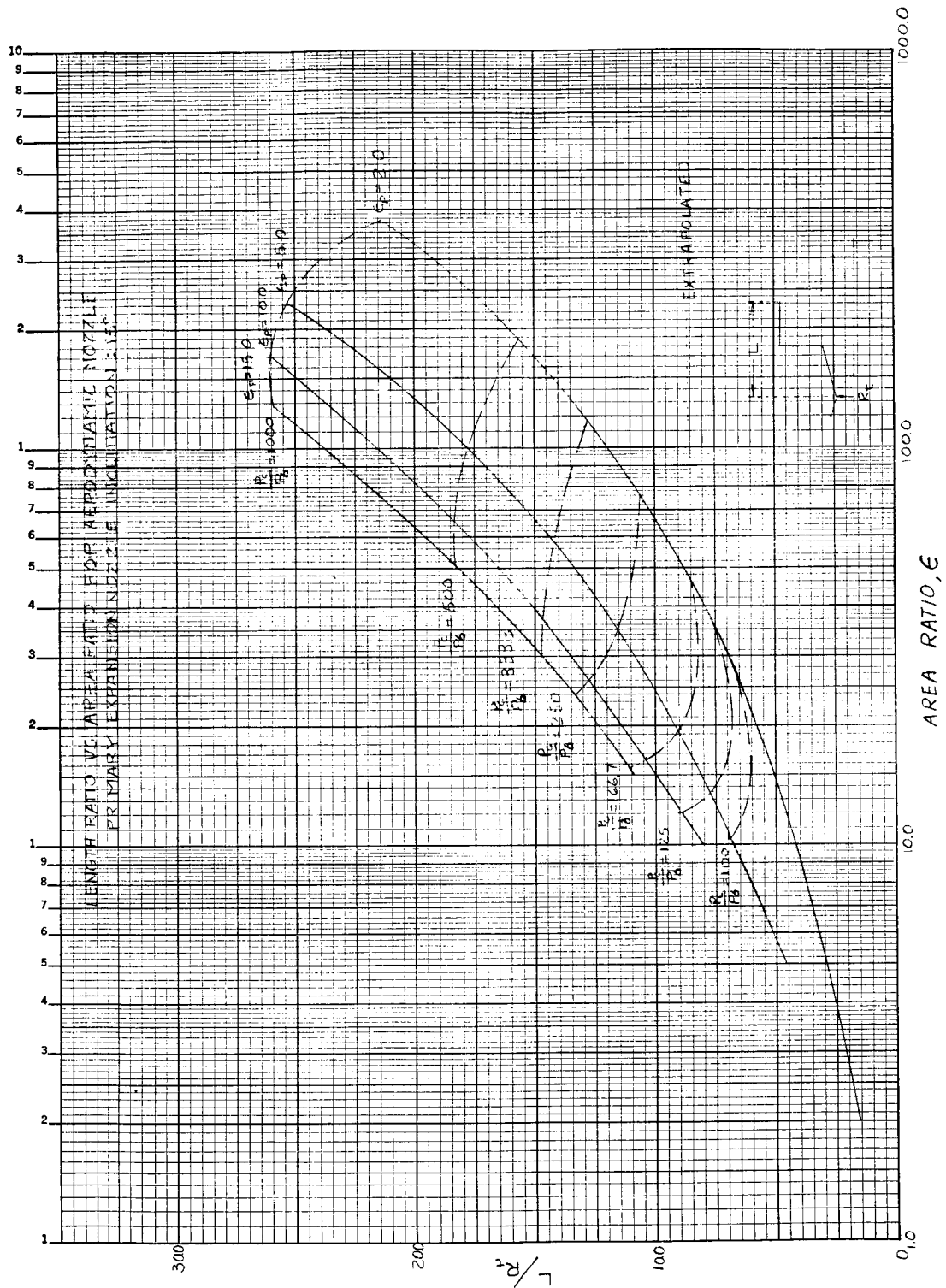


Figure 2

Aerodynamic-Nozzle Length, Primary Contour is a 15° Cone

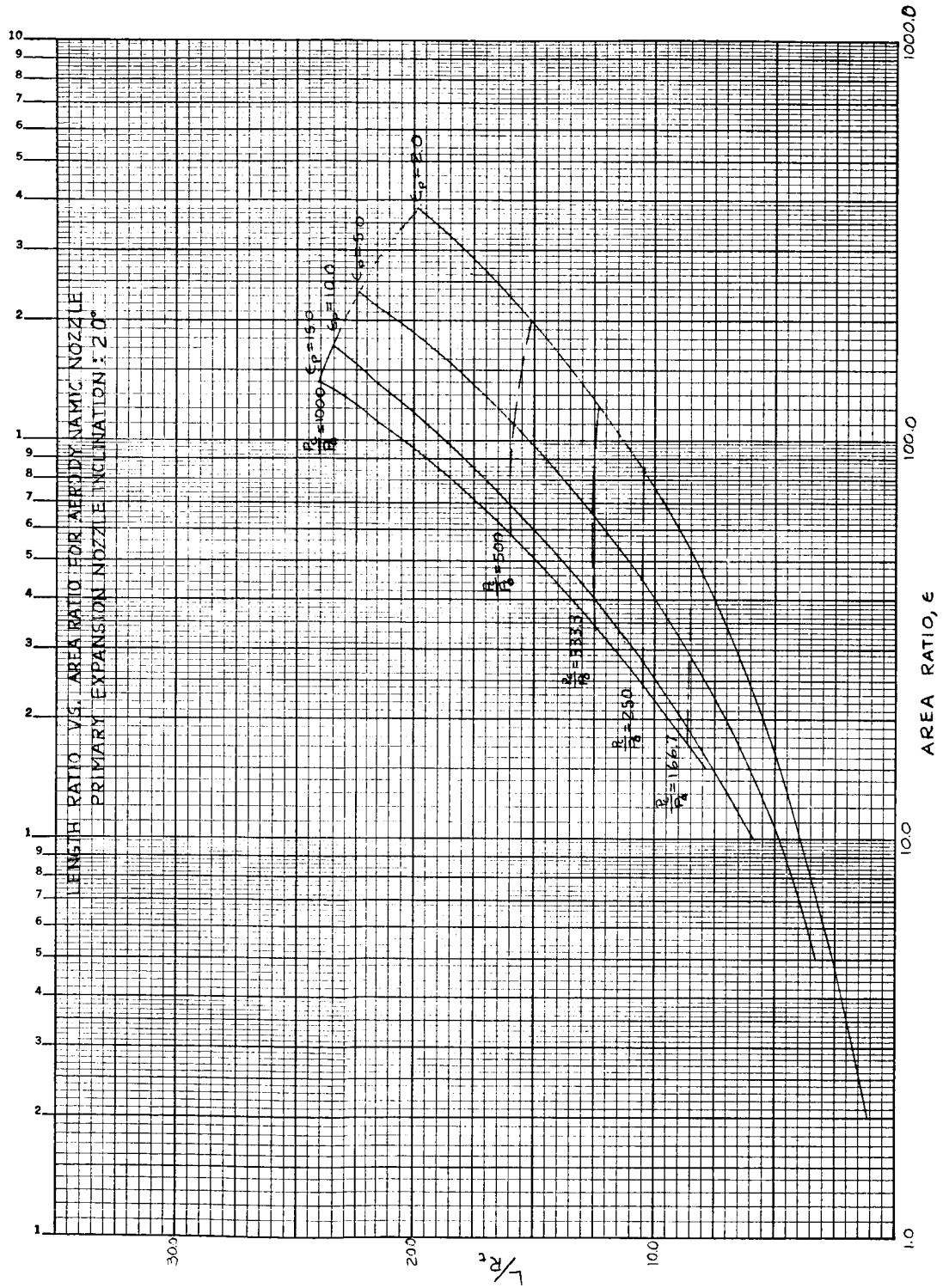
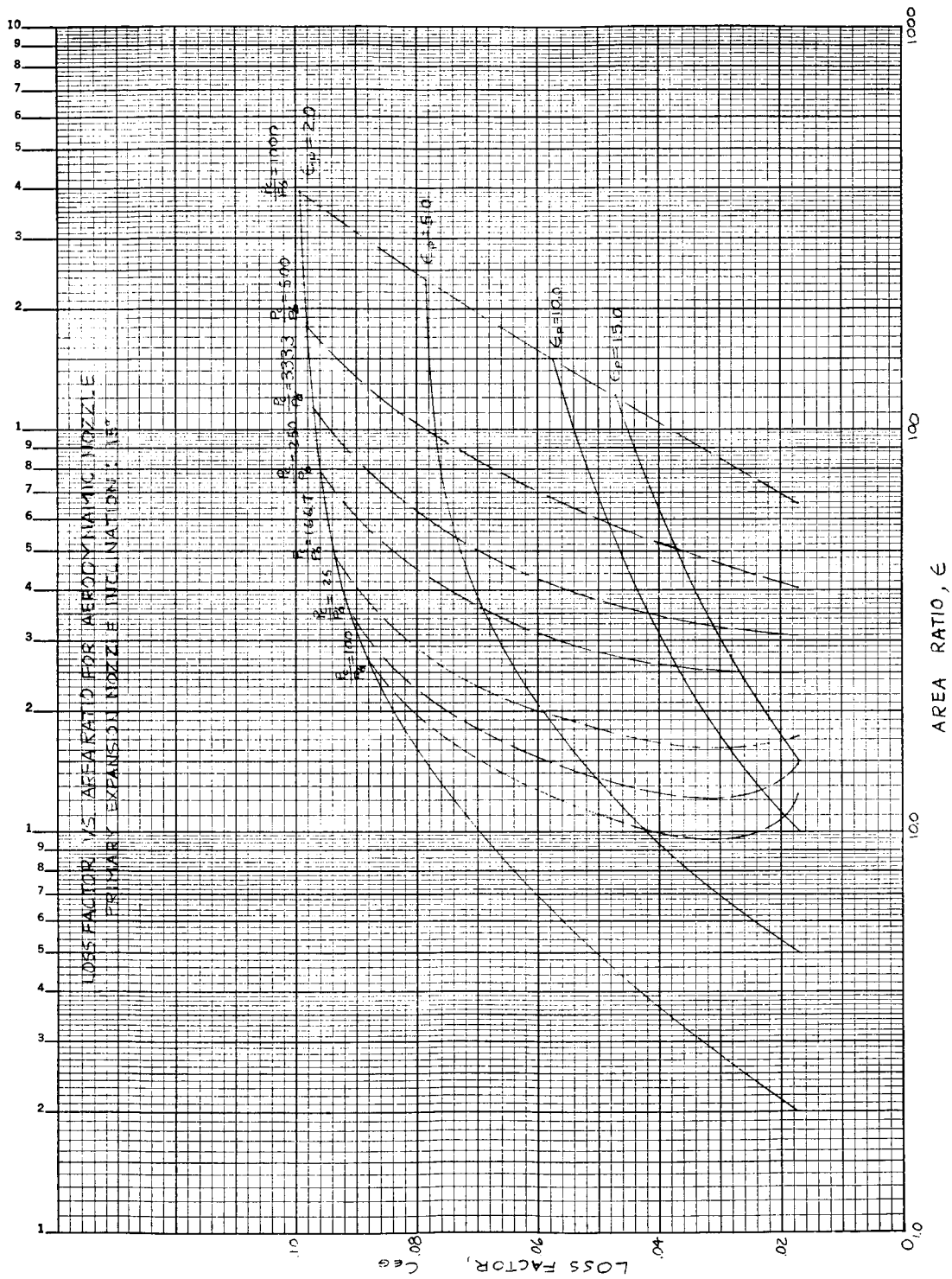


Figure 3

Aerodynamic-Nozzle Length, Primary Contour is a 20° Cone



Aerodynamic-Nozzle Loss Factor, Primary Contour is a 15° Cone

Figure 4

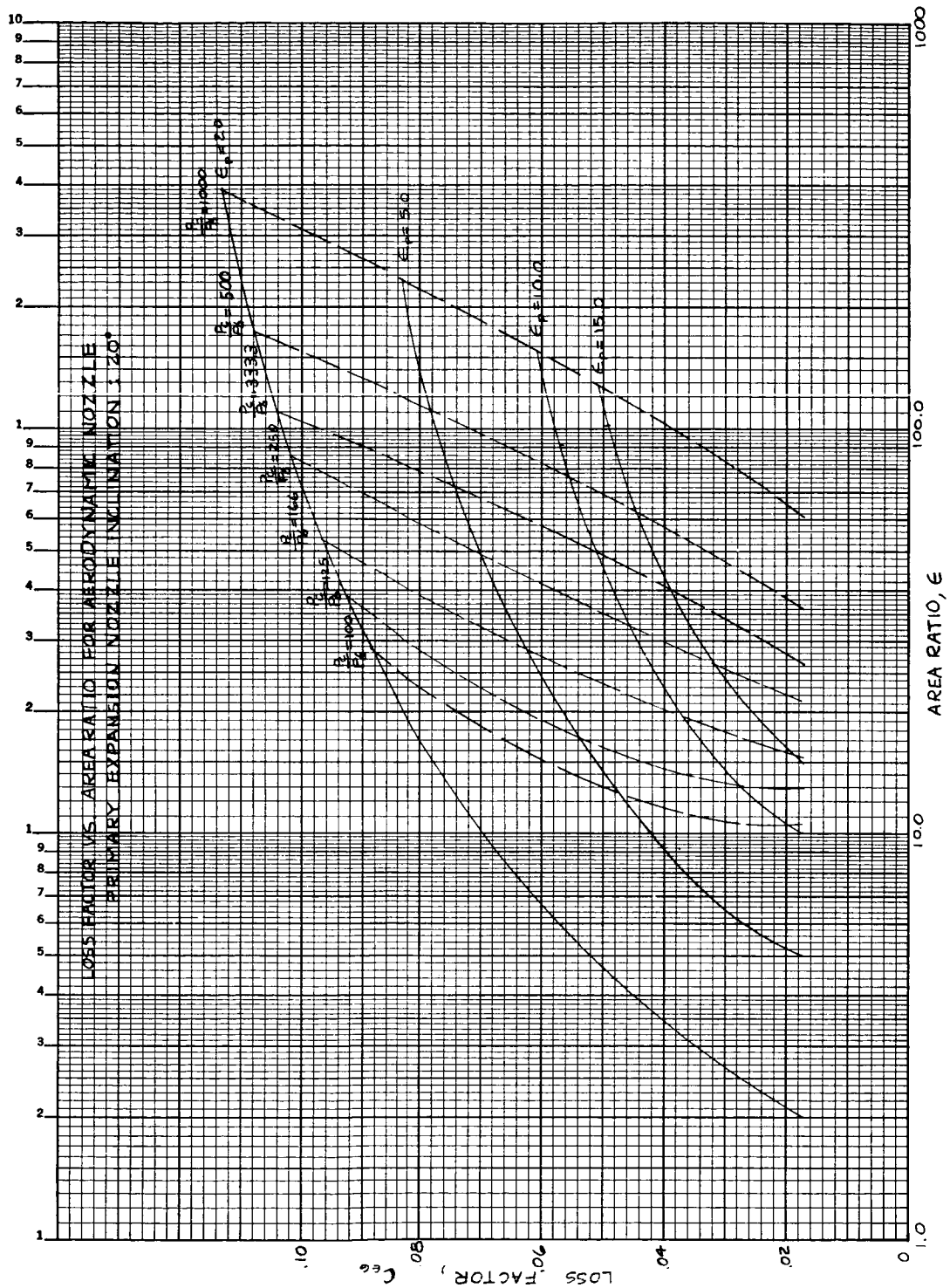
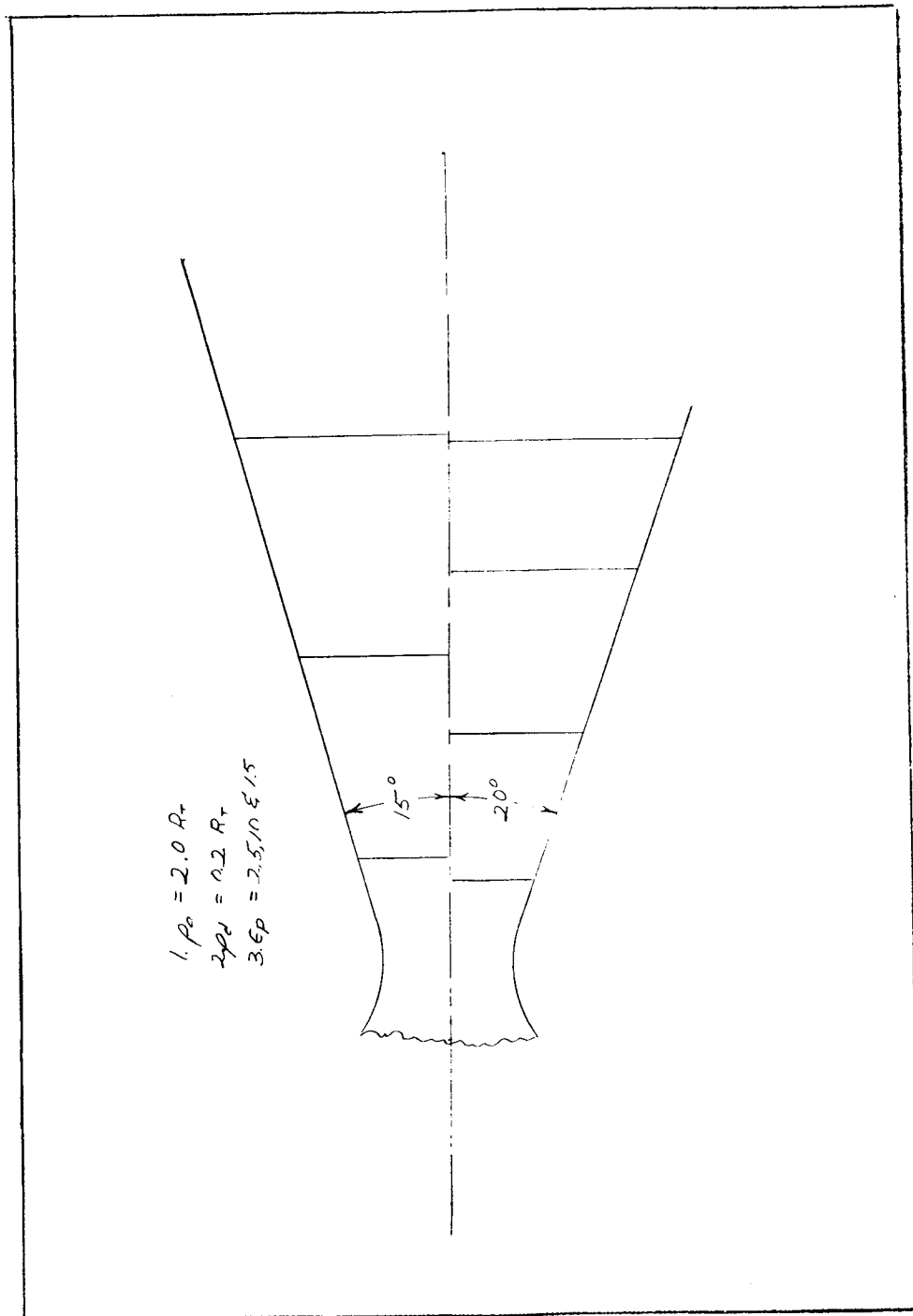


Figure 5

Aerodynamic-Nozzle Loss Factor, Primary Contour is a 20° Cone



Conical Primary Nozzles

Figure 6

CONSTANT PRESSURE, CONSTANT MACH NUMBER
FREE BOUNDARY

1. Conical Primary Nozzle, 15° Half-Angle
2. $C_p = 2$

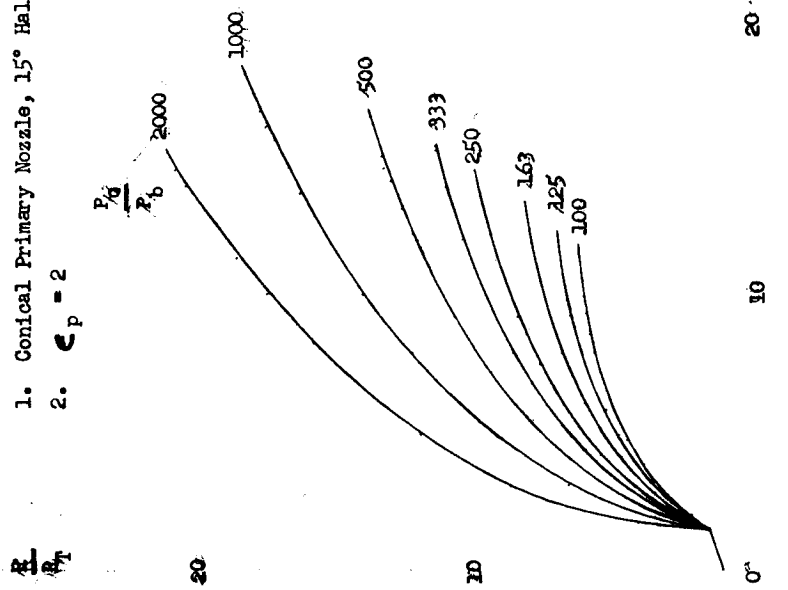


Figure 7

Free Boundaries, 15° Half-Angle Primary Nozzle

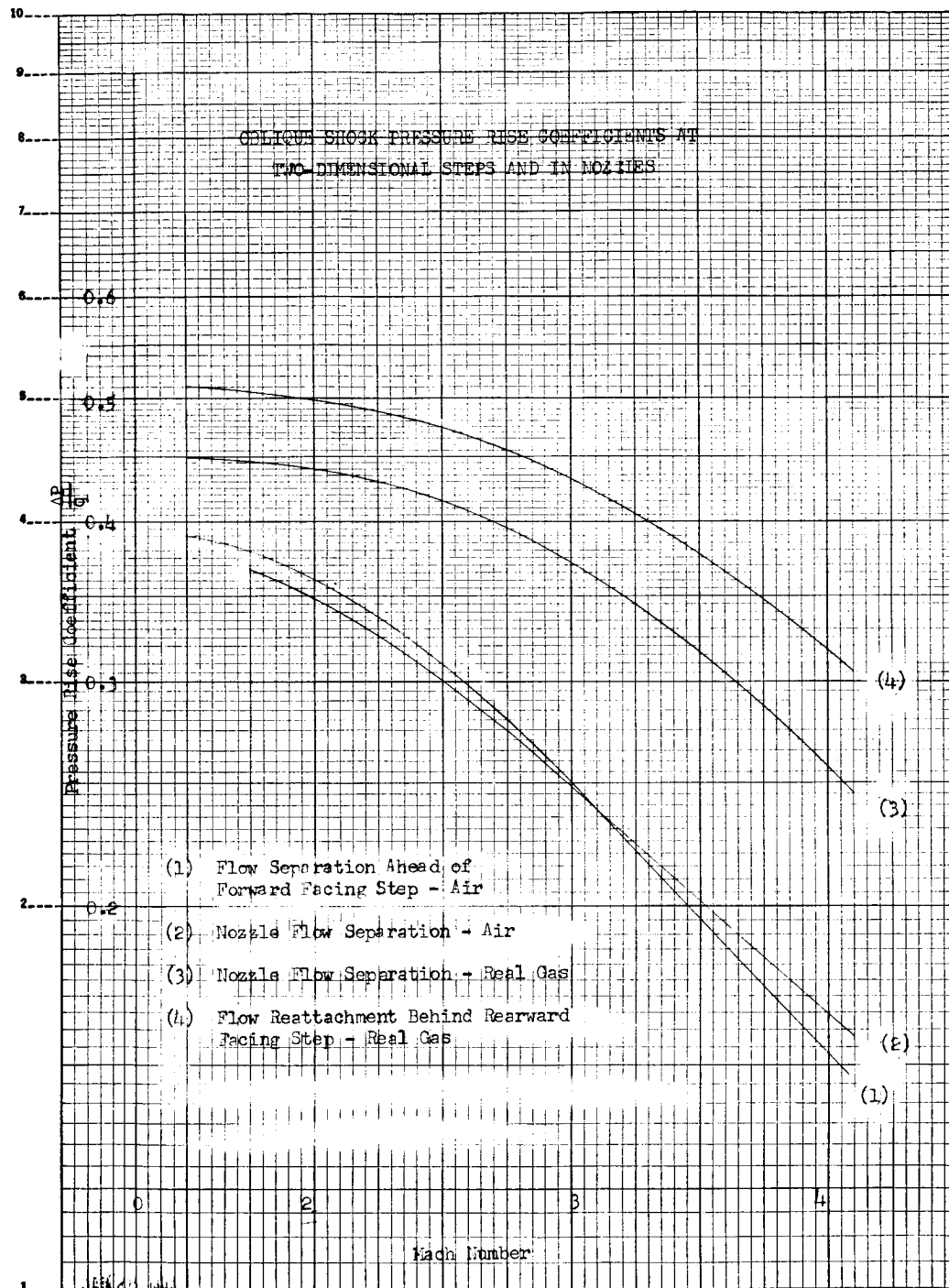


Figure 8

Report NAS 7-136-F

APPENDIX G

MISSION ANALYSIS

FIGURE LIST

FIGURE

Length of Contour (Rao) Nozzle from Bottom of Propellant Tank to Nozzle Exit	1
Length of Conical Nozzle from Bottom of Propellant Tank to Nozzle Exit	2
Length of Clustered Bell Nozzles from Bottom of Propellant Tank to Nozzle Exit	3
Length of Annular Nozzle from Bottom of Propellant Tank to Nozzle Exit	4
Length of Forced-Deflection Nozzle from Bottom of Propellant Tank to Nozzle Exit	5
Length of 20% Plug Nozzle from Bottom of Propellant Tank to Nozzle Exit	6
Length of Star Nozzle from Bottom of Propellant Tank to Nozzle Exit	7
Length of Swirl Nozzles from Bottom of Propellant Tank to Nozzle Exit	8
Length of Aerodynamic Nozzle from Bottom of Propellant Tank to Nozzle Exit	9
Weight of Contoured (Rao) Nozzle	10
Weight of Conical Nozzle	11
Weight of Clustered-Bell Nozzles	12
Weight of Annular Nozzle	13
Weight of Forced-Deflection Nozzle	14
Weight of Plug Nozzle	15
Weight of Star Nozzle	16
Weight of Swirling Flow Nozzle	17
Weight of Aerodynamic Nozzle	18

I. ASSUMPTIONS

To make the results of the mission analysis study meaningful for the comparative evaluation of real vehicles designed to carry out different missions, it was necessary to make the following assumptions:

A. Propellant outage is 1% of the usable propellant weight. This is a reasonable percentage to allow for outage, on the basis of outage propellant weights of current boost vehicles. The selected 1% figure is not of great importance in itself; the important thing is that the percentage is held constant for all nozzles so that a nozzle payload comparison will not be invalidated.

B. Propellant tank ullage is 1% of the usable propellant volume. The same remarks apply here as under the previous assumption.

C. For cryogenic propellant tanks, the tank stiffening factor decreases parabolically from 2.0 for a tank pressure of 0 psi to 1.15 for tank pressures above 400 psi. For storable propellant tanks, the tank stiffening factor decreases parabolically from 1.25 for a tank pressure of 0 psi, to 1.0 for tank pressures above 400 psi. These assumptions were arrived at by fitting parabolic curves through propellant tank "stiffness points" that were calculated for existing or planned vehicles such as Saturn S-IV, Able-star, and Titan II-A. The extra stiffness in the case of the last vehicle mentioned was taken into account.

D. A titanium alloy, Ti 6Al-4V, was chosen for the fuel tank and pressure bottle material, and an aluminum alloy, 7075-T6, was selected for the oxidizer tank material. The former was selected for its high strength-to-weight ratio, but was not considered suitable for use as an oxidizer tank material because of its sensitivity to oxidation.

E. Cryogenic tank insulation and baffle weights are 15% and 10%, respectively, of total spherical tank weight for liquid hydrogen tanks, and 4% and 10%, respectively, of total spherical tank weight for liquid oxygen tanks. Storable tank insulation and baffle weights are combined and are 15% of total spherical tank weight.

I, Assumptions (cont.)

weight for both N_2O_4 and Aerozine 50 tanks. For the cryogenic propellants, these percentages were arrived at after referring to the proposal indicated in footnote*, which details the Saturn S-II vehicle. For the storable propellants, the 15% figure was selected to make the tank weights of the Titan II-A, corrected for spherical tanks and lower stiffness factors, yield a tank factor commensurate with that obtained for the cryogenic propellant tanks.

F. If a tank is not completely spherical, as in the case of pump-fed systems, its weight is multiplied by a "frustum factor" to account for the increase in weight from the conical tank bottom. The frustum factor includes the weight of a toroidal transition section between the conical bottom and the spherical top of the tank.

G. For pump-fed systems, average tank pressures of 30 psi are used, whereas for pressure-fed systems, tank pressures are 130% of chamber pressure. In the former case, the tank factors would be slightly changed for different tank pressures in the range of 15 psi to 50 psi which would slightly affect the payload capability curves; but since all the vehicles were analyzed at the same average tank pressure, the most important consideration of comparing nozzle performance was effectively treated. For pressure-fed systems, the 130% figure represents an average loss of pressure in the lines and injectors of existing vehicles of 30% of chamber pressure.

H. Propellant tank pressures are constant during firing until propellant depletion. This is the natural consequence of the assumption that the pressurization system bottle pressure is constant until propellant depletion. This is a good assumption except perhaps for the last few seconds of firing.

* SATURN S-II Proposal, Aerojet-General Corporation Proposal
No. AGC-61002, July, 1961 (CONFIDENTIAL)

I, Assumptions (cont.)

I. Tank pressures resulting from propellant dynamic loads are small with respect to tank design pressures and are neglected. That this assumption is reasonable may be seen by the fact that for the worst possible condition, i.e., for the high density storable propellants in a Mars space vehicle subjected to a 4g acceleration during the boost-to-earth-orbit phase, the tank pressure increase above the design pressure of 30 psi, is only 10 psi. Because the design tank weight is multiplied by a safety factor of 1.5 as well as by a stiffness factor of at least 1.2, the tank may be considered to be adequately designed if the propellant dynamic loads are neglected.

J. The temperature of the gases that pressurize the cryogenic propellants is raised to 150°F above the propellant saturation temperature to preclude condensation.

K. The pressure in the hydrogen spherical pressure bottle is regulated to twice the fuel tank pressure. This regulation is sufficient to give a great enough pressure differential between the hydrogen pressure bottle and the fuel tank for efficient pressurization of the tank.

L. Helium is stored in a titanium alloy (Ti6Al-4V) pressure sphere at 5,000 psi. The high pressure of helium reduces its storage requirements.

M. The perfect-gas law is valid near the liquid state of a gas. This assumption affects the volume of the helium bottle and probably is valid only at pressures far above the critical pressure, which is the case for the stored helium.

N. Burst-to-proof and proof-to-working pressure ratios are 1.33 and 1.2, respectively.*

* Tanforan, F. M., "Preliminary Design Data for Low Thrust Rocket Propulsion Systems", Aerojet-General Report No. PDR-60-7 (LRP), 18 August 1960

I, Assumptions (cont.)

O. The pressurization system safety factor is 1.1, pressure tolerance factor is 1.1, valves, lines, and fittings factor is 1.1, weight contingency and structural support factor is 1.25, and the heating element factor is 1.01.*

P. Structural safety factors of 1.5 are used for all structures. This is common practice for man-rated systems.

Q. The minimum wall thickness for propellant tanks and the hydrogen pressure bottle is 0.01-in. This limitation was imposed to preclude tank thicknesses which would be unattainable under the present state of the art of tank manufacture.

R. Intertank and interstage structure is made of a sandwich material that has 7075-T6 aluminum outer panels and an inner filler material that weighs 0.01 lb/in³. This material was selected for its high strength-to-weight ratio.** This weight was increased as described in section IV.C.3 and Appendix J to account for the effect of increased bending moment on the lower stages as the interstage length is increased.

S. Structural rings at the ends of the interstage and intertank sections change the direction of the applied loads, thus reducing the bending and compressive stress in the sections. The weight of these rings is approximately 10% of the weight of the interstage or intertank section to which they are attached. This estimate of ring weight may be a little conservative.

* Tanforan, F. M., "Preliminary Design Data for Low Thrust Rocket Propulsion Systems", Aerojet-General Report No. PDR-60-7 (LRP), 18 August 1960

** Sandorff, P. E., "Structures Considerations in Design for Space Boosters," ARS Journal, November 1960

I, Assumptions (cont.)

T. The maximum angle of the lower interstage skirt is limited to 20° for vehicle designs in which the nozzle exit diameter exceeds the larger tank diameter, whereas a straight cylindrical skirt is selected for the designs in which the larger tank diameter equals or exceeds the nozzle exit diameter. This assumption was made to avoid large payload losses resulting from excessive aerodynamic drag on a wide-angle interstage skirt. A study of many existing vehicle designs showed that in all cases the interstage angles were less than 20°.

II. PRINCIPAL EQUATIONS

A. WEIGHT RATIO EQUATION

$$W_I = W_O \exp (- \Delta v / g I_s)$$

B. PRESSURIZATION SYSTEM WEIGHT EQUATION *

$$W_{ps} = 144 \text{ PV} \left[\frac{30.3}{\gamma} r_t + \frac{1}{RT} \right] \left[1 + \frac{r_t}{r_p} \right]$$

$$\text{where } r_t = \frac{P_i \rho_f}{P_f \rho_i} \quad \text{and} \quad r_p = \frac{P_i}{P_f}$$

The terms in the first bracket represent the pressure bottle weight and the pressurant weight needed to expel all the propellant from the tanks. The last term in the second bracket represents the additional pressure bottle weight and pressurant weight required to allow for residual pressurants in the pressure bottle upon propellant depletion.

* op. cit., Tanforan, F. M.

II, Principal Equations (cont.)

C. DIAMETER OF PRESSURE SPHERES OR SPHERICAL TANKS

$$D_g = \sqrt[3]{\frac{6}{\pi} V_g}$$

D. HELIUM BOTTLE WEIGHT

The helium bottle weight is usually found from one application of the Pressurization System Weight Equation given above, except for the case when the helium is used to pressurize two different containers. When this is the case, two applications of the Pressurization System Weight Equation, one for each container, are necessary to find the helium bottle weight from the following equation:

$$W_{HEB} = \left[\frac{W_{HEB_I} + W_{HEB_{II}}}{V_I + V_{II}} \right] V_{HEB}$$

where W_{HEB_I} and $W_{HEB_{II}}$ are the helium bottle weights required in pressurizing containers I and II, and V_I and V_{II} are the volumes of the containers.

E. SKIN THICKNESS EQUATION

$$t = \frac{W_g}{\rho_s \pi D_g^2}$$

F. TANK WEIGHT EQUATION

$$W_T = f f_1 f_2 \frac{k}{Y} PV$$

This equation represents the sum of the container wall weight, the insulation weight and baffle weight. The derivation follows:

$$W_T = f f_1 f_2 \rho_s \pi D_g^2 t + k_1 W_T + k_2 W_T$$

II, F, Tank Weight Equation (cont.)

where k_1 and k_2 represent insulation and baffle weight factors, respectively.

$$W_T = \frac{f f_1 f_2 \rho_s \pi D^2 t}{1 - (k_1 + k_2)}$$

Representing thickness, t , as a function of tank pressure and diameter:

$$t = \frac{PD}{4\sigma} \quad \text{where } \sigma \text{ is the material ultimate strength (lb/in}^2\text{)}$$

$$W_T = \frac{f f_1 f_2 \rho_s \pi D^2 PD}{[1 - (k_1 + k_2)] 4\sigma} = \frac{f f_1 f_2 D^3}{[1 - (k_1 + k_2)] 6} \quad (1.5)(1.33)(1.2)(1728) \frac{P}{\gamma}$$

$$\text{let } k = \frac{(1.5)(1.33)(1.2)(1728)}{1 - (k_1 + k_2)}$$

which now accounts for type of units used as well as the pressurizing safety factors of 1.33 and 1.2.

$$\text{Then } W_T = f f_1 f_2 \frac{k}{\gamma} PV$$

G. LOWER TANK DIAMETER FOR PUMP-FED SYSTEM

Let c represent the length of a chord across the widest base of the frustum section of the tank bottom and h represent the altitude of this frustum.

$$\text{Then } c = x_1 D \text{ and } h = x_2 D$$

The new lower tank diameter D_1 in terms of the old spherical diameter, D , x_1 , and x_2 is then:

$$D_1 = D \sqrt[3]{1 + x_2 \left[6 x_2 (x_1 + 1) - 8 x_2^2 - 3 x_1^2 \right]}$$

II, Principal Equations (cont.)

H. FRUSTUM FACTOR EQUATION

The frustum factor which accounts for the increased tank weight because of the conical bottom and toroidal transition section is:

$$f_2 = 1/2 \left[1 + 3 \sqrt{2} x_2 (x_1 - x_2) + \left(\frac{D_1}{D} + x_1 \right) \sqrt{2} (1/2 - x_2) \right]$$

where x_1 and x_2 are the same as in G.

I. PUMP WEIGHT EQUATION *

$$W_{\text{pmp}} = 100 + .463 Q^{0.67} P_c^{0.74}$$

where the propellant flow rate, Q , in ft^3/sec is derived as follows:

$$\dot{w} = F/I_s$$

$$\rho_b = \rho_{fu} \frac{MR + 1.0}{1.0 + MR \left(\frac{\rho_{fu}}{\rho_{ox}} \right)}$$

$$Q = \frac{\dot{w}}{\rho_b}$$

J. INTERTANK AND INTERSTAGE WEIGHT EQUATIONS

These equations have the same form and may be written

$$W_g = 1.1 \pi \frac{E}{8} (D + d)^2 \left[\frac{4 \rho_s \bar{t}}{D + d} \right]$$

* "Unconventional Nozzle Study", Douglas Aircraft Co., MSSD Report No. SM 41358, Jan., 1962 (C)

II, Principal Equations (cont.)

Where D and d are the large and small diameters respectively of the ends of the intertank or interstage section. The bracketed expression is given by the curve for sandwich structures in the reference indicated in footnote**.

K. PAYLOAD WEIGHT EQUATION

$$W_{PL} = W_o - (W_{PP} + W_{ft} + W_{oxt} + W_{PS} + W_{lines} + W_{PMP} + W_e + W_{its})$$

where the meaning of each term is given in the list of symbols on page 12.

III. DERIVATION OF BURNOUT WEIGHT-SPECIFIC IMPULSE TRADE FACTOR

$$\Delta v = gI_s \ln \left(\frac{W_o}{W_I} \right)$$

$$d \left(\frac{\Delta v}{g} \right) = dI_s \ln \left(\frac{W_o}{W_I} \right) + \left(\frac{I_s}{\left(\frac{W_o}{W_I} \right)} - \frac{W_o}{W_I^2} \right) dW_I$$

keeping the ideal velocity increment constant, $d \left(\frac{\Delta v}{g} \right) = 0$.

$$\therefore \frac{I_s}{W_I} dW_I = dI_s \left(\frac{W_o}{W_I} \right)$$

Replacing $\ln \left(\frac{W_o}{W_I} \right)$ by $\frac{\Delta v}{gI_s}$, and replacing differentials by finite differences, the burnout weight-specific impulse trade factor is obtained.

$$\frac{\Delta W_I}{\Delta I_s} = \frac{\Delta v}{gI_s^2} W_I$$

** Op. cit., Sandorff, P. E.

IV. DERIVATION OF TRADE FACTOR OF PERCENTAGE CHANGE IN PAYLOAD WEIGHT PER PERCENTAGE CHANGE IN SPECIFIC IMPULSE

From the derivation of the burnout weight-specific impulse trade factor given in III.

$$\Delta W_I = \left(\frac{\Delta v \frac{W_I}{2}}{g I_s} \right) \Delta I_s$$

$$\frac{\Delta W_I}{W_{PL}} = \left(\frac{W_I}{W_{PL}} \right) \left(\frac{W_I}{W_I} \right) = \left(\frac{\Delta v}{g I_s} \right) \left(\frac{W_I}{W_{PL}} \right) \left(\frac{\Delta I_s}{I_s} \right)$$

and since $\Delta W_{PL} = \Delta W_I$

$$\left(\frac{\Delta W_{PL}}{W_{PL}} \right) / \left(\frac{\Delta I_s}{I_s} \right) = \frac{\Delta v \frac{W_I}{W_{PL}}}{g I_s} = \frac{\Delta v \left[W_o (1 - \lambda) + \lambda W_{PL} \right]}{g I_s W_{PL}}$$

V. DERIVATION OF TRADE FACTOR OF PERCENTAGE CHANGE IN PAYLOAD WEIGHT PER PERCENTAGE CHANGE IN ENGINE WEIGHT

Because both payload weight and engine weight are inert weights, they must be one-to-one correspondence.

$$\Delta W_{PL} = - \Delta W_e$$

$$\frac{\Delta W_{PL}}{W_e W_{PL}} = - \frac{\Delta W_e}{W_{PL} W_e}$$

$$\left(\frac{\Delta W_{PL}}{W_{PL}} \right) / \left(\frac{\Delta W_e}{W_e} \right) = - \frac{W_e}{W_{PL}}$$

VI. DERIVATION OF TRADE FACTOR OF PERCENTAGE CHANGE IN PAYLOAD WEIGHT PER PERCENTAGE CHANGE IN INTERSTAGE WEIGHT

$$W_{PL} = (W_{Lo} - W_{Iss}) \left[1 - \frac{1}{\lambda} (1 - e^{-\Delta V / g I_s}) \right]$$

$$\frac{dW_{PL}}{dW_{Iss}} = \frac{1 - e^{-\Delta V / g I_s}}{\lambda} - 1 = 1 - \frac{W_{PL}}{W_{Lo} - W_{Iss}} - 1 = \frac{W_{PL}}{W_{Lo} - W_{Iss}}$$

$$\therefore \left(\frac{\Delta W_{PL}}{W_{PL}} \right) / \left(\frac{\Delta W_{Iss}}{W_{Iss}} \right) = \frac{W_{Iss}}{W_{Lo} - W_{Iss}}$$

SYMBOLS

D	Spherical propellant tank diameter, unless otherwise noted (in.)
d	Denotes differentiation, unless otherwise noted
D_1	Lower propellant tank diameter for pump fed systems (in.)
E	Slant height of conical frustum (in.)
F	Space vehicle thrust (lb)
f	Tank stiffening factor (dimensionless)
f_1	Structural safety factor (dimensionless)
f_2	Frustum factor (1.0 for perfectly spherical tanks-dimensionless)
g	Reference gravitational constant (32.2 ft/sec ²)
I_s	Vacuum specific impulse (sec)
k	Parameter that is a function of units used, pressurization safety factors, and insulation and baffle weights (in/ft ³)
MR	Mixture ratio, oxidizer to fuel (dimensionless)
P	Tank pressure (lb/in. ²)
P_c	Combustion chamber pressure (lb/in. ²)
Q	Propellant flow rate (ft ³ /sec)
R	Gas constant ($\frac{\text{ft-lb}}{\text{lb}^\circ\text{R}}$)
r_p	Ratio of initial pressure to final pressure of a pressurizing gas (dimensionless)
r_t	Ratio of initial temperature to final temperature of a pressurizing gas (dimensionless)
T	Final temperature of a pressurizing gas (°R)
t	Skin thickness (in.)
\bar{t}	Equivalent thickness of an intertank or interstage section (in.)
V	Tank volume unless otherwise noted (ft ³)
Δv	Ideal velocity increment required for the space vehicle to perform its mission (ft/sec)
W_e	Engine weight (lb)
W_{ft}	Fuel tank weight (lb)
W_I	Vehicle burnout weight (lb)
W_{Iss}	Interstage skirt weight (lb)
W_{its}	Intertank skirt weight (lb)

SYMBOLS (cont.)

W_{lines}	Propellant line weight (lb)
W_o	Vehicle liftoff weight (lb)
W_{ox}	Oxidizer tank weight (lb)
W_{PL}	Payload weight (lb)
W_{pmp}	Pump weight (lb)
W_{pp}	Propellant weight (lb)
W_{ps}	Pressurization system weight (lb)
W_T	Propellant tank weight (lb)
\dot{w}	Propellant weight flow (lb/sec)
γ	Material strength to weight ratio (in.)
Δ	Denotes finite differences
ϵ	Ratio of nozzle exit area to throat area (dimensionless)
ρ	Density (lb/in ³) for solids, lb/ft ³ for liquids and gases)
λ	Stage mass fraction = $W_{pp}/(W_{pp} + W_I - W_{PL})$
σ	Material ultimate strength (lb/in. ²)

Subscripts

B	Bulk propellant (fuel plus oxidizer)
f	Final condition
fu	Fuel
g	A general quantity
HEB	Helium pressure bottle
i	Initial condition
ox	Oxidizer
s	Structure or material

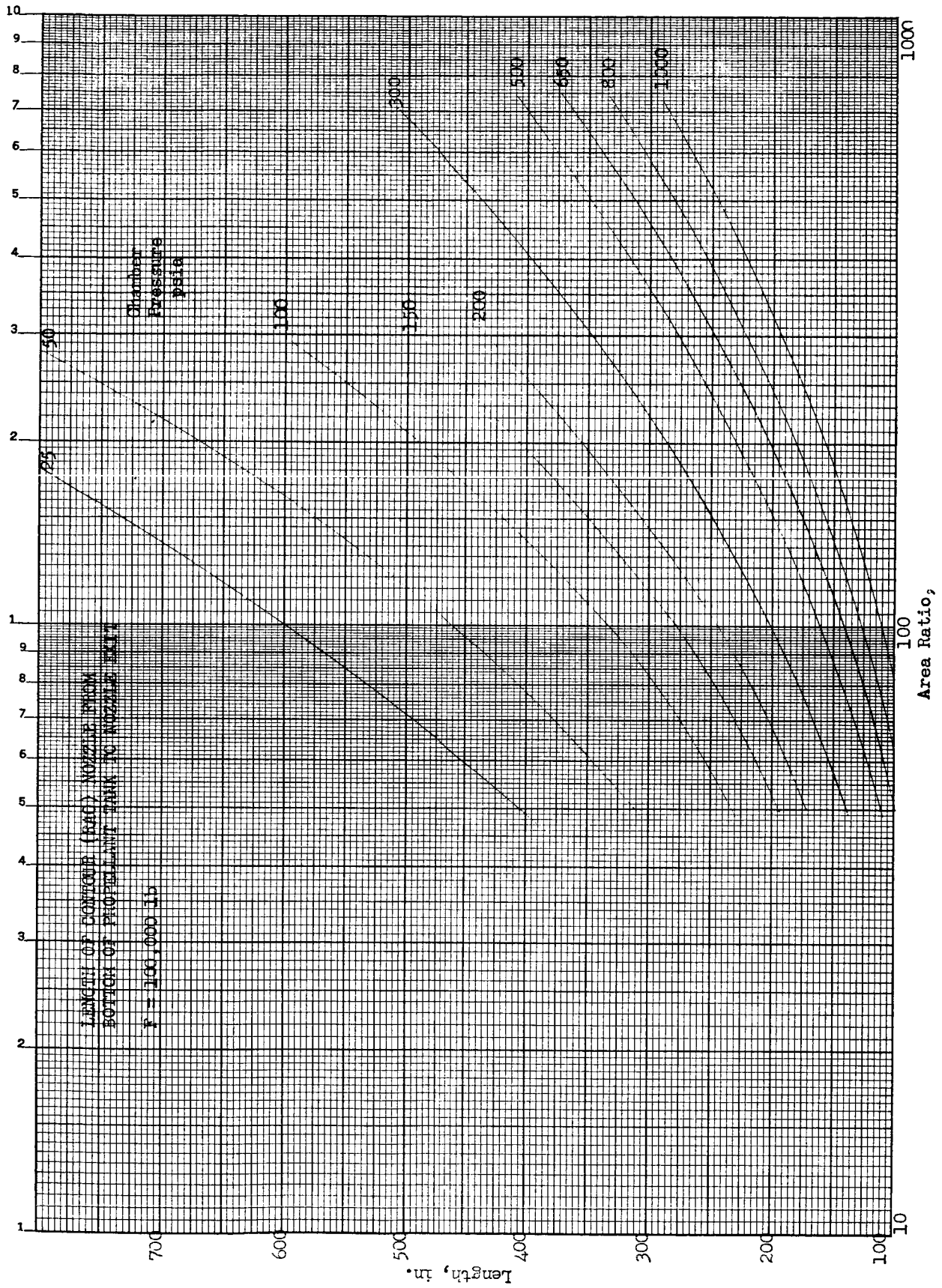


Figure 1

Length of Contour (Rao) Nozzle from Bottom of Propellant Tank to Nozzle Exit

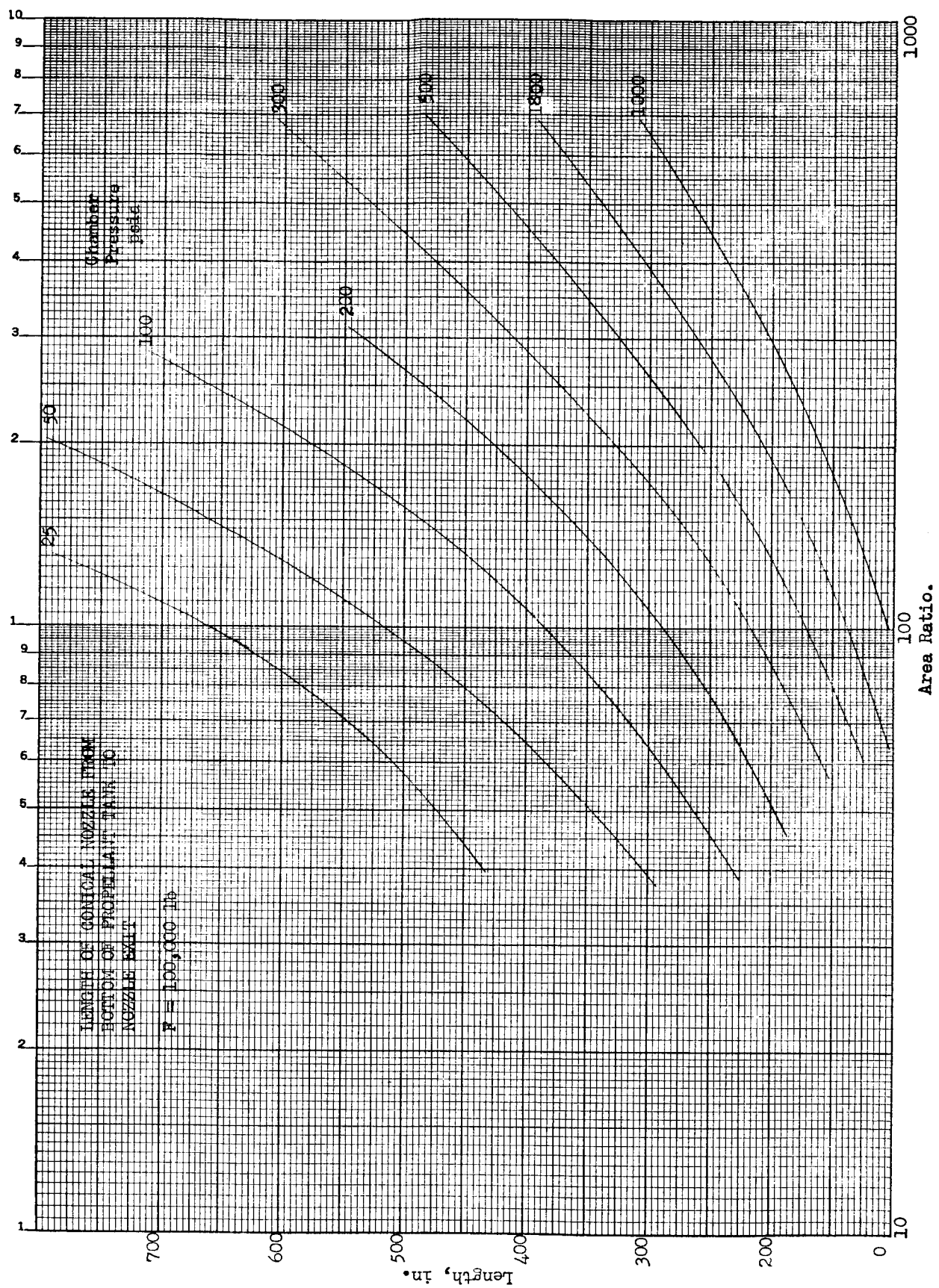


Figure 2

Length of Conical Nozzle from Bottom of Propellant Tank to Nozzle Exit

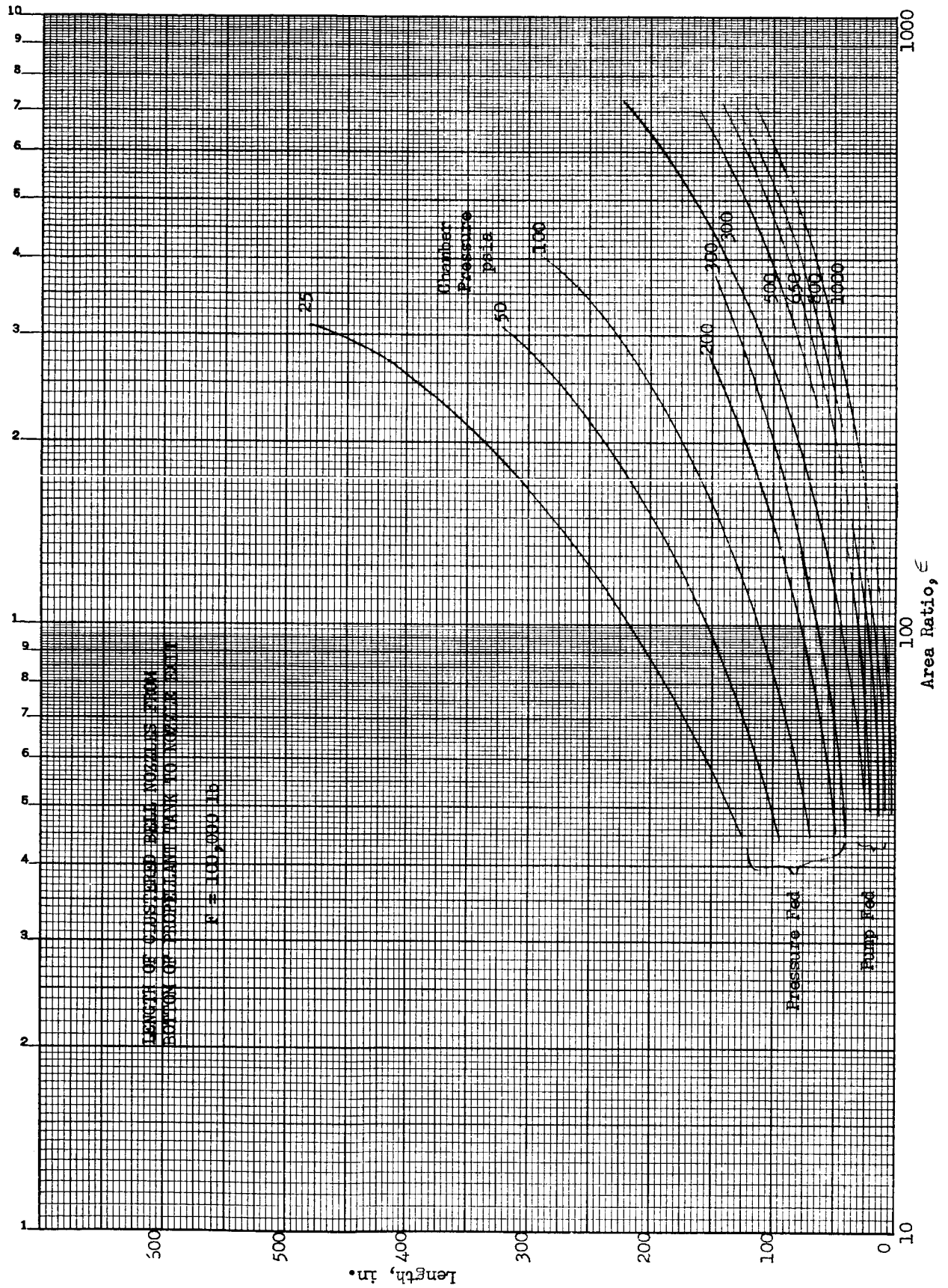


Figure 3

Length of Clustered Bell Nozzles from Bottom of Propellant Tank to Nozzle Exit

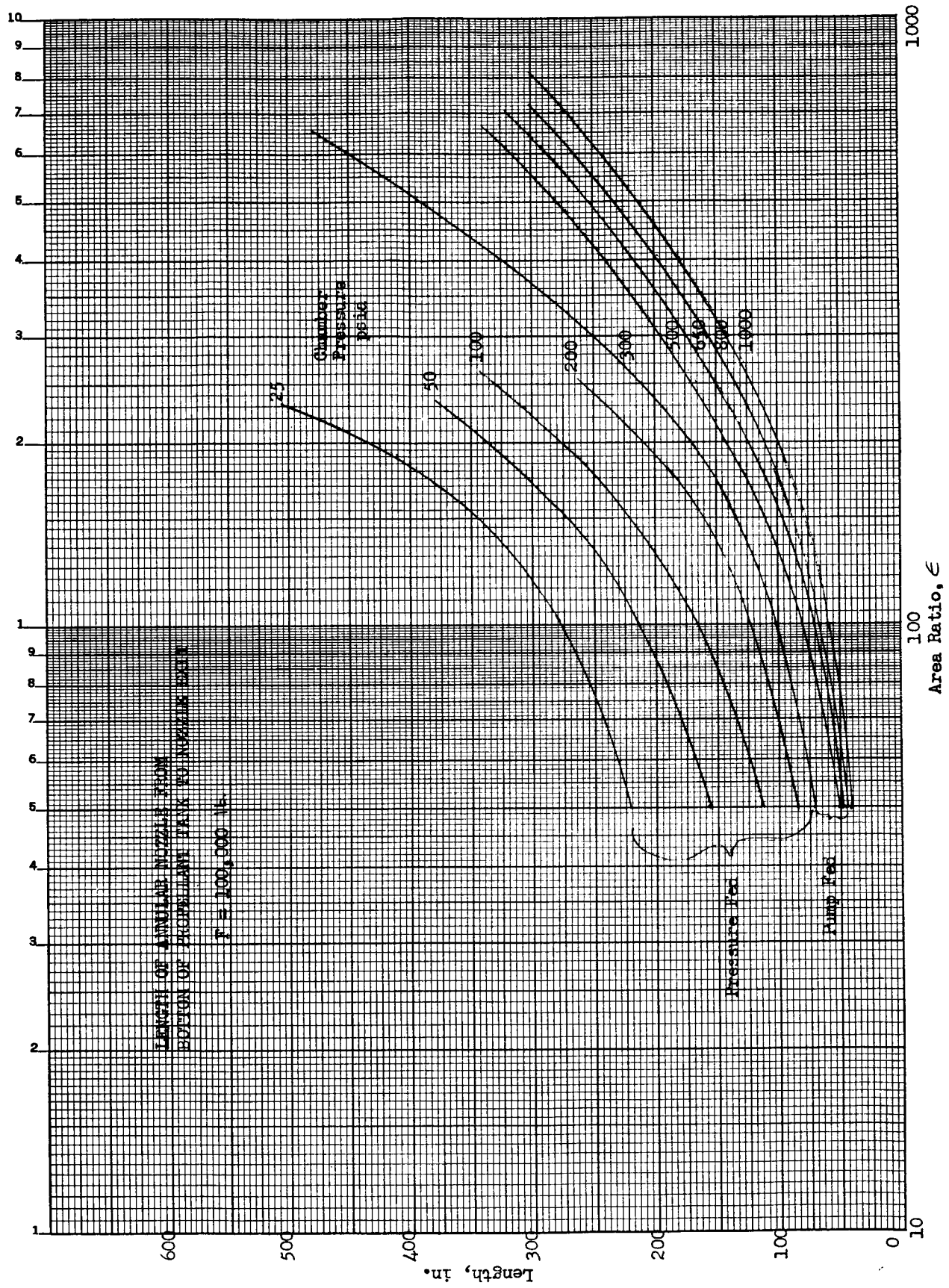


Figure 4

Length of Annular Nozzle from Bottom of Propellant Tank to Nozzle Exit

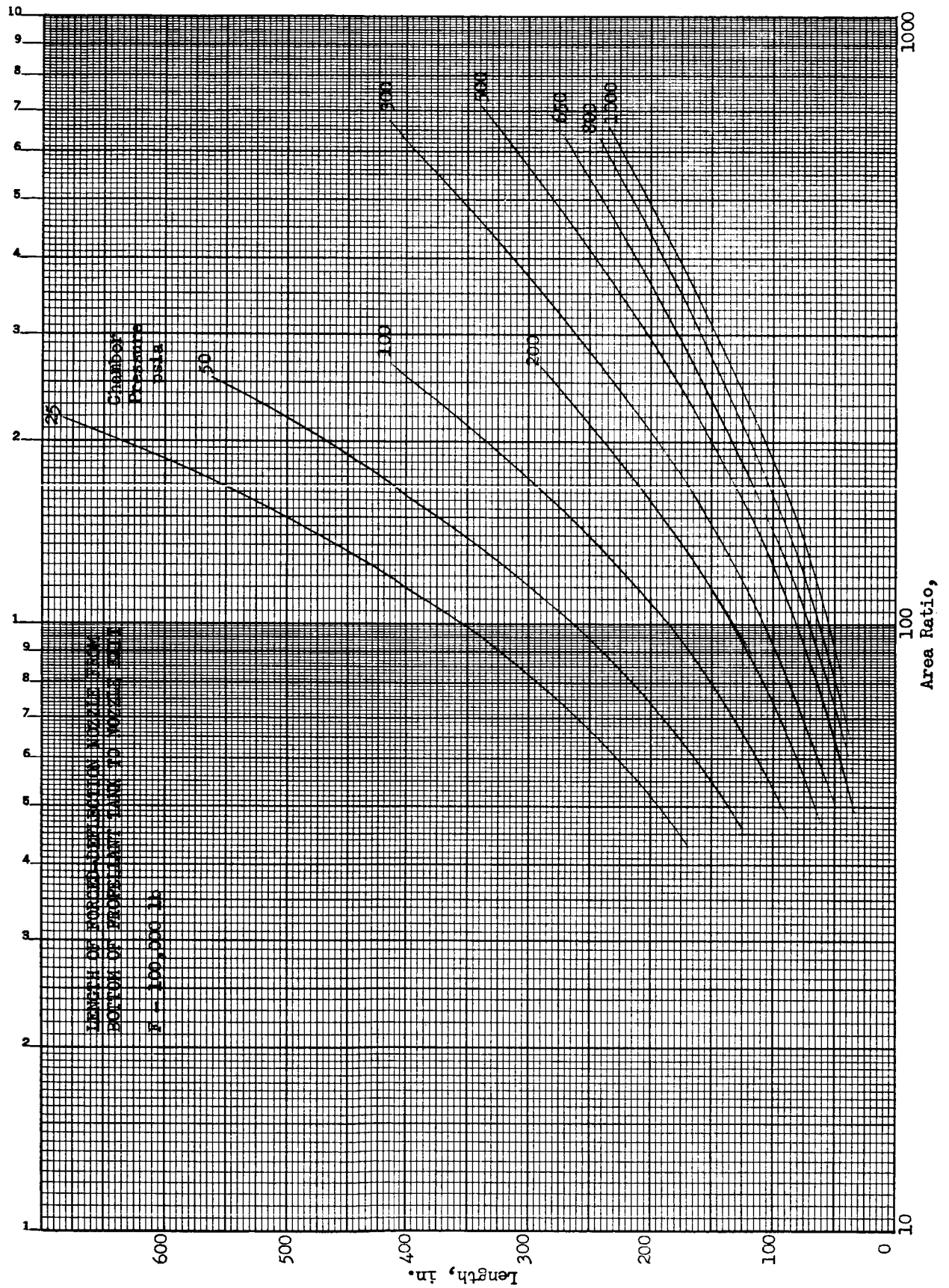


Figure 5

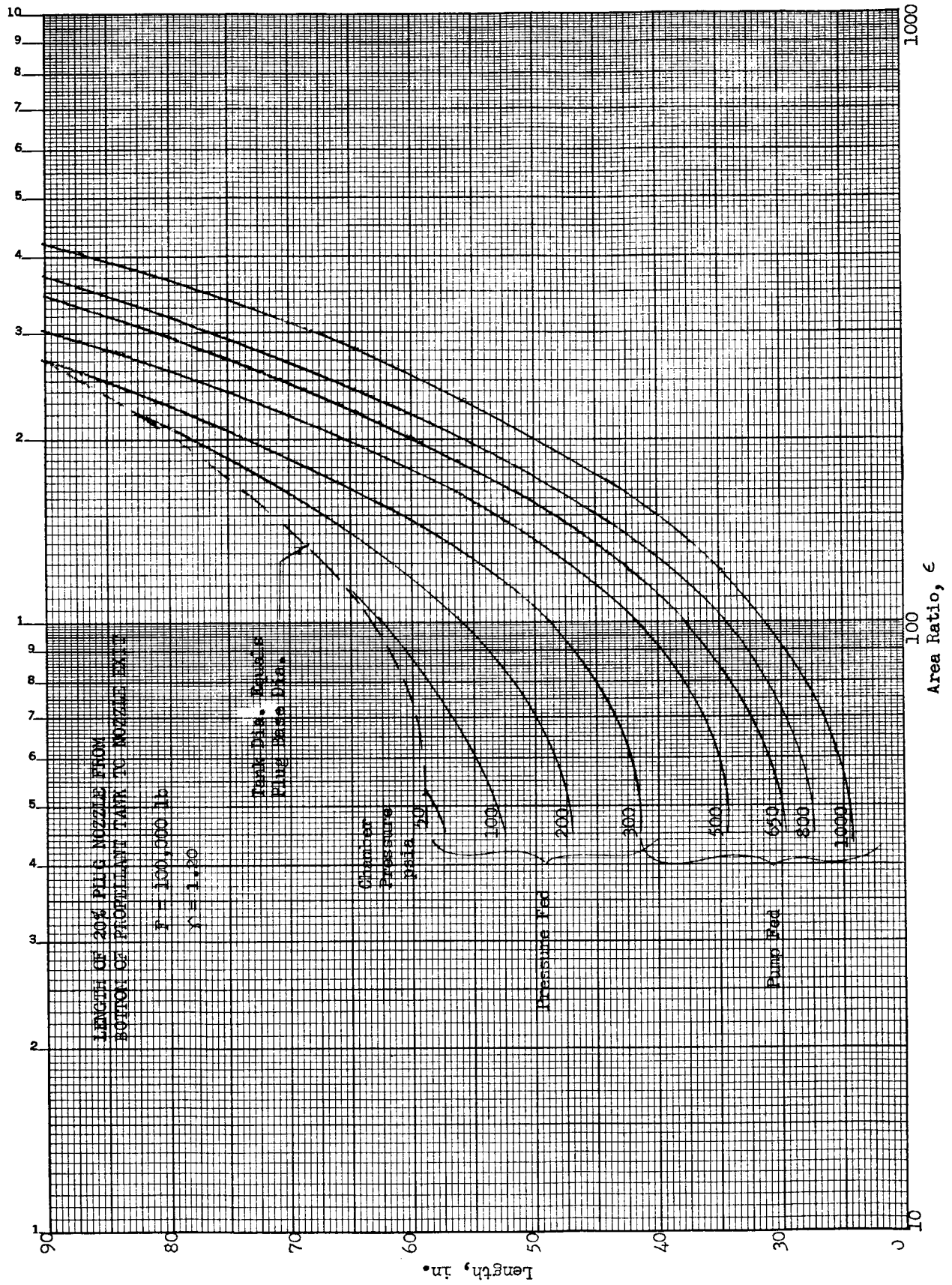


Figure 6

Length of 20% Plug Nozzle from Bottom of Propellant Tank to Nozzle Exit

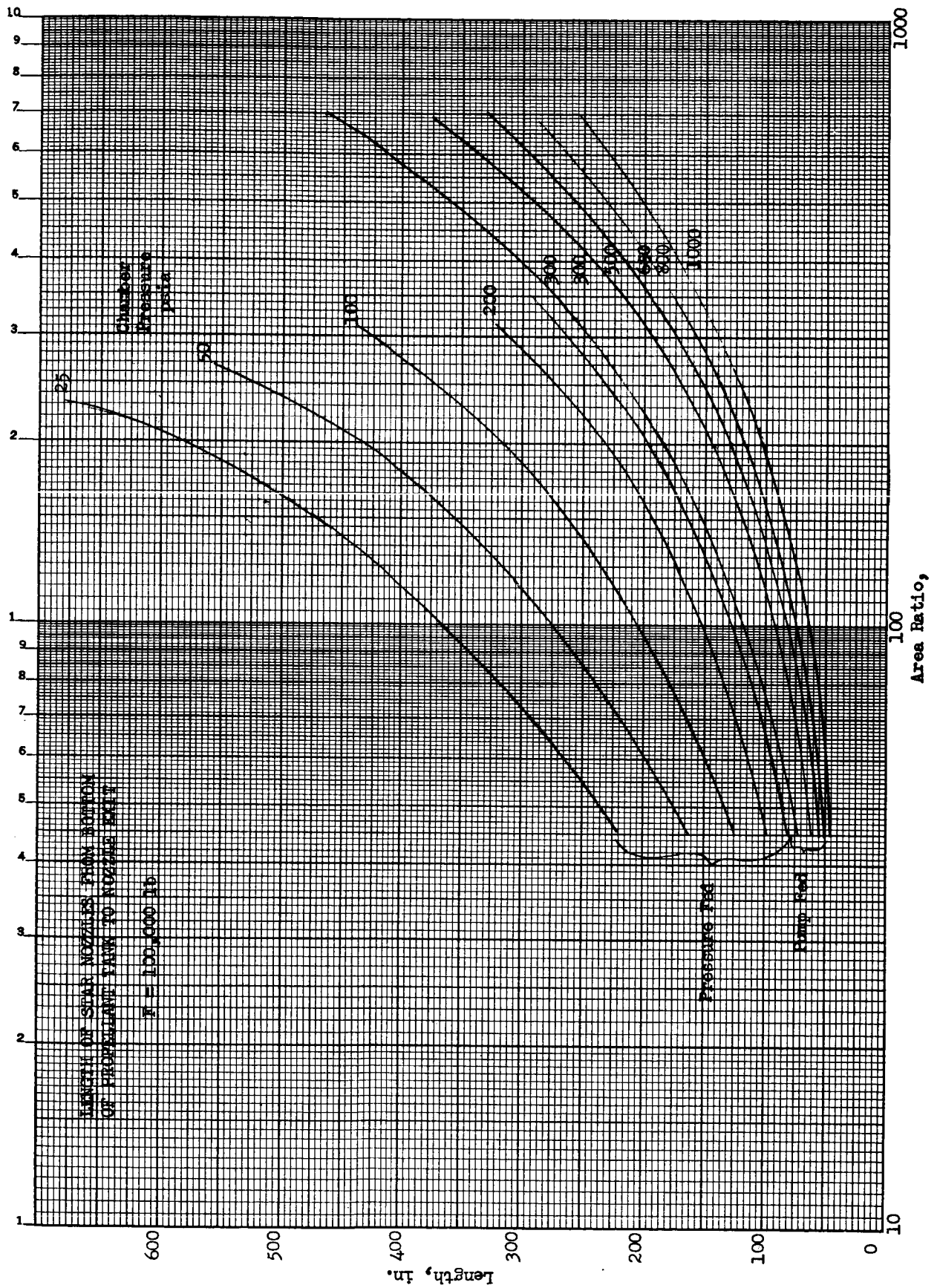


Figure 7

Length of Star Nozzle from Bottom of Propellant Tank to Nozzle Exit

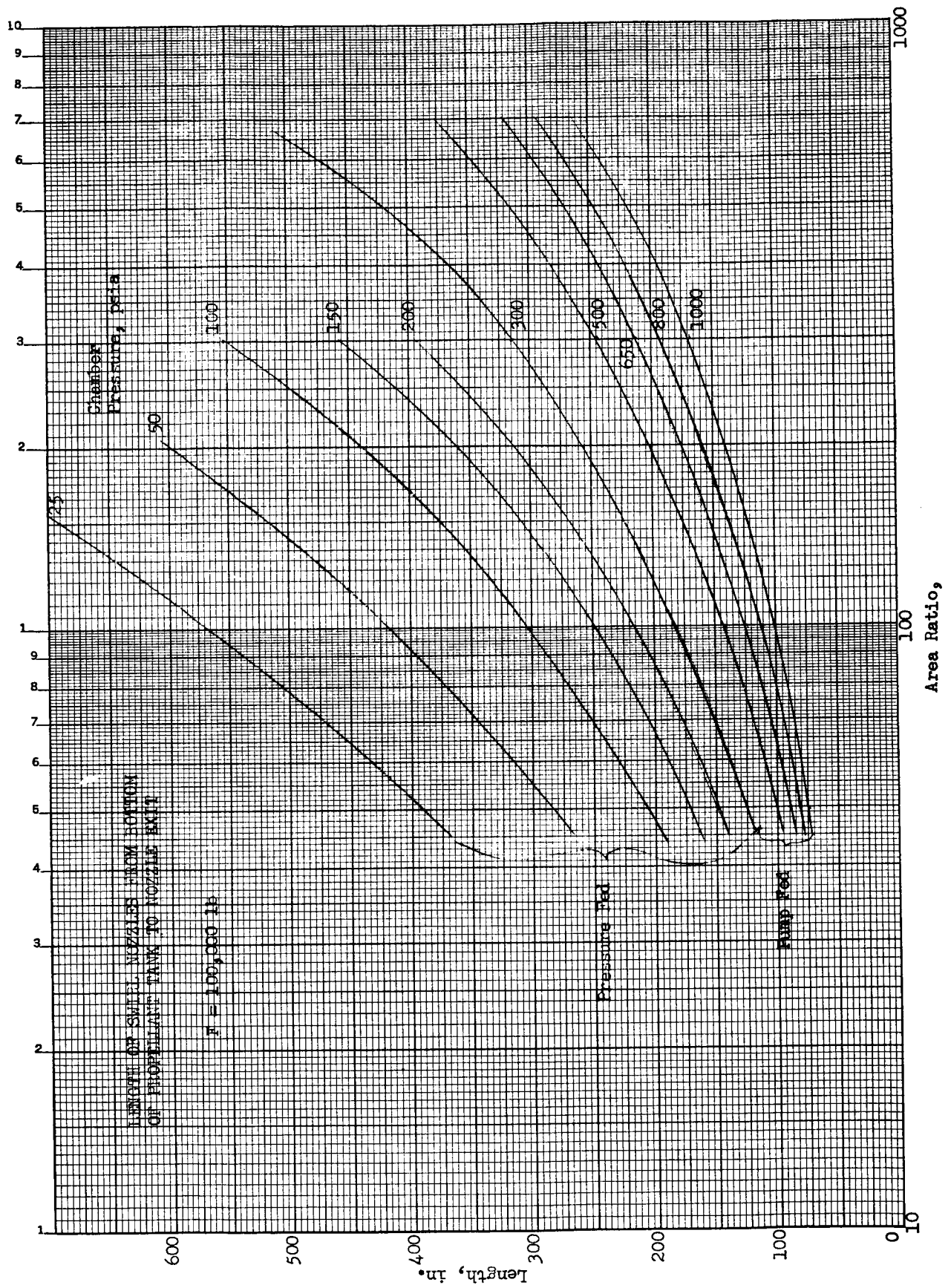


Figure 8

Length of Swirl Nozzles from Bottom of Propellant Tank to Nozzle Exit

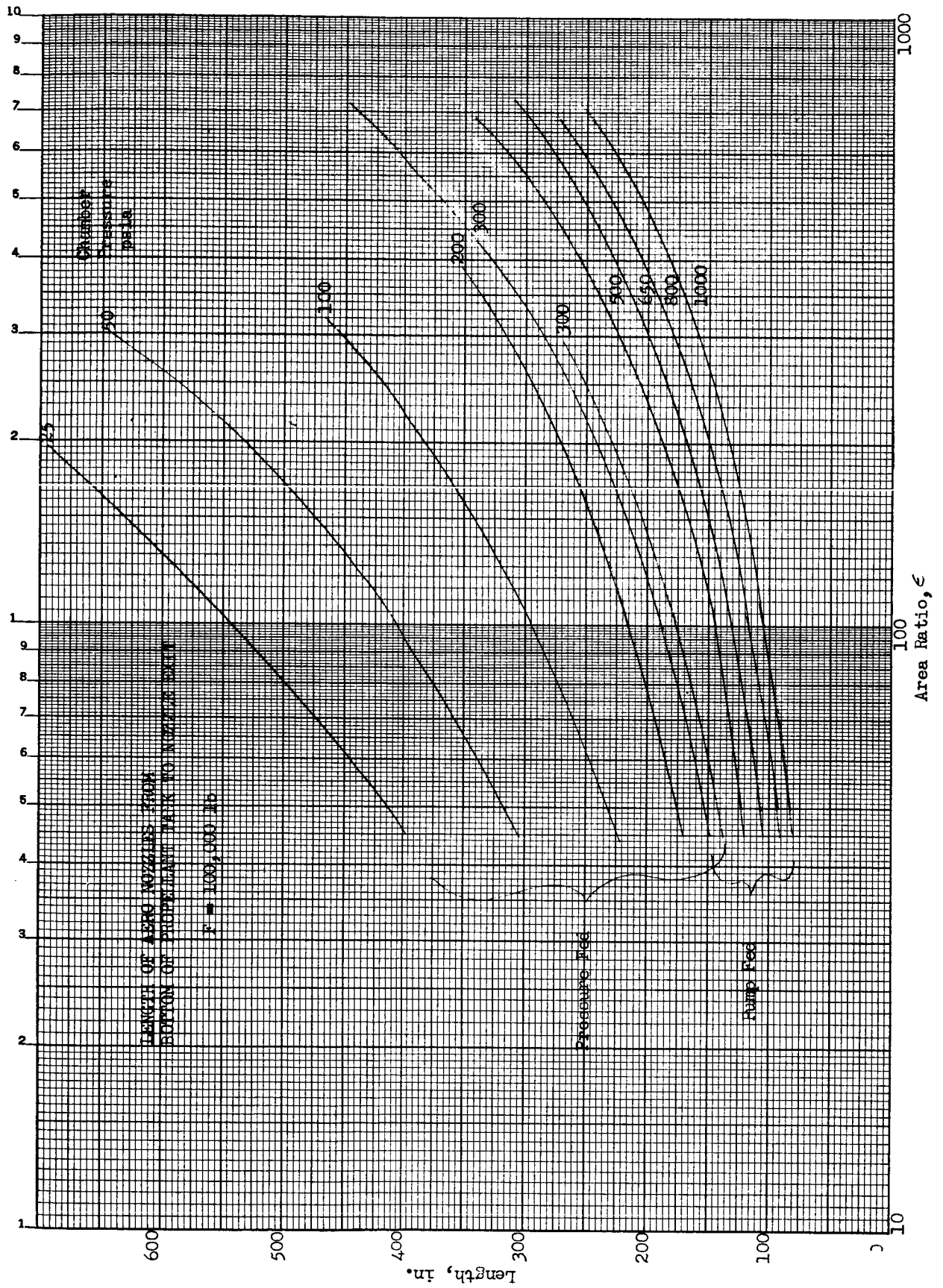


Figure 9

Length of Aerodynamic Nozzle from Bottom of Propellant Tank to Nozzle Exit

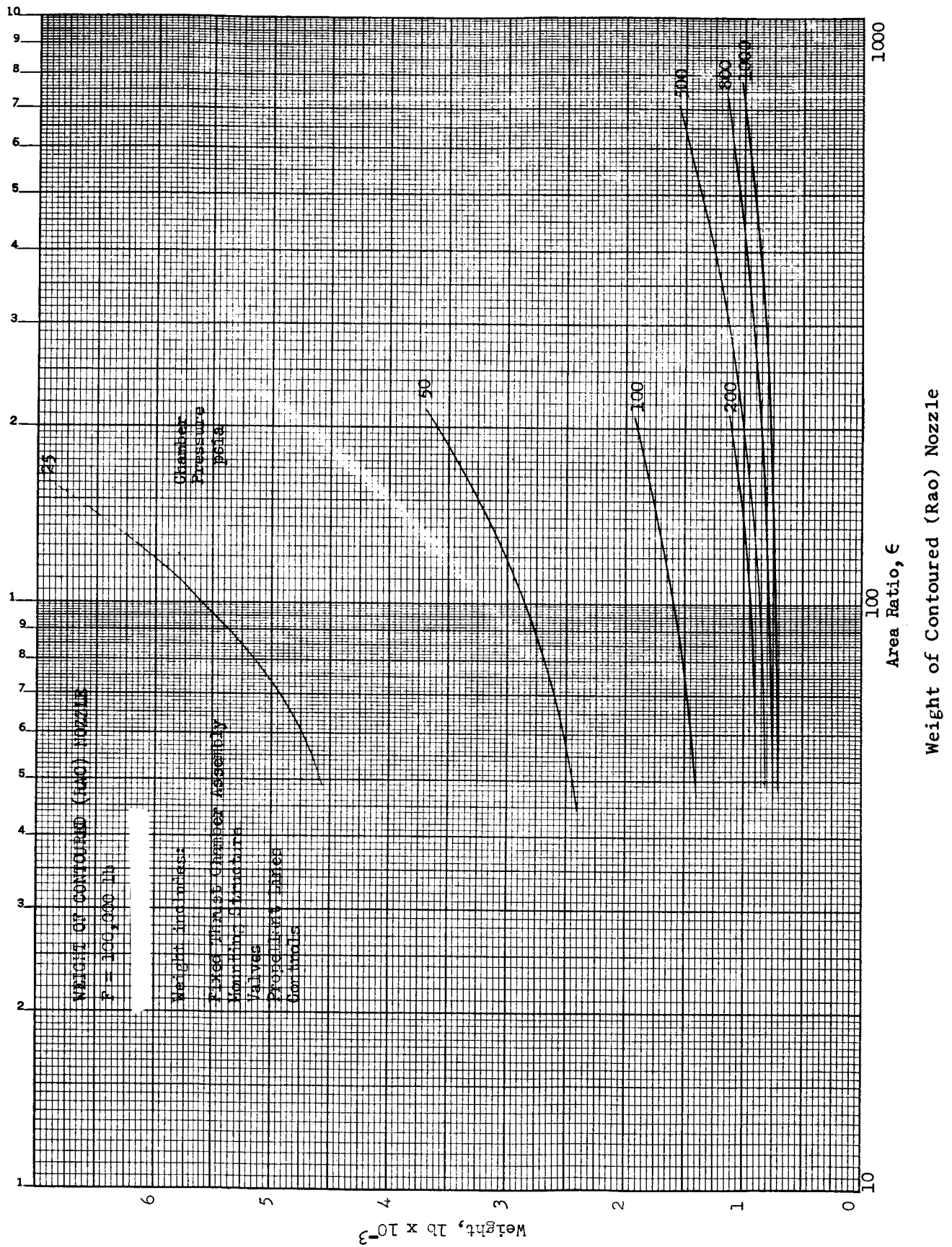


Figure 10

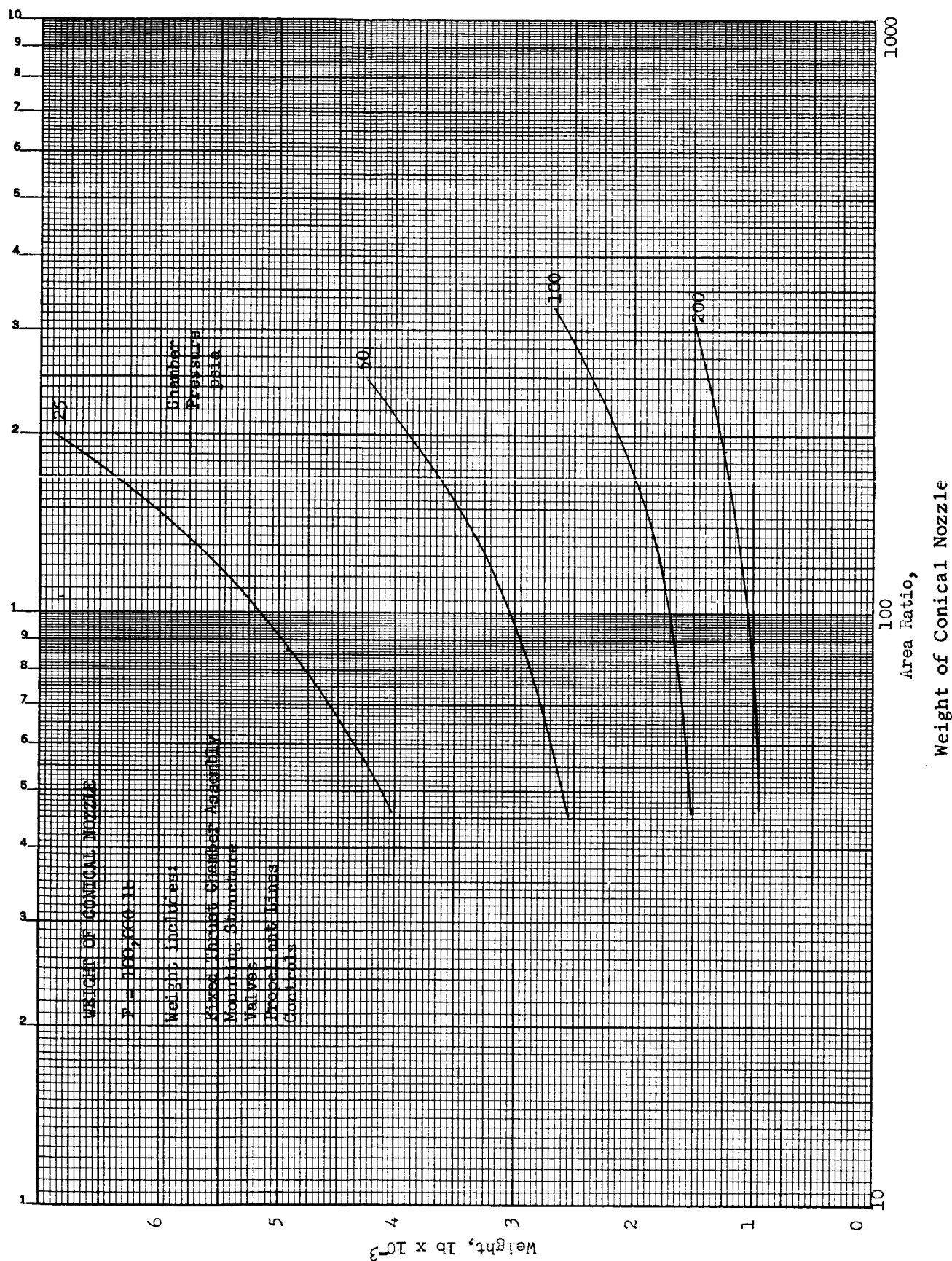


Figure 11

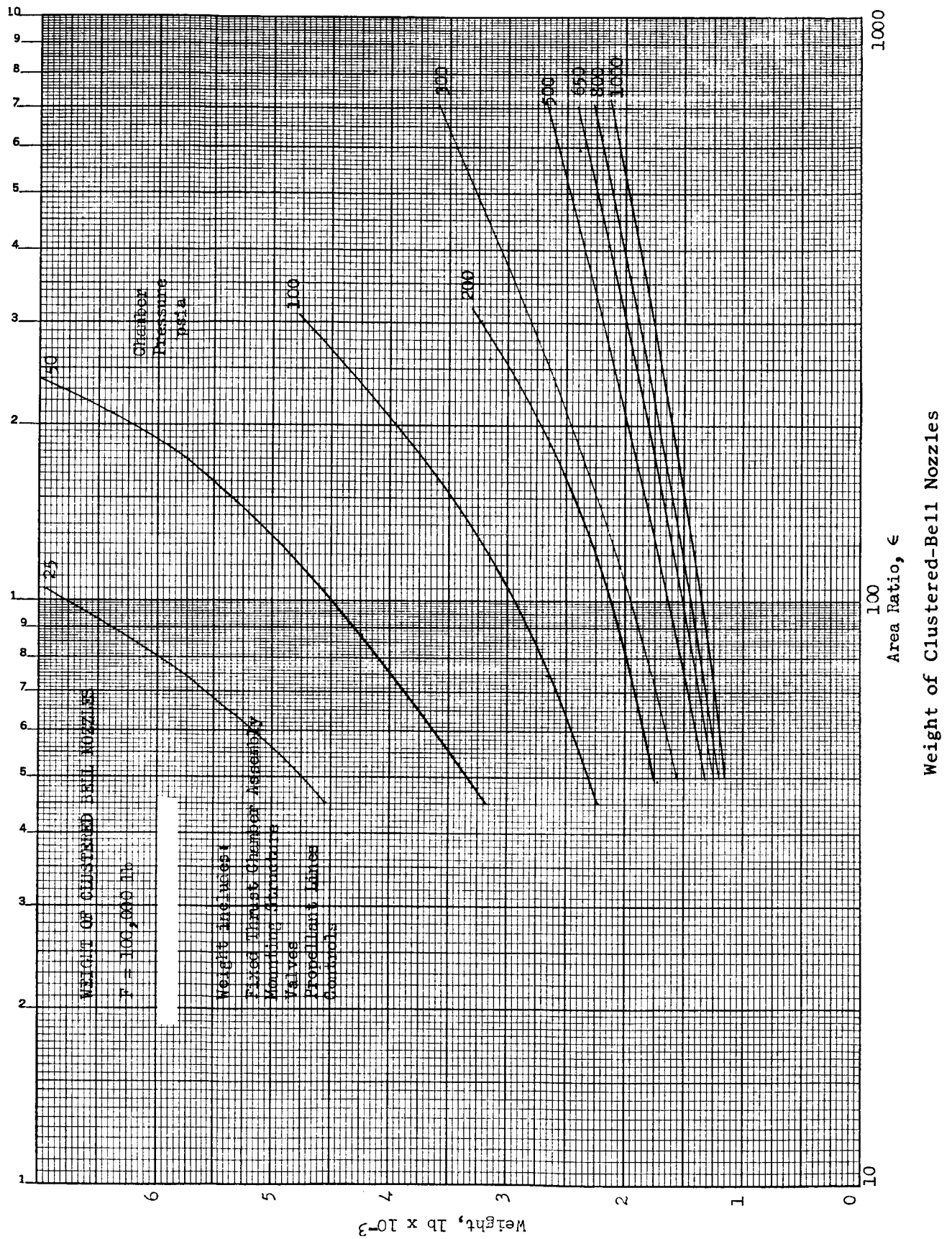


Figure 12

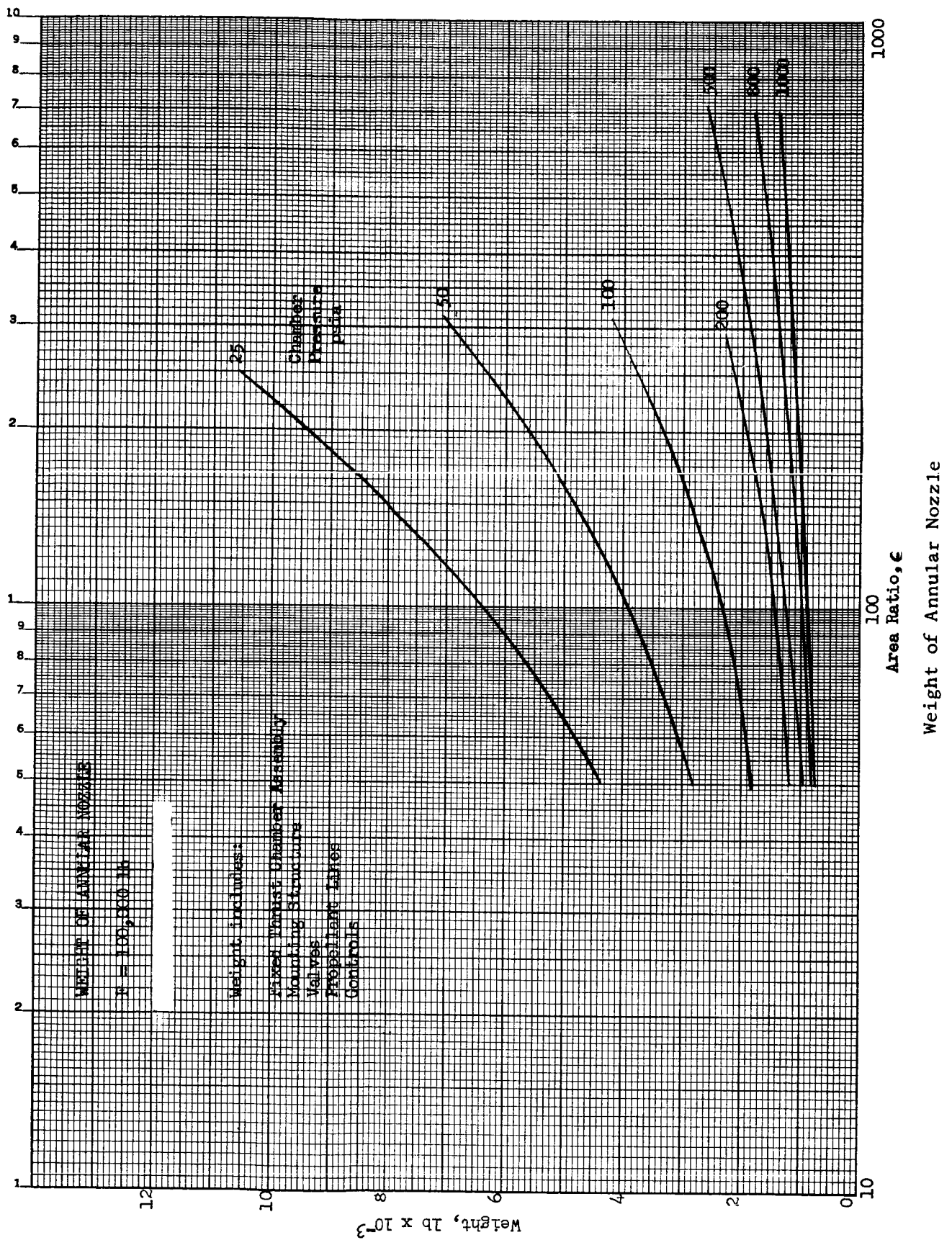


Figure 13

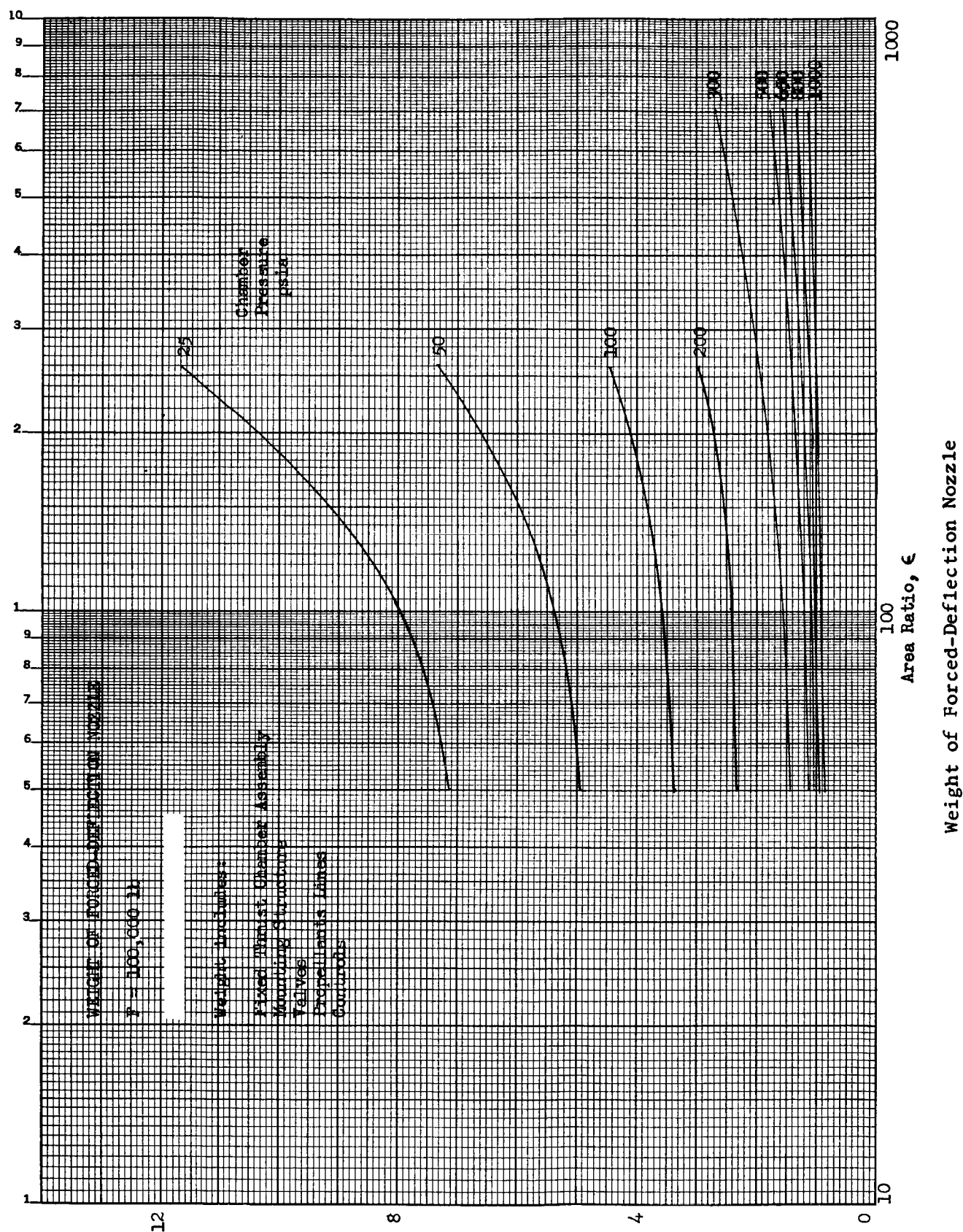


Figure 14

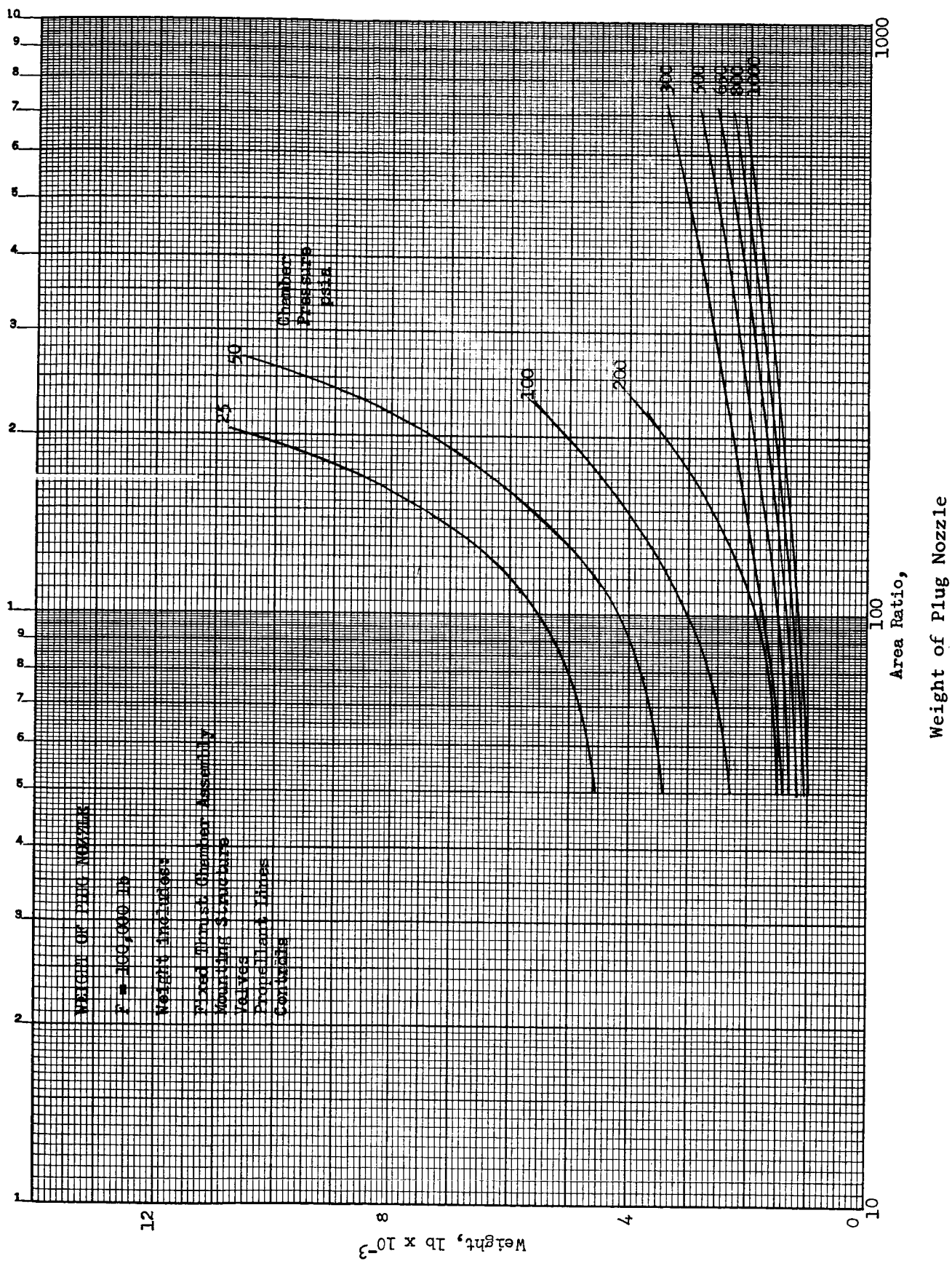


Figure 15

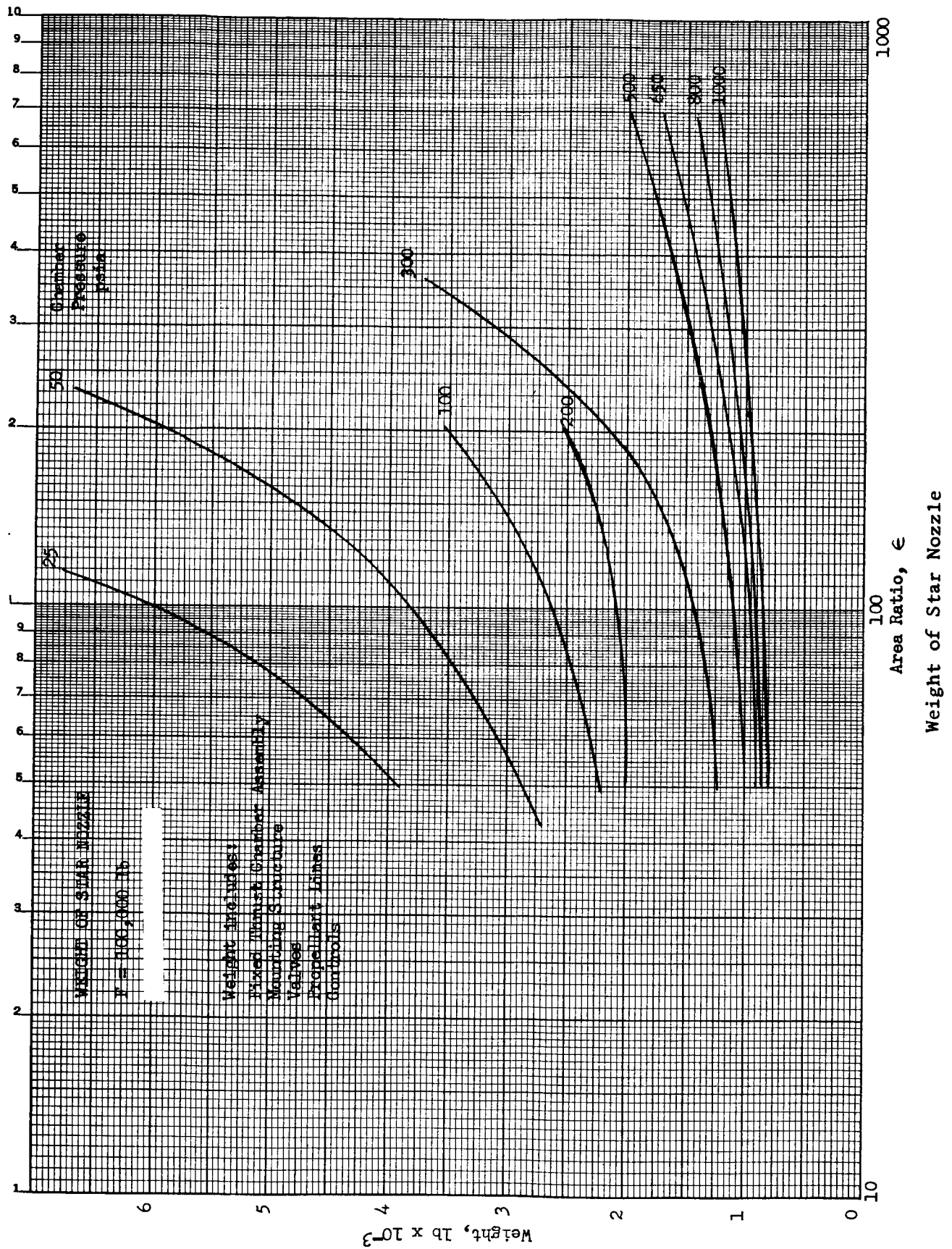


Figure 16

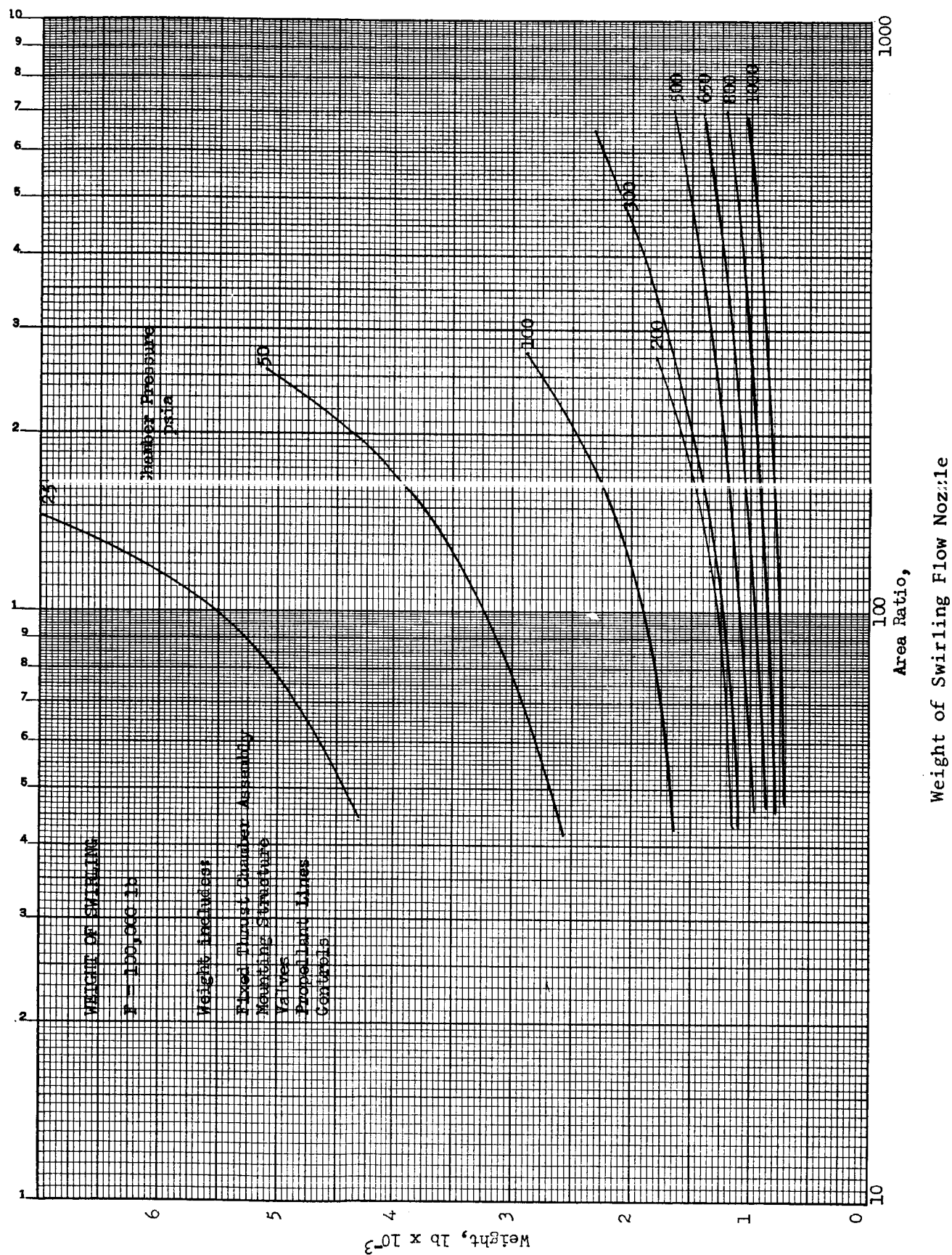


Figure 17

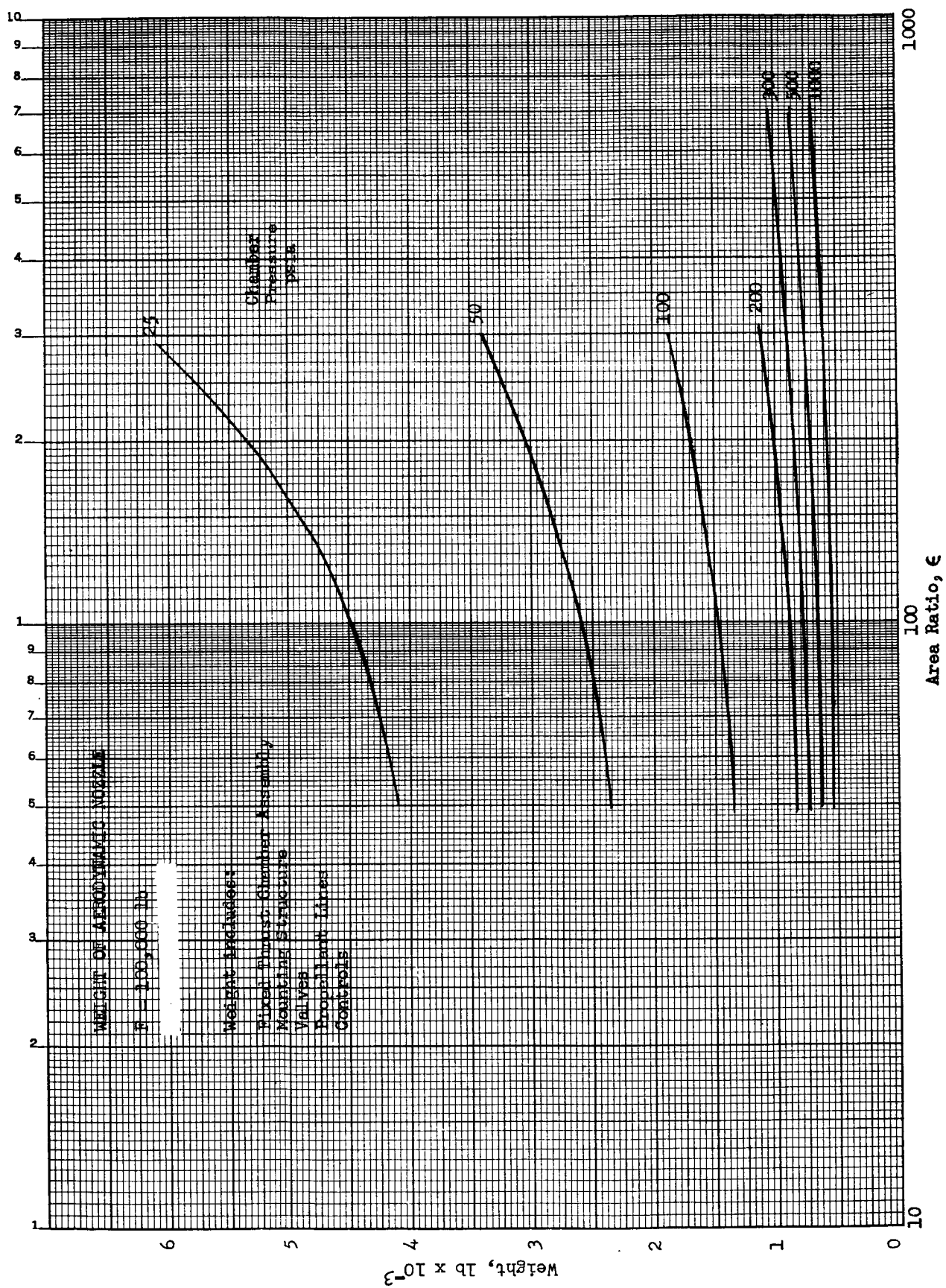


Figure 18

Weight of Aerodynamic Nozzle

APPENDIX H

ANALYSIS OF THE RADIAL PRESSURE AND MACH-NUMBER
DISTRIBUTION IN A SWIRLING-FLOW NOZZLE

This appendix describes the method used to obtain the theoretical curves of static pressure ratio and Mach number in Figures VI-18, VI-19 and VI-22. The velocity of the gas at any point in the nozzle is divided into tangential and axial components; the radial component is neglected. The angle between the axial component and the total velocity is designated ϕ_w , so that:

$$\begin{aligned} V_a &= V \cos \phi_w \\ V_t &= V \sin \phi_w \\ V &= \sqrt{V_t^2 + V_a^2} \end{aligned}$$

The axial component V_a is assumed to be constant across any plane normal to the nozzle axis. The tangential component is expressed:

$$V_t = K/r$$

in a potential vortex, and:

$$V = \omega r$$

in solid body rotation*. Then using the one-dimensional steady isentropic flow relations:

$$\begin{aligned} \frac{P}{P_T} &= \left(1 + \frac{\gamma-1}{2} M^2\right)^{-\frac{\gamma}{\gamma-1}} \\ \frac{T}{T_W} &= \left(\frac{P}{P_W}\right)^{\frac{\gamma-1}{\gamma}} \\ M &= \frac{V}{\sqrt{\gamma g R T}} \end{aligned}$$

* Shapiro, A. H. The Dynamic and Thermodynamics of Compressible Fluid Flow, the the Ronald Press Co., New York, 1953.

an expression for the static pressure ratio and Mach number may be obtained as a function of the radius ratio for a given wall Mach number and flow angle. In a potential vortex, the relations are:

$$\frac{P}{P_W} = \left[1 + \frac{\gamma-1}{2} M_W^2 \sin^2 \phi_W \left\{ 1 - \left(\frac{r_W}{r} \right)^2 \right\} \right]^{\frac{\gamma}{\gamma-1}}$$

$$M = M_W \sqrt{\frac{(r_W/r)^2 \sin^2 \phi_W + \cos^2 \phi_W}{(P/P_W)^{\frac{\gamma-1}{\gamma}}}}$$

The Mach number and flow angle at the wall were obtained from the one-dimensional analysis described in Section II, C, 6. The values used are given in the table below:

Swirl configuration	1	2	
Location	Chamber	Chamber	Exit
Wall Mach No., M_W	0.1007	0.1367	7.48
Wall Flow Angle, ϕ_W , °	84.2	87.3	2.78

Note that P/P_W for a potential vortex may be differentiated and substituted into the Mach number relation to obtain, after rearranging:

$$M^2 = \frac{r'^3 \tan^2 \phi_W}{\gamma p'} \frac{dp'}{dr'}$$

where the primes indicates the value divided by the value at the wall. When the wall angle ϕ_W is close to 90° , this relation simplifies to:

$$M^2 = \frac{r'}{\gamma p'} \frac{dp'}{dr'}$$

which is the equation used by Keyes* to compute the Mach number distribution from the measured pressure distribution.

* Keyes, J. J., Jr., "An Experimental Study of Gas Dynamics in High Velocity Vortex Flow," Proceedings of the 1960 Heat Transfer and Fluid Mechanics Institute, Stanford, Stanford University Press, Stanford, California.

SYMBOL LIST

g	Gravitational constant, 32.2 ft/sec^2
K	Constant
M	Mach Number
P	Pressure, psia
R	Gas constant, $\text{ft lb/lb } ^\circ\text{R}$
T	Static temperature, $^\circ\text{R}$
V	Velocity, ft/sec
γ	Ratio of specific heats
ϕ	Angle, deg
ω	Angular velocity, rad/sec

Subscripts

a	Axial
t	Tangential
T	Total
w	Wall

APPENDIX I

THE METEOROID HAZARD

FIGURE LIST

Figure No.

Most Probable Rate of Puncture

1

The lower and upper velocity limits of meteoroids have been established as 11 and 33 km/sec, respectively. To date, most of the data concerning meteoroids has been gathered by means of photography and radar. A few determinations of the meteoroid flux using earth satellites have also been made. The flux found by the Explorer XVI earth satellite, the latest of these, is given in Reference I-1 and previous estimates based on both ground and satellite observation are given in Reference I-2. Figure I-1, reproduced from Reference I-2, shows several estimates of the most probable number of punctures by meteoroids of aluminum sheet per square feet per day as a function of the sheet thickness. The estimate used in this study is the one based on Whipples' 1961 determination of the flux and Bjork penetration equation. Whipples' 1961 determination, since it is the most recent of the earth-based observations, is hopefully the best. It, when combined with the Bjork penetration equation, gives results which are conservative compared with those derived from Explorer XVI.

The effect on nozzle performance of meteoroids puncturing the unprotected radiation cooled portion of a parabolic nozzle having an exit area ratio of 731:1 was determined for an engine operating at a chamber pressure of 500 psia and a thrust of 100,000 lb. The propellant was taken to be N_2O_4 /Aerozine 50 with a mixture ratio of 2.0. As shown in Figure II-40 of Reference I-3, radiation cooling will not suffice below an area ratio of 15 for an engine using O_2/H_2 at a mixture ratio of 5.0 and a chamber pressure of 500 psia. Since N_2O_4 /Aerozine 50 at a M.R. of 2.0 burns at a higher temperature, considering the radiation cooled portion to be attached at an area ratio of 15, will give an upper bound to its surface area. The skirt will most probably be made from either titanium or stainless steel, about 0.002-in. thick. Because most of the meteoroid puncture data is presented for aluminum, the skirt was considered as being made out of this material. Titanium and stainless steel sheet are at least equivalent to and probably superior to aluminum sheet of the same thickness (Reference I-4).

The penetration data given in Figure I-1 were computed assuming a meteoroid density of 2.7 gm/cm^3 . For the purposes of finding the area of the punctures in the nozzle, the density of the meteoroids was conservatively taken to be 0.5 gm/cm^3 .

(One study of meteoroid density found the average density to be 1.75 gm/cm^3 . Reference I-5). The exposed surface area, A_s , of the nozzle skirt is 1578 ft^2 . From Table 1, Reference I-2, Whipple's 1961 estimate, most of the meteoroids striking the nozzle will weigh less than 10^{-2} gm . The most probable number of penetrations per square foot per day, ψ , by particles larger than 10^{-2} gm , is less than 10^{-7} . The most probable number of penetrations by particles larger than 10^{-2} gm for a 14 day trip, then, is

$$\begin{aligned}\phi &= \psi A_s \tau = 10^{-7} \frac{(\text{penetrations})}{\text{ft}^2 - \text{day}} (1578 \text{ ft}^2)(14 \text{ days}) \\ &= 0.00221\end{aligned}$$

The probability, $p(0)$, of the skirt not being struck by a particle larger than 10^{-2} grams is: (from Reference I-2)

$$\begin{aligned}p(0) &= e^{-\phi} \\ &= e^{-0.00221} = 0.9978\end{aligned}$$

The average mass of the meteoroids striking the vehicle can thus conservatively be taken at 10^{-2} gm .

To compute the thrust losses from meteoroids, the nozzle was divided into transverse sections. The surface area of the section was calculated assuming it to be a cone, and the sum of the absolute values of side thrusts calculated assuming the average of the highest and lowest static pressures in the section, P_{avg} , to be the pressure throughout the section. A thrust coefficient, C_F , of 1.23 was assumed for each puncture. This is the thrust coefficient at the nozzle throat for $\text{N}_2\text{O}_4/\text{Aerzine 50}$ at a M.R. of 2.0, for a wide range of chamber pressures.

Tests made at the Aerojet-General Corporation show that punctures made in radiation cooled skirts are not enlarged during an engine firing. Therefore, the area of each puncture was assumed to be equal to the area of projection of a sphere having a mass of 10^{-2} gm and a density of 0.5 gm/cc; i.e., 0.01378 in.². From Figure I-1, the most probable number of punctures per square foot per day for 0.002-in. thick aluminum is 0.45. This same figure shows that approximately one-tenth of the particles that puncture a single sheet of aluminum would puncture two separated sheets, each sheet being of the same thickness as the single sheet. Therefore, one tenth of the particles puncturing one side of the nozzle was assumed to pass on through the nozzle and puncture the other side also; i.e., the overall puncture rate is 0.495. The sum of the absolute values of the side thrusts in each section is then:

$$\sum |F| = (A_s) (\gamma) (\psi) C_F (A_{\text{puncture}})(P_{\text{avg}})$$

Between $\epsilon = 15.7$ and $\epsilon = 47.4$

$$\begin{aligned}\sum |F| &= (40.8 \text{ ft}^2)(14 \text{ days}) (.495 \frac{\text{punctures}}{\text{ft}^2\text{-day}})(1.23)(.01378 \frac{\text{in}^2}{\text{puncture}}) (2.43 \text{ psia}) \\ &= 11.64 \text{ lb}\end{aligned}$$

Between $\epsilon = 47.4$ and $\epsilon = 106.8$

$$\begin{aligned}\sum |F| &= (87.7 \text{ ft}^2)(14 \text{ days})(.495 \frac{\text{punctures}}{\text{ft}^2\text{-day}})(1.23)(.01278 \frac{\text{in}^2}{\text{puncture}}) (.60 \text{ psia}) \\ &= 6.17 \text{ lb}\end{aligned}$$

Between $\epsilon = 106.8$ and $\epsilon = 271.8$

$$\begin{aligned}\sum |F| &= (303 \text{ ft}^2)(14 \text{ days})(.495 \frac{\text{punctures}}{\text{ft}^2\text{-day}})(1.23)(.01378 \frac{\text{in}^2}{\text{puncture}}) (.215 \text{ psia}) \\ &= 7.63 \text{ lb}\end{aligned}$$

Between $\epsilon = 271.8$ and $\epsilon = 731$

$$\sum |F| = (1146 \text{ ft}^2) \dots = 6.73 \text{ lb}$$

$$\sum |F|_{\text{Total}} = 11.64 \text{ lb} + 6.7 \text{ lb} + 7.63 \text{ lb} + 6.73 \text{ lb} = 32.17 \text{ lb}$$

The probability that the actual number of punctures will be less than double the most probable number can be calculated from the equation

$$P(2\phi) = e^{-\phi} \sum_{n=0}^{2\phi} \frac{\phi^n}{n!}$$

The most probable number of punctures sustained by the nozzle is very large, 10,950. From the tables in Reference I-6, one can see that $p > 0.999$. Therefore, one can safely take $\sum |F|$ total to be less than 64. The net side thrust is undoubtedly much less than 64 lb and is most probably close to zero. An upper bound to the loss in specific impulse caused by the punctures may be found from the relation:

$$I_{sp} = \frac{F}{\dot{w}}$$

Then,

$$1 - \frac{I_{sp}(\text{puncture})}{I_{sp}} < \frac{\sum |F|_{\text{total}}}{|F|_{\text{engine}}} = \frac{64}{100,000} = 0.00064$$

Since the punctures will not all occur at the beginning of the trip, the average loss in specific impulse will depend upon when during the trip the engine is operating, but in any case, the loss should not exceed 0.00064.

To try to protect the nozzle so that there would be a 0.99 probability of no punctures would require that there be less than

$$\psi = \frac{0.01005}{(1578)(14)} = 4.56 (10^{-7}) \text{ penetrations/ft}^2/\text{day}$$

To achieve this, two sheets, spaced several inches apart, having a total thickness of aluminum of 0.2-in. or a single sheet of 0.3-in. thick aluminum would be required (Figure I-1). The weight of this protection in the first case, ignoring the weight of any spacers between the sheets, is 4430 lb, and in the second case is 6650 lb. Since the weight of the entire engine is less than 2000 lb (Reference I-3), the amount of shielding is obviously too high and would make the use of large area ratio nozzles impracticable were it necessary.

However, to protect the nozzle from $\epsilon = 1$ to $\epsilon = 15$ sufficiently so that the probability of receiving no punctures is 0.999 requires that

$$\psi = \frac{.001}{(15.26)(14)} = 4.68 (10^{-6}) = \frac{\text{penetrations}}{\text{ft}^2 \text{ day}}$$

The single sheet thickness required is, from Figure I-1, approximately 0.15-in. The weight of this sheet is 32.1 lb. The weight of the shielding needed to protect the ablatively or regeneratively cooled portions of the nozzle does not appear to be excessive.

As more meteoroid data becomes available, the conclusions presented herein may need revision. If the penetration data from the Explorer XVI satellite were used, the number of punctures received by the nozzle would be reduced by a factor of 10.

REFERENCES

- I-1. Hastings, Carl C., "The Explorer SVI Micrometeoroid Satellite," NASA Tech. Memo., X-810, February 1963.
- I-2. Davidson, J. R., Sandorff, Paul E., "Environmental Problems of Space Flight Structures," II. Meteoroid Hazard, NASA TW-1493, January 1963.
- I-3. "Study of High Effective Area Ratios for Spacecraft Engines," Aerojet-General Corp. Report No. NAS 7-1361F, 14 June 1963.
- I-4. "Rockets in Space Environment," Vol. I, Aerojet-General Corp. Report No. 2484, 4 February 1963.
- I-5. "Rockets in Space Environment," Vol. II, Aerojet-General Corp. Report No. 2484, 4 February 1963.
- I-6. Owen, D. B., Handbook of Statistical Tables, Addison-Wesley Publishing Co., Reading, Massachusetts, 1962.

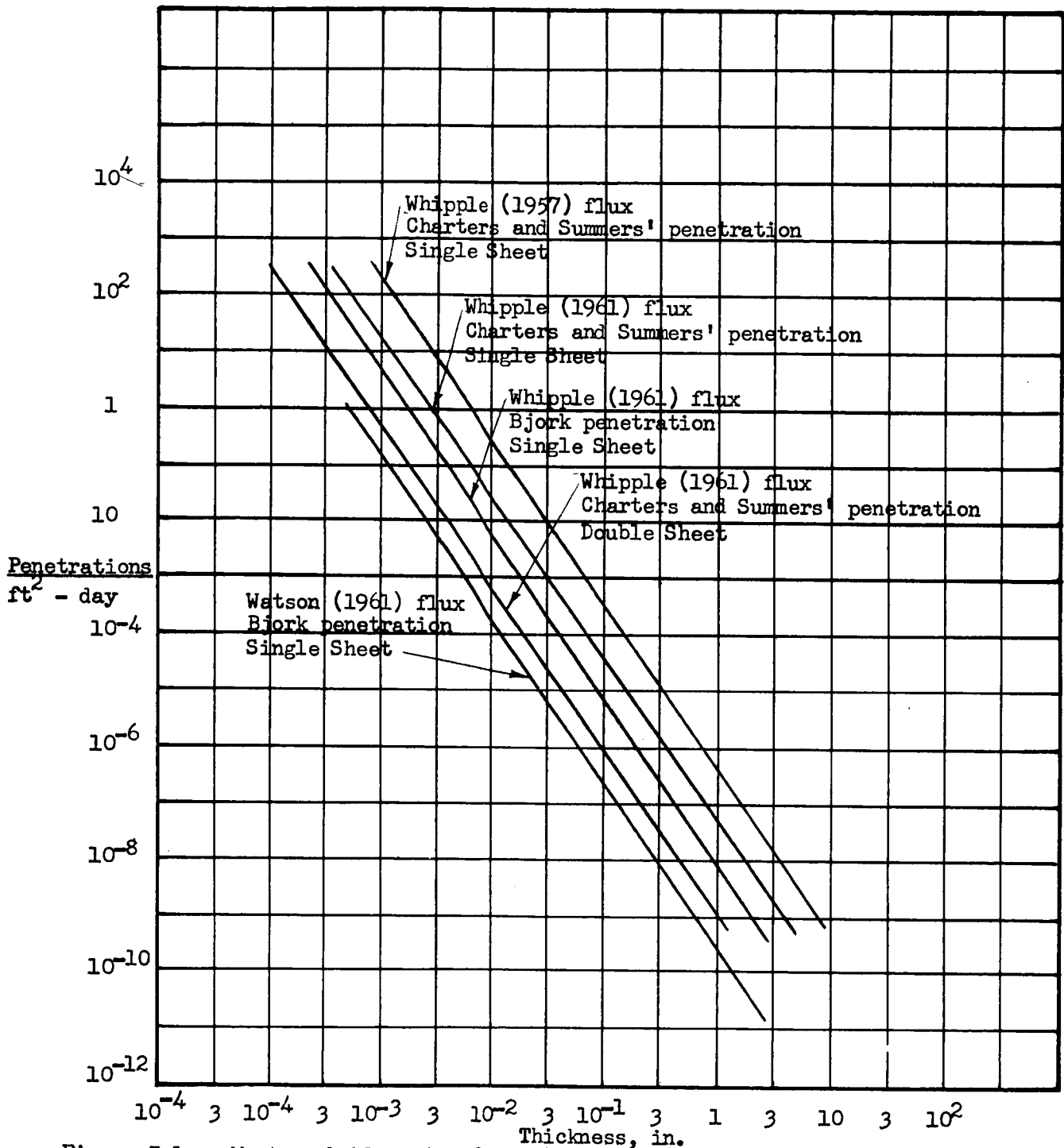


Figure I-1. - Most probable rate of puncture as a function of total aluminum skin thickness as determined by various methods. For the purpose of comparison a meteoroid density of 2.7 g/cm³ was assumed in all cases.

Reproduced from Reference I-2

Most Probable Rate of Puncture

Figure 1

APPENDIX J

EFFECTS OF INCREASED BENDING MOMENT
ON THE BOOST STAGES DUE TO AN INCREASE IN INTERSTAGE WEIGHT
BETWEEN THE BOOSTER AND SPACE VEHICLE

FIGURE LIST

	<u>Figure No.</u>
Moment from 1 "G" Transverse Acceleration	1
Typical Stage Construction	2

I. INTRODUCTION

As the interstage structure is lengthened, the transverse acceleration of the booster vehicle causes an increase of bending moment on the structure proportional to the change in interstage structure length. Consequently, to maintain a constant stress in the structure a larger cross-sectional moment of inertia is required and hence an increase in booster weight.

The three stage booster (Figure 1) was analyzed as a conventional stringer-panel-frame vehicle with 4 "g's" axial and 1 "g" transverse accelerations. Other specifications for the booster vehicle are given below:

<u>Stage</u>	<u>Propellant</u>	<u>Change in Velocity</u> <u>ft per sec</u>	<u>Isp</u>	<u>Mixture</u> <u>Ratio</u>	<u>Initial Mass</u> <u>Fraction</u>
1	O ₂ - RP-1	12000	248	2.2	.942
2	O ₂ - H ₂	9100	353	5.33	.848
3	O ₂ - H ₂	8900	428	5.33	.884

Booster stage configuration is determined from the size requirements of the fuel and oxidizer tanks. The stage diameter of the first and second stages was determined from the diameter of the spherical oxidizer tank. To prevent the third stage diameter from becoming less than the payload diameter, the oxidizer tank was made cylindrical with hemispherical ends and a diameter equal to the payload diameter.

In order to obtain structural weights, initial mass fractions of the boost stages were assumed as shown. Since changes in weights rather than actual values were required from this study, no detailed designs of the vehicles were attempted.

Propellant requirements for the first stage were calculated from,

$$W_p = W_{LO} (1 - e^{-\Delta V / g Isp})$$

$$W_{LO} = \text{Light off weight} = 12,386,500 \text{ lb}$$

I, Introduction (cont.)

ΔV = Velocity increment

$e = 2.71828$

g = acceleration of gravity

Fuel and oxidizer tankage requirements are determined from stage mixture ratio and propellant densities.

From the basic configuration of the stage the forward structure, fuel tank, fuel tank forward heat skirt, stringers, frames, oxidizer tank and oxidizer tank upper and lower headskirts, the change in weights as the bending moment is increased were calculated by methods outlined below. The change in stage weight is the summation of changes in component weights.

The payload of the first stage is then calculated from

$$W_{PL} = W_{LO} \left[1 - \frac{1}{\lambda} (1 - e^{-\Delta V / g I_{sp}}) \right]$$

Where W_{PL} is the weight of all higher stages, or the lightoff weight of the second stage. This procedure is repeated successively for the second and third stages to determine the overall booster effects.

The increase in bending moment on the boost vehicle as the interstage length is increased was calculated by assuming a transverse acceleration of 1 "g". The weight of the vehicle is then summed along its length, and the area under the resulting curve is the bending moment at that location. A change in length of the vehicle results in a change in bending moment which was used to compute the increase in load on the structural components.

The forward structure length for the first and second stages was considered to be 30% of the upper stage oxidizer tank diameter.

I, Introduction (cont.)

Basic material selections for the analysis were 6Al4V Titanium for all fuel components and 7075 Aluminum for the remainder of the vehicles.

Results of this study indicate that the total booster weight increases approximately 81 lb per inch of interstage structure. Of this amount, 31 lb per inch are attributable to the first stage and 27 and 23 lb per inch to the second and third stages, respectively, as shown in Figure IV-53. This is also shown in terms of percent change in weight, and as a change in the mass fraction of the boost stages on the same figure.

II. ANALYSIS

A. FORWARD STRUCTURE

The forward structure is the transition between the booster vehicle stages.

The total change in weight of this structure is analyzed by summing the change in weight of the components as a function of the change in moment from lengthening the interstage structure.

Basic components affecting the weight of the forward structure, stringers, forward frame, center frame, and aft frame, are shown schematically in Figure 2.

1. Stringers

The area of the stringers in the forward structure is given by the equation

$$A_{ST} = \frac{\pi D_{12} [F_c]_{ult}}{\sigma_c} \quad (1.1)$$

II, A, Forward Structure (cont.)

Where $[F_c]$ ult is the ultimate compressive load on the stringers

$$[F_c] \text{ ult} = \frac{1.4}{\cos \phi} \frac{M}{\pi R_1^2} + \frac{P}{\pi D_1} \quad (1.2)$$

And σ_c is the allowable stress for elastic stability.

The weight of the stringers is given by the basic equation

$$W_{ST} = A_{ST} L \rho \quad (1.3)$$

Since by definition for this analysis $L = .3D_1$ the change in weight of the stringers as a function of the change in moment is given by

$$\Delta W_{ST} = \frac{1.68 R_{12} \rho \Delta M}{R_1 \sigma_c \cos \phi} \quad (1.4)$$

2. Forward Frame

The critical compressive load in the forward frame due to "kick load" is

$$F_{CR} = \frac{3EI}{R_c^3} \quad (\text{Ref 5 Page 307}) \quad (1.5)$$

Taking a frame section as shown in Figure 2 the moment of inertia and area may be expressed by

$$I_{FF} = \frac{t h^3}{4} \quad (1.6)$$

$$A_{FF} = \frac{5 h t}{3} \quad (1.7)$$

II, A, Forward Structure (cont.)

By combining equations (1.5) and (1.6) the critical frame thickness is determined to be

$$t_{cR} = \frac{4 F' R_c^3}{3 E h^3} \quad (1.8)$$

where

$$F' = [F_c]_{ult} \frac{R_2 - R_1}{L} \quad (1.9)$$

and $[F_c]_{ult}$ is obtained from Equation (1.2)

The change in critical thickness as a function of change in moment may be expressed by

$$\Delta t_{cR} = \frac{5.6 \Delta M R_c^3}{3 E h^3 \pi R_1^2} \quad (1.9)$$

In addition to the compressive stress in the frame due to kick load, there is a bending moment in the frame caused by unequal shear loads around the frame perimeter which tend to deflect or warp the frame radially. The magnitude of this load is

$$[V_{FF}]_{ult} = \frac{1.4 \text{ WPL x transverse "g's"}}{\text{No. of fittings}} \quad (1.10)$$

The compressive stress in the frame from the kick loads are given by

$$\sigma_c = \frac{Mc}{I_{FF}} + \frac{Pax}{A_{FF}} \quad (1.11)$$

II, A, Forward Structure (cont.)

where

$$M = K_{\text{bend}} R_c [V_{\text{FF}}]_{\text{ult}} \quad (1.12)$$

and

$$P_{\text{ax}} = \frac{[F_c]_{\text{ult}} R_1}{A_{\text{FF}}} + \frac{K_{\text{AX}} [V_{\text{FF}}]_{\text{ult}} R_c}{A_{\text{FF}}} \quad (1.13)$$

The change in frame area as a function of change in moment may be expressed by

$$\Delta A_{\text{FF}} = \frac{1.4 \Delta M}{\pi R_1 \sigma_c} \quad (1.14)$$

and from equation (1.7) it follows that

$$\Delta t = \frac{.84 \Delta M}{R_1 \sigma_c h} \quad (1.15)$$

The total change in frame area is proportional to $(\Delta t_{\text{cr}} + \Delta t)$ and is given by

$$\Delta A_{\text{FF}} = \frac{5h}{3} \left[\frac{5.6 \Delta M R_c^3}{3E h^3 \pi R_1^2} + \frac{.84 \Delta M}{\pi R_1 \sigma_{\text{ch}}} \right] \quad (1.16)$$

By letting $R_1 = R_1 c$

$$\Delta A_{\text{FF}} = \frac{\Delta M}{\pi} \left[\frac{3.11 R_1}{E h^2} + \frac{1.4}{R_1 \sigma_c} \right] \quad (1.17)$$

II, A, Forward Structure (cont.)

Since weight of the forward frame is given by

$$W_{FF} = \pi D_1 \Delta A_{FF} \rho \quad (1.18)$$

the change in weight as a function of change in moment is given by

$$\Delta W_{FF} = \Delta M \rho \left[\frac{6.22 R_1^2}{E h^2} + \frac{2.8}{\sigma_c} \right] \quad (1.19)$$

3. Center Frame

The required cross-sectional area of the center frame to resist instability failure is given by Ref 1 to be

$$A_{cF} = \sqrt{\frac{C_F M D_{12}^2}{K_4 L E}} \quad (1.20)$$

then the change in area as a function of change in moment is

$$\Delta A_{cF} = \frac{\Delta M \pi \rho}{2 \sqrt{\frac{C_F M}{K_4 L E}}} \quad (1.21)$$

where

C_F = dimensionless coefficient = $\frac{1}{16000}$

M = bending moment at frame

K_4 = dimensionless shape parameter = 5.24

L = .115 D_{12} optimum frame spacing

E = modulus of elasticity

II, A, Forward Structure (cont.)

Center frame weight is given by the expression

$$W_{CF} = A_{CF} \pi D_{12} \rho \quad (1.21)$$

from which the change in weight can be derived to be

$$\Delta W_{CF} = \frac{\Delta M \pi \rho}{2 \sqrt{\frac{C_F M}{K_4 L E}}} \quad (1.22)$$

4. Aft Frame

The compressive frame load on the aft frame is

$$[F_c]_{ult} = \left[\frac{M_2}{\pi R_2^2} + \frac{P_2}{\pi D_2} \right] 1.4 \quad (1.23)$$

therefore the change in load is

$$\Delta [F_c]_{ult} = \frac{1.4 \Delta M}{\pi R_2^2} \quad (1.24)$$

In addition to the compressive load it can be seen from Fig 2 that a tensile load also exists on the aft frame. The change in magnitude of this load as a function of change in moment is

$$F_2' = \frac{1.4 \Delta M_2}{\pi R_2^2} \tan \phi \quad (1.25)$$

II, A, Forward Structure (cont.)

The area and weight of the aft frame is expressed by equations (1.26) and (1.27) from which the change of weight is derived in equation (1.28).

$$A_{AF} = \frac{[F_c] \text{ ult } \tan \phi R_2}{\sigma_c} \quad (1.26)$$

$$W_{AF} = \pi D_{12} A_{AF} \rho \quad (1.27)$$

$$\Delta W_{AF} = \frac{2.8 \Delta M_2 \tan \phi}{\sigma_c} \quad (1.28)$$

5. Total Structure

The total change in weight of the forward structure is given by summing the delta weight of the individual components, so that

$$\Delta W_{FS} = \Delta W_{ST} + \Delta W_{FF} + \Delta W_{CF} + \Delta W_{AF}$$

B. STAGE WEIGHT

The stage change in weight as a function of change in bending moment from lengthening the interstage structure can also be calculated from summing the weight change of the structural components.

The schematic diagram shown in Figure 2 shows the components, forward head skirt fuel tank, fuel tank stringers and frames and oxidizer tank upper and lower head skirts, whose weights are affected by this change in moment.

II, B, Stage Weight (cont.)

1. Forward Head Skirt Fuel Tank

Load on the structure is given by equations (2.1)

$$[F]_{ult} = \left[\frac{M}{\pi R_2^2} + \frac{P}{\pi D_2} \right] 1.4 \quad (2.1)$$

and

$$t = \frac{R_2^{.612} [F]_{ult}^{.388}}{2.24 E^{.388}} \quad (2.2)$$

The thickness equation (2.2) was developed from NACA TN 3783 Figure 7 and is valid within the range

$$60 < \frac{R}{T} < 3000$$

Combining equations (2.1) and (2.2) the change in weight of the forward head skirt can be expressed as a function of the change in moment in equation (2.3)

$$\Delta W_{FHS} = \frac{.242 \Delta M A_{FHS} \rho}{E^{.388} \pi R_2^{1.388} [F]_{ult}^{.612}} \quad (2.3)$$

2. Fuel Tank Stringers

The compressive load on the stringers is given by equation (2.4)

$$F_c = \left[\frac{M}{\pi R^2} + \frac{P}{\pi D} \right] \quad (2.4)$$

II, B, Stage Weight (cont.)

where

$$F_c \text{ ult} = 1.4 F_c \quad (2.5)$$

If the stringers carry 100% of load then

$$A'_{ST} = \frac{\pi D_2 [F_c] \text{ ult}}{\sigma_c} \quad (2.6)$$

The fuel tank skin, however, carries some load and an estimate is made for stringer area

$$A_{ST \text{ est}} = K A'_{ST} \quad (2.7)$$

and the equivalent skin thickness for the stringers

$$t'_{st} = \frac{A_{ST \text{ est}}}{\pi D} \quad (2.8)$$

The gross tensile stress

$$\left(\frac{P}{A}\right)_{\text{gross}} = \frac{\text{PRESS} \times R_2}{2(t'_{st} + t_{\text{skin}})} \quad (2.9)$$

where t_{skin} is the tank cylinder wall thickness.

For combined stringer-skin-frame type structure, the stringer tensile load, therefore, is

$$F_{t \text{ st}} = t'_{st} \left(\frac{P}{A}\right)_{\text{gross}} \times .4 \quad (2.10)$$

II, B, Stage Weight (cont.)

and compressive load in the skin is

$$\frac{.3Et^2 \text{ skin}}{R_2} \quad (2.11)$$

The net compressive load in the stringer is determined from

$$[\text{NET } F_c]_{\text{ult}} = [F_c - F_{c \text{ skin}} - F_{t \text{ st}}] \quad 1.4 \quad (2.12)$$

It can be determined from Equation (2.7) that

$$\Delta A_{\text{ST est}} = \frac{2.8 K \Delta M}{\sigma_c R} \quad (2.13)$$

and Equation (2.12) that

$$\Delta [\text{NET } F_c]_{\text{ult}} = 1.4 \Delta M \frac{1}{\pi R^2} + \frac{.56 K \pi D t_{\text{tank}} \text{ Press}}{\sigma_c (A_{\text{ST est}} + \pi D t_{\text{tank}})^2} \quad (2.14)$$

The change in stringer area is therefore

$$\Delta A_{\text{ST}} = \frac{\pi D}{\sigma_c} 1.4 \Delta M \frac{1}{\pi R^2} + \frac{.56 \pi D K t_{\text{tank}} \text{ Press}}{\sigma_c (A_{\text{ST est}} + \pi D t_{\text{tank}})^2} \quad (2.15)$$

Equation 2.15 and 2.13 are iterated until the values are equal. The change in weight is then given by the expression

$$\Delta W_{\text{ST}} = \frac{1.4 L \pi D \Delta M}{\sigma_c} \frac{1}{\pi R^2} + \frac{.56 K \pi D t_{\text{tank}} \text{ press}}{\sigma_c (A_{\text{ST est}} + D t_{\text{tank}})^2} \quad (2.16)$$

II, B, Stage Weight (cont.)

3. Fuel Tank Frames

The compressive load on the frames is determined from

$$F_c = \frac{M}{\pi R^2} + \frac{P}{\pi D} \quad (2.17)$$

and the tensile load from tank internal pressure is

$$F_t = \frac{\text{PRESS } R_2}{2} \quad (2.18)$$

The net ultimate loading is then

$$[\text{NET } F_c]_{\text{ult}} = 1.4 [F_c - F_t] \quad (2.19)$$

and the equivalent bending moment M' is

$$M' = \pi R^2 [\text{NET } F_c]_{\text{ult}} \quad (2.20)$$

By substituting M' for M in Equation (1.25) the change in frame area can be determined. The change in weight of the frames is then given by

$$\Delta W_F = \Delta A_F \pi D N_F \rho \quad (2.21)$$

where

$$N_F = \frac{L_{\text{cyl}}}{.115D} + 1 \quad (2.22)$$

4. Oxidizer Tank Forward Head Skirt

The compressive load on the oxidizer tank forward head skirt is

$$F_c = \frac{M}{\pi R^2} + \frac{P}{\pi D} \quad (2.23)$$

II, B, Stage Weight (cont.)

and the tensile load from tank internal pressure determined from equation (2.18). By combining equations (2.23) and (2.18) net ultimate compressive load is determined to be

$$[NET F_c]_{ult} = 1.4 [F_c - F_t]$$

By substituting the appropriate values in Equation (2.3) the change in weight of the oxidizer tank forward head skirt can be determined.

5. Oxidizer Tank Aft Head Skirt

The change in weight of the aft head skirt is solved the same as 4 above except that the tensile load from tank internal pressure is equal to zero.

LIST OF SYMBOLS

A	area in. ²
C	distance from neutral axis to extreme edge of beam
D	diameter, inches
E	modulus of elasticity, lb/in. ²
F	load, lb/in.
F'	kick load
K	estimated % load supported by stringers
L	length inches
M	bending moment, in-lb
P	axial load lb x axial acceleration "g"s
PRESS	pressure, lb/in. ²
R	radius, inches
R _c	radius at c.g.
V	shear load, lb
W	weight, lb
WPL	weight of payload, lb
a	frame spacing, inches
b	stringer spacing, inches
h	length at base of U section - see Figure 2
t _{cr}	critical thickness, inches
t	thickness, inches
t'st	equivalent skin thickness of stringer
Δ	incremental change
ρ	density of material, lb/in. ³
σ	allowable material stress, lb/in. ²
φ	angle of forward structure

LIST OF SYMBOLS (cont.)

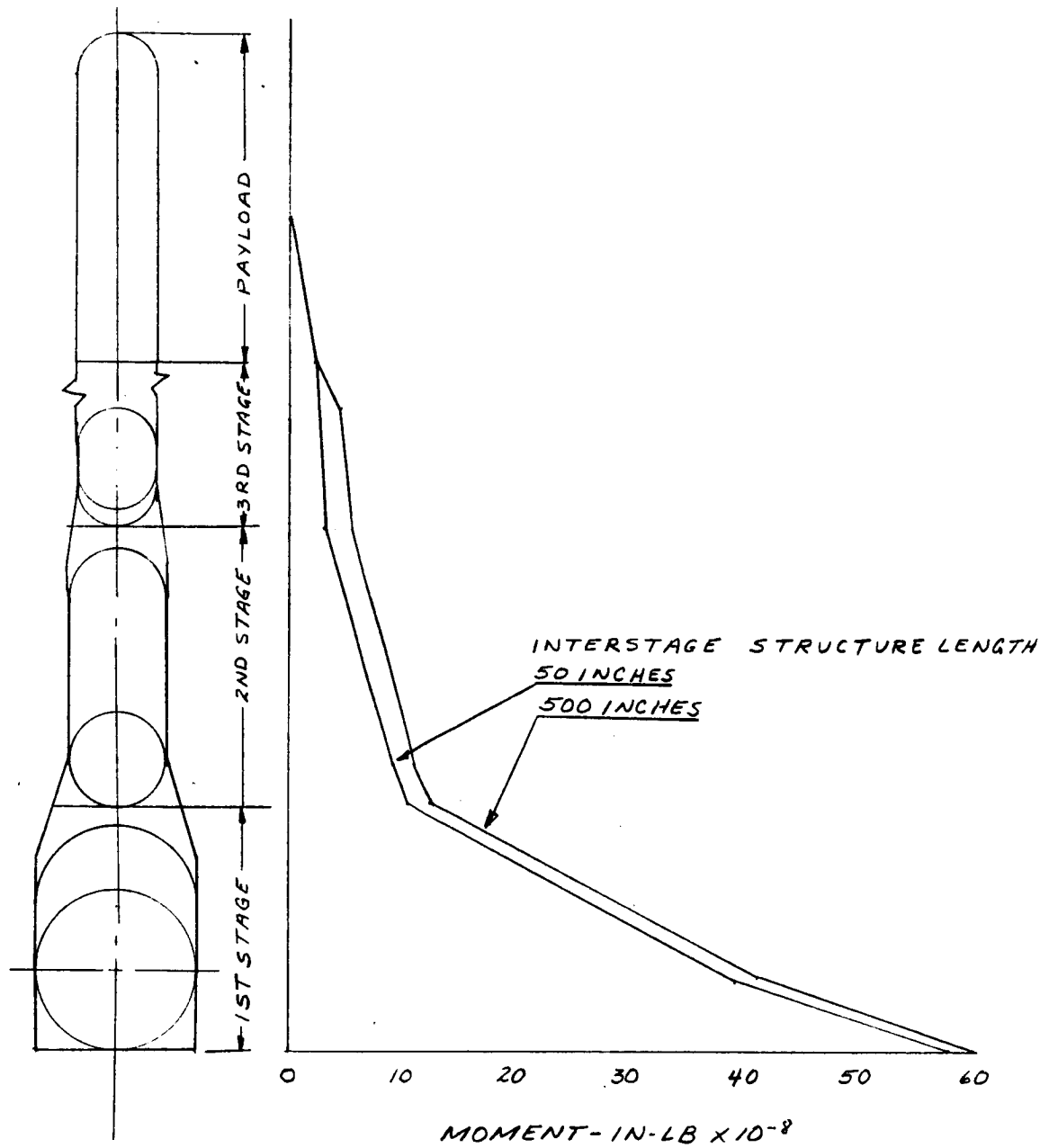
Subscripts:

AF	aft frame
c	compression
cr	critical
CR	center frame
F	frame
FF	forward frame
FHS	fuel tank head skirt
mat'l	material
prop	propellant
s	shear
ST	stringers
t	tension
ult	ultimate
1	upper
2	lower
12	average

REFERENCES

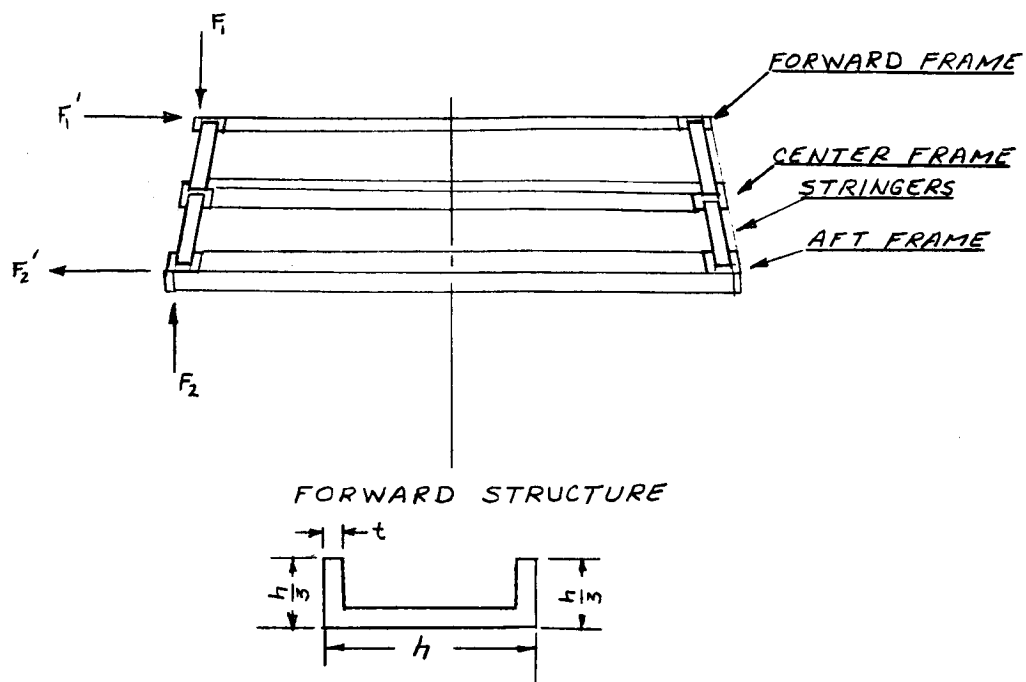
1. F. R. Shanley, Weight-Strength Analysis of Aircraft Structures, New York, McGraw, 1952
2. David J. Perry, Aircraft Structures, New York, McGraw, 1950
3. E. L. Bruhn and A. F. Schmitt, Analysis and Design of Airplane Structures, Vol. I, Analysis for Stress and Strain, Cincinnati Tristate Offset Co., 1958
4. George Gerard and Herbert Becker, "Handbook of Structural Stability, Part 3, Buckling of Curved Plates and Shells," NACA TN 3783, August 1957
5. Raymond J. Roark, Formulas for Stress and Strain, New York, McGraw, 1954

MOMENT FROM 1 "G" TRANSVERSE
ACCELERATION VS BOOSTER LENGTH

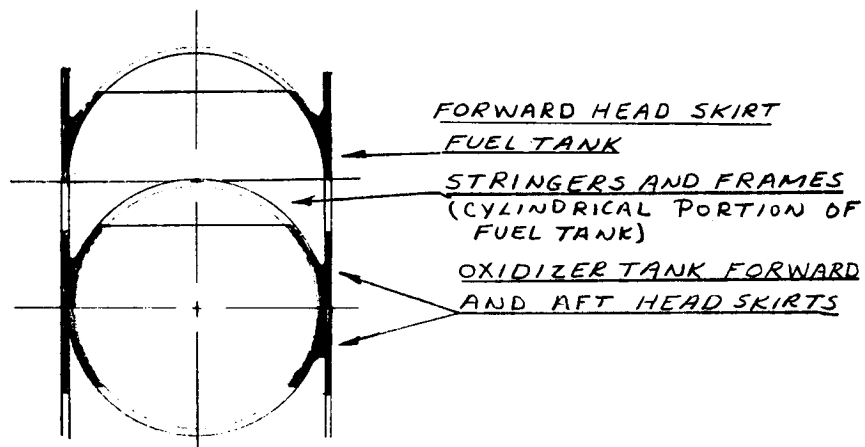


Moment from 1 "G" Transverse Acceleration

Figure 1



FORWARD STRUCTURE CROSS-SECTION OF FRAME



TYPICAL STAGE CONSTRUCTION

Typical Stage Construction

Figure 2

Report NAS 7-136-F

APPENDIX K

STRUCTURAL DYNAMIC ANALYSIS
OF NOZZLE EXTENSIONS

FIGURE LIST

	<u>FIGURE</u>
Vibrating Coupled System Nomenclature	1

I. ASSUMPTIONS

In the present analysis, the following assumptions are made:

- (1) The overall engine motions (due to $\theta(t)$) have no effect on the buckling motions of the nozzle extensions.
- (2) The power spectral density, $q(\omega)$, is a step function in a given spectral range.
- (3) The generalized mass, M_N , is approximately equal to the mass, m_N , of the undeformed nozzle.

II. FORMULATION OF EQUATIONS OF MOTION

The equations of motion for forced vibrations of a fixed-free thin conical shell nozzle attached to a rigid nozzle free to move in a given rotational direction, $\theta(t)$, are derived herein.

Consider the vibrating coupled system shown in Figure 1, where the various displacements, distances, forces, and masses of the flexible nozzles and engine are defined. Let the displacements, $u(x, \phi, t)$, $v(x, \phi, t)$, and $w(x, \phi, t)$ be expressed as

$$\left. \begin{aligned} u(x, \phi, t) &= u_s(x, \phi) \xi_s(t) \\ v(x, \phi, t) &= v_s(x, \phi) \xi_s(t) \\ w(x, \phi, t) &= w_s(x, \phi) \xi_s(t) + x' \theta(t) \end{aligned} \right\} [\text{in.}] \quad (1)$$

$s = 1, 2, 3, \dots$

where

u_s, v_s and w_s = modal shapes of nozzle
 $\xi_s(t)$ = normalized coordinate, [in.]
 $x' = c + x$, (Figure 1), [in.]
 s = mode number
 θ = coupled system rotational angle
 x, ϕ = nozzle coordinates
 t = time, [sec.]

II, Formulation of Equations of Motion (cont.)

The kinetic energy may be written as

$$T = \frac{1}{2} \int_{M_\theta} (\dot{u}^2 + \dot{v}^2 + \dot{w}^2) dM_\theta = \frac{1}{2} M_N \dot{z}_s^2 + S_\theta \dot{z} \dot{\theta} + \frac{1}{2} I_\theta \dot{\theta}^2 \quad [\text{lb}_f \cdot \text{in.}] \quad (2)$$

where

$$dM_\theta = \text{differential mass of the coupled system, } \left[\frac{\text{lb}_f \text{ sec}^2}{\text{in.}} \right]$$

$$M_N = \text{generalized mass of the nozzle, } \left[\frac{\text{lb}_f \text{ sec}^2}{\text{in.}} \right]$$

$$= \int_V \rho_0 (u_s^2 + v_s^2 + w_s^2) dV$$

$$\rho_0 = \text{mass density of the nozzle, } \left[\frac{\text{lb}_m}{\text{in}^3} \right]$$

$$1 \text{ lb}_m = \frac{1}{32.2 \times 12} \left[\frac{\text{lb}_f \text{ sec}^2}{\text{in.}} \right]$$

$$V = \text{volume of the nozzle, } [\text{in}^3]$$

$$S_\theta = \text{static unbalance of the coupled system about its elastic axis, } [\text{lb}_f \text{ sec}^2]$$

$$= M_\theta X_{CG}$$

$$M_\theta = \text{total mass of the coupled system, } \left[\frac{\text{lb}_f \text{ sec}^2}{\text{in.}} \right]$$

$$X_{CG} = \text{location of center of gravity of the coupled system, } [\text{in.}]$$

$$I_\theta = \text{mass moment of inertia of the coupled system, } M_\theta, \text{ about } O \text{ (Figure 1), } [\text{lb}_f \text{ in. sec}^2]$$

II, Formulation of Equations of Motion (cont.)

The potential energy may be written as

$$U = \frac{1}{2} K_N \zeta_s^2 + \frac{1}{2} K_\theta \theta^2, \quad [1b_f \text{ in.}] \quad (3)$$

where

$$\begin{aligned} K_N &= \text{spring constant of the flexible wall nozzle} \\ &= \omega_N^2 M_N, \quad \left[\frac{1b_f}{\text{in.}} \right] \end{aligned} \quad (3a)$$

$$\begin{aligned} K_\theta &= \text{spring constant of the coupled system} \\ &= \omega_\theta^2 I_\theta, \quad [1b_f \text{ in.}] \end{aligned} \quad (3b)$$

$$\omega_N = \text{natural frequency of the nozzle, } \left[\frac{1}{\text{sec}} \right]$$

$$\omega_\theta = \text{natural frequency of the coupled system, } \left[\frac{1}{\text{sec}} \right]$$

Lagrange's equations of motion can be written as

$$\frac{d}{dt} \left(\frac{\partial T}{\partial \dot{\alpha}_i} \right) - \frac{\partial T}{\partial \alpha_i} + \frac{\partial U}{\partial \alpha_i} = Q_i \quad \alpha_i = 1, 2, 3, \dots \quad (4)$$

where

$$\alpha_1 = \zeta_s \quad \text{and} \quad \alpha_2 = \theta \quad \text{for the present system}$$

$$Q_i = \text{external force acting on the system}$$

The substitution of Eqs. (2) and (3) into Eq. (4) yields

$$\left. \begin{aligned} M_N \ddot{\zeta}_s + C_N \dot{\zeta}_s + K_N \zeta_s + S_\theta \ddot{\theta} &= Q_{\zeta_s}, \quad [1b_f] \\ S_\theta \ddot{\zeta}_s + I_\theta \ddot{\theta} + C_\theta \dot{\theta} + K_\theta \theta &= Q_\theta, \quad [1b_f] \end{aligned} \right\} \quad (5)$$

II, Formulation of Equations of Motion (cont.)

where

$$G_N = \text{damping coefficient of the nozzle, } \left[\frac{\text{lb}_f \text{ sec}}{\text{in}} \right]$$

$$G_\theta = \text{damping coefficient of the coupled system, } [\text{lb}_f \text{ in. sec}]$$

Let

$$\left. \begin{aligned} Q_{z_s} &= \bar{F}_0 e^{i\omega t}, [\text{lb}_f] \\ Q_\theta &= \bar{F}_0 L e^{i\omega t}, [\text{lb}_f \text{ in.}] \end{aligned} \right\} \quad (6)$$

where

$$L = \text{distance from the elastic axis } O \text{ (Figure 1) to the point of application of the driving force, } \bar{F}_0 e^{i\omega t}, [\text{in}]$$

The substitution of Eq. (6) into Eq. (5) yields

$$\ddot{z}_s + \beta_N \dot{z}_s + \omega_N^2 z_s + \gamma_N \ddot{\theta} = \bar{F}_{z_0} e^{i\omega t}, \left[\frac{\text{in}}{\text{sec}^2} \right] \quad (7)$$

$$\ddot{\theta} + \beta_\theta \dot{\theta} + \omega_\theta^2 \theta + \gamma_\theta \ddot{z}_s = \bar{F}_{\theta_0} e^{i\omega t}, \left[\frac{1}{\text{sec}^2} \right] \quad (8)$$

where

$$\begin{aligned} \beta_N &= \text{damping parameter of the nozzle, } \left[\frac{1}{\text{sec}} \right] \\ &= \frac{G_N}{M_N} \end{aligned}$$

$$\begin{aligned} \beta_\theta &= \text{damping parameter of the coupled system, } \left[\frac{1}{\text{sec}} \right] \\ &= \frac{G_\theta}{I_\theta} \end{aligned}$$

$$\gamma_N = \frac{S_\theta}{M_N}, [\text{in}] ; \quad \gamma_\theta = \frac{S_\theta}{I_\theta}, \left[\frac{1}{\text{in.}} \right]$$

$$\bar{F}_{z_0} = \frac{\bar{F}_0}{M_N}, \left[\frac{\text{in}}{\text{sec}^2} \right] ; \quad \bar{F}_{\theta_0} = \frac{\bar{F}_0 L}{I_\theta}, \left[\frac{1}{\text{sec}^2} \right] \quad (7a); (8a)$$

III. SOLUTION OF EQUATIONS OF MOTION

The solutions of Eqs. (7) and (8) are of the form, respectively,

$$\bar{z}_s(t) = \bar{z}_s e^{i\omega t} \quad [in] \quad (9)$$

$$\bar{\theta}(t) = \bar{\theta} e^{i\omega t} \quad (10)$$

The substitution of Eqs. (9) and (10) into Eqs. (7) and (8) yields, respectively,

$$\left. \begin{aligned} \bar{z}_s [(\omega_N^2 - \omega^2) + i\omega\beta_N] - \bar{\theta} \gamma_N \omega^2 &= \bar{F}_{z_0} \\ -\bar{z}_s \gamma_\theta \omega^2 + \bar{\theta} [(\omega_\theta^2 - \omega^2) + i\omega\beta_\theta] &= \bar{F}_{\theta_0} \end{aligned} \right\} \quad (11)$$

Solving Eq. (11) for \bar{z}_s and $\bar{\theta}$ gives

$$\bar{z}_s = \frac{[(\omega_\theta^2 - \omega^2) + i\omega\beta_\theta] \bar{F}_{z_0} + \gamma_N \omega^2 \bar{F}_{\theta_0}}{[(\omega_N^2 - \omega^2) + i\omega\beta_N][(\omega_\theta^2 - \omega^2) + i\omega\beta_\theta] - \gamma_N \gamma_\theta \omega^4} \quad (12)$$

$$\bar{\theta} = \frac{[(\omega_N^2 - \omega^2) + i\omega\beta_N] \bar{F}_{\theta_0} + \gamma_\theta \omega^2 \bar{F}_{z_0}}{[(\omega_N^2 - \omega^2) + i\omega\beta_N][(\omega_\theta^2 - \omega^2) + i\omega\beta_\theta] - \gamma_N \gamma_\theta \omega^4} \quad (13)$$

The denominator of Eqs. (12) and (13) can be written as

$$\sqrt{A\omega^8 + B\omega^6 + C\omega^4 + D\omega^2 + E} \quad e^{i\psi_0} \quad (14)$$

III, Solution of Equations of Motion (cont.)

where

$$A = (1 - \gamma_N \gamma_\theta)^2$$

$$B = (\beta_N + \beta_\theta)^2 - 2(1 - \gamma_N \gamma_\theta)(\omega_N^2 + \omega_\theta^2 + \beta_N \beta_\theta)$$

$$C = (\omega_N^2 + \omega_\theta^2 + \beta_N \beta_\theta)^2 + 2(1 - \gamma_N \gamma_\theta)\omega_N^2 \omega_\theta^2 - 2(\beta_N + \beta_\theta)(\beta_N \omega_\theta^2 + \beta_\theta \omega_N^2)$$

$$D = (\beta_N \omega_\theta^2 + \beta_\theta \omega_N^2) - 2(\omega_N^2 + \omega_\theta^2 + \beta_N \beta_\theta)\omega_N^2 \omega_\theta^2$$

$$E = \omega_N^4 \omega_\theta^4$$

$$\Psi_D = \tan^{-1} \left[\frac{(\beta_N \omega_\theta^2 + \beta_\theta \omega_N^2) \omega - (\beta_N + \beta_\theta) \omega^3}{[(1 - \gamma_N \gamma_\theta) \omega^4 - (\omega_N^2 + \omega_\theta^2 + \beta_N \beta_\theta) \omega^2 + \omega_N^2 \omega_\theta^2]} \right]$$

The numerator of Eq. (12) can be written as

$$\sqrt{F_1 \omega^4 + G_1 \omega^2 + H_1} e^{i \Psi_Z} \bar{F}_{Z_0} \quad (15)$$

where

$$F_1 = (1 - L J \gamma_N)^2, \quad J = \frac{M_N}{I_\theta}$$

$$G_1 = -2 \omega_\theta^2 \left(1 - L J \gamma_N - \frac{\beta_\theta^2}{2 \omega_\theta^2} \right)$$

$$H_1 = \omega_\theta^4$$

$$\Psi_Z = \tan^{-1} \left[\frac{\beta_\theta \omega}{(L J \gamma_N - 1) \omega^2 + \omega_\theta^2} \right]$$

The numerator of Eq. (13) can be written as

$$\sqrt{F_2 \omega^4 + G_2 \omega^2 + H_2} e^{i \Psi_\theta} \bar{F}_{\theta_0} \quad (16)$$

III, Solution of Equations of Motion (cont.)

where

$$\begin{aligned}
 F_2 &= \left(1 - \frac{Y_0}{LJ}\right)^2 \\
 G_2 &= -2\omega_N^2 \left(1 - \frac{Y_N}{LJ} - \frac{\beta_N^2}{2\omega_N^2}\right) \\
 H_2 &= \omega_N^4 \\
 \psi_0 &= \tan^{-1} \left[\frac{\beta_N \omega}{\left(\frac{Y_N}{LJ} - 1\right)\omega^2 + \omega_N^2} \right]
 \end{aligned}$$

Hence Eqs. (12) and (13) become, respectively,

$$\bar{z}_s = \sqrt{\frac{F_1 \omega^4 + G_1 \omega^2 + H_1}{A\omega^8 + B\omega^6 + C\omega^4 + D\omega^2 + E}} e^{i(\psi_3 - \psi_0)} \bar{F}_{z_0} \text{ [in.]} \quad (17)$$

$$\bar{\theta} = \sqrt{\frac{F_2 \omega^4 + G_2 \omega^2 + H_2}{A\omega^8 + B\omega^6 + C\omega^4 + D\omega^2 + E}} e^{i(\psi_0 - \psi_0)} \bar{F}_{\theta_0} \quad (18)$$

The substitution of Eqs. (17) and (18) into Eqs. (9) and (10) yields, respectively,

$$z_s(t) = \sqrt{\frac{F_1 \omega^4 + G_1 \omega^2 + H_1}{A\omega^8 + B\omega^6 + C\omega^4 + D\omega^2 + E}} e^{i(\omega t + \psi_3 - \psi_0)} \bar{F}_{z_0} \text{ [in]} \quad (19)$$

$$\theta(t) = \sqrt{\frac{F_2 \omega^4 + G_2 \omega^2 + H_2}{A\omega^8 + B\omega^6 + C\omega^4 + D\omega^2 + E}} e^{i(\omega t + \psi_0 - \psi_0)} \bar{F}_{\theta_0} \quad (20)$$

The mean square of $\bar{z}_s(t)$ is defined as

$$\widehat{z}_s^2 \triangleq \lim_{T \rightarrow \infty} \frac{1}{2T} \int_{-T}^T \bar{z}_s^2(t) dt, \quad [\text{in}^2] \quad (21)$$

III, Solution of Equations of Motion (cont.)

In Eq. (6), if the real part is chosen, namely,

$$\left. \begin{aligned} Q_{zs} &= \operatorname{Re} \{ \bar{F}_0 e^{i\omega t} \} = \bar{F}_0 \cos \omega t, \quad [\text{lb f}] \\ Q_{\theta} &= \operatorname{Re} \{ \bar{F}_0 L e^{i\omega t} \} = \bar{F}_0 L \cos \omega t, \quad [\text{lb f-in.}] \end{aligned} \right\} \quad (22)$$

the solutions (19) and (20) then become, respectively,

$$\xi_s(t) = \sqrt{\frac{F_1 \omega^4 + G_1 \omega^2 + H_1}{A \omega^8 + B \omega^6 + C \omega^4 + D \omega^2 + E}} \cos(\omega t + \psi_z - \psi_0) \bar{F}_{z_0}, \quad [\text{in}] \quad (23)$$

$$\theta(t) = \sqrt{\frac{F_2 \omega^4 + G_2 \omega^2 + H_2}{A \omega^8 + B \omega^6 + C \omega^4 + D \omega^2 + E}} \cos(\omega t + \psi_{\theta} - \psi_0) \bar{F}_{\theta_0} \quad (24)$$

The substitution of Eq. (23) into Eq. (21) yields

$$\begin{aligned} \hat{\xi}_s^2 &= \bar{\xi}_s^2 \left[\lim_{T \rightarrow \infty} \frac{1}{2T} \int_{-T}^T \cos^2(\omega t + \psi_z - \psi_0) dt \right] \bar{F}_{z_0}^2 \\ &= \frac{1}{2} \bar{\xi}_s^2 \bar{F}_{z_0}^2 \end{aligned} \quad (25)$$

where

$$\bar{\xi}_s^2 = \frac{F_1 \omega^4 + G_1 \omega^2 + H_1}{A \omega^8 + B \omega^6 + C \omega^4 + D \omega^2 + E}, \quad [\text{sec}^4] \quad (25a)$$

The mean square of $\theta(t)$ is defined as

$$\hat{\theta}^2 \triangleq \lim_{T \rightarrow \infty} \frac{1}{2T} \int_{-T}^T \theta^2(t) dt \quad (26)$$

III, Solution of Equations of Motion (cont.)

The substitution of Eq. (24) into Eq. (26) yields

$$\begin{aligned} \hat{Q} &= \bar{\Delta}^2 \left[\lim_{T \rightarrow \infty} \frac{1}{2T} \int_{-T}^T \cos^2(\omega t + \psi_0 - \psi_0) dt \right] \bar{F}_0^2 \\ &= \frac{1}{2} \bar{\Delta}^2 \bar{F}_0^2 \end{aligned} \quad (27)$$

where

$$\bar{\Delta}^2 = \frac{F_2 \omega^4 + G_2 \omega^2 + H_2}{A \omega^2 + B \omega^6 + C \omega^4 + D \omega^2 + E}, \quad [\text{sec}^4] \quad (27a)$$

The mean square values of Q_{zs} and Q_θ are, respectively,

$$\hat{Q}_{zs}^2 = \lim_{T \rightarrow \infty} \frac{1}{2T} \int_{-T}^T \bar{F}^2 \cos^2 \omega t dt = \frac{1}{2} \bar{F}_0^2, \quad [\text{lb}_f^2] \quad (28)$$

$$\hat{Q}_\theta^2 = \lim_{T \rightarrow \infty} \frac{1}{2T} \int_{-T}^T (\bar{F}_0 L)^2 \cos^2 \omega t dt = \frac{1}{2} (\bar{F}_0 L)^2, \quad [\text{lb}_f^2 \text{ in}^2] \quad (29)$$

From Eqs. (7a), (8a), (28), and (29),

$$\frac{\hat{Q}_{zs}^2}{M_N^2} = \frac{1}{2} \bar{F}_{z0}^2, \quad \left[\frac{\text{in}^2}{\text{sec}^4} \right] \quad (28a)$$

$$\frac{\hat{Q}_\theta^2}{I_\theta^2} = \frac{1}{2} \bar{F}_{\theta 0}^2, \quad \left[\frac{1}{\text{sec}^4} \right] \quad (29a)$$

III, Solution of Equations of Motion (cont.)

The substitution of Eqs. (28a) and (29a) into Eqs. (25) and (27) yields

$$\hat{\xi}_s^2 = \bar{\xi}^2 \frac{\hat{Q}_{zs}^2}{M_N^2}, \quad [in] \quad (30)$$

$$\hat{\theta}^2 = \bar{\theta}^2 \frac{\hat{Q}_\theta^2}{I_\theta^2} \quad (31)$$

The substitution of Eqs. (25a) and (27a) into Eqs. (30) and (31) gives, respectively,

$$\hat{\xi}_s^2 = \frac{\frac{\hat{Q}_{zs}^2}{M_N^2}}{\left(\frac{A\omega^8 + B\omega^6 + C\omega^4 + D\omega^2 + E}{F_1\omega^4 + G_1\omega^2 + H_1} \right)} = \frac{\frac{\hat{Q}_{zs}^2}{M_N^2}}{|Z_{zs}(\omega)|^2}, \quad [in^2] \quad (32)$$

$$\hat{\theta}^2 = \frac{\frac{\hat{Q}_\theta^2}{I_\theta^2}}{\left(\frac{A\omega^8 + B\omega^6 + C\omega^4 + D\omega^2 + E}{F_2\omega^4 + G_2\omega^2 + H_2} \right)} = \frac{\frac{\hat{Q}_\theta^2}{I_\theta^2}}{|Z_\theta(\omega)|^2} \quad (33)$$

where

$|Z_{zs}(\omega)|^2$ = the absolute square of the impedance of the flexible wall nozzle

$|Z_\theta(\omega)|^2$ = the absolute square of the impedance of the coupled system

From Eqs. (28) and (29)

$$\hat{Q}_\theta^2 = L^2 \hat{Q}_{zs}^2, \quad [lb_f in^2] \quad (34)$$

III, Solution of Equations of Motion (cont.)

The substitution of Eq. (34) into Eq. (33) yields

$$\hat{\theta}^2 = \frac{\frac{\hat{Q}_{zs}^2}{M_N^2}}{\left(\frac{1}{JL}\right)^2 \left(\frac{A\omega^8 + B\omega^6 + C\omega^4 + D\omega^2 + E}{F_2\omega^4 + G_2\omega^2 + H_2} \right)} \quad (35)$$

If $Q_{zs}(t)$ is not sinusoidal, but a random function, $Q_{zs}(t)$ needs only to be defined by the square mean value as follows:

$$\hat{Q}_{zs}^2 \triangleq \int_0^\infty g(\omega) d\omega, \quad [lb_f^2] \quad (36)$$

where

$$g(\omega) = \text{power spectral density of an input force, } [lb_f^2 \cdot \text{sec}]$$

Similarly, let the power spectral density of $\xi_s(t)$ be defined by

$$\hat{\xi}_s^2 \triangleq \int_0^\infty g(\omega) d\omega, \quad [in^2] \quad (37)$$

where

$g(\omega)$ is given as

$$g(\omega) = \frac{\frac{q(\omega)}{M_N^2}}{|Z_{\xi_s}(\omega)|^2}, \quad [in^2 \cdot \text{sec}] \quad (38)*$$

*Bisplinghoff, R. L., Ashely, H., and Halfman, R. L., "Aeroelasticity," Addison-Wesley Publishing Company, Inc., 1955, pp. 813-825.

III, Solution of Equations of Motion (cont.)

and hence, from Eqs. (37) and (38),

$$\hat{\xi}_s^2 = \int_0^\infty \frac{\frac{g(\omega)}{M_N^2}}{|Z_{\xi_s}(\omega)|^2} d\omega, \quad [in^2] \quad (39)$$

If $g(\omega)$ is assumed to be a slowly varying function compared to the variation of the impedance with ω ,

$$\hat{\xi}_s^2 = \frac{g(\omega_N)}{M_N^2} \int_0^\infty \frac{F_1 \omega^4 + G_1 \omega^2 + H_1}{A \omega^8 + B \omega^6 + C \omega^4 + D \omega^2 + E} d\omega, \quad [in^2] \quad (40)$$

Let

$$\int_0^\infty \frac{F_1 \omega^4 + G_1 \omega^2 + H_1}{A \omega^8 + B \omega^6 + C \omega^4 + D \omega^2 + E} d\omega = I_{\xi_s}, \quad [sec^3] \quad (41)$$

where I_{ξ_s} is a function of $\beta_N, \beta_\theta, \omega_N, \omega_\theta, M_N, M_\theta, X_{CG}$, and I_θ .

From Eqs. (40) and (41),

$$\hat{\xi}_s^2 = \frac{g(\omega_N)}{M_N^2} \cdot I_{\xi_s}, \quad [in^2] \quad (42)$$

Substituting Eq. (42) into the square mean value, $\hat{w}^2(x, \phi)$, of the displacement, $w(x, \phi, t)$, given in Eqs. (1) and then deleting $x' \hat{\theta}^2$ (only one degree of freedom, namely, only the motion of the nozzle is considered here) gives

$$\hat{w}^2(x, \phi) = w_s^2(x, \phi) \frac{g(\omega_N)}{M_N^2} I_{\xi_s}, \quad [in^2] \quad (43)$$

III, Solution of Equations of Motion (cont.)

If the modal shape, $w_s(x, \varphi)$, is assumed to be of the form*

$$w_s(x, \varphi) = \bar{w}_{s0} (A_1 \eta^2 + A_2 \eta^3 + A_3 \eta^4) \sin(s\varphi) \quad (44)$$

where

\bar{w}_{s0} = the modal amplitude and the function of mode number, s (see Section VII)

$$\eta = \frac{x}{l_1}, \quad l_1 = l - l_0, \quad (\text{see Figure 1}),$$

the maximum value of \hat{w}^2 of Eq. (43) will then be

$$\hat{w}_{\max}^2 = \bar{w}_{s0}^2 A_s^2 \frac{f(\omega_N)}{M_N^2} I_{zs}, \quad [in^2] \quad (44a)$$

where

$$A_s = A_1 + A_2 + A_3 \quad (\text{see Reference 1}) \quad (44b)$$

The critical radial deflection required for buckling, w_{crit} , is obtained as*

$$w_{\text{crit}} = \frac{k K s^4 l_1^2 h^2}{12(1-\nu^2) r_0^3} = \frac{k K s^4 h^2 \lambda^2}{12(1-\nu^2) r_0}, \quad [in] \quad (45)$$

where k , K , h , and r_0 are introduced in Reference * and $\lambda = l_1/r_0$.

The critical force which gives rise to buckling of the cone can be approximately determined by equating Eq. (44a) to the square of Eq. (45), i.e.,

$$\hat{w}_{\max}^2 = w_{\text{crit}}^2, \quad [in^2] \quad (45a)$$

*"Study on Bell-Mode Vibrations of Conical Nozzles," Aerojet-General Corporation Space Propulsion Division of the Liquid Rocket Plant, Azusa, California. Aerojet-General Report No. 2581, May 1963.

III, Solution of Equations of Motion (cont.)

This result provides for a relationship between the critical force, $q_c(\omega_N)$, and λ , which is directly related to area ratio, as follows:

$$q_c(\omega_N) = \frac{\frac{k K s^4 h^2 \lambda^2}{12(1-\nu^2) r_0}}{\bar{w}_{s_0}^2 A_s^2 I_{z_s}} M_N^2, \quad [lb_f^2 \text{ sec}] \quad (46)$$

If the modal amplitude, \bar{w}_{s_0} , and the coefficient, A_s , are known for a given mode number, s , the evaluation of $q_c(\omega_N)$ by Eq. (46) depends upon the evaluation of the integral, I_{z_s} . This integral can be evaluated in closed form. It would be, however, difficult to obtain simple physical parameters from its evaluation. On the basis of engineering simplicity and on the fact that the overall engine motions (due to θ) would have little or no effect on the buckling motions of the nozzle extensions, the following approximation is developed by substituting $I_\theta = \infty$ into Eq. (25a):

$$\frac{F_1 \omega^4 + G_1 \omega^2 + H_1}{A \omega^8 + B \omega^6 + C \omega^4 + D \omega^2 + E} \approx \frac{1}{\omega_N^2 - \omega^2 + \beta_N^2 \omega^2} \quad (47)$$

Eq. (47) implies that θ motion is excluded in the determination of nozzle extension motion, ξ_s . Based on Eq. (47), the integral, I_{z_s} , becomes:

$$I_{z_s} = \int_0^\infty \frac{d\omega}{(\omega_N^2 - \omega^2)^2 + \beta_N^2 \omega^2} \approx \frac{\pi}{2} \frac{1}{\beta_N \omega_N^2}, \quad [\text{sec}^3] \quad (48)$$

Thus, the final expression for the critical force becomes, from Eqs. (46) and (48),

$$q_c(\omega_N) = \frac{2}{\pi} \frac{\left[\frac{k K s^4 h^2 \lambda^2}{12(1-\nu^2) r_0} \right]^2}{\bar{w}_{s_0}^2 A_s^2} M_N^2 \beta_N \omega_N^2, \quad [lb_f^2 \text{ sec}] \quad (49)$$

IV. AERODYNAMIC FORCES INDUCED BY VIBRATION OF THE NOZZLE

When a gas flows through the nozzle, aerodynamic forces act over the nozzle surface. If the nozzle is deformed, there is a change in the magnitude and distribution of these surface forces. The functional relation between the deformation and the change in surface forces produced by the deformation, $w(x, \varphi, t)$, can be obtained as**

$$F_A(t) = l_1 \int_0^1 \int_0^{2\pi} A(w) w_s(x, \varphi) \frac{r}{\cos \alpha} d\eta d\varphi, \quad [lb_f] \quad (50)$$

where

$$A(w) = -\frac{\rho_A U^2}{\sqrt{M^2-1}} \frac{\partial w}{\partial x} - \frac{\rho_A U}{\sqrt{M^2-1}} \frac{M^2-2}{M^2-1} \frac{\partial w}{\partial t}, \quad \left[\frac{lb_f}{in^2} \right] \quad (50a)^*$$

$$\rho_A = \text{mass density of the gas, } \left[\frac{lb_f \text{ sec}^2}{in^4} \right]$$

$$U = \text{velocity of the gas, } \left[\frac{in}{sec} \right]$$

$$M = \text{Mach number}$$

$$w(x, \varphi, t) = w_s(x, \varphi) \xi_s(t), \quad [in.]$$

$$\left. \begin{aligned} w_s(x, \varphi) &= \bar{w}_{s0} (A_1 \eta^2 + A_2 \eta^3 + A_3 \eta^4) \sin(s\varphi) \\ \xi_s(t) &= \bar{\xi}_s f(t), \quad [in] \end{aligned} \right\} \quad (50b)$$

$f(t)$ = a random function of time

$$\eta = \frac{x}{l_1}, \quad l_1 = l - l_0$$

*Eq. (50a) represents a first order approximation to the aerodynamic theory in which the influence of three-dimensional aerodynamic effects is neglected and the Mach number should be greater than approximately 1.6.

**R. L. Bisplinghoff and H. Ashley, "Principles of Aero-Elasticity," John Wiley & Sons, Inc., 1962, p. 443.

IV, Aerodynamic Forces Induced by Vibration of the Nozzle (cont.)

By one dimensional isentropic flow theory,

$$\frac{\rho_A U^2}{\sqrt{M^2-1}} = \frac{\gamma P_c M^2}{\sqrt{M^2-1} \left(1 + \frac{\gamma-1}{2} M^2\right)^{\frac{\gamma}{\gamma-1}}} \quad , \quad \left[\frac{\text{lb}_f}{\text{in}^2} \right] \quad (51)$$

$$\frac{\rho_A U}{\sqrt{M^2-1}} \cdot \frac{M^2-2}{M^2-1} = \frac{M \rho_c \sqrt{\gamma R T_c} \left(\frac{M^2-2}{M^2-1}\right)}{\sqrt{M^2-1} \left(1 + \frac{\gamma-1}{2} M^2\right)^{\frac{\gamma+1}{2(\gamma-1)}}} \quad , \quad \left[\frac{\text{lb}_f \text{ sec}}{\text{in}^3} \right] \quad (52)$$

where

P_c, ρ_c, T_c = chamber pressure, density, temperature, $\left[\frac{\text{lb}_f}{\text{in}^2} \right], \left[\frac{\text{lb}_m}{\text{in}^3} \right], [^\circ R]$
 γ = specific heat ratio

R = gas constant, $\left[\frac{\text{lb}_f \text{ ft}}{\text{lb}_m \text{ } ^\circ R} \right]$

Let the mean Mach number of fluid in the nozzle be denoted by M_m and hence the mean values of Eqs. (51) and (52) be denoted as, respectively,

$$- \frac{\gamma P_c M_m^2}{\sqrt{M_m^2-1} \left(1 + \frac{\gamma-1}{2} M_m^2\right)^{\frac{\gamma}{\gamma-1}}} = H_{A1}(M_m) \quad , \quad \left[\frac{\text{lb}_f}{\text{in}^2} \right] \quad (53)$$

$$- \frac{M_m \rho_c \sqrt{\gamma R T_c} \left(\frac{M_m^2-2}{M_m^2-1}\right)}{\sqrt{M_m^2-1} \left(1 + \frac{\gamma-1}{2} M_m^2\right)^{\frac{\gamma+1}{2(\gamma-1)}}} = H_{A2}(M_m) \quad , \quad \left[\frac{\text{lb}_f \text{ sec}}{\text{in}^3} \right] \quad (54)$$

Thus Eq. (50a) is written in the form

$$A(w) = H_{A1} \frac{\partial w}{\partial x} + H_{A2} \frac{\partial w}{\partial t} \quad (55)$$

From the geometry (Figure 1), Eq. (50) is written in the form:

$$F_A(t) = \frac{r_0 l_1}{\cos \alpha} \int_0^1 \int_0^{2\pi} A(w) w_s d\eta d\varphi + \frac{l_1^2 \sin \alpha}{\cos^2 \alpha} \int_0^1 \int_0^{2\pi} \eta A(w) w_s d\eta d\varphi \quad , \quad [\text{lb}_f] \quad (56)$$

IV, Aerodynamic Forces Induced by Vibration of the Nozzle (cont.)

The substitution of Eq. (50b) into Eq. (55) yields

$$A(w) \bar{w}_s = \frac{H_{A1} \bar{w}_{s0}^2 \ddot{\xi}_s(t)}{l_1} (2A_1 \eta + 3A_2 \eta^2 + 4A_3 \eta^3) (A_1 \eta^2 + A_2 \eta^3 + A_3 \eta^4) \sin^2(s\phi) + H_{A2} \bar{w}_{s0}^2 \dot{\xi}_s(t) (A_1 \eta^2 + A_2 \eta^3 + A_3 \eta^4) \sin^2(s\phi), \left[\frac{\text{lb f}}{\text{in}^2} \right] \quad (57)$$

The substitution of Eq. (57) into Eq. (56) yields

$$\begin{aligned} F_A(t) = & \left(\frac{H_{A1} I_{11} r_0}{\cos \alpha} + \frac{H_{A1} I_{21} \sin \alpha}{\cos^2 \alpha} l_1 \right) \bar{w}_{s0}^2 \ddot{\xi}_s(t) \\ & + \left(\frac{H_{A2} I_{12} r_0}{\cos \alpha} l_1 + \frac{H_{A2} I_{22} \sin \alpha}{\cos^2 \alpha} l_1^2 \right) \bar{w}_{s0}^2 \dot{\xi}_s(t), \quad [\text{lb f}] \end{aligned} \quad (58)*$$

Let

$$\left. \begin{aligned} \left(\frac{H_{A1} I_{11} r_0}{\cos \alpha} + \frac{H_{A1} I_{21} \sin \alpha}{\cos^2 \alpha} l_1 \right) \bar{w}_{s0}^2 &= K_A \\ \left(\frac{H_{A2} I_{12} r_0}{\cos \alpha} l_1 + \frac{H_{A2} I_{22} \sin \alpha}{\cos^2 \alpha} l_1^2 \right) \bar{w}_{s0}^2 &= G_A \end{aligned} \right\} \quad (59)$$

Then Eq. (58) is written as

$$\boxed{F_A(t) = G_A \dot{\xi}_s(t) + K_A \ddot{\xi}_s(t), \quad [\text{lb f}]} \quad (60)$$

* I_{11} , I_{21} , I_{12} , and I_{22} are given in the foot-note of the next page.

IV, Aerodynamic Forces Induced by Vibration of the Nozzle (cont.)

This force, $F_A(t)$, is the aerodynamic force induced by vibration of the nozzle.

Eq. (50a) reduces to the case of piston theory when $\sqrt{M^2-1} \rightarrow M$ and $\frac{M^2-2}{M^2-1} \rightarrow 1$.

In this case, Eqs. (53) and (54) become

$$-\frac{\gamma P_c M_m}{\left(1 + \frac{\gamma-1}{2} M_m^2\right)^{\frac{\gamma}{\gamma-1}}} = H_{A1}(M_m) \quad , \quad \left[\frac{lb_f}{in^2} \right] \quad (61)$$

$$-\frac{P_c \sqrt{\gamma R T_c}}{\left(1 + \frac{\gamma-1}{2} M_m^2\right)^{\frac{\gamma+1}{2(\gamma-1)}}} = H_{A2}(M_m) \quad , \quad \left[\frac{lb_f}{in^2} \right] \quad (62)$$

* I_{11} , I_{21} , I_{12} , and I_{22} of Eq. (58):

$$\left. \begin{aligned} I_{11} &= \int_0^1 \int_0^{2\pi} (2A_1\eta + 3A_2\eta^2 + 4A_3\eta^3)(A_1\eta^2 + A_2\eta^3 + A_3\eta^4) \sin^2(s\phi) d\eta d\phi \\ I_{21} &= \int_0^1 \int_0^{2\pi} (2A_1\eta + 3A_2\eta^2 + 4A_3\eta^3)(A_1\eta^2 + A_2\eta^3 + A_3\eta^4) \eta \sin^2(s\phi) d\eta d\phi \\ I_{12} &= \int_0^1 \int_0^{2\pi} (A_1\eta^2 + A_2\eta^3 + A_3\eta^4)^2 \sin^2(s\phi) d\eta d\phi \\ I_{22} &= \int_0^1 \int_0^{2\pi} (A_1\eta^2 + A_2\eta^3 + A_3\eta^4)^2 \eta \sin^2(s\phi) d\eta d\phi \end{aligned} \right\} \quad (58a)$$

V. PREDICTION OF INPUT SPECTRUM FORCE WHEN THE AERODYNAMIC FORCE, $F_A(t)$, ACTS OVER THE NOZZLE SURFACE

In Section II, the critical spectrum force, $q_c(\omega_N)$, was obtained as

$$q_c(\omega_N) = \frac{w_{crit}^2 M_N^2 \beta_N \omega_N^2}{\frac{\pi}{2} \bar{w}_{so}^2 A_s^2}, \quad [lb_f^2 sec] \quad (49)$$

by solving the equation of motion of the nozzle (Ref. Eq. (7)):

$$M_N \ddot{z}_s + G_N \dot{z}_s + K_N z_s = F_c(t) \quad (63)$$

In the analysis, the square-mean value of $F_c(t)$ was defined (Ref. Eq. (36)) as

$$\hat{F}_c^2 \triangleq \int_0^\infty q(\omega) d\omega \quad (64)$$

In the present section, the equation of motion of the nozzle is written in the form

$$M_N \ddot{z}_s + G_N \dot{z}_s + K_N z_s = F_A(t) + F_D(t) \quad (65)$$

where

$F_D(t)$ = input force acting over the nozzle surface

The substitution of Eq. (60) into Eq. (65) yields

$$M_N \ddot{z}_s + G_B \dot{z}_s + K_B z_s = F_D(t) \quad (66)$$

where

$$\left. \begin{aligned} G_B &= G_N - G_A \\ K_B &= K_N - K_A \end{aligned} \right\} \quad (66a)$$

V, Prediction of Input Spectrum Force When the Aerodynamic Force, $F_A(t)$, Acts Over the Nozzle Surface (cont.)

Let the square-mean value of $F_D(t)$ be defined as

$$\hat{F}_D^2 \triangleq \int_0^\infty f_D(\omega) d\omega \quad (67)$$

Then the input spectrum force, $f_D(\omega_N)$, may be obtained as

$$f_D(\omega_N) = \frac{\hat{W}_D^2(x, \phi) M_N^2 \beta_B \omega_B^2}{\frac{\pi}{2} W_S^2(x, \phi)}, \quad [lb_f^2 sec] \quad (68)$$

where

$\hat{W}_D^2(x, \phi)$ = the square-mean value of the displacement, $W_D(x, \phi, t)$, which is produced by the input force, $F_D(t)$,

$$\left. \begin{aligned} \beta_B &= \frac{G_B}{M_N}, \quad \left[\frac{1}{sec} \right] \\ \omega_B^2 &= \frac{K_B}{M_N}, \quad \left[\frac{1}{sec^2} \right] \end{aligned} \right\} \quad (69)$$

When the maximum value of $\hat{W}_D^2(x, \phi)$ is considered, the input spectrum force, $f_D(\omega_N)$, is rewritten by substituting $x = l$, and $s\phi = \frac{\pi}{2}$ into Eq. (68) as

$$f_D(\omega_N) = \frac{\hat{W}_{D, max}^2 M_N^2 \beta_B \omega_B^2}{\frac{\pi}{2} \bar{W}_{S_0}^2 A_S^2}, \quad [lb_f^2 sec] \quad (70)$$

From Eqs. (49) and (70),

$$\frac{f_D(\omega_N)}{f_C(\omega_N)} = \left(\frac{\hat{W}_{D, max}}{W_{crit}} \right)^2 \cdot \frac{\beta_B \omega_B^2}{\beta_N \omega_N^2} \quad (71)$$

V, Prediction of Input Spectrum Force When the Aerodynamic Force, $F_A(t)$, Acts Over the Nozzle Surface (cont.)

If the input spectrum force, $f_D(\omega_N)$, produces a critical displacement at the nozzle surface,

$$\hat{W}_{D, \max} = W_{\text{crit}} \quad (72)$$

In this case, Eq. (71) becomes

$$\frac{f_D(\omega_N)}{f_C(\omega_N)} = \frac{\beta_B \omega_B^2}{\beta_N \omega_N^2} \quad (73)$$

The substitution of Eqs. (66a) and (69) into Eq. (73) yields

$$\frac{f_D(\omega_N)}{f_C(\omega_N)} = 1 - (R_G + R_K) + R_G R_K \quad (74)$$

where

$$R_G = \frac{G_A}{G_N} \quad \text{and} \quad R_K = \frac{K_A}{K_N} \quad (74a)$$

From Eqs. (49) and (74),

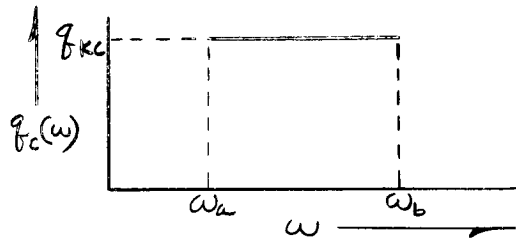
$$f_D(\omega_N) = \frac{2}{\pi} \left(\frac{W_{\text{crit}}^2 M_N^2 \beta_N \omega_N^2}{W_{s0}^2 A_s} \right) [1 - (R_G + R_K) + R_G R_K] \quad (75)$$

VI. POWER SPECTRAL DENSITY, G^2/CPS , OF VIBRATING NOZZLE IN TERMS OF ACCELERATION

It is assumed for the present case that the power spectral density, $g_c(\omega)$, of critical force is expressed in the form:

$$g_c(\omega) = \begin{cases} 0, & \omega < \omega_a \\ g_{kc}, & \omega_a \leq \omega \leq \omega_b \\ 0, & \omega > \omega_b \end{cases} \quad [lb_f^2 \text{ sec}] \quad (76)$$

as shown in the figure below:



(The spectral range is from ω_a to ω_b)

For the case of Eq. (76), Eq. (64) becomes

$$\hat{F}_c^2 \triangleq \int_0^{\infty} g_c(\omega) d\omega = \int_{\omega_a}^{\omega_b} g_c(\omega) d\omega = g_{kc} (\omega_b - \omega_a), [lb_f^2] \quad (77)$$

Let

$$g_{kc} = \frac{\omega_N}{\omega_b - \omega_a} g_c(\omega_N), \quad [lb_f^2 \text{ sec}] \quad (78)$$

then substituting Eq. (78) into Eq. (77) gives

$$\hat{F}_c^2 = \omega_N g_c(\omega_N), \quad [lb_f^2] \quad (79)$$

VI, Power Spectral Density, G^2/CPS , of Vibrating Nozzle in Terms of Acceleration (cont.)

Similarly if the power spectral density, $g_D(\omega)$, of input force is assumed to be of the form

$$g_D(\omega) = \begin{cases} 0, & \omega < \omega_a \\ g_{KD}, & \omega_a \leq \omega \leq \omega_b \\ 0, & \omega > \omega_b \end{cases} \quad [lb_f^2 \text{ sec}] \quad (80)$$

where

$$g_{KD} = \frac{\omega_N}{\omega_b - \omega_a} g_D(\omega_N) \quad [lb_f^2 \text{ sec}] \quad (80a)$$

then Eq. (67) becomes

$$\hat{F}_D^2 = \omega_N g_D(\omega_N) \quad [lb_f^2] \quad (81)$$

The functions, G_c^2 and G_D^2 , are defined as, respectively,

$$G_c^2 \triangleq \frac{\hat{F}_c^2}{M_N^2 g_D^2} \quad (82)$$

$$G_D^2 \triangleq \frac{\hat{F}_D^2}{M_N^2 g_0^2} \quad (83)$$

where

$$g_0 = \text{acceleration due to gravity, } \left[\frac{in}{sec^2} \right]$$

The substitution of Eq. (79) into Eq. (82) yields

$$G_c^2 = \frac{\omega_N g_c(\omega_N)}{M_N^2 g_0^2} \quad (84)$$

VI, Power Spectral Density, G^2/CFS , of Vibrating Nozzle in Terms of Acceleration (cont.)

The substitution of Eq. (81) into Eq. (83) yields

$$G_D^2 = \frac{\omega_N g_D(\omega_N)}{M_N^2 g_0^2} \quad (85)$$

From Eqs. (49), (70), (72), (84), and (85)

$$G_c^2 = \frac{2 W_{crit}^2 \beta_N \omega_N^3}{\pi \bar{W}_{s_0}^2 A_s^2 g_0^2} \quad (86)$$

$$G_D^2 = \frac{2 W_{crit}^2 \beta_B \omega_B^2 \omega_N}{\pi \bar{W}_{s_0}^2 A_s^2 g_0^2} \quad (87)$$

where

$$A_s = A_1 + A_2 + A_3, \quad [eq. (44b)]$$

$$\bar{W}_{s_0}^2 = \frac{\pi (r_0 + r_t + l \tan \alpha)}{I_M} \left(\frac{l}{\cos \alpha} - \frac{r_0 - r_t}{\sin \alpha} \right), \quad [eq. (96)]$$

From Eqs. (74), (84), and (85),

$$\frac{G_D^2}{G_c^2} = 1 - (R_G + R_K) + R_G R_K \quad (88)$$

VII. DETERMINATION OF MODAL AMPLITUDE, \bar{w}_{s0}

The generalized mass, M_N , of the nozzle wall was introduced in Eq. (2). For the present case, it may be approximated for $S = 6$ by

$$M_N = \rho_0 \iiint w_s^2 dV = \rho_0 h \int_0^{l_1} \int_0^{2\pi} w_s^2 \frac{r}{\cos \alpha} dx d\varphi, \left[\frac{\text{lb}_f \text{sec}^2}{\text{in}} \right] \quad (89)$$

where h is a thickness of the nozzle wall.

The substitution of Eq. (44) into Eq. (89) yields

$$M_N = \rho_0 h \int_0^{l_1} \int_0^{2\pi} \bar{w}_{s0}^2 (A_1 \eta^2 + A_2 \eta^3 + A_3 \eta^4)^2 \sin^2(s\varphi) \frac{r}{\cos \alpha} dx d\varphi, \left[\frac{\text{lb}_f \text{sec}^2}{\text{in}} \right] \quad (90)$$

Let

$$\int_0^{l_1} \int_0^{2\pi} (A_1 \eta^2 + A_2 \eta^3 + A_3 \eta^4)^2 \sin^2(s\varphi) \frac{r}{\cos \alpha} dx d\varphi = I_M, \quad [\text{in}^2] \quad (91)$$

Then Eq. (90) is written as

$$M_N = \rho_0 h I_M \bar{w}_{s0}^2, \left[\frac{\text{lb}_f \text{sec}^2}{\text{in}} \right] \quad (92)$$

Let the mass of undeformed nozzle wall be denoted by m_N . It is assumed in the present study that the generalized mass, M_N , is approximately equal to the mass, m_N ,

$$M_N \cong m_N, \quad \left[\frac{\text{lb}_f \text{sec}^2}{\text{in}} \right] \quad (93)$$

The substitution of Eq. (93) into Eq. (92) yields

$$\bar{w}_{s0} \cong \sqrt{\frac{m_N}{\rho_0 h I_M}} \quad (94)$$

VII, Determination of Modal Amplitude, \bar{w}_{s0} (cont.)

The mass, m_N , of undeformed nozzle wall is obtained as

$$m_N = \pi \rho h (r_0 + r_t + l \tan \alpha) \left(\frac{l}{\cos \alpha} - \frac{r_0 - r_t}{\sin \alpha} \right) \quad , \quad \left[\frac{\text{lb} \cdot \text{sec}^2}{\text{in}} \right] \quad (95)$$

The substitution of Eq. (95) into Eq. (94) yields

$$\bar{w}_{s0} \cong \sqrt{\frac{\pi (r_0 + r_t + l \tan \alpha)}{I_M} \left(\frac{l}{\cos \alpha} - \frac{r_0 - r_t}{\sin \alpha} \right)} \quad (96)$$

VIII. SAMPLE CALCULATIONS

The procedure for determining the input spectrum force, G_D^2 , in terms of acceleration when the aerodynamic force, $F_A(t)$, acts over the nozzle surface is outlined here.

- (1) I_M given by Eq. (91)

$$I_M = \int_0^1 \int_0^{2\pi} (A_1 \eta^2 + A_2 \eta^3 + A_3 \eta^4)^2 \sin^2(s\varphi) \frac{r}{\cos \alpha} dx d\varphi$$

- (2) \bar{w}_{s0} given by Eq. (96)

$$\bar{w}_{s0} \cong \sqrt{\frac{\pi (r_0 + r_t + l \tan \alpha)}{I_M} \left(\frac{l}{\cos \alpha} - \frac{r_0 - r_t}{\sin \alpha} \right)}$$

- (3) I_{11} , I_{21} , I_{12} , and I_{22} given by Eq. (58a)

$$I_{11} = \int_0^1 \int_0^{2\pi} (2A_1 \eta + 3A_2 \eta^2 + 4A_3 \eta^3) (A_1 \eta^2 + A_2 \eta^3 + A_3 \eta^4) \sin^2(s\varphi) d\eta d\varphi$$

$$I_{21} = \int_0^1 \int_0^{2\pi} (2A_1 \eta + 3A_2 \eta^2 + 4A_3 \eta^3) (A_1 \eta^2 + A_2 \eta^3 + A_3 \eta^4) \eta \sin^2(s\varphi) d\eta d\varphi$$

$$I_{12} = \int_0^1 \int_0^{2\pi} (A_1 \eta^2 + A_2 \eta^3 + A_3 \eta^4)^2 \sin^2(s\varphi) d\eta d\varphi$$

$$I_{22} = \int_0^1 \int_0^{2\pi} (A_1 \eta^2 + A_2 \eta^3 + A_3 \eta^4)^2 \eta \sin^2(s\varphi) d\eta d\varphi$$

VIII, Sample Calculations (cont.)

(4) $\rho_c \sqrt{\gamma R T_c}$ given in Eq. (54)

$$\rho_c \sqrt{\gamma R T_c} = \frac{\gamma P_c}{\gamma R T_c} \sqrt{\gamma R T_c} = \frac{\gamma P_c}{\sqrt{\gamma R T_c}}$$

(5) H_{A1} and H_{A2} given in Eqs. (53) and (54)

$$H_{A1} = - \frac{\gamma P_c M_m^2}{\sqrt{M_m^2 - 1} \left(1 + \frac{\gamma-1}{2} M_m^2 \right)^{\frac{\gamma}{\gamma-1}}}$$

$$H_{A2} = - \frac{\rho_c \sqrt{\gamma R T_c} M_m}{\sqrt{M_m^2 - 1} \left(1 + \frac{\gamma-1}{2} M_m^2 \right)^{\frac{\gamma+1}{2(\gamma-1)}}}$$

(6) K_A and G_A given by Eq. (59)

$$K_A = \left(\frac{H_{A1} I_{11} l_0}{\cos \alpha} + \frac{H_{A1} I_{21} \sin \alpha}{\cos^2 \alpha} l_1 \right) \bar{W}_{s_0}^2$$

$$G_A = \left(\frac{H_{A2} I_{12} l_0}{\cos \alpha} l_1 + \frac{H_{A2} I_{22} \sin \alpha}{\cos^2 \alpha} l_1^2 \right) \bar{W}_{s_0}^2$$

(7) M_N given by Eq. (92)

$$M_N = \rho_0 h I_M \bar{W}_{s_0}^2$$

(8) K_N and G_N given in Eq. (63)

$$K_N = \omega_N^2 M_N, \left[\frac{lb_f}{in} \right]$$

$$G_N = \omega_N M_N g_N \left[\frac{lb_f \sec}{in} \right]^*$$

* g_N is the structural damping coefficient of the mode S and seldom exceeds a value of 0.05. In the present study g_N is assumed to be a value of 0.015.

VIII, Sample Calculations (cont.)

- (9)
- R_G and R_K given by Eq. (74a)

$$R_G = \frac{G_A}{G_N}$$

$$R_K = \frac{K_A}{K_N}$$

- (10)
- $q_c(\omega_N)$ given by Eq. (49)

$$q_c(\omega_N) = \frac{W_{crit}^2 M_N^2 \beta_N \omega_N^2}{\frac{\pi}{2} W_{s0}^2 A_s^2}, \quad [lb_f \text{ sec}] ; \beta_N = \frac{G_N}{M_N}$$

$$W_{crit} = \frac{k K \epsilon^4 h^2}{12(1-\nu^2)\rho_0} \left(\frac{l_1}{\lambda_0}\right)^2, \quad [in] \quad [see \text{ eq (45)}]$$

From Reference*, $k \cong 24$ and $K \cong .24$

$$A_s^2 = (A_1 + A_2 + A_3)^2$$

- (11)
- $q_D(\omega_N)$ given by Eq. (74)

$$q_D(\omega_N) = [1 - (R_G + R_K) + R_G R_K] q_c(\omega_N)$$

- (12)
- G_D^2/G_C^2 given by Eq. (88)

$$\frac{G_D^2}{G_C^2} = 1 - (R_G + R_K) + R_G R_K$$

- (13)
- G_C^2 given by Eq. (84)

$$G_C^2 = \frac{\omega_N q_c(\omega_N)}{M_N^2 g_0^2}$$

*See reference at bottom of page K-15.

VIII, Sample Calculations (cont.)

(14) G_D^2 given by Eq. (12)

$$G_D^2 = G_c^2 \left(\frac{G_p^2}{G_c^2} \right)$$

Thus, if a driving force of G_D g's of "white noise" is uniformly applied to the nozzle extension, which may be caused by combustion instability, aerodynamic noise from the missile, boundary layer transitions, etc., then this force represents the limit in terms of initial buckling of the nozzle extension.

LIST OF SYMBOLS

A_i	see Equation 44
c	distance from origin to extension attachment point, in.
G_C	critical acceleration, g's
G_D	driving acceleration, g's
G_N	damping coefficient of the nozzle
G_θ	damping coefficient of the coupled system
h	extension thickness, in.
I_θ	mass moment of inertia of the coupled system about the origin, lbf-in.-sec ²
K_N	spring constant of the nozzle extension, lbf-in.
K_θ	spring constant of the coupled system, lbf-in.
l	distance from throat to nozzle exit, in.
l_o	distance from throat to extension attachment point, in.
M	Mach number
M_o	total mass of the coupled system, lbm
P_c	chamber pressure, psia
$q(\omega)$	power spectral density of the input force, lbf ² -sec
Q_i	external force acting on the system, lbf
r_e	nozzle exit radius, in.
r_o	nozzle radius at attachment point, in.
r_t	nozzle throat radius, in.
R	gas constant, lbf-ft/(lbm-°R)
S_o	static unbalance of the coupled system about its elastic axis, lbm-in.
t	time, sec
T	kinetic energy, lbf-in.
T_c	chamber temperature, °Rankine
u	displacement along nozzle wall, in.
u_s	modal shape
U	potential energy, lbf-in.
v	circumferential displacement, in.
v_s	modal shape

LIST OF SYMBOLS (cont.)

V	volume of the nozzle, in. ³
w	displacement normal to nozzle wall
w_s	modal shape
x	distance from extension attachment point, in.
x'	distance from origin, in.
$x_{c.g.}$	distance from origin to c.g. of engine, in.
$Z_s(w)$	impedance of the nozzle extension
$Z_{\theta}(w)$	impedance of the coupled system
α	cone half angle
K_N	damping parameter of the nozzle, 1/sec
K_{θ}	damping parameter of the coupled system, 1/sec
γ	ratio of specific heats
θ	rotational angle
ν	Poisson's ratio
$\xi_s(t)$	normalized coordinate, in.
ρ_A	density of gas, lbm/in. ³
ρ_D	mass density, lbm/in. ³
ω	frequency, 1/sec
ω_N	natural frequency, 1/sec

Report NAS 7-136-F

APPENDIX L

BIBLIOGRAPHY

NOZZLE CONCEPTS

- Berman, K., "The Plug Nozzle--A New Approach to Engine Design," *Astronautics*, Vol. 5, No. 4, April 1960.
- Berman, K., "Plug Nozzle Rocket Engine," *Franklin Inst. Journal*, Vol. 272, August 1961
- Berman, K., and Crimp, F. W., Jr., "Performance of Plug-Type Rocket Exhaust Nozzles," *ARS Journal*, Vol. 31, No. 1, January 1961.
- Berman, K., and Neuffer, B., "Plug Nozzle Flexibility, *Astronautics*, Vol. 5, No. 9, September 1960.
- Chamay, A., Horgan, J. J., and Megdal, D., "Evaluation of Plug Cluster Nozzles, Presented at ARS Solid Rocket Conference, February 1-3, 1961 (ARS preprint 1608-61).
- Diels, M. F., "Inverse-Plug Nozzle Characteristics," *Aerojet-General Technical Memo No. 170 SRP*, November 1961.
- Douglas Aircraft Co., "Unconventional Nozzle Study," *MSSD Report No. SM 41358*, January 1962.
- General Electric, "Analytical and Experimental Investigations of Unconventional Nozzle Designs Contract AF 04(611)-6016, Quarterly Report No. 3 for period ending February 28, 1961.
- Hug, D.P., "The Truncated Isentropic Spike Nozzle," *ABL/Z-33*, Contract NOrd 16640, paper prepared for sixth AFBMD-Aerospace Corporation Symposium on Ballistic Missile and Space Technology, Los Angeles, 28-30 August 1961.
- Ilsen, V., "Nozzles with Forced Deflection of Gas Flow," *Aerojet-General Report No. LRP 209*, 24 February 1961.
- Jacobs, T. A., Penner, S. S., Gill, G., and Eckel, E. F., "Approximate Theoretical Performance Evaluation for a Diverging Rocket," *Journal of the International Astronautical Federation*, Vol VI, Fasc. 2-3, 1960.
- Machel, W. G., and Graham, A.R., "Plug Nozzle Program," *General Electric Contract NAS W-40, Task III, Final Report April 1960*.
- Mager, A., "Approximate Solution of Isentropic Swirling Flow Through a Nozzle," *ARS Journal* 31:1140-1141, August 1961.

Nozzle Concepts (cont.)

Rand, "An Adiabatic-Isothermal Nozzle," V. F. Stepanchuk, Contract AF 49(638)-700 DC 1961, RM-2930-PR.

Ranson, V. H., Lorenc, S. A., Williams, J. J., and De Young, T. L., "Results of a Program for Theoretical and Experimental Evaluation of the Plug Nozzle Concept," Aerojet-General Tech. Memo 159 SRP, 8 March 1961.

Rao, G. V. R., "Analysis of a New Concept Rocket Nozzle," Liquid Rockets and Propellants Progress on Astronautics and Rocketry, Vol 2, M. Summerfield (ed) Academic Press, New York, 1960.

Rao, G. V. R., "The E-D Nozzle," Astronautics, September 1960.

Rao, G. V. R., "Recent Developments in Rocket Nozzle Configurations," ARS Journal Vol 31, No. 11, November 1961.

Rocketdyne, "Multichamber Engine Investigation," Liquid Advanced Projects Report 63-69, Interim Report, Contract NAS 8-4000, May 14, 1963.

Rocketdyne, "Advanced Design Analysis on Annular Nozzles," Contract NOW 60-0509-d Summary Report for Period 1 June 1960 to 30 July 1960, Report No. R-2354-3P, 18 September 1961.

Rocketdyne, "Aerodynamic Nozzle Study," Contract NAS 8-2654, Volume 1 Summary, Interim Report No. R-5381, October 1, 1963. (Confidential, title unclassified)

NOZZLE PERFORMANCE AND GAS FLOW

- Beale, W. T., and Povolny, J. H., "Internal Performance of Two-Dimensional Wedge Exhaust Nozzles," NACA RME 56K296, February 28, 1957.
- Branstetter, J. R., Kaufman, W. B., and Smith, A. L., "Experimental Behavior of Combustion Products of HEEF-2 and Air During Expansion in Exhaust Nozzles," December 1960, 61p, NASA TM X-381.
- Bryant, R. A. A., "One Dimensional Irreversible Gas Flow in Nozzles," University of South Wales, Bull. No. 3, 1960.
- Bryant, R. A. A., "Adiabatic Nozzle Flows," ARS Journal Vol. 31, No. 6, June 1961, pp 828-830.
- Corson, B. W., and Mercer, C. E., "Static Thrust of an Annular Nozzle with a Concave Central Base," NASA TN D-418, September 1960, 18p.
- Delyagin, G. N., "Convection Heat Transfer in a Vortex Flow Under Pressure," A Paper for Presentation at the Heat Transfer Conference, June 5-10, 1961, at Minsk, USSR.
- Goethert, B. H., "Studies of the Flow Characteristics and Performance of Multi-Nozzle Rocket Exhausts," Contract No. AF 40(600)-800, AEDC TR-59-16, October 1959.
- Grisman, P., Goldwasser, S., and Petrozzi, P., "Proceedings of the Propellant Thermodynamics and Handling Conference," Engineering Experiment Station Special Report No. 12, Ohio State University, June 1960.
- Hanzel, P. C., "A General Method for Calculating the Equilibrium Compositions and Temperature and the Thermodynamic Performance Parameters of Rocket-Propellant Systems," JPL Report No. 3-3, April 13, 1959.
- Malina, F. J., "Characteristics of the Rocket Motor Based on the Theory of Perfect Gases," Journal Franklin Inst., Vol. 230, 1940.
- Mickey, F., "A Study on the Equations Governing Gas Flow in a Low-Density Nozzle," Contract AF 40(600)-897, Proj. 8952 AEDC TDR 63-59, Report No. USCEC-R-78-101, March 1963, 92p.
- Mercer, C. E., and Simonson, A. J., "Effect of Geometric Parameters on the Static Performance of an Annular Nozzle with a Concave Central Base," NASA TN D-1006, February 1962, 33p.

Nozzle Performance and Gas Flow (cont.)

- Musial, N. T., and Ward, J. J., "Base Flow Characteristics for Several Four-Clustered Rocket Configurations at Mach Numbers from 2.0 to 3.5," NASA TN D-1093, December 1961, 55p.
- Pai, S. I., and Cary, B. B., Jr., "Two Dimensional Jet Mixing of Supersonic Flow," 50 Jahre Grenzschichtforschung, H. Gortler and W. Tollmier, eds, Friedr, Vieweg & Son (Braunschweig) 1955.
- Penner, S. S., "Chemical Reactions in Flow Systems," AGARD ograph No. 7, Butterworths Scientific Publications, London, 1955.
- Ransonn, V. H., "Gas Dynamic Considerations for Design of Discrete and Annular Throat External Expansion Nozzles," Aerojet-General Technical Memo. 150 LRP, 14 May 1962.
- Sauer, R., "General Characteristics of the Flow Through Nozzles at Near Critical Speeds," NACA TM 1147, 1946.
- Sauer, R., "Practical Numerical Methods of Three Dimensional Supersonic Flow," Final Report, Contract AF 61(052)-377, 1 June 1961.
- Shapiro, A. H., "The Dynamics and Thermodynamics of Compressible Fluid Flow," Vol. 1, The Ronald Press Co., New York, 1953
- Sievers, G. K., Tomazic, W. A., and Kinnery, G. R., "Theoretical Performance of Hydrogen-Oxygen Rocket Thrust Chambers," NASA TR R-111, 1961.
- Snyder, W. T., "Non-Isentropic Nozzle Flow," ARS Journal Vol. 30, No. 3, March 1960, pp 270-271.
- Thiokol, R. M. D., "Feasibility Study of Vortex Injection Techniques," Contract No. AF 04(611)-7429, Report RMD 5500-F, July 1962.
- United Technology Corp., "Dynamics of Two-Phase Flow Rocket Nozzles," Quarterly Technical Progress Report No. 7, INOV 62-31 January 1963, by R. Dunlap, C. E. Woldridge and others, 28 February 1963, 29p.
- Williams, J. J., "Results of Plug-Nozzle Cold-Flow Experiments," Aerojet-General Technical Memo No. 160 SRP, 20 April 1961.

NOZZLE LOSSES

Geometry

- Ahlberg, J. H., Hamilton, S., Migdal, D., and Nilson, E. N., "Truncated Perfect Nozzles in Optimum Nozzle Design," ARS Journal, pp 614-620, May 1961.
- Bloomer, H. E. Antl, R. J., Renas, P. E., "Experimental Study of Effects of Geometric Variables on Performance of Conical Rocket-Engine Exhaust Nozzles," NASA TN D-846, June 1961, 61p.
- Burrows, M. C., "Effect of Nozzle Convergence Length on Performance of a Heptane-Oxygen Combustor," NASA TN D-579, December 1960, 22p.
- Demuth, O. J., and Ditore, M. J., "Graphical Methods for Selection of Nozzle Contours," presented at ARS Solid Propellant Rocket Research Conf. Princeton, N. J., January 28-29, 1960, (ARS preprint No. 1945-60).
- Dillaway, R. B., "A Philosophy for Improved Rocket Nozzle Design," Jet Propulsion Vol. 27, No. 10, October 1957.
- Farley, J. M., and Campbell, C. E., "Performance of Several Method-of-Characteristics Exhaust Nozzles," NASA TN D-293, October 1960, 33p.
- Foelseh, K., "New Method of Designing Two-Dimensional Laval Nozzles for a Parallel and Uniform Jet," NAA NA-46-235-2, 27 May 1962.
- Foelsh, K., "The Analytic Design of an Axially Symmetric Laval Nozzle for a Parallel and Uniform Jet," Journal of Aero Science, Vol. 16, No. 3, March 1949.
- General Electric, "Analytical and Experimental Investigations of Unconventional Nozzle Designs," Contract AF 04(611)-6016, Quarterly Report No. 1, for period ending August 31, 1960.
- Greer, H., "Rapid Method for Plug Nozzle Design," ARS Journal Vol. 31, No. 4 April 1961, pp560-561.
- Guderly, G., and Hantsch, E., "Beste Formen Fur Achsensymmetrische Überschall-schubdrisen," Zerts. fur Flugwissen-Schaften, Vol. 3, September 1955.
- Guderly, G., "On Rao's Method for the Computation of Exhaust Nozzles," Zeits, fur Flugwissenschaften, December 1959.
- Guentert, E. C., and Neumann, H. E., "Design of Axisymmetric Exhaust Nozzles by Method of Characteristics Incorporating a Variable Isentropic Exponent," NASA TR R-33, September 1959.

Nozzle Losses (cont.)

- Johnson, C. B., Boney, L. R., Ellison, J. C., and Erickson, W. D., "Real-Gas Effects on Hypersonic Nozzle Contours with a Method of Calculation," NASA TN D-1622, April 1963, 52p.
- Knuth, E. L., "Optimum Contours for Propulsion Nozzles," ARS Journal Vol. 30, No. 10, October 1960, p983.
- Krull, H. G., and Beale, W. T., "Effect of Plug Design of Performance Characteristics of Convergent-Plug Exhaust Nozzles," NACA RME54 H05, October 1954.
- Krull, H. G., and Beale, W. T., "Effect of Outer Shell Design on Performance Characteristics of Convergent-Plug Exhaust Nozzles," NACA RME54K22, 1955.
- Krull, H. G., Beale, W. T., and Schmiedlin, R. F., "Effect of Several Design Variables on Internal Performance of Convergent-Plug Exhaust Nozzles, NACA RME56 G20, October 1956.
- Landsbaum, E. M., "Thrust of a Conical Nozzle," ARS Journal Vol. 29, No. 3, March 1959, pp212-213.
- Landsbaum, E. M., "Contour Nozzles," ARS Journal Vol. 30, No. 3, March 1960, pp244-250.
- Mercer, C. E., and Simonson, A. J., "Effect of Geometric Parameters on the Static Performance of an Annular Nozzle with a Concave Central Base," NASA TN D-1006 February 1962, 33p.
- Overall, R. E., "An Experimental Conclusion of Contoured and Conical Nozzles," presented at ARS Solid Propellant Rocket Research Conf. Princeton, N. J., January 28-29, 1960 (ARS preprint 1044-60).
- Rao, G. V. R., "Exhaust Nozzle Contour for Optimum Thrust," Jet Propulsion Vol. 28, No. 6, June 1958.
- Rao, G. V. R., "Contoured Rocket Nozzles," Proc. 9th International Astro. Fed. Congress, Amsterdam, 1958.
- Rao, G. V. R., Optimum Performance of Contoured Nozzles," Proc. Liquid Propellant Information Agency, JANAF Vol. 1, 1959.
- Rao, G. V. R., "Evaluation of Conical Nozzle Thrust Coefficient," ARS Journal Vol. 29, No. 8, August 1959.
- Rao, G. V. R., "Approximation of Optimum Thrust Nozzle Contour," ARS Journal Vol. 30, No. 6, June 1960.
- Rao, G. V. R., "Spike Nozzle Contour for Optimum Thrust," Ballistic Missile and Space Technology, Vol. 2, C. W. Morrow (ed) Pergamon Press, New York, 1961.

Nozzle Losses (cont.)

Rocketdyne, "High Expansion Area Ratio Nozzle Investigation," Phase III Hot Firing Program, Contract AF 04(611)-8509, Project No. 3058, Task No. 305802, First Quarterly Progress, Report, July 1963.

Vlachos, N. D., "Correction Factor for Annular Nozzles," ARS Journal Vol. 31, No. 6, June 1961, p822.

DRAG

- Braun, W. H., "Turbulent Boundary Layer on a Yawed Cone in a Supersonic Stream," NASA TR R-7, 1959, 16 p.
- Brinich, P. F., and Diaconis, N. S., "Boundary Layer Development and Skin Friction at Mach No. 3.05," NACA TN 2742, 1952.
- Chapman, D. R., and Kester, R. H., "Turbulent Boundary-Layer and Skin Friction Measurements in Axial Flow Along Cylinders at Mach Nos Between 0.5 and 3.6," NACA TN 3097, 1954.
- Cole, J. K., "Preliminary Investigation of the Interaction of an Oblique Shock Wave and a Turbulent Boundary Layer," Masters Thesis, University of New Mexico, 1961.
- Dhawan, S., "Direct Measurements of Skin Friction," NACA Rep. 1121 (1953).
- Elliot, D. G., Bartz, D. R., and Silver, S., "Calculation of Turbulent Boundary Layer Growth and Heat Transfer in Axisymmetric Flow," NASA TR 3-387.
- Englert, G. W., and Kochendorfer, F. D., "Estimated Performance of Radial-Flow Exit Nozzles for Air in Chemical Equilibrium," NASA MEMO 1-5-59E, February 1959, 53p. diagrs.
- Gruber, G., "Boundary Layer Correction to Nozzle Design and Performance," AGC Report F-7372, 1961.
- John Hopkins University Applied Physics Laboratory, "Task R Quarterly Progress Report No. 9," 1 April - 30 June 1961, Report No. TG331-9, Contract NOrd 7386, ARPA Order No. 22-59, Task 5.
- Mager, A., "On the Model of the Free- Shock Separated Turbulent Boundary Layer," J. Aeronaut. Sci., February 1956.
- Matting, F. W., et.al., "Turbulent Skin Friction at High Mach Numbers and Reynolds Nos in Air and Helium," NASA Tech. Rept. R-82, 1961.
- Monaghan, R. J., "Comparison Between Experimental Measurements and a Suggested Formula for the Variation of Turbulent Skin Friction in Compressible Flow," Aero. Res. Council, 1951.
- O'Donnell, R. M., "Experimental Investigation at Mach Numbers of 2.41 of Average Skin Friction Coefficients and Velocity Profiles for Laminar and Turbulent Boundary Layers and Assessment of Probe Effects," NACA TM 3122, 1954.

Drag (cont.)

- Pfyl, F. A., and Presley, L. L., "Experimental Determination of the Recovery Factor and Analytical Solution of the Conical Flow Field for a 20° Included Angle Cone at Mach Numbers of 4.6 and 6.0 and Stagnation Temperatures to 2600°R , NASA TN D-353, June 1961, 64p.
- Rubesin, M. W., Maydew, R. C., and Varga, S. A., "An Analytical and Experimental Investigation of the Skin Friction of the Turbulent Boundary Layer on a Flat Plate at Supersonic Speeds," NACA TN 2305, 1951.
- Schlichting, H., "Boundary Layer Theory," McGraw-Hill Book Co., 1960.
- Schubauer, G. B., and Klebanoff, P. S., "Contributions on the Boundary Layer Transition," NACA Report No. 1289, 1956.
- Summer, S. C., and Short, B. J., "Free Flight Measurements of Turbulent Boundary-Layer Skin Friction in the Presence of Severe Aerodynamic Heating at Mach Nos From 2.8 to 7.0," NACA TN 3391, 1955.
- Space Technology Laboratory, "Research in the Field of Low-Thrust Devices for Attitude and Velocity Control in Space Missions," Semi-Annual Report 1 January - 30 June 1960, Report No. STL/TR-60-0000-09229, Contract AF 04(647)-309, AF BMD TR 60-139.
- Tanner, R. F., "The Turbulent Boundary Layer in Zero-Pressure Gradient with Transpiration," Contract DA 44-177-AMC-892(T), TRECOM TR-63-35; Rept. 40, July 1963, 48p, 7 refs.
- Tucker, M., "Approximate Calculation of Turbulent Boundary Layer Development in Compressible Flow," NACA TN 2337, 1951.
- Wilson, R. E., "Turbulent Boundary Layer Characteristics at Supersonic Speeds-Theory and Experiment," Journal of the Aeronautical Sciences, Vol. 17, No. 9, 1950.

DISSOCIATION

Aeroneutronic, "An Investigation of Recombination and Condensation Effects in Rocket Nozzles," Contract NORD 17980, Task 3(P), Aeroneutronic Publication No. C-1277
15 June 1961.

Aerospace

Aukerman, C. A., and Church, B. E., "Experimental Hydrogen-Fluorine Rocket Performance at Low Pressures and High Area Ratios," NASA TM X-724, September 1963, 31p.

Blythe, P. A. - "Nonequilibrium Flow through Nozzles," Journal of Fluid Mechanics, September 1963.

Bray, K. N. C. and Appleton, J. P. - "The Choice of an Optimum Set of Measurements to Study Atomic Recombination in Nozzles," A.A.S.U. Report No. 120, University of Southampton, November 1959.

Bray, K. N. C., "Simplified Sudden-Freezing Analysis for Nonequilibrium Nozzle Flows," ARS Journal Vol. 31, No. 6, June 1961.

Bray, K. N. C., "Atomic Recombination in a Hypersonic Wind Tunnel Nozzle," Journal of Fluid Mechanics, No. 6, 1959.

Bray, K. N. C., "Atomic Recombination in Nozzles: Methods of Analysis for Flows With Complicated Chemistry," University of South Hampton, Aero and Astro Report No. 166, 1961.

Buchele, D. R., "Recombination of Hydrogen-Air Combustion Products in an Exhaust Nozzle," NASA TN D-1052, August 1961, 43p.

Capiaux, R. and Washington, M. - "Nonequilibrium Flow Past a Wedge," AIAA Journal, March 1963.

Chen, C. J. - "Experimental Investigation of Atomic Recombination in a Supersonic Nozzle," Journal of Fluid Mechanics, November 1963.

Cornell Aeronautical Lab., Inc., "Nonequilibrium Gas Dynamics Related to Propulsion Systems," Fourth Quarterly Report, 4 July 1961 to 4 October 1961, N62-10697.

Der, J. J. "Linearized Supersonic Nonequilibrium Flow Past an Arbitrary Boundary," NASA TR R-1119, August 1961.

Ehlers, F. E. - "Method of Characteristics and Velocity of Sound for Reacting Gases," AIAA Journal, June 1963.

Dissociation (cont.)

- Eschenroeder, A. Q., and Lori, J. A., - "Catalysis of Recombination in Nonequilibrium Nozzle Flows," Ninth Symposium (International) on Combustion, Academic Press, New York, 1963.
- Freeman, N. C., "Nonequilibrium Theory of an Ideal-Dissociating Gas Through a Conical Nozzle," Aeronautical Research Council (Great Britain) ARC Report No. 20, 340; FM2708; TP597, 5 August 1958.
- John Hopkins University Applied Physics Laboratory, "Task R Quarterly Progress Report No. 9," 1 April - 30 June 1961, Report No. TG331-9, Contract NORD 7386, ARPA Order No. 22-59, Task 5.
- Lezberg, E. A. and Fraciscus, L. C. - "Effects of Exhaust Nozzle Recombination on Hypersonic Ramjet Performance," AIAA Journal, September 1963.
- Lighthill, M. J. - "Dynamics of a Dissociation Gas, Part I: Equilibrium Flow," Journal of Fluid Mechanics, V.2, n. 1, 1957
- Marrone, P. V. - Treavor, C. E. - "Efforts of Dissociation on the Rate of Vibrational Relaxation," Physics of Fluids, 1962
- Olsen, W. T., "Problems of High Energy Propellants for Rockets," Rocket and Missile Technology Chem. Engineering Progress Symposium Series No. 33, Vol. 57, AICHE, 1961, pp28-37.
- Olsen, W. T., "Recombination and Condensation Processes in High Area Ratio Nozzles," ARS Journal Vol. 32, May 1962, p672.
- Space Technology Laboratories, "Semi Annual Report on Investigation of Nonequilibrium Phenomena in Rocket Nozzles," Contract AF 04(647)-165, Report GM-TR-0165-00581, 1 July - 31 December 1958.
- Space Technology Laboratories, "Nonequilibrium Phenomena in Rocket Nozzles, Contract AF 04(674)-309, TR-59-000-00707, Semi-Annual Report, 1 January 1959-30 June 1959.
- Watson, R., "Effect of Scale Size on a Rocket Engine with Suddenly Frozen Nozzle Flow," ARS Journal, Vol. 31, No. 3, March 1961, pp 452-453.
- Wegener, P. O. - "A Review of Investigations of Stationary Supersonic Nozzle Flow with a Reacting Gas Mixture," Combustion and Propulsion, Fourth Agard Colloquium, Pergamo Press, New York, 1961.
- Wilde, K. A. - "Numerical Study of Hydrogen-Fluorine Kinetics in Nozzles," AIAA Journal, February 1964

REDUCTION OF NOZZLE LOSSES

SHEAR DRAG REDUCTION

- Black, T. J., and Sarnecki, A. J., The Turbulent Boundary Layer with Suction or Injection. A.R.C. 20, 501, 1958.
- Clarke, J. H. Menkes, H. R., and Libby, P. A., A Provisional Analysis of Turbulent Boundary Layers with Injection, Jour. Aero. Sci., V22, 1955.
- Dorrance, W. H., The Effect of Mass Transfer on the Compressible Turbulent Boundary Layer Skin Friction and Heat Transfer--An Addendum, Jour. Aero. Sci., Vol. 23, 1956.
- Dorrance, W. H., and Dore, F. J., The Effect of Mass Transfer on the Compressible Turbulent Boundary Layer Skin Friction and Heat Transfer, Jour. Aero. Sci. V21, 1954.
- Leadon, B. M., and Scott, C. J., Transpiration Cooling Experiments in a Turbulent Boundary Layer at $M=3$, Jour. Aero. Sci., V23, 1956.
- Mickley, H. S., and Davis, R. S., Momentum Transfer for Flow Over a Flat Plate with Blowing, NACA TN 4017, 1957.
- Morduchow, M., On Heat Transfer over a Sweat-Cooled Surface in Laminar Compressible Flow with a Pressure Gradient, Jour. Aero. Sci., V19, 1952.
- Ness, N., Foreign Gas Injection Into a Compressible Turbulent Boundary Layer on a Flat Plate, Jour. Aero. Sci., Vol 28, 1961.
- Mickley, H. S., Ross, R. C., Squyers, A. L., Stewart, W. E., Heat Mass, and Momentum Transfer for Flow over a Flat Plate with Blowing or Suction, NACA TN 3208, 1954.
- Pappas, C. C., The Effect of Injection of a Foreign Gas on the Skin Friction and Heat Transfer of the Turbulent Boundary Layer, I.A.S. Preprint 59-78, 1959.
- Pappas, C. C. and Okuno, A. F., Measurements of Skin Friction of the Compressible Turbulent Boundary Layer on a Cone with Foreign Gas Injection, Jour. Aero. Sci., Vol 28, May 1960.
- Rubesin, M. W., An Analytical Estimation of the Effect of Transpiration Cooling on the Heat Transfer and Skin Friction Characteristics of a Compressible Turbulent Boundary Layer, NACA TN 3341, 1954.
- Rubesin, M. W., The Influence of Surface Injection on Heat Transfer and Skin Friction Associated with the High Speed Turbulent Boundary Layer, NACA RM A55L13, 1956.

Reduction of Nozzle Losses (cont.)

- Rubesin, M. W., and Pappas, C. C., An Analysis of the Turbulent Boundary Layer Characteristics on a Flat Plate with Distributed Light Gas Injection, NACA TN 4149, 1958.
- Rubesin, M. W., Pappas, C. C., Okuno, A. F., The Effect of Fluid Injection on the Compressible Turbulent Boundary Layer, NACA RM A55119, 1955.
- Tendeland, T., and Okuno, A. F., The Effect of Fluid Injection on the Compressible Turbulent Boundary Layer-The Effect on Skin Friction of Air Injected into the Boundary Layer of a Cone at M-2.7, NACA RM A56D05, 1956.
- Tewfik, O. E., Some Characteristics of the turbulent Boundary Layer with Air Injection, AIAA Journal, Vol 1. No. 6, 1963.

CONTINUUM LIMITS

- Cybulski, R. J., Baldwin, L. V., "Heat Transfer from Cylinders in Transition from Slip Flow to Free-Molecule Flow," NASA MEMO 4-27-59E, May 1959, 49p. diags., tabs.
- Eckert, E. R. G., "Heat and Mass Transfer," McGraw-Hill Book Co., Inc., New York, 1959.
- Hayes & Probstein, "Hypersonic Flow Theory," Academic Press, New York 1959.
- Liepmann, H. W., and Roshko, A., "Elements of Gas Dynamics," John Wiley & Sons, Inc., New York, 1957.
- Schlichting, H., "Boundary Layer Theory," McGraw-Hill Book Co., 1960.
- Shapiro, A. H., "The Dynamics and Thermodynamics of Compressible Fluid Flow," Vol. 1, The Ronald Press Co., New York, 1953.
- Stalder, J. R., Goodwin, G., and Creager, M. O., "Heat Transfer to Bodies in a High Speed Rarefied-Gas Stream," NACA Rep. 1093, 1952.
- Tsien, Hsue-Shen, "Superaerodynamics, Mechanics of Rarefied Gases," Journal of the Aeronautical Sciences, Vol. 13, No. 12, December 1946, p653.

VIBRATION

Aerojet-General Corp., "Study on Bell Mode Vibrations of Conical Nozzles," Contract NASr-111, Final Report AGC Report No. 2581, May 1963.

Barrett, R. E., "Techniques for Predicting Localized Vibratory Environments of Rocket Vehicles," NASA TN D-1836, October 1963, vii, 58p.

Bisplinghoff, R. L., and Ashley, H. L., "Principles of Aero Elasticity," John Wiley, New York, 1962.

Bisplinghoff, R. L., Ashley, H., and Halfman, R. L., "Aeroelasticity," Addison-Wesley Publishing Co., Inc., 1955.

Report NAS 7-136-F

APPENDIX M

Report NAS 7-136-F, Appendix M

Contract NAS 7-136 -- Aerojet-General Corporation
"High Effective Area Ratio Nozzles for Space Engines"

<u>COPIES</u>	<u>RECIPIENT</u>
	NASA Western Operations Office 150 Pico Boulevard Santa Monica, California 90406
1	Office of Technical Information
1	Contracting Officer
1	Patent Office
	NASA Headquarters Washington, D. C. 20546
4	Mr. Henry Burlage, Jr. Chief, Liquid Propulsion Technology, RPL
1	Mr. Vernon E. Jaramillo Advanced Manned Missions, MTA
25	Scientific and Technical Information Facility Attn: NASA Representative, Code CRT P. O. Box 5700 Bethesda, Maryland 20014
1	Mr. Richard Cannova Jet Propulsion Laboratory California Institute of Technology 4800 Oak Grove Drive Pasadena, California 91103

NASA FIELD CENTERS

<u>COPIES</u>	<u>RECIPIENT</u>	<u>DESIGNEE</u>
2	NASA Ames Research Center Moffett Field, California 94035	H. Hornby Mission Analysis Div.
2	NASA Goddard Space Flight Center Greenbelt, Maryland 20771	M. Moseson Code 624
2	Jet Propulsion Laboratory California Institute of Technology 4800 Oak Grove Drive Pasadena, California 91103	R. F. Rose Propulsion Div., 38
2	NASA Langley Research Center Langley Station Hampton, Virginia 23365	F. L. Thompson Director
2	NASA Lewis Research Center 21000 Brookpark Road Cleveland, Ohio 44135	Dr. A. Silverstein Director
2	NASA Marshall Space Flight Center Huntsville, Alabama 35812	H. Weidner Code R-P&VED
2	NASA Manned Spacecraft Center Houston, Texas 77001	Robert R. Gilruth Director

GOVERNMENT INSTALLATIONS

<u>COPIES</u>	<u>RECIPIENT</u>	<u>DESIGNEE</u>
1	Advanced Research Projects Agency Pentagon, Room 3D154 Washington 25, D. C.	D. E. Mock
1	Aeronautical Systems Division Air Force Systems Command Wright-Patterson Air Force Base Dayton, Ohio	D. L. Schmidt Code ASRCNC-2
1	Air Force Missile Development Center Holloman Air Force Base, New Mexico	MAJ R. E. Bracken Code MDGRT
1	Air Force Missile Test Center Patrick Air Force Base, Florida	L. J. Ullian
1	Air Force Systems Command, Dyna-Soar Air Force Unit Post Office Los Angeles 45, California	COL Clark (Technical Data Center)
1	U. S. Army Missile Command Redstone Arsenal, Alabama 35809	Dr. Walter Wharton
1	Arnold Engineering Development Center Arnold Air Force Station Tullahoma, Tennessee	Dr. H. K. Doetsch
1	Bureau of Naval Weapons Department of the Navy Washington 25, D. C.	J. Kay Code RTMS-41
1	Central Intelligence Agency 2430 E Street, N. W. Washington 25, D. C. Attn: Miss Elizabeth F. Kernan	XXXXXXX
1	Defense Documentation Center Headquarters Cameron Station, Building 5 5010 Duke Street Alexandria, Virginia 22314 Attn: TISIA	XXXXXXX

GOVERNMENT INSTALLATIONS

<u>COPIES</u>	<u>RECIPIENT</u>	<u>DESIGNEE</u>
1	Headquarters, United States Air Force Washington 25, D. C.	COL C. K. Stambaugh Code AFRST
1	Picatinny Arsenals Dover, New Jersey	I. Forsten, Chief Liquid Propulsion Lab.
1	Rocket Research Laboratories Edwards Air Force Base Edwards, California 93523	COL H. W. Norton
1	U. S. Naval Ordnance Test Station China Lake, California 93557	Chief Missile Propulsion Div. Code 451
1	U. S. Atomic Energy Commission Technical Information Services Box 62 Oak Ridge, Tennessee	XXXXXXXX

CPIA

1	Chemical Propulsion Information Agency Johns Hopkins University Applied Physics Laboratory 8621 Georgia Avenue Silver Spring, Maryland	Neil Safeer
---	--	-------------

COMMERCIAL CONTRACTORS

<u>COPIES</u>	<u>RECIPIENT</u>	<u>DESIGNEE</u>
1	Aerojet-General Corporation P. O. Box 296 Azusa, California	L. F. Kohrs
1	Aerojet-General Corporation P. O. Box 1947 Technical Library, Bldg. 2015, Dept. 2410 Sacramento 9, California	R. Stiff
1	Aeronutronic A Division of Ford Motor Company Ford Road Newport Beach, California	D. A. Carrison
1	Aerospace Corporation 2400 East El Segundo Boulevard P. O. Box 95085 El Segundo, California 90045	John G. Wilder MS-2293 Propulsion Department
1	Aerospace Corporation Post Office Box 95085 Los Angeles 45, California	Library Technical Documents Group
1	Arther D. Little, Inc. Acorn Park Cambridge 40, Massachusetts	A. C. Tobey
1	Astropower, Inc., Subsidiary of Douglas Aircraft Company, Inc. 2968 Randolph Avenue Costa Mesa, California	Dr. George Moc Dir., Research
1	Astrosystems, Inc. 1275 Bloomfield Avenue Caldwell Township, New Jersey	A. Mendenhall
1	Atlantic Research Corporation Edsall Road and Shirley Highway Alexandria, Virginia	A. Scurlock

COMMERCIAL CONTRACTORS

<u>COPIES</u>	<u>RECIPIENT</u>	<u>DESIGNEE</u>
1	Beech Aircraft Corporation Boulder Facility Box 631 Boulder, Colorado	J. H. Rodgers
1	Bell Aerosystems Company P. O. Box 1 Buffalo 5, New York	W. M. Smith
1	Bendix Systems Division Bendix Corporation Ann Arbor, Michigan	John M. Brueger
1	Boeing Company P. O. Box 3707 Seattle 24, Washington	J. D. Alexander
1	General Dynamics/Astonautics Library and Information Services (128-00) P. O. Box 1128 San Diego, California 92212	Frank Dore
1	Curtiss-Wright Corporation Wright Aeronuatic Division Wood-ridge, New Jersey	G. Kelley
1	Douglas Aircraft Company, Inc. Missile and Space Systems Division 3000 Ocean Park Boulevard Santa Monica, California 90406	R. W. Hallet Chief Engineer Advanced Space Technology
1	Fairchild Stratos Corporation Aircraft Missiles Division Hagerstown, Maryland	J. S. Kerr
1	General Electric Company Missile and Space Vehicle Department Box 8555 Philadelphia, Pennsylvania	L. S. Beers

COMMERCIAL CONTRACTORS

<u>COPIES</u>	<u>RECIPIENT</u>	<u>DESIGNEE</u>
1	General Electric Company Flight Propulsion Lab Department Cincinnati 15, Ohio	D. Suichu
1	Grumman Aircraft Engineering Corporation Bethpage, Long Island, New York	Joseph Gavin
1	Chrysler Corporation Missile Division Warren, Michigan	John Gates
1	Kidde Aero-Space Division Walter Kidde and Company, Inc. 675 Main Street Belleville 9, New Jersey	R. J. Hanville Director of Research Engineering
1	Lockheed Missile and Space Company Attn: Technical Information Center P. O. Box 504 Sunnyvale, California	Y. C. Lee Power Systems R&D
1	Lockheed Propulsion Company P. O. Box 111 Redlands, California	H. L. Thackwell
1	Marquardt Corporation 16555 Saticoy Street Box 2013 - South Annex Van Nuys, California	Warren P. Boardman, Jr.
1	Martin Division Martin Marietta Corporation Baltimore 3, Maryland	John Calathes (3214)
1	Martin Denver Division Martin Marietta Corporation P. O. Box 179 Denver, Colorado 80201	J. D. Goodlette Mail No. A-241
1	McDonnell Aircraft Corporation P. O. Box 6101 Lambert Field, Missouri	R. A. Herzmark

COMMERCIAL CONTRACTORS

<u>COPIES</u>	<u>RECIPIENT</u>	<u>DESIGNEE</u>
1	North American Aviation, Inc. Space & Information Systems Division Downey, California	H. Storms
1	Northrop Corporation 1001 East Broadway Hawthorne, California	W. E. Gasich
1	Pratt & Whitney Aircraft Corporation Florida Research & Development Center P. O. Box 2691 West Palm Beach, Florida 33402	R. J. Coar
1	Lockheed California Company 10445 Glen Oaks Boulevard Pacoima, California	G. D. Brewer
1	Radio Corporation of America Astro-Electronics Division Defense Electronic Products Princeton, New Jersey	S. Fairweather
1	Reaction Motors Division Thiokol Chemical Corporation Denville, New Jersey 07832	A. Sherman
1	Republic Aviation Corporation Farmingdale Long Island, New York	Dr. Wm. O'Donnell
1	Rocketdyne (Library Dept. 586-306) Division of North American Aviation, Inc. 6633 Canoga Avenue Canoga Park, California 91304	E. B. Monteath
1	Space General Corporation 9200 Flair Avenue El Monte, California	C. E. Roth
1	Space Technology Laboratories P. O. Box 95001 Air Port Station Los Angeles 45, California	G. W. Elverum

Report NAS 7-136-F, Appendix M

COMMERCIAL CONTRACTORS

<u>COPIES</u>	<u>RECIPIENT</u>	<u>DESIGNEE</u>
1	Stanford Research Institute 333 Ravenswood Avenue Menlo Park, California 94025	Thor Smith
1	TAPCO Division Thompson-Ramo-Wooldridge, Inc. 23555 Euclid Avenue Cleveland 17, Ohio	P. T. Angell
1	Thiokol Chemical Corporation Redstone Division Huntsville, Alabama	John Goodloe
1	United Aircraft Corporation East Hartford Plant 400 Main Street Hartford, Connecticut 06108	Erle Martin
1	United Technology Corporation 587 Methilda Avenue Sunnyvale, California	B. Abelman
1	Vought Astronautics Box 5907 Dallas 22, Texas	Warren C. Trent